^{99m}Tc-labeled interleukin-8

for imaging of infection and inflammation

^{99m}Tc-labeled interleukin-8
for imaging of infection and inflammation

een wetenschappelijke proeve

op het gebied van de Medische Wetenschappen

PROEFSCHRIFT

ter verkrijging van de graad van doctor aan de

Katholieke Universiteit Nijmegen,

op gezag van de Rector Magnificus Prof. Dr. C.W.P.M. Blom,

volgens besluit van het College van Decanen in het

openbaar te verdedigen op vrijdag 20 februari 2004

des namiddags om 1.30 uur precies

door

Hubertus Johannes Johanna Maria Rennen

geboren op 24 januari 1959 te Woensdrecht

Promotores: Prof. Dr. F.H.M. Corstens
                     Prof. Dr. W.J.G. Oyen

Co-Promotor: Dr. O.C. Boerman

Manuscriptcommissie: Prof. Dr. J.W.M. van der Meer
                     Prof. Dr. J.M.D. Galama
                     Prof. Dr. R.M.J. Liskamp (Universiteit Utrecht)

Table of contents

Abbreviations

BSA	bovine serum albumin
C5adR	C5a des Arg[74]
CFU	colony forming units
CI	colitis index
EDDA	ethylenediaminediacetic acid
[18]FDG FDG	^{18}F-fluorodeoxyglucose
FPLC	fast performance liquid chromatography
[67]Ga	radionuclide gallium-67
h	hour
HMPAO	hexamethylpropyleneamine oxime
HPLC	high performance liquid chromatography
HYNIC	hydrazinonicotinamide
IBD	inflammatory bowel disease
ID	injected dose
IgG	immunoglobulin G
IL-8	interleukin-8
i.m.	intramuscular(ly)
ITLC	instant thin layer chromatography
i.v.	intravenous(ly)
MBq	megabecquerel
mCi	millicurie
MW	molecular weight
NAP-2	neutrophil activating peptide 2
p.i.	post injection
PBS	phosphate buffered saline
PET	positron emission tomography
PMN	polymorphonuclear cell
RBC	red blood cell
RBF	receptor binding fraction
ROI	region of interest
SD	standard deviation
SEM (s.e.m.)	standard error of the mean
S-HYNIC	succinimidyl hydrazinonicotinamide
T/B T/BGr	target to background ratio
[99m]Tc	radionuclide technetium-99m
TPPTS	triphenylphosphinetrisulfonate
WBA	whole body activity
WBC	white blood cell

Preface: Outline of the thesis

Nuclear medicine offers ideal techniques to visualize inflammatory processes using noninvasive methods of whole-body scanning, enabling the determination of both the localization and the extent of the inflammatory process throughout the body. Although autologous leukocytes, labeled with ^{111}In or ^{99m}Tc, is still considered the 'gold standard' nuclear medicine technique to image infection and inflammation, there is a great need for a less cumbersome and less hazardous approach. Over the last few decades a series of radiopharmaceuticals to investigate infectious and non-microbial inflammatory disorders has been proposed. Radiolabeled monoclonal antibodies and antibody-fragments, radiolabeled chemotactic peptides and cytokines, and radiolabeled antibiotics are new approaches for this application. Chapter 1 presents an overview of these newly developed agents, their potential and their drawbacks.

Most encouraging results have been obtained with radiolabeled receptor-specific small proteins and peptides, such as interleukin-1 (IL-1), interleukin-2 (IL-2) and interleukin-8 (IL-8). IL-8 is a chemotactic cytokine involved in activation and recruitment of neutrophilic granulocytes to areas of infection. This protein binds to two types of receptors on neutrophils with high affinity. Previous studies by Van der Laken et al. in our group showed excellent infection imaging characteristics of radioiodinated IL-8 in a rabbit model of intramuscular infection. However, for clinical imaging, ^{123}I is not a very suitable radionuclide: It has a limited availability, it is expensive and the adopted labeling method is rather laborious and the specific activities obtained were low. For clinical application, a simple and rapid labeling procedure, using the radiometal ^{99m}Tc, is preferable. The studies presented in this thesis focus on the labeling of IL-8 with ^{99m}Tc and the suitability of ^{99m}Tc-labeled IL-8 to image infection and inflammation in various animal models.

IL-8 is labeled with ^{99m}Tc using a derivative of hydrazinonicotinamide (HYNIC) as a molecule linking protein to radiometal. First, the chemistry of labeling proteins with ^{99m}Tc via HYNIC is investigated. In chapter 2, the conditions of conjugating HYNIC to proteins are varied in order to find the optimal conditions to obtain a maximal labeling efficiency while preserving the receptor binding.

In chapter 3, the contribution of non-specific accumulation of ^{99m}Tc-labeled proteins in inflammatory foci in rats is studied. Eleven proteins of various molecular weights without specific interaction with components in inflammatory sites are labeled with ^{99m}Tc via HYNIC and studied in rats with intramuscular infection. The question which characteristic of a protein determines its nonspecific localization in infectious foci is addressed here.

Chapter 4 presents the first in vivo characterization of ^{99m}Tc-HYNIC-IL-8 in rabbits with an intramuscular infection. The results are compared with those obtained with radioiodinated IL-8.

In Chapter 5 a further optimization of the labeling of IL-8 with ^{99m}Tc via HYNIC is described. Improvement of stability, specific activity and infection imaging characteristics are sought in a slight modification of the HYNIC-linker and in the use of alternative co-ligand systems.

In the addendum to chapter 5 the importance of a careful choice of the radiolabeling conditions for the imaging characteristics is discussed.

In chapters 6 and 7 the utility of ^{99m}Tc-HYNIC-IL-8 as an imaging agent in rabbit models of colitis and pulmonary infection is explored .

The pharmacokinetic behavior of ^{99m}Tc-labeled IL-8 is studied in chapter 8. These studies aim to demonstrate the specificity of uptake of IL-8 in the abscess and to elucidate the mechanism of uptake IL-8 in the abscess.

In chapters 9 and 10 the scope of the study is broadened from IL-8 as infection imaging agent to other leukocyte receptor binding proteins. Complement factors C5a and C5a-des-Arg[74], binding with high affinity to a common receptor on neutrophils, are labeled with ^{99m}Tc and tested for imaging of infection in a rabbit model (Chapter 9).

Several chemokines, closely related to IL-8, are compared for their capabilities to image infection in chapter 10. These proteins show various affinities for receptors on neutrophils and the relationship between neutrophil receptor affinity and suitability for infection imaging is investigated. Special attention is given to Neutrophil-Activating-Petide-2 (NAP-2) and three NAP-2 variants.

In chapter 11, the results of the presented studies are discussed and ^{99m}Tc-IL-8 scintigraphy is put in perspective with other new approaches to visualize infection scintigraphically such as positron emission tomography (PET) using ^{18}F-Fluorodeoxyglucose (FDG).

Chapter 1

Imaging infection/inflammation in the new millennium

Huub J.J.M. Rennen, Otto C. Boerman, Wim J.G. Oyen, Frans H.M. Corstens

Abstract

In the past century a wide variety in approaches to visualise infections and inflammations by gamma scintigraphy has been developed. Autologous leukocytes, labelled with ^{111}In or ^{99m}Tc, is still considered the 'gold standard' nuclear medicine technique to image infection and inflammation. The range of radiopharmaceuticals to investigate infectious and non-microbial inflammatory disorders is vastly expanding. Developments in protein/peptide chemistry and in radiochemistry should lead to agents with very high specific activities. Recently, positron emission tomography (PET) with ^{18}FDG has been introduced and has been shown to delineate infectious and inflammatory foci with high sensitivity. The third millennium will show a gradual shift from basal (nonspecific) or cumbersome, even hazardous techniques (radiolabelled leukocytes) to more sophisticated approaches. Here a survey is presented of the different approaches in use or under investigation.

Introduction

Scintigraphic detection of infection and inflammation allows the determination of both the localisation and the number of infectious and inflammatory foci throughout the body. Since scintigraphic images are based on functional (physiological and/or biochemical) changes of tissues, infectious and inflammatory foci can be visualised in their early phases, when anatomical changes are not yet apparent. Over the last 30 years multiple approaches to visualise infections and inflammations using radionuclides and gamma cameras have been developed. Recently, positron emission tomography (PET) with ^{18}FDG has been introduced in the field of infection/inflammation imaging. To understand the way of action of many of these new agents, the pathophysiology of inflammation needs to be elucidated.

Infection and inflammation

Inflammation can be described as the reaction of the body to any kind of injury (1). Such injury can vary from trauma to ischaemia, to neoplasm, and also to invasion of micro-organisms, in which case we speak of infection. Infection simply means "contamination with micro-organisms". There can be infection without inflammation, as in the case of a severely immunocompromised patient. Especially in such cases it is clear that for the purpose of imaging one would need an agent that directly interacts with the micro-organisms. There can be inflammation without infection when tissue injury is not due to the invasion of micro-organisms but caused by "stimuli" as trauma, ischaemia, neoplasm or foreign particles (e.g. asbestos).

Components of the inflammatory response
The response to acute infection/inflammation can be characterized by:
- Locally increased blood supply
- Increased vascular permeability in the affected area
- Enhanced transudation of plasma proteins
- Enhanced influx of leukocytes

In response to tissue damage powerful defense mechanisms are activated, consisting of cells (leukocytes) and plasma proteins (opsonins, antibodies, complement). A complex variety of mediators, both vasoactive and chemotactic, is involved in the process. These mediators are generated in the focus of inflammation/infection and amplify the local response by the recruitment of cells and plasma components from the blood. Vasodilatation and increased endothelial permeability are induced to facilitate the extravasation of proteins and cells. In addition, the expression of adhesion molecules on endothelial cells and leukocytes is stimulated. In this way leukocytes migrate actively from the circulation into inflamed tissue. First, they adhere to the vascular endothelium due to locally enhanced expression of adhesion molecules (rolling, arrest and adhesion). Subsequently, they pass through the endothelium and the basal membrane (diapedesis) and migrate into the inflammatory focus (chemotaxis). In acute inflammation/infection the infiltrating cells are predominantly polymorphonuclear cells (PMN).

In chronic inflammation/infection the cellular response is different from that of acute inflammation/infection. Infiltrating cells are predominantly mononuclear cells: lymphocytes, monocytes and macrophages.

Non-specific and specific radiopharmaceuticals to image infection
Non-specific radiotracers of infection
Increased blood supply, increased vascular permeability and enhanced transudation are processes that can be utilized for non-specific accumulation of radiotracers. It must be emphasized that all radiopharmaceuticals accumulate to some extent in this non-specific way at the site of infection. Examples of non-specific radiotracers for detection of infection based on increased vascular permeability are:
- ^{67}Ga-citrate
- Radiolabelled non-specific immunoglobulins
- Radiolabelled liposomes
- Radiolabelled avidin-biotin

Table 1. Strategies in infection imaging with specific radiotracers

_____

A   Target leukocytes moving to and present in the focus of infection:
- direct labelling of leukocytes (ex vivo labelling)
- indirect labelling of leukocytes (in vivo labelling):
  - antibody-antigen interactions: radiolabelled antigranulocyte monoclonal antibodies/antibody-fragments
  - binding to receptors on leukocytes:
    - radiolabelled chemotactic peptides: formyl-Met-Leu-Phe
    - radiolabelled cytokines: the interleukins, platelet factor 4

B   Target mediators that are already present in or migrate to the site of infection by radiopharmaca:
- anti-E-selectin antibodies or anti-E-selectin $F(ab')_2$ fragments

C   Administer radiolabelled mediators that migrate to the site of infection:
- radiolabelled mediators binding to leukocytes (see above: indirect labelling of leukocytes)

D   Target the locally present micro-organisms:
- radiolabelled ciprofloxacin
- radiolabelled antimicrobial peptides

E   Target the increased glucose uptake of infiltrated granulocytes and tissue macrophages:
- ^{18}FDG in positron emission tomography (PET)

_____

Specific radiotracers of infection

Specific processes of accumulation comprise a number of possible interactions between radiopharmaceutical and target, e.g. receptor binding and antibody-antigen binding. Several pathways can be distinguished in infection imaging based on specific processes of accumulation of the radiopharmaceutical, as shown in table 1. Leukocytes preferentially target infection by chemotaxis and can therefore be used to transport radionuclides to the infected area (A). They move massively to the site of infection and localise there in great numbers. Detection of infection can be accomplished by direct labelling of leukocytes (ex vivo labelling) or by labelling leukocytes indirectly, i.e. in vivo. Ex vivo labelling requires withdrawal of blood from the patient, purification of leukocytes, labelling and reinjection of the radiolabelled cells. Autologous leukocytes labelled with ^{111}In or ^{99m}Tc can lead to positive imaging due to the fact that leukocytes, even after ex-vivo labelling, have the capacity to migrate to the inflamed area. In vivo labelling of leukocytes can be based on antibody-antigen interactions (e.g. radiolabelled antigranulocyte monoclonal antibodies) or on leukocyte receptor binding (e.g. radiolabelled chemotactic peptides and cytokines). With respect

to pathway B and C, vasoactive or chemotactic mediators of the inflammatory process could either be targeted in vivo by radiopharmaca or could be radiolabelled in vitro and injected. So, either we label in vivo a particular component that is already present in or goes to the inflamed area, or we inject in a radiolabelled form the mediator itself. Pathway D can be said to be truly infection imaging, in the way that radiopharmaceuticals are used that specifically target micro-organisms. A completely different mechanism of accumulation at the inflammatory site is underlying PET scans using ^{18}FDG: Enhanced uptake of radiolabelled glucose by infiltrated granulocytes and tissue macrophages with increased metabolic requirements (Pathway E). The accumulation of ^{18}FDG in cells with increased glucose metabolism is specific. However, ^{18}FDG is taken up also by e.g. tumour cells. So, accumulation of ^{18}FDG is not specific for infection and inflammation processes as such.

Characteristics of the ideal conditions for infection imaging
A lot of radiopharmaceuticals for the diagnosis of infection have been developed in the last decades, each with its own advantages and disadvantages. Criteria for the ideal radiotracer are summarised in Table 2. It will be clear that there exists no radiopharmaceutical that meets all these criteria in a perfect way. In clinical practice the choice of the imaging agent is based on careful examination of each individual case. Early diagnostic imaging is preferable but not always necessary as in the case of osteomyelitis or in infected bone/joint prostheses. A one-day protocol is favorable in cases of severe and acute illness like lung infections for example. Imaging with high radiation doses or the occurrence of minor transient side-effects after administration of the radiopharmaceutical is in general unfavorable and should be considered only when significant clinical benefit is to be expected.

Table 2. Criteria for an ideal radiotracer

- Efficient accumulation and good retention in inflammatory foci
- Rapid clearance from the background
- No accumulation in non-target organs
- No toxicity
- Early diagnostic imaging
- Ready availability and low cost
- Easy low-hazard preparation
- Differentiation between infection and non-microbial inflammation
- Low radiation burden

Developing new radiotracers

For the development of new infection imaging radiopharmaceuticals the following route can be designed. Once a potential new radiopharmaceutical has passed the laboratory level of synthesis, purification and quality control, in vitro and in vivo testing starts. In case the potential new radiotracer aims at binding to certain cell types in vivo (e.g. leukocytes, lymphocytes, bacteria), in vitro binding assays with the target cells can give an indication of the potential of the product. Target cells for binding studies can be isolated from the blood or cell lines can be generated bearing receptors from original cells by cDNA transfection techniques. Reproducibility of receptor binding assays is generally better using these cell cultures bearing the desired transfected receptors. In binding assays the affinity and specificity of the agent for the target cells can be determined.

Subsequently, the new radiotracer can be tested in one of the simple and easy to use animal models of infection. Mice or rats with soft tissue infections induced by S.aureus or E.coli can serve as a good model for these first explorations. Biodistribution data generated in such a model can give a first impression of the imaging potential of the new tracer and allow the first comparison with known agents (2,3). Data on accumulation in the target (%ID/g), target/non-target ratios, blood clearance and the primary route of clearance (hepatobiliary/renal) can be obtained.

The next and in most cases last step in preclinical testing will involve more advanced models of infection in animals of more closely related species like rabbits and dogs. High costs and strict legal regulations will in most cases impede the use of primates for these studies. Moreover, the new information that experiments in primates could reveal does not outweigh the investments in money and energy in general. Besides the soft tissue infection mentioned above, more complicated models of infection can be used, which are of more clinical relevance: colitis (4,5), osteomyelitis (6,7), endocarditis (8,9), meningitis (10,11) and respiratory tract infections (12,13). In many cases these models require more specialised skills and experience. The model of choice depends on the intended application of the new radiotracer. In the rabbit and dog model(s) a direct comparison between the new radiotracer and the 'gold standard' [111]In or ^{99m}Tc labelled purified granulocytes can be carried out.

Once a new radiotracer has successfully passed these stages of laboratory and preclinical research, the agent should be tested in clinical trials in patients suspected of infectious or inflammatory diseases.

Detection of infection by non-specific radiotracers

^{67}Ga-citrate

^{67}Ga-citrate is used in clinical practice in several pathological conditions, including infection and many skeletal disorders (14,15). ^{67}Ga-citrate binds, once injected in the circulation, to circulating transferrin. This complex extravasates at the site of infection due to the locally enhanced vascular permeability (16), and is partly bound there to lactoferrin excreted by leukocytes or to siderophores produced by microorganisms (17). The agent is excreted partly via the kidneys (especially during the first 24 hours after injection), and via the gastrointestinal tract. Physiological uptake of the radiolabel occurs in liver, bone, bone marrow and bowel. Although ^{67}Ga-citrate scintigraphy has high sensitivity for both acute and chronic infection and noninfectious inflammation (18), there are several shortcomings that limit its clinical application. The specificity of the technique is low, due to physiological bowel excretion and accumulation in malignant tissues and areas of bone modeling (19-21). In addition, the radiopharmaceutical has unfavourable imaging characteristics (long physical half-life and high energy gamma radiations), causing high radiation absorbed doses. Furthermore, optimal imaging often requires delayed recordings up to 72 hours. These unfavorable characteristics, in combination with the development of newer radiopharmaceuticals, have narrowed the clinical indication for gallium scintigraphy to certain conditions such as lung infections and chronic osteomyelitis (18,21).

Non-specific immunoglobulins

Initially it was hypothesized that human polyclonal immunoglobulin (HIG) was retained in infectious foci due to the interaction with Fc-γ receptors as expressed on infiltrating leukocytes (22). Later studies have shown that radiolabelled HIG accumulates in infectious foci by nonspecific extravasation due the locally enhanced vascular permeability (23).

For clinical use HIG has been labelled with ^{111}In as well as ^{99m}Tc. Both agents have slow blood clearance and physiological uptake in the liver, the spleen and the kidneys. The ^{99m}Tc-labelled preparation has the known ideal radiation characteristics, while the ^{111}In-labelled preparation allows imaging at time points beyond 24 h postinjection. ^{111}In or ^{99m}Tc-labelled HIG has been extensively tested in a large number of clinical studies. It has shown excellent performance in the localisation of musculoskeletal infection and inflammation (24). In addition, good results have been reported in pulmonary infection - particularly in immunocompromised patients – (25,26), and abdominal inflammation (27). In a comparative study, Dams et al. showed that ^{99m}Tc-HIG labelled with the Tc-99m chelator hydrazinonicotinamid (HYNIC), has in

vivo characteristics highly similar to those of ^{111}In-HIG, and in most cases can replace the ^{111}In-labelled compound (28). Poor sensitivity of radiolabelled HIG is found in the diagnosis of endocarditis and vascular lesions in general, due to long lasting high levels of circulating activity. A general limitation is the long time span between injection and final diagnosis (24-48 h).

Liposomes

Liposomes are spheres consisting of one ore more lipid bilayers surrounding an aqueous space. They were proposed as vehicles to image infection some 20 years ago, but the preparations used in those early years were cleared from the circulation very rapidly by the mononuclear/phagocyte system (MPS). However, if the surface of the liposomes is coated with a hydrophylic polymer such as polyethyleneglycol (PEG), they circumvent recognition by the MPS, leading to a prolonged residence time in the circulation and enhanced uptake in pathological sites by extravasation due to locally enhanced vascular permeability (29). Such stabilized PEG-liposomes can be labelled with ^{111}In-oxinate and with ^{99m}Tc using either HMPAO as an internal label or via HYNIC as an external chelator. Labelling is easy and takes only minutes (30). The first clinical evaluation showed good imaging of focal infection (31). In patients suspected of infectious or inflammatory disease, ^{99m}Tc-PEG-liposomes were directly compared to ^{111}In-IgG-scintigraphy. ^{99m}Tc-PEG-liposomes scintigraphy showed high sensitivity (94%) and specificity (89%). Visualization of muscuskeletal and abdominal pathology was better than with ^{111}In-IgG. Unfortunately, in another clinical study self-limiting side-effects were observed in three out of nine patients (32).

The avidin-biotin system

Avidins are a family of proteins present in the eggs of amphibians, reptiles and birds; streptavidin is a member of the same family. Avidin and streptavidin (MW 64-60 kDa) bind to biotin with extremely high affinity ($K_d = 10^{-15}$ M). Biotin is a compound of low molecular weight that can be radiolabelled. The avidin-biotin approach is based on the fact that avidin (or streptavidin) will non-specifically localise at sites of infection due to increased vascular permeability. Avidin (or streptavidin) is injected as a pretargeting agent, followed hours later by a second injection with radiolabelled biotin (33). Good diagnostic accuracy was demonstrated in a study of vascular infection (34) and of chronic osteomyelitis (35).

Limitations in the use of non-specific radiotracers to image infections

Infectious foci can be visualised with radiotracers without a specific interaction between the agent and a tissue component in the infectious focus, in a non-specific

process of localisation due to the locally enhanced vascular permeability. Extravasation of (macro)molecules via diffusion is a slow process. Prolonged high blood levels are needed to allow (sufficient) diffusion into the target tissue. However, high blood levels implicate relatively high background levels, especially in well-perfused tissues. Secondly, in chronic inflammation the vascular permeability tends to normalize. Furthermore, because nonspecific agents accumulate due to a common feature of infection and inflammation, these agents cannot distinguish between infection and inflammation. As a result, non-specific radiotracers are principally limited in their ability to detect (and discriminate between) infections and inflammations. In this ^{67}Ga-citrate, radiolabelled HIG, radiolabelled liposomes and the avidin-biotin approach face the same inherent limitations.

Detection of infection by specific radiotracers

As outlined in Table 1, different strategies in imaging infection using specific radiotracers can be employed. These agents will be presented in more detail. An overview of agents that are currently being developed for infection imaging is presented in Table 3.

Table 3. Overview of studies in infection imaging with new specific radiotracers (including [18]FDG).

Agent	Number of patients studied	Year of publication	Ref.
Antigranulocyte antibodies:			
Anti-NCA-95: BW 250/183	>300	1989-2000	42-48
Anti-CD66: LeukoScan®	>100	1994-2000	49-51
Anti-CD15: LeuTech®	>200	1996-2000	52-55
Chemotactic peptide analogs	preclinical	1991-1997	59-63
Interleukin-1ra	5	2000	66
Interleukin-2	>400	1999,2000	69-71
Interleukin-8	8	1996-2000	3,72-74
PF-4 derivative: P483H	30	1996,1999	75,76
Anti E-selectin antibodies	25	1996-1997	80,81
Ciprofloxacin: Infecton	>1000	1996-2000	82,83
Neutrophil defensins: HNP-1	preclinical	1998,1999	84,85
[18]FDG (PET)	>250	1996-2000	91-98

Detection of infection by direct labelling of leukocytes

Ex vivo labelled leukocytes
Radiolabelled autologous leukocytes have been developed in the seventies and eighties (36-38) and are still considered the "gold standard" nuclear medicine technique for infection and inflammation imaging. After intravenous administration, there is initial sequestration of the labelled leukocytes in the lungs with subsequent rapid clearance of the activity from the lungs. The radiolabel rapidly clears from the blood and in most cases there is high uptake in granulocytic infiltrates, while a substantial portion of the leukocytes (presumably the damaged cells) accumulate in the spleen. Thus, as a radiopharmaceutical, radiolabelled leukocytes are a specific indicator for leukocytic infiltration, but not for infection. McAfee et al. developed a technique to label autologous leukocytes with ^{111}In using oxinate as a chelate to transfer the radiolabel into the cell (36). Peters et al. developed a labelling technique using HMPAO, a lipophilic chelator, that allows efficient labelling of white blood cells with [99m]Tc (37). In contrast to ^{111}In-oxinate some of the ^{99m}Tc-HMPAO is released from the leukocytes after injection and subsequently excreted renally (within minutes) and hepatobiliary (after hours) (38). Due to the more optimal radiation characteristics ^{99m}Tc-labelled leukocytes have replaced ^{111}In-labelled leukocytes for most indications. For evaluation of kidney, bladder and gall bladder infections the use of leukocytes labelled with ^{111}In is preferred. The excellent performance of radiolabelled leukocytes for imaging infection and inflammation was demonstrated in a series of studies: for imaging infectious/inflammatory foci sensitivity exceeded 95% (38,39). There was some concern that more chronic infections could be missed with labelled leukocyte scans, because such infections generate a smaller granulocyte response than acute infections. However, a study in 155 patients showed that the sensitivity of labelled leukocytes for acute infections (90%) was not significantly different from the sensivity for detection chronic infections (86%) (40). With regard to diagnostic accuracy there is no need for a better imaging agent than labelled autologous leukocytes. However, the preparation of this radiopharmaceutical is laborious, requires specialized equipment and could be hazardous. Isolating and labelling a patient's white blood cells takes a trained technician approximately 3 hours. In addition, the need to handle potentially contaminated blood could lead to transmission of blood-born pathogens such as HIV and HBV (41).

Detection of infection by in vivo labelling of leukocytes
A gross division can be made in radiotracers that bind leukocytes by receptor-binding (relatively small molecules; MW < 20 kDa) and radiotracers that bind leukocytes by

antibody-antigen interaction (relatively large molecules). The antibodies range in molecular weight from 50 kDa (antibody fragments) via 150 kDa (IgG) to 900 kDa (IgM).

Antigranulocyte antibodies and antibody fragments

Ever since it became clear that radiolabelled autologous leukocytes could visualise infectious foci, investigators have tried to develop a method that would label leukocytes in the circulation or in the infectious foci. Instead of isolating the white blood cells from a patient and labelling the cells *ex vivo,* these methods aimed to label white blood cells in vivo. Labelling procedures are easier and do not require handling of potentially contaminated blood. The use of radiolabelled monoclonal antibodies against surface antigens as present on granulocytes was one of the first attempts to accomplish in vivo labelling of leukocytes. Several monoclonal antibodies reactive with antigens expressed on granulocytes (NCA, CD15, CD66 and CD67) have been developed. At least three anti-granulocyte antibodies have been tested for infection imaging: anti-NCA-95 IgG (BW250/183) (42-48), anti-NCA-90 Fab' (Immu-MN3, leukoscan®: anti-CD66) (49-51), and anti-SSEA-1 IgM (LeuTech®: anti-CD15) (52-55). Each of these anti-granulocyte antibodies labelled with ^{99m}Tc or ^{123}I allowed accurate delineation of infection.

It was soon realized that the in vivo behavior of these labelled anti-granulocyte antibody preparations, did not mimick the behavior of radiolabelled leukocytes. In general, blood clearance of the IgG preparations was much slower, giving a high background radioactivity that decreases slowly with time. For that reason the time interval between injection of the labelled antibodies and the acquisition of images is relatively long in order to get good target-background ratios. Furthermore, no initial lung entrapment was seen and splenic uptake was much lower, while the preparations based on antibody fragments (Fab, Fab') had a much higher renal excretion. Similarly, the IgM antibody had a much higher liver uptake as compared to the *ex vivo* labelled white blood cells. Becker et al. showed that less than 10% of the radiolabelled BW250/183 antibody as present in the blood was actually associated with granulocytes (42). These observations indicated that the anti-granulocyte antibody approach for infection imaging, although feasible did not represent a method to label white blood cells in vivo. It is now generally accepted that radiolabelled anti-granulocyte antibodies localise in infectious foci mainly by nonspecific extravasation due to the locally enhanced vascular permeability, and that binding of the antibody to infiltrated leukocytes in the inflamed tissue may contribute to the retention of the radiolabel in the focus. Perhaps an exception should be made for anti-SSEA-1 IgM (LeuTech®: anti-CD15) (52). This antibody recognizes CD-15 antigens on PMNs with high affinity

($K_d = 10^{-11}$M) and the in vivo PMN binding exceeds 50%, pointing towards more specific processes in infected tissue accumulation. Recently, a ^{99m}Tc-labelled anti-CD15 IgM monoclonal antibody has shown promising results in patients with equivocal appendicitis (53).

The anti-granulocyte antibody-based radiopharmaceuticals visualised infectious foci in patients with a sensitivity between 80 and 90% (56). ^{99m}Tc-BW250/183 scintigraphy was useful in the evaluation of vascular graft infection and prosthetic heart valve infection. Good results were also obtained in the evaluation of patients with inflammatory bowel disease (43,56), although the agent appeared to be less accurate compared to labelled leukocytes (45,46). Pulmonary infections - with the exception of lung abscesses - were not visualised. Peripheral bone infections were adequately visualised, but the sensitivity decreased in case the focus was located closer to the spine (50). Due to the relatively slow blood clearance of the agent, a 24-hour postinjection scan is generally necessary for correct localisation of the inflammatory focus. A major disadvantage of the murine monoclonal antibodies is that they may induce human antimouse antibodies (HAMA), which can result in altered biodistribution after subsequent injections (56,57). In this respect, the use of antibody fragments instead of the whole antibody seems to be more advantageous, since such fragments appeared to be less immunogenic (56). In addition, antibody fragments show faster blood clearance and may thus provide earlier diagnosis. The ^{99m}Tc-labelled antigranulocyte Fab'-fragment (Leukoscan®) has been registered in Europe as an infection imaging agent (49). Further clinical studies will help to define the utility of these new agents in clinical practice.

Chemotactic peptides

Like anti-granulocyte antibodies, peptides with high affinity for receptors expressed preferentially on granulocytes, could be suitable for targeting granulocytes in vivo. A wide variety of peptides that bind to receptors as expressed on white blood cells has been tested for the detection of infection. One of the first receptor-binding peptides that was tested for its ability to image infectious foci was the chemotactic peptide formyl-Met-Leu-Phe. This tripeptide that is N-terminally formylated, is a chemotactic factor produced by bacteria. It binds to receptors on granulocytes and monocytes with high affinity (K_d = 10-30 nM). The first work on this radiolabelled chemotactic peptide was reported almost twenty years ago. Zoghbi et al. and later McAfee et al. labelled f-Met-Leu-Phe and investigated its in vivo characteristics (58). They found that even low doses of peptide induced a transient granulocytopenia. In 1991, Fischman et al. described the synthesis of four DTPA-derivatized chemotactic peptide analogs and their labelling with ^{111}In (59). All peptides maintained biologic activity and receptor binding affinity. The

peptides were tested in rats with *Escherichia coli* infections. All analogs showed preferential localisation in the focal infection within one hour after injection. In a comparative study in rabbits with *E. coli* infections, it was demonstrated that localisation of infection using ^{99m}Tc-labelled f-Met-Leu-Phe was superior to that of ^{111}In-labelled leukocytes (60). However, although a high specific activity ^{99m}Tc-labelling method was applied, a peptide dose as low as 10 ng/kg still had an effect on the peripheral leukocyte counts (61). Several antagonists were developed to circumvent this undesirable biologic activity of the radiolabelled chemotactic peptide. However, these antagonists had lower uptake in the infectious focus, most likely due to reduced affinity for the receptor (62,63). In summary, rapid imaging of infection and inflammation is feasible with radiolabelled chemotactic peptides, however, the undesired biologic side-effects of these peptides seem to impede further clinical development.

Cytokines

Labelled cytokines are an interesting class of protein radiopharmaceuticals of small molecular weight (< 20 kDa). Cytokines act through an interaction with specific cell-surface receptors expressed on known cell populations. Binding affinities are usually high (nanomolar range). Cytokine receptors are expressed at low levels on non-excited cells, but their expression can be upregulated during activation.

Interleukin-1 (IL-1)

IL-1 binds receptors as expressed mainly on granulocytes, monocytes and lymphocytes, with high affinity. Studies in mice with focal *Staphylococcus aureus* infections showed specific uptake of radioiodinated IL-1 at the site of infection (2). Using IL-1 receptor blocking antibodies, it could be demonstrated that accumulation of the agent in the infectious foci was due to binding to the IL-1 type II receptor (64). Unfortunately, the biologic effects (e.g., hypotension, headache) of IL-1 even at very low doses (10 ng/kg) precluded clinical application of radiolabelled IL-1. Therefore, the naturally occurring IL-1 receptor antagonist (IL-1ra) was tested as an imaging agent. This equally-sized (17 kDa) protein binds IL-1 receptors with similar high affinity but lacks any biologic activity. In a comparative study in rabbits with focal *E. coli* infections, the abscess uptake of radioiodinated IL-1ra was half that of radioiodinated IL-1 (65). ^{123}I-IL-1ra was tested in patients with rheumatoid arthritis. In these patients, inflamed joints were nicely visualised, however, major retention of the radiolabel in the intestinal tract indicated that this agent can not be used to visualise infectious and inflammatory lesions in the abdomen (66).

Interleukin-2 (IL-2)

Chronic inflammation is characterized by infiltration of the target tissue by lymphocytes. These infiltrates have been successfully targeted with radiolabelled IL-2. The IL-2 is considered to bind specifically to IL-2 receptors as expressed on activated T-lymphocytes. In a study in an animal model of human autoimmune diabetes mellitus, Signore et al. showed that lymphocytic infiltration in the pancreas could be visualised with ^{123}I-labelled IL-2 between five and fifteen minutes after injection (67). A method was developed that allowed the preparation of a ^{99m}Tc-IL-2 preparation with a high specific activity (68). Studies in patients with chronic inflammatory conditions, including insulin-dependent diabetes, Hashimoto thyroiditis, Graves' disease, Crohn's disease, coeliac disease and other autoimmune diseases, demonstrated localisation of [123]I- or ^{99m}Tc-labelled IL-2 at the site of lymphocytic infiltration (69-71). These results suggest that radiolabelled IL-2 might be a suitable agent for in vivo targeting of mononuclear cell infiltration as present in autoimmune diseases.

Interleukin-8 (IL-8)

IL-8 is a small protein (8.5 kDa) belonging to the CXC subfamily of the chemokines, or chemotactic cytokines, in which the first two cysteine residues are separated by one aminoacid residue. IL-8 binds to receptors on neutrophils with high affinity (0.3 – 4 nM). Hay and collegues (72) studied the in vivo behaviour of radioiodinated IL-8 in a rat model with carrageenan-induced sterile inflammations. The uptake peaked at 1-3 hours after injection and declined thereafter. Target-to-background ratios remained relatively low. In a pilot study in 8 patients these investigators showed that a ^{123}I-IL-8 could visualise inflammatory foci (73). The labelling method appeared to have major effects on the in vivo biodistribution of radioiodinated IL-8. The scintigraphic imaging characteristics of IL-8 labelled via the Bolton-Hunter method were clearly superior to IL-8 labelled via the iodogen method, despite similar in vitro cell binding characteristics (3). In rabbits with focal *E. coli* infection, accumulation of ^{123}I-labelled IL-8 in the abscess was rapid and high. The specific activity of this IL-8 preparation was relatively low resulting in a transient drop of peripheral leukocyte counts to 45% after a dose of 25 µg/kg ^{123}I-IL-8, followed by a leukocytosis (170 % of preinjection level) during several hours. Recently, a ^{99m}Tc-labelled IL-8 preparation was developed using HYNIC as a chelator. In rabbits with *E. coli* infection, high abscess uptake of ^{99m}Tc-HYNIC-IL-8 and high abscess-background ratios were obtained compared to those using the radioiodinated preparation (74). The higher specific activity of the ^{99m}Tc-labelled IL-8 preparation ameliorates concerns about the influence on WBC counts.

Platelet Factor 4 (PF-4)

PF4 is like IL-8 a member of the CXC chemokines. PF4 binds the CXC type II (= IL-8 type B) receptors expressed on neutrophils and monocytes. PF4 has been called the "body's heparin neutralizing agent". At Diatide Inc. the peptide P483H was synthesized. This peptide contains the heparin-binding region of PF4 - complexed with heparin - and a lysine-rich sequence to facilitate rapid renal clearance. In a rabbit model of infection, ^{99m}Tc-P483H clearly delineated the infectious foci as early as 4 hours after injection. No systemic side effects were observed: the transient neutropenia observed with IL-8 and f-Met-Leu-Phe was not encountered after i.v. injection of P483H (75). ^{99m}Tc-P483H has been studied in patients to test its applicability as imaging agent for scintigraphic detection of infection and inflammation with fair results (82% sensitivity, 77% specificity) (76). However, in some patients excessive thyroid uptake was observed, suggesting the release of ^{99m}Tc from the agent in vivo.

Detection of infection by targeting adhesion molecules

Anti-E-selectin antibodies or anti-E-selectin F(ab')$_2$ fragments

E-selectin is an endothelial adhesion molecule exclusively expressed on the luminal surface of activated endothelial cells and capable of binding to leukocytes. Radiolabelled anti-E-selectin monoclonal antibodies (77) or anti-E-selectin F(ab')$_2$ fragments (78) have been successfully used to image arthritis and chronic inflammatory bowel disease (79-81). To overcome the possible induction of human anti-mouse antibodies, a bioengineered single-chain antibody construct has been developed.

Detection of infection by radiolabelled antibiotics

Ciprofloxacin (Infecton)

None of the agents discussed above can make a differential diagnosis between infection and inflammation as they accumulate in the focus due to a common feature of infection and inflammation. Ciprofloxacin, a fluoroquinolone antimicrobial agent, binds to the DNA gyrase enzyme present in all dividing bacteria, even to those resistant to ciprofloxacin. Fluoroquinolones are thought not to bind to dead bacteria nor to accumulate in non-microbial inflammatory processes such as Crohn's disease. It is claimed that with these ^{99m}Tc-labelled agents it is possible to discriminate between infection and sterile inflammation (82). First clinical studies in several centers so far show high accuracy in the detection of bacterial infection. Data on the efficacy of ^{99m}Tc-Infecton imaging in 90 patients with suspected infective disorders reveal a

sensitivity of 70% and a specificity of 93% (83). Since this agent is not taken up in bone marrow it could be very helpful in the evaluation of infection of orthopaedic prostheses.

Antimicrobial peptides

Neutrophil defensins (human neutrophil peptides, HNP) are stored in the granules of neutrophils. In addition to their direct antimicrobial activity, the peptides have chemo-attractive activity for various monocytes and lymphocytes. It has been hypothesized that their cationic charge facilitates binding of these peptides to various micro-organisms. HNP-1 was labelled with ^{99m}Tc using a direct method by reducing the disulfide bridges of the molecule. Using this agent in experimental thigh infections in mice abscess-to-background ratios were low and decreasing with time (84,85). In the peritoneal cavity of the infected mice, ^{99m}Tc-HNP-1 bound to bacteria rather than to leukocytes. However, this agent needs extensive optimisation and tailoring to become able to distinguish between bacterial infection and sterile inflammation.

Detection of infection by positron emission tomography (PET) using ^{18}FDG

The use of ^{18}F fluorodeoxyglucose positron emission tomography (FDG-PET) has become increasingly important for differentiating malignant from benign tumours, for tumour staging, and for evaluating treatment efficacy in cancer patients (86,87). As early as 1931, Warburg has demonstrated an increased glucose metabolism in malignant tumours in vitro (88). FDG accumulates quantitatively in malignant tumours in vivo mainly due to their increased glucose metabolism. However, during staging and follow-up of malignant tumours, false-positive findings occasionally occurred, mainly due to infectious or granulomatous processes (89). Ever since Tahara et al. first demonstrated high FDG uptake in human abdominal abscesses in 1989 (90), FDG has been reported to accumulate in various inflammatory processes. Infection imaging with FDG-PET is based on the fact that granulocytes and macrophages use glucose as an energy source. When activated through infection, metabolism and thus FDG-uptake increases. The usefulness of FDG-PET to image infections has recently been demonstrated in several patient studies (Table 3) (91-98). FDG-PET has been studied in a wide variety of infections, including lesions of baterial, tuberculous and fungal origins, soft tissue infections as well as bone infections. Sensitivities and specificities generally exceeded 90%. FDG-PET has been especially successful in cases of osteomyelitis (93,95-98). The high spatial resolution allows differentiation between osteomyelitis or inflammatory spondylitis and infection of the soft tissue surrounding the bone (97). High spatial resolution and rapid accumulation into infectious foci are significant advantages over conventional imaging techniques as labelled leukocytes.

However, the high degree of unspecificity due to uptake in any cell type with high glycolytic activity is a serious limitation of the use of FDG-PET for infection imaging. E.g., FDG-PET does not allow the discrimination between tumour lesions and inflammatory lesions. Depending on the clinical setting, this may restrict the usefulness of FDG-PET in the imaging of infection. Moreover, FDG uptake in infectious foci is affected by serum glucose levels and by conditions as diabetes mellitus. Cost is another issue. FDG-PET is a rather expensive imaging modality and prospective studies in various patient populations will have to show the cost-effectiveness of FDG-PET for imaging of inflammatory and infectious diseases.

Conclusion

In the third millennium we will face a gradual shift in the field of nuclear medicine from the basal (non-specific) and cumbersome, even hazardous techniques (radiolabelled leukocytes) to more intelligent approaches based on small agents binding their targets with high affinity. Classes of agents will be designed to specifically distinguish between infection and non-infectious inflammation and between acute and chronic processes. The advantages of ^{99m}Tc as radionuclide will be fully explored. Labelling with high specific activity will reduce doses to be used, so that undesirable agonistic activities will be non-existent. In a totally different approach, undesirable agonistic activities will be coped with by chemical modification of the agonist. Furthermore, ^{18}FDG-PET may prove to be as useful in the rapid detection and management of human infections, as it is for management of malignant diseases.

References

1. Roitt IM. *Essential immunology, 9th edn.* Oxford: Blackwell Scientific, 1997.
2. van der Laken CJ, Boerman OC, Oyen WJG, van de Ven MTP, Claessens RAMJ, van der Meer JWM, Corstens FHM. Specific targeting of infectious foci with radioiodinated human recombinant interleukin-1 in an experimental model. *Eur J Nucl Med* 1995;22:1249-1255.
3. van der Laken CJ, Boerman OC, Oyen WJG, van de Ven MTP, van der Meer JWM, Corstens FHM. Radiolabeled interleukin-8: scintigraphic detection of infection within a few hours. *J Nucl Med* 2000;41:463-469.
4. Rogler G, Andus T. Cytokines in inflammatory bowel disease. *World J Surg* 1998;22:382-389.
5. Neurath M, Fuss I, Strober W. TNBS-colitis. *Int Rev Immunol* 2000;19:51-62.
6. Smeltzer MS, Thomas JR, Hickmon SG, Skinner RA, Nelson CL, Griffith D, Parr TR Jr, Evans RP. Characterization of a rabbit model of staphylococcal osteomyelitis. *J Orthop Res* 1997;15:414-421.
7. Dams ET, Nijhof MW, Boerman OC, Laverman P, Storm G, Buma P, Lemmens JA, van der Meer JW, Corstens FH, Oyen WJ. Scintigraphic evaluation of experimental chronic osteomyelitis. *J Nucl Med* 2000;41:896-902.
8. Veltrop MH, Bancsi MJ, Bertina RM, Thompson J. Role of monocytes in experimental Staphylococcus aureus endocarditis. *Infect Immun* 2000;68:4818-4821.
9. Hershberger E, Coyle EA, Kaatz GW, Zervos MJ, Rybak MJ. Comparison of a rabbit model of bacterial endocarditis and an in vitro infection model with simulated endocardial vegetations. *Antimicrob Agents Chemother* 2000;44:1921-1924.
10. Koedel U, Pfister HW. Models of experimental bacterial meningitis. Role and limitations. *Infect Dis Clin North Am* 1999;13:549-577.
11. Sorensen KN, Sobel RA, Clemons KV, Pappagianis D, Stevens DA, Williams PL. Comparison of fluconazole and itraconazole in a rabbit model of coccidioidal meningitis. *Antimicrob Agents Chemother* 2000;44:1512-1517.
12. Dei-Cas E, Brun-Pascaud M, Bille-Hansen V, Allaert A, Aliouat EM. Animal models of pneumocystosis. *FEMS Immunol Med Microbiol* 1998;22:163-168.
13. Cere N, Polack B. Animal pneumocystosis: a model for man. *Vet Res* 1999;30:1-26.
14. Lavender JP, Lowe J, Barker JR, Burn JI, Chaudhri MA. Gallium 67 citrate scanning in neoplastic and inflammatory lesions. *Br J Radiol* 1971;44:361-366.
15. Staab EV, McCartney WH. Role of gallium-67 in inflammatory disease. *Semin Nucl Med* 1978;8:219-234.
16. Tsan MF. Mechanism of gallium-67 accumulation in inflammatory lesions. *J Nucl Med* 1985;26:88-92.
17. Weiner R. The role of transferrin and other receptors in the mechanism of 67Ga localization. *Int J Rad Appl Instrum B* 1990;17:141-149.
18. Palestro CJ. The current role of gallium imaging in infection. *Semin Nucl Med* 1994;24:128-141.
19. Perkins PJ. Early gallium-67 abdominal imaging: Pitfalls due to bowel activity. *Am J Roentgenol* 1981;136:1016-1017.
20. Bekerman C, Hoffer PB, Bitran JD. The role of gallium-67 in the clinical evaluation of cancer. *Semin Nucl Med* 1984;14:296-323.
21. Seabold JE, Nepola JV, Conrad GR, et al. Detection of osteomyelitis at fracture nonunion sites: comparison of two scintigraphic methods. *Am J Roentgenol* 1989;152:1021-1027.
22. Fischman AJ, Rubin RH, White JA, Locke E, Wilkinson RA, Nedelman M, Callahan RJ, Khaw BA, Strauss HW. Localization of Fc and Fab fragments of nonspecific polyclonal IgG at focal sites of inflammation. *J Nucl Med* 1990;31:1199-1205.
23. Fischman AJ, Fucello AJ, Pellegrino-Gensey JL, Geltofsky J, Yarmush ML, Rubin RH, Strauss HW. Effect of carbohydrate modification on the localization of human polyclonal IgG at focal sites of bacterial infection. *J Nucl Med* 1992;33:1378-1382.
24. Nijhof MW, Oyen WJ, van Kampen A, Claessens RA, van der Meer JW, Corstens FHM. Evaluation of infections of the locomotor system with indium-111-labelled human IgG scintigraphy. *J Nucl Med* 1997;38:1300-1305.
25. Oyen WJG, Claessens RAMJ, Raemaekers JMM, de Pauw BE, van der Meer JWM, Corstens FHM. Diagnosing infection in febrile granulocytopenic patients with indium-111 labeled human IgG. *J Clin Oncol* 1992;10:61-68.
26. Buscombe JR, Oyen WJG, Grant A, et al. Indium-111-labeled human polyclonal immunoglobulin: identifying focal infection in patients positive for human immunodeficiency virus (HIV). *J Nucl Med* 1993;34:1621-1625
27. Mairal L, Lima PD, Martin Comin J, et al. Simultaneous administration of ^{111}In-human immunoglobulin and ^{99m}Tc-HMPAO labelled leukocytes in inflammatory bowel disease. *Eur J Nucl Med* 1995;22:664-670.

28. Dams ET, Oyen WJ, Boerman OC, Claessens RA, Wymenga AB, van der Meer JW, Corstens FHM. Technetium-99m labeled to human immunoglobulin G through the nicotinyl hydrazine derivative: a clinical study. *J Nucl Med* 1998;39:119-1124.

29. Boerman OC, Storm G, Oyen WJG, van Bloois L, van der Meer JWM, Claessens RAMJ, Corstens FHM. Sterically stabilized liposomes labeled with ^{111}In to image focal infection in rats. *J. Nucl. Med.* 1995;36:1639-1644.

30. Laverman P, Dams ETM, Oyen WJG, Storm G, Koenders EB, Prevost R, van der Meer JWM, Corstens FHM, Boerman OC. A novel method to label liposomes with Tc-99m via the hydrazino nicotinyl derivative: a comparison with Tc-99m-HMPAO-labeled PEG-liposomes. *J Nucl Med* 1999;40: 192-197.

31. Dams ETM, Oyen WJG, Boerman OC, Laverman P, Meeuwis APM, Koenders EB, Buijs WCAM, Storm G, Bakker J, van der Meer JWM, Corstens FHM. Tc-99m-PEG-liposomes for the scintigraphic detection of infection and inflammation: Clinical evaluation. *J Nucl Med* 2000;41:622-30.

32. Brouwers AH, de Jong DJ, Dams ETM, et al. Tc-99m-PEG-Liposomes for the evaluation of colitis in Crohn's disease. *J Drug Targeting* 2000;8:225-233.

33. Hnatowich D, Virzi F, Rusckowski M. Investigation of avidin and biotin for imaging investigation. *J Nucl Med* 1987;28:1294-1302.

34. Samuel A, Paganelli G, Chiesa R et al. Detection of prosthetic vascular graft infection using avidin/indium-111-biotin scintigraphy. *J Nucl Med* 1996;37:55-61.

35. Rusckowski M, Paganelli, Hnatowich D et al. Imaging osteomyelitis with streptavidin and indium-111-labeled biotin. *J Nucl Med* 1996;37:1655-1662.

36. McAfee JG, Thakur ML. Survey of radioactive agents for the in vitro labeling of phagocytic leucocytes. I Soluble agents. II Particles. *J Nucl Med* 1976;17:480-492.

37. Peters AM, Danpure HJ, Osman S, et al. Preliminary clinical experience with 99mTc-hexamethylpropylene-amineoxime for labelling leucocytes and imaging infection. *Lancet* 1986;ii:945-949.

38. Peters AM. The utility of ^{99m}Tc-HMPAO-leukocytes for imaging infection. *Semin Nucl Med* 1994;24:110-127.

39. Datz FL. Indium-111-labeled leukocytes for the detection of infection: current status. *Semin Nucl Med* 1994;24:92-109.

40. Datz FL, Thorne DA . Effect of chronicity of infection on the sensitivity of the In-111-labeled leukocyte scan. *AJR Am J Roentgenol* 1986;147:809-812.

41. Lange JMA, Boucher CAB, Hollak CEM, Wiltink EH, Reiss P, van Royen EA, Roos M, Danner SA, Goudsmit J. Failure of zidovudine prophylaxis after accidental exposure to HIV-1. *N Eng J Med* 1990; 323:915-916.

42. Becker W, Borst U, Fischbach W, Paurka B, Schafer R, Borner W. Kinetic data of in vivo labelled granulocytes in humans with a murine Tc-99m-labelled monoclonal antibody. *Eur J Nucl Med* 1989;15:361-366.

43. Becker W, Saptogino A, Wolf F. The single late Tc-99m granulocyte antibody scan in inflammatory diseases. *Nucl Med Commun* 1992;13:186-192.

44. Schubiger PA, Hasler PH, Novak-Hofer I, Blauenstein P. Assessment of the binding properties of Granuloszint. *Eur J Nucl Med* 1989;15:605-608.

45. Papos M, Nagy F, Narai G, et al. Anti-granulocyte immunoscintigraphy and (99mTc)hexamethylpropylene-amine-oxime-labeled leukocyte scintigraphy in inflammatory bowel disease. *Dig Dis Sci* 1996;41:412-420 .

46. Segarra I, Roca M, Baliellas L, et al. Granulocyte specific monoclonal antibody technetium-99m-BW 250/183 and indium-111 oxine labelled leukocyte scintigraphy in inflammatory bowel disease. *Eur J Nucl Med* 1991;18:715-719.

47. Krause T, Reinhardt M, Nitzsche E, Moser E. Photopenic lesions in bone marrow scintigraphy using technetium-99m labeled antigranulocyte antibody without known tumour.*Nuklearmedizin* 1999;38:85-89.

48. Gyorke T, Duffek L, Bartfai K, Mako E, Karlinger K, Mester A, Tarjan Z. The role of nuclear medicine in inflammatory bowel disease. A review with experiences of aspecific bowel activity using immunoscintigraphy with 99mTc anti-granulocyte antibodies. *Eur J Radiol* 2000;35:183-192.

49. Becker W, Palestro CJ, Winship J, Feld T, Pinsky CM, Wolf F, Goldenberg DM. Rapid imaging of infections with a monoclonal antibody fragment (Leukoscan). *Clin Orthopeadics* 1996;329:263-272.

50. Becker W, Bair J, Behr T, et al. Detection of soft-tissue infections and osteomyelitis using a technetium-99m labelled anti granulocyte monoclonal antibody fragment. *J Nucl Med* 1994;35:1436-1443.

51. Gratz S, Raddatz D, Hagenah G, Behr TM, Meller J, Becker W. Tc99m-labelled antigranulocyte monoclonal antibody Fab' fragments (LeukoScan) versus echocardiography in subacute infective endocarditis. *Int J Cardiology* 2000 (in press).

52. Thakur ML, Marcus CS, Henneman P, Butler J, Sinow R, Diggles L, Minami C, Mason G, Klein S, Rhodes B. Imaging inflammatory diseases with neutrophil-specific technetium-99m-labeled monoclonal antibody anti-SSEA-1. *J Nucl Med* 1996;37:1789-1795.

53. Kipper SL, Rypins EB, Evans DG, Thakur ML, Smith TD, Rhodes B. Neutrophil-specific 99mTc-labeled anti-CD15 monoclonal antibody imaging for diagnosis of equivocal appendicitis. *J Nucl Med* 2000;41:449-455.

54. Gratz S, Behr T, Herrmann A, Dresing K, Tarditi L, Franceschini R, Rhodes B, Sturmer KM, Becker W. Intraindividual comparison of 99mTc-labelled anti-SSEA-1 antigranulocyte antibody and 99mTc-HMPAO labelled white blood cells for the imaging of infection. *Eur J Nucl Med* 1998;25:386-393.

55. Rypins EB, Kipper SL. Scintigraphic determination of equivocal appendicitis. *Am Surg* 2000;66:891-895.

56. Becker W, Goldenberg DM, Wolf F. The use of monoclonal antibodies and antibody fragments in the imaging of infectious lesions. *Semin Nucl Med* 1994;24:142-153.

57. Sakahara H, Reynolds JC, Carrasquillo JA, et al. In vitro complex formation and biodistribution of mouse antitumor monoclonal antibody in cancer patients. *J Nucl Med* 1989;30:1311-1317.

58. Zoghbi S, Thakur M, Gottschalk A. Selective cell labelling: a potential radioactive agent for labeling of human neutrophils. *J Nucl Med* 1981;22:32P.

59. Fischman AJ, Pike MC, Kroon D, Fucello AJ, Rexinger D, ten Kate C, Wilkinson R, Rubin RH, Strauss HW. Imaging focal sites of bacterial infection in rats with indium-111-labeled chemotactic peptid analogs. *J Nucl Med* 1991;32:483-491.

60. Babich JW, Graham W, Barrow SA, et al. Technetium-99m-labeled chemotactic peptides: comparison with indium-111-labeled white blood cells for localizing acute bacterial infection in the rabbit. *J Nucl Med* 1993;34:2176-2181.

61. Fischman AJ, Rauh D, Solomon H, et al. In vivo bioactivity and biodistribution of chemotactic peptide analogs in nonhuman primates. *J Nucl Med* 1993;34:2130-2134.

62. Pollak A, Goodbody AE, Ballinger JR, Duncan GS, Tran LL, Dunn-Dufault R, Meghji K, et al. Imaging inflammation with Tc-99m labelled chemotactic peptides: analogues with reduced neutropenia. *Nucl Med Commun* 1996;17:132-139.

63. Babich JW, Dong Q, Graham W, Barzana M, Ferrill K, Pike M, Fischman AJ. A novel high affinity chemotactic peptide antagonist for infection imaging. *J Nucl Med* 1997;38:268P.

64. van der Laken CJ, Boerman OC, Oyen WJG, van de Ven MTP, Chizzonite R, Corstens FHM, van der Meer JWM. Preferential localization of systemically administered radiolabeled interleukin-1α in experimental inflammation in mice by binding to the type II receptor. *J Clin Invest* 1997;100:2970-2976.

65. van der Laken CJ, Boerman OC, Oyen WJG, van de Ven MTP, van der Meer JWM, Corstens FHM. Imaging of infection in rabbits with radioiodinated interleukin-1 (α and β), its receptor antagonist and a chemotactic peptide: a comparative study. *Eur J Nucl Med* 1998;25:347-352.

66. Barrera P, van Der Laken CJ, Boerman OC, Oyen WJ, van De Ven MT, van Lent PL, van De Putte LB, Corstens FH. Radiolabelled interleukin-1 receptor antagonist for detection of synovitis in patients with rheumatoid arthritis. *Rheumatology* 2000;39:870-874.

67. Signore A, Chianelli M, Toscano A, et al. A radiopharmaceutical for imaging areas of lymphocytic infiltration, ^{123}I-interleukin-2 labeling procedure and animal studies. *Nucl Med Commun* 1992;13:713-722.

68. Chianelli M, Signore A, Fritzberg AR, Mather SJ. The development of technetium-99m-labelled interleukin-2: a new radiopharmaceutical for the in vivo detection of mononuclear cell infiltrates in immune-mediated diseases. *Nucl Med Biol* 1997;24:579-586.

69. Signore A. Interleukin-2 scintigraphy: An overview. *Nucl Med Commun* 1999;20:938.

70. Signore A, Chianelli M, Annovazzi A, Rossi M, Maiuri L, Greco M, Ronga G, Britton KE, Picarelli A. Imaging active lymphocytic infiltration in coeliac disease with iodine-123-interleukin-2 and the response to diet. *Eur J Nucl Med* 2000;27:18-24.

71. Signore A, Chianelli M, Annovazzi A, Bonanno E, Spagnoli LG, Pozzilli P, Pallone F, Biancone L. 123I-interleukin-2 scintigraphy for in vivo assessment of intestinal mononuclear cell infiltration in Crohn's disease. *J Nucl Med* 2000;41:242-249.

72. Hay RV, Skinner RS, Newman OC, Kunkel SL, Lyle LR, Shapiro B, Gross MD. Scintigraphy of acute inflammatory lesions in rats with radiolabelled recombinant human interleukin-8. *Nucl Med Commun* 1997;18:367-378.

73. Gross MD, Shapiro B, Skinner RS, Shreve P, Fig LM, Hay RV. Scintigraphy of osteomyelitis in man with human recombinant interleukin-8. *J Nucl Med* 1996;37:25P.

74. Rennen HJJM, Boerman OC, Oyen WJG, van der Laken CJ, Corstens FHM. Specific and rapid scintigraphic detection of infection with Tc-99m-labeled interleukin-8. *J Nucl Med* 2001 (in press).

75. Moyer BR, Vallabhajosula S, Lister-James J, Bush LR, Cyr JE, Snow DA, Bastidas D, Lipszyc H, Dean RT Technetium-99m-white blood cell-specific imaging agent developed from platelet factor 4 to detect infection. *J Nucl Med* 1996;37:673-679.

76. Palestro CJ, Tomas MB, Bhargava KK, Afriyie MO, Nicodemus CF, Lister-James J, Dean RT. Tc-99m P483H for imaging infection: phase 2 multicenter trial results. *J Nucl Med* 1999;40:15P.

77. Keelan E, Chapman P, Binns R, Peters A, Haskard D. Imaging vascular endothelial activation: An approach using radiolabeled monoclonal antibodies against the endothelial cell adhesion molecule E-selectin. *J Nucl Med* 1994;35:276-281.

78. Jamar F, Chapman PY, Harrison AA, Binns RM, Haskard DO, Peters AM. Inflammatory arthritis: imaging of endothelial cell activation with an In-111 labeled $F(ab')_2$ fragment of anti-E-selectin monoclonal antibody. *Radiology* 1995;194:843-850.

79. Bhatti M, Chapman P, Jamar F et al. Immunolocalization of active inflammatory bowel disease (IBD) using a monoclonal antibody against E-selectin. *J Nucl Med* 1996;37(suppl.5):114P.

80. Chapman PT, Jamar F, Keelan ET, Peters AM, Haskard DO. Use of a radiolabeled monoclonal antibody against E-selectin for imaging of endothelial activation in rheumatoid arthritis. *Arthritis Rheum* 1996;39:1371-1375.

81. Jamar F, Chapman PT, Manicourt DH, Glass DM, Haskard DO, Peters AM. A comparison between 111In-anti-E-selectin mAb and 99Tcm-labelled human non-specific immunoglobulin in radionuclide imaging of rheumatoid arthritis. *Br J Radiol* 1997;70:473-481.

82. Vinjamuri S, Hall AV, Solanki KK et al. Comparison of ^{99m}Tc Infecton imaging with radiolabelled white-cell imaging in the evaluation of bacterial infection. *Lancet* 1996;347:233-235.

83. Hall AV, Solanki KK, Vinjamuri S, Britton KE, Das SS. Evaluation of the efficacy of 99mTc-Infecton, a novel agent detecting sites of infection. *J Clin Pathol* 1998;51:215-219.

84. Welling MM, Hiemstra PS, van den Barselaar MT, Paulusma-Annema A, Nibbering PH, Pauwels EKJ, Calame W. Antibacterial Activity of Human Neutrophil Defensins in Experimental Infections in Mice Is Accompanied by Increased Leukocyte Accumulation. *J Clin Invest* 1998;102:1583-1590.

85. Welling MM, Nibbering PH, Paulusma-Annema A, Hiemstra PS, Pauwels EK, Calame W. Imaging of bacterial infections with 99mTc-labeled human neutrophil peptide-1. *J Nucl Med* 1999;40:2073-2080.

86. O'Doherty MJ. PET in oncology I--lung, breast, soft tissue sarcoma. *Nucl Med Commun* 2000;21:224-229.

87. Nunan TO, Hain SF. PET in oncology II--other tumours. *Nucl Med Commun* 2000;21:229-233.

88. Warburg O. *On the origin of cancer cells. The metabolism of tumors*. New York: Richard R. Smith; 1931:129-169.

89. Strauss LG. Fluorine-18 deoxyglucose and false-positive results: a major problem in the diagnostics of oncological patients. *Eur J Nucl Med* 1996;23:1409-1415.

90. Tahara T, Ichiya Y, Kuwabara Y, Otsuka M, Miyake Y, Gunasekera R, Masuda K. High (18F)-fluorodeoxyglucose uptake in abdominal abscesses: a PET study. *J Comput Assist Tomogr* 1989;13:829-831.

91. Ichiya Y, Kuwabara Y, Sasaki M, Yoshida T, Akashi Y, Murayama S, Nakamura K, Fukumura T, Masuda K. FDG-PET in infectious lesions: The detection and assessment of lesion activity. *Ann Nucl Med* 1996;10:185-191.

92. O'Doherty MJ, Barrington SF, Campbell M, Lowe J, Bradbeer CS. PET scanning and the human immunodeficiency virus-positive patient. *J Nucl Med* 1997;38:1575-1583.

93. Guhlmann A, Brecht-Krauss D, Suger G, Glatting G, Kotzerke J, Kinzl L, Reske SN. Chronic osteomyelitis: detection with FDG PET and correlation with histopathologic findings. *Radiology* 1998;206:749-754.

94. Sugawara Y, Braun DK, Kison PV, Russo JE, Zasadny KR, Wahl RL. Rapid detection of human infections with fluorine-18 fluorodeoxyglucose and positron emission tomography: preliminary results. *Eur J Nucl Med* 1998;25:1238-1243.

95. Guhlmann A, Brecht-Krauss D, Suger G, Glatting G, Kotzerke J, Kinzl L, Reske SN. Fluorine-18-FDG PET and technetium-99m antigranulocyte antibody scintigraphy in chronic osteomyelitis. *J Nucl Med* 1998;39:2145-2152.

96. Zhuang H, Duarte PS, Pourdehand M, Shnier D, Alavi A. Exclusion of chronic osteomyelitis with F-18 fluorodeoxyglucose positron emission tomographic imaging. *Clin Nucl Med* 2000;25:281-284.

97. Kalicke T, Schmitz A, Risse JH, Arens S, Keller E, Hansis M, Schmitt O, Biersack HJ, Grunwald F. Fluorine-18 fluorodeoxyglucose PET in infectious bone diseases: results of histologically confirmed cases. *Eur J Nucl Med* 2000;27:524-528.

98. Stumpe KD, Dazzi H, Schaffner A, von Schulthess GK. Infection imaging using whole-body FDG-PET. *Eur J Nucl Med* 2000;27:822-832.

Chapter 2

Labeling proteins with ^{99m}Tc via Hydrazinonicotinamide (HYNIC): Optimization of the conjugation reaction

Huub J.J.M. Rennen, Otto C. Boerman, Emile B. Koenders,
Wim J.G. Oyen, Frans H.M. Corstens

ABSTRACT

At present there is considerable interest in labeling peptides with Tc-99m for the development of target specific radiopharmaceuticals for imaging purposes. In the present study the conjugation of the bifunctional coupling agent succinimidyl-hydrazinonicotinamide (S-HYNIC) was studied and optimized in a series of peptides (MW 6.5 – 14.3 kDa).

Methods: Aprotinin (MW 6.5 kDa), cytochrome C (MW 12.4 kDa), α-lactalbumin (MW 14.2 kDa) and lysozyme (MW 14.3 kDa) were conjugated with S-HYNIC via the ε-aminogroups of their lysine-residues. The effects of molar conjugation ratio, reaction temperature, pH and protein concentration were studied. Reaction products were analyzed both with respect to the HYNIC-substitution ratio (spectrophotometrically) as well as to the labeling efficiency (SG-ITLC) and molecular size (FPLC). The effects of conjugation on biological activity were studied in three proteins binding to receptors on leukocytes: interleukin-8 (MW 8.5 kDa), interleukin-1α (MW 17 kDa) and interleukin-1 receptor antagonist (MW 17 kDa).

Results: The labeling efficiency of aprotinin, cytochrome c, α-lactalbumin and lysozyme conjugated under optimal conjugation conditions exceeded 90%. Specific activities obtained were up to 7.5 MBq/μg. Conjugation was most efficient at 0 ^{0}C (as compared to 20 and 40 ^{0}C), at pH 8.2 (as compared to 6.0, 7.2 and 9.5) and at protein concentrations $\geq$ 2.5 mg/ml. In general, efficiency increased with increasing molar conjugation ratio (protein-HYNIC-ratio 1:3 < 1:6 < 1:15 < 1:30). For the receptor binding proteins, biological activity was preserved only under mildest conjugation conditions. For each of these proteins an inverse relation between labeling efficiency and receptor binding capacity was found.

Conclusion: Labeling proteins with ^{99m}Tc using S-HYNIC is easy, rapid and efficient and preparations with high specific activity can be obtained. However, biological activity of proteins may be lost at high HYNIC-substitution ratios. With the proteins tested here a careful balancing of reaction conditions resulted in acceptable, be it suboptimal, labeling efficiencies and preservation of biological activity.

INTRODUCTION

Nowadays there is considerable interest in labeling proteins and peptides with ^{99m}Tc for the development of target specific imaging agents. Three main strategies for labeling proteins with ^{99m}Tc can be distinguished: (i) direct labeling, (ii) preformed chelate approach, and (iii) indirect labeling using a bifunctional coupling agent (BCA) (*1;2*). The direct labeling approach uses a reducing agent to convert the cystine disulfide bridges of a protein into free thiols, which are able to bind ^{99m}Tc in a very efficient way. However, this method applies only to proteins with disulfide bonds. More importantly, these bonds are often critical for maintaining the biological properties of the protein. In the preformed chelate approach first a complex of ^{99m}Tc with a bifunctional coupling agent (BCA) is formed. In a second step the ^{99m}Tc-BCA complex is conjugated to a protein. However, a two-step radiochemical synthesis is not very suitable for routine clinical applications. In the indirect labeling approach the BCA is attached first to a protein to form a BCA-protein conjugate. Secondly, the conjugate is labeled with ^{99m}Tc either directly by reduction of ^{99m}TcO$_4^-$ or indirectly by ligand exchange with an intermediate ^{99m}Tc-complex (such as ^{99m}Tc-glucoheptonate, ^{99m}Tc-diphosphonate or ^{99m}Tc-tricine). In general, the latter approach is easy to carry out and has a well-defined chemistry. Succinimidyl-hydrazinonicotinamide (S-HYNIC) as developed by Abrams and coworkers (*3*) appears to be an ideal BCA for ^{99m}Tc-labeling, because it allows rapid and efficient labeling of proteins. In addition, it can be used in relatively low concentrations. Thus, preparations can be produced with high specific activities. The S-HYNIC approach consists of a conjugation step and a labeling step. In the conjugation step S-HYNIC reacts with ε-amino groups of lysine-residues in the protein, resulting in a HYNIC-protein conjugate. This conjugate can be labeled with ^{99m}Tc in the second step. In our study, tricine (N-[Tris(hydroxymethyl)-methyl]glycine) was used as co-ligand. In the resulting ^{99m}Tc-HYNIC-protein complex the ^{99m}Tc species is coordinated by two tricine molecules and the terminal N-atom of the hydrazine-group of HYNIC (*4*).

The aim of the present study was to characterize and optimize the labeling of small-sized proteins using S-HYNIC. In our laboratory we develop and test new agents for scintigraphic imaging of infections (*5;6*). ^{99m}Tc-labeled small-sized proteins binding to leukocyte receptors are most attractive candidates in this, for leukocytes are abundantly present in the area of infection. Receptors for interleukin-1 and interleukin-8 are highly expressed on activated leukocytes. In this study we used three leukocyte receptor binding proteins: interleukin-8 (MW 8.5 kDa) binding to interleukin-8 receptors; interleukin-1α (MW 17 kDa) and interleukin-1 receptor antagonist (MW 17 kDa) both binding to interleukin-1 receptors. To study and optimize the conjugation of

S-HYNIC to proteins we selected four easily available proteins of similar molecular weight (6.5 – 14.3 kDa): Aprotinin, cytochrome c, α-lactalbumin and lysozyme. The effects of the six reaction parameters of the reaction were investigated: molar conjugation ratio S-HYNIC to protein, reaction temperature, S-HYNIC administration mode, pH, protein concentration and duration of the conjugation reaction. The effects of each of the parameters on HYNIC substitution ratio and on labeling efficiency were studied. Next, the three leukocyte receptor binding proteins were studied for effects of conjugation on labeling efficiency and receptor binding capacity.

MATERIALS AND METHODS

Seven proteins were selected for these studies. Four proteins were purchased from Sigma (St. Louis, MO): Aprotinin (from bovine lung, molecular weight (MW) 6.5 kDa); cytochrome c (from horse heart, MW 12.4 kDa), α-lactalbumin (from bovine milk, MW 14.2 kDa); lysozyme (from chicken egg white, MW 14.3 kDa). Human recombinant interleukin-8 (IL-8, MW 8.5 kDa), human recombinant interleukin-1α (IL-1α, MW 17 kDa) and interleukin-1 receptor antagonist (IL-1ra, MW 17 kDa) were kindly provided by Dr I. Lindley (Novartis, Vienna, Austria), Dr P.T. Lomedico (Hoffman-La Roche, Nutley, NJ) and Dr R.C. Thompson (Synergen, Boulder, CO), respectively. Succinimidyl-hydrazino-nicotinamide (S-HYNIC, MW 286 Da) was synthesized as described by Abrams et al. (*3*).

Conjugation of S-HYNIC to protein
The proteins were conjugated to S-HYNIC essentially as described by Abrams et al. (*3*). Briefly, in a 1.5 ml vial 10% (v/v) of buffer solution was added to the solution of the protein under investigation. Buffer solutions to adjust the pH of the protein solution were: 1.0 M NaAc pH 6.0, phosphate-buffered saline (PBS) in 10-fold concentration pH 7.2, 1.0 M NaHCO$_3$ pH 8.2 and 1.0 M Na$_2$CO$_3$/NaHCO$_3$ pH 9.5. Subsequently an excess of S-HYNIC in DMSO was added dropwise to the solution. Reactions with durations shorter than 60 minutes were stopped by addition of an excess of 1.0 M glycine (Merck, Darmstadt, Germany) in PBS. Finally, precooled PBS was added to all reaction mixtures. To remove excess unbound S-HYNIC the mixture was extensively dialyzed against PBS (0.1-0.5 ml dialysis cell 3.5 MWCO, Pierce, Rockford, IL). Dialyzed samples were stored at –20 ^{0}C. Six reaction parameters of the conjugation reaction were investigated:

- The amount of S-HYNIC added to the reaction mixture was varied: from a 1 to 1 molar ratio S-HYNIC to protein, to a 30-fold excess S-HYNIC;

- The S-HYNIC solution was added to the protein preparation either dropwise (1 drop per minute) or as a single bolus;
- The reaction temperature was varied: from 0°C to 40°C;
- The pH of the reaction was varied: from pH 6.0 to 9.5;
- The protein concentration was varied: from 0.5 mg/ml to 10 mg/ml;
- The reaction time was varied; from 3 minutes to 60 minutes.

The various conjugation reaction conditions are summarized in table 1 and 2. All conjugation reactions were performed on a microgram scale of 40 to 200 μg protein per reaction. The number of HYNICs incorporated in the HYNIC-protein conjugate was determined spectrophotometrically by converting the hydrazine group of HYNIC into a hydrazone using o-sulfonic benzaldehyde (*7*). In brief, samples of HYNIC-protein conjugate (10-20 μg) to be analyzed were diluted into 0.1 ml of o-sulfonic benzaldehyde (Aldrich, Zwijndrecht, Netherlands; 1 mg/ml, 0.1 M NaAc, pH 4.7). The reaction was incubated at room temperature in the dark overnight. Samples of unconjugated protein were taken as a negative control. The absorption of the hydrazone adduct was read at 343 nm. The hydrazine concentration was calculated using a molar extinction coefficient of $\varepsilon_{343nm} = 17000$ mol^{-1}.l.cm^{-1} for the adduct.

Technetium-99m labeling of HYNIC conjugated protein

Tricine-SnSO$_4$-kits were prepared containing 20 mg tricine (N-[Tris(hydroxymethyl)-methyl]glycine, Fluka, Buchs, Switzerland) and 0.01 mg SnSO$_4$ (Merck) in 0.2 ml PBS pH 7.0. Stannous sulphate dissolved in 2 M HCl was added to a solution of tricine in PBS and the pH was subsequently adjusted to 7.0 with 1.0 M NaOH. To a thawed protein-HYNIC vial (5 μg) a 0.2 ml tricine-SnSO$_4$-kit and 0.1-0.3 ml 20-30 MBq ^{99m}TcO$_4^-$ in saline were added. The mixture was then incubated at room temperature for 30 minutes.

The radiochemical purity was determined by instant thin-layer chromatography (ITLC) on ITLC-SG strips (Gelman Laboratories, Ann Arbor, MI) with 0.1 M citrate, pH 6.0, as the mobile phase.

Analytical FPLC was carried out on a Pharmacia (Roosendaal, Netherlands) Superdex 75 HR 10/30 column using 0.05 M phosphate buffer with 0.15 M NaCl, pH 7.0 as eluens.

Receptor binding assays

The receptor binding fraction (RBF) of the various ^{99m}Tc-HYNIC-IL-8, ^{99m}Tc-HYNIC-IL-1α and ^{99m}Tc-HYNIC-IL-1ra preparations was determined in receptor binding assays essentially as described by Lindmo et al. (*8*). First the radiolabeled conjugates were purified on a Sephadex G-25 column (PD-10; Pharmacia) with 0.5 % BSA in PBS as eluens in order to remove non protein-bound label.

For ^{99m}Tc-HYNIC-IL-8 a receptor binding assay with human leukocytes was used. Heparinized human whole blood (10 ml) was mixed with 2.5 ml 5% Dextran (Sigma). Following red blood cell sedimentation for 1 hr at room temperature, the blood free of red blood cells, was washed in incubation buffer (1 mM NaH_2PO_4, 5 mM Na_2HPO_4, 140 mM NaCl, 0.5 mM $MgCl_2$, 0.15 mM $CaCl_2$, 0.5% (w/v) BSA, pH 7.4) and centrifuged at 500xg for 20 min. The cell pellet was then resuspended in 7 ml incubation buffer and layered on 5 ml Ficoll-Hypaque (Pharmacia), followed by centrifugation at 500xg for 20 min. Contaminating erythrocytes were removed from the pellet, rich of polymorphonuclear cells (PMNs), by hypotonic lysis. The PMN pellet was washed once and subsequently resuspended in incubation buffer supplemented with 0.5% BSA. A series of serially diluted PMN suspension (0.5 - 8 x 10^6 PMN/ml) was incubated with 10,000 cpm of ^{99m}Tc-labeled IL-8. A duplicate of the lowest cell concentration was incubated in the presence of a 100-fold molar excess of unlabeled IL-8 to correct for nonspecific binding. After 3 hr incubation at 4 ^{0}C, PMNs were centrifuged (5 min, 2000xg) and the radioactivity in the pellet (total bound activity) was measured in a shielded well-type gamma counter (Wizard; Pharmacia). The data were graphically analyzed in a modified Lineweaver-Burk plot: a double inverse plot of the conventional binding plot (specifically bound fraction versus cell concentration). The receptor-binding fraction at infinite cell excess was calculated by linear extrapolation to the ordinate.

The murine cell line EL-4-6.1, a variant subline of EL-4 thymoma cells (*9*), a kind gift of Dr H.R. MacDonald (Ludwig Institute for Cancer Research Epalinges, Switzerland), was used for determination of the receptor binding capacity of the ^{99m}Tc-HYNIC-IL-1α and ^{99m}Tc-HYNIC-IL-1ra preparations. The cell line was cultured at 37°C in a humidified atmosphere of air/CO_2 (95:5) in RPMI 1640 medium (GIBCO, Gaithersburg, MD) containing 10% fetal calf serum. Live EL-4-6.1 cells were washed once with cold medium. A series of serially diluted cell suspension (0.2-3 x 10^7 cells/ml) was incubated with 10,000 cpm of ^{99m}Tc-HYNIC-IL-1α or ^{99m}Tc-HYNIC-IL-1ra in assay buffer (RPMI 1640, 0.5% BSA, 0.05% NaN_3). A duplicate of the lowest cell concentration was incubated in the presence of at least a 100-fold molar excess of unlabeled IL-1α or IL-1ra to correct for non-specific binding. After 30 minutes incubation at 37°C, cells were centrifuged (5 min, 2000xg) and the radioactivity in the pellet (total bound radioactivity) was measured in a shielded well-type gamma counter (Wizard; Pharmacia). Data analysis was similar to that of the leukocyte receptor binding assay.

RESULTS

Optimization of the conjugation reaction: effects on HYNIC substitution and labeling efficiency

The number of HYNIC-groups incorporated in the HYNIC-protein conjugates as determined by the hydrazine assay and the labeling efficiencies of the ^{99m}Tc-labeled HYNIC-protein conjugates is presented in table 1 and figure 1. Labeling efficiencies of all proteins conjugated under optimal conjugation conditions exceeded 90%. Specific activities of up to 7.5 MBq/μg were obtained.

Table 1. *Schematic presentation of the reaction conditions of the conjugation reaction of S-HYNIC with four different proteins. For labeling experiments 5 μg of HYNIC-conjugated protein was labeled with 20-30 MBq ^{99m}Tc. The resulting HYNIC-substitution ratios and labeling efficiencies are presented.*

	Reaction conditions				Results							
	Conjugation ratio S-HYNIC:protein	S-HYNIC Admininistration Mode *	Reaction Temperature	Reaction pH	Protein Concentration	Substitution ratio HYNIC:protein				Labeling Efficiency %			
						Apr	**Cyt**	**Lac**	**Lys**	**Apr**	**Cyt**	**Lac**	**Lys**
1	**1 : 1**	d	20°C	8.2	5 mg/ml	0.1	0.3	0.4	0.1	49	70	79	26
2	**3 : 1**	d	20°C	8.2	5 mg/ml	0.9	1.0	0.6	0.6	76	89	88	58
3	**6 : 1**	d	20°C	8.2	5 mg/ml	1.5	1.8	2.0	0.9	86	92	84	78
4	**15 : 1**	d	20°C	8.2	5 mg/ml	2.0	2.2	4.6	2.3	94	91	88	90
5	**30 : 1**	d	20°C	8.2	5 mg/ml	3.6	3.9	7.8	2.4	83	88	92	85
6	6 : 1	d	**0°C**	8.2	5 mg/ml	1.9	1.8	2.4	1.4	87	92	85	81
=3	6 : 1	d	**20°C**	8.2	5 mg/ml	1.5	1.8	2.0	0.9	86	92	84	78
7	6 : 1	d	**40°C**	8.2	5 mg/ml	0.8	0.7	1.8	0.7	80	88	84	58
8	6 : 1	**b**	**0°C**	8.2	5 mg/ml	1.3	1.7	2.2	1.3	87	90	87	75
9	6 : 1	**b**	**20°C**	8.2	5 mg/ml	1.1	1.7	1.4	0.8	87	91	79	59
10	6 : 1	**b**	**40°C**	8.2	5 mg/ml	0.6	1.1	1.0	0.5	77	89	63	43
11	6 : 1	d	20°C	**6.0**	5 mg/ml	0.4	0.1	0.2	0.3	69	60	39	33
12	6 : 1	d	20°C	**7.2**	5 mg/ml	1.0	1.0	1.0	1.0	82	84	66	72
=3	6 : 1	d	20°C	**8.2**	5 mg/ml	1.5	1.8	2.0	0.9	86	92	84	78
13	6 : 1	d	20°C	**9.5**	5 mg/ml	1.2	1.0	2.1	0.5	86	80	72	45
14	6 : 1	d	20°C	8.2	**0.5 mg/ml**	0.1	0.1	0.1	0.0	10	25	17	10
15	6 : 1	d	20°C	8.2	**2.5 mg/ml**	0.9	1.1	2.1	0.7	84	75	30	58
=3	6 : 1	d	20°C	8.2	**5 mg/ml**	1.5	1.8	2.0	0.9	86	92	84	78
16	6 : 1	d	20°C	8.2	**10 mg/ml**	1.7	0.8	1.8	1.2	87	86	80	82

*Reaction time = 60 minutes. Apr: aprotinin; Cyt: cytochrome c; Lac: α-lactalbumin; Lys: lysozyme. * d = dropwise addition of 10 drops (1 drop/minute); b = addition as a single bolus.*

At increasing conjugation ratio HYNIC to protein an increasing number of HYNICs was conjugated per protein molecule (Fig. 1A). At increasing conjugation ratios labeling efficiency increased as well but stabilized at higher ratios (Fig. 1B). The FPLC patterns of labeled cytochrome c (Fig. 2A) showed higher molecular weight species appearing at increasing conjugation ratio. This formation was found for cytochrome c only; for aprotinin, α-lactalbumin and lysozyme higher conjugation ratios did not result in the formation of high molecular weight species (demonstrated for aprotinin in Fig. 2B). It should be noted that highest conjugation ratios (30:1) occasionally resulted in precipitation.

The reaction temperature clearly affected the HYNIC substitution ratio (Fig. 1C) and labeling efficiency (Fig. 1D): most efficient conjugation and highest labeling efficiency were obtained at 0^0C. Additionally, adding S-HYNIC to the protein as a single bolus appeared less effective than a dropwise addition (Fig. 1C, 1D).

At pH 6.0 conjugation and labeling was less efficient (Fig. 1E, 1F). Best results were obtained at pH 8.2 with each of the four proteins tested.

At lowest protein concentrations (0.5 mg/ml) hardly any HYNIC was conjugated to the protein and thus labeling efficiencies were very low (Fig. 1G, 1H). More efficient conjugation and subsequent labeling was obtained at higher concentrations ($\geq$2.5 mg/ml).

Optimization of the conjugation reaction: effects on biological activity

Table 2 summarizes the results of the conjugation reactions with three receptor binding proteins. Labeling of IL-8, IL-1α and IL-1ra was more efficient at higher molar conjugation ratios. At a fixed molar conjugation ratio a higher labeling efficiency was obtained with longer reaction times. The capacity of ^{99m}Tc-labeled IL-8, IL-1α and IL-1ra to bind their receptors on leukocytes (IL-8) or EL-4-6.1 cells (IL-1α and IL-1ra) was clearly affected by the conjugation reaction conditions. Milder conjugation conditions (low conjugation ratio S-HYNIC to protein and/or short reaction time) resulted in a higher receptor binding capacity. Increasing conjugation ratios and/or increasing reaction times resulted in higher labeling efficiency and a decrease of the receptor binding fraction. For each of the three proteins most optimal preparations were obtained when the protein was reacted five minutes at an 3:1 S-HYNIC:protein ratio. These conditions revealed preparations with a good receptor binding capacity ($\geq$65%) with a reasonable labeling efficiency (20-52%).
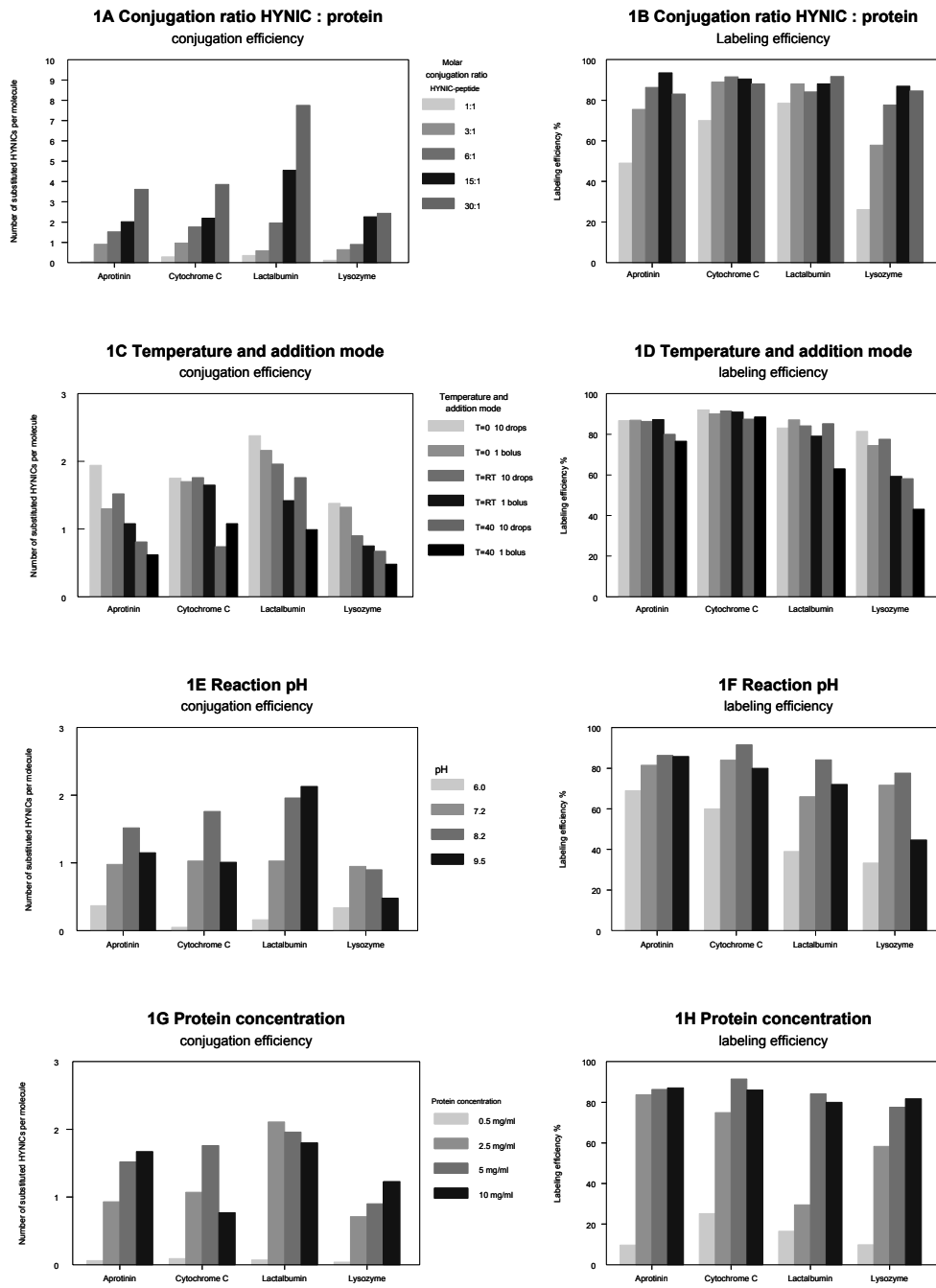
Figure 1. *Effects of varying reaction conditions of the conjugation reaction of S-HYNIC with 4 different proteins on: i) the number of substituted HYNIC-groups per molecule of protein conjugate; and ii) the labeling efficiency of the labeled protein conjugate. Data are taken directly from Table 1.*
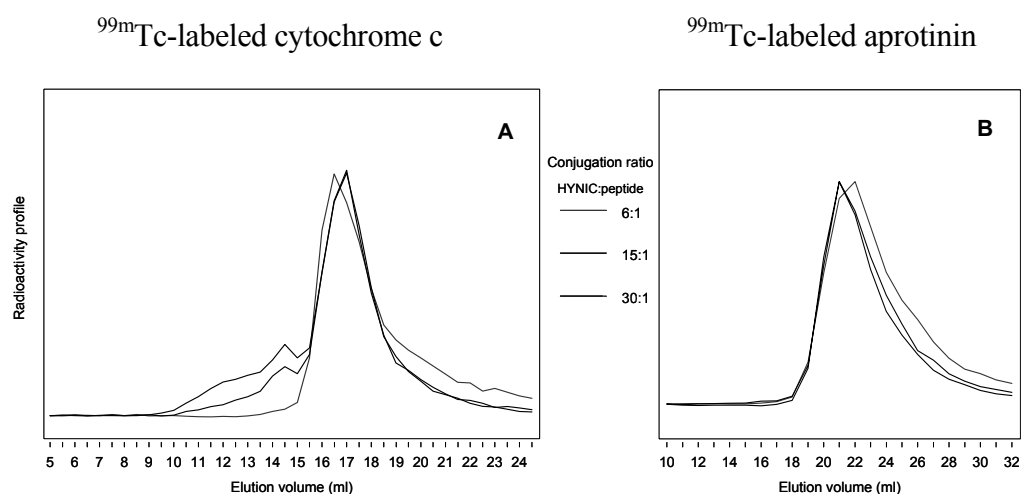
Figure 2. *HPLC radioactivity profiles of preparations ^{99m}Tc-labeled cytochrome c and aprotinin. Effect of increasing conjugation ratios S-HYNIC : protein.*

Table 2. *Schematic presentation of the reaction conditions of the conjugation reaction of S-HYNIC with interleukin-8 (IL-8), interleukin-1α (IL-1α) and interleukin-1 receptor antagonist (IL-1ra). For labeling experiments 5 μg of HYNIC-conjugated protein was labeled with 20-30 MBq ^{99m}Tc. The resulting labeling efficiencies and binding capacities to receptors on human granulocytes (IL-8) or EL-4-6.1 cells (IL-1α, IL-1ra) are presented.*

	Reaction conditions		Results					
	Conjugation ratio S-HYNIC:protein	Reaction Time	Labeling Efficiency			Receptor Binding Fraction		
			IL8	IL1α	IL1ra	IL8	IL1α	IL1ra
1	1 : 1	5 min.	15%	16%	24%	65%	98%	84%
2	1 : 1	60 min.	87%	44%	29%	31%	62%	71%
3	3 : 1	5 min.	20%	35%	52%	65%	70%	65%
4	3 : 1	10 min.	71%	43%	61%	37%	54%	56%
5	3 : 1	60 min.	95%	57%	83%	21%	54%	18%
6	10 : 1	60 min.	97%	82%	94%	16%	38%	17%

IL8: interleukin-8; IL1α: interleukin-1α; IL1ra: interleukin-1 receptorantagonist. S-HYNIC admininistration mode = dropwise; reaction temperature = 20°C; reaction pH = 8.2; protein concentration = 5 mg/ml.

DISCUSSION

The aim of this study was to characterize and optimize the conjugation of S-HYNIC to proteins in order to obtain a conjugate that could be labeled efficiently with ^{99m}Tc. In addition, the effects of conjugation on receptor binding capacity of proteins were studied for three proteins. The effects of six conjugation reaction parameters on HYNIC substitution and labeling efficiency were investigated. Higher conjugation ratios S-HYNIC to protein resulted in increasing efficiency on the one hand, but could lead to the formation of higher molecular weight aggregates and even to precipitation. The influence of the conjugation ratio on the number of introduced HYNIC-groups per protein molecule has been investigated in earlier studies for larger proteins like polyclonal IgG (MW 150 kDa) (*10*) and for human serum albumin (HSA, MW 67 kDa) (*11*). A fourfold molar excess of S-HYNIC was required in order to incorporate one HYNIC-group per IgG-molecule or HSA-molecule at protein concentrations of 4.6 mg/ml (IgG) or 20 mg/ml (HSA). This is in line with our results with smaller proteins. Also, incorporation of more than ten HYNIC-groups per IgG-molecule resulted in precipitation of the protein (*10*).

Conjugation of small proteins was most efficient at 0 ^{0}C as compared to 20 and 40 ^{0}C. This could be due to the fact that S-HYNIC can either be conjugated to the protein or be hydrolysed. Lower reaction temperatures might favor the conjugation reaction, while at higher temperatures hydrolysis dominates. The effect of reaction temperature on conjugation has not been reported so far. Conjugations are routinely carried out at room temperature (*3;10;11*).

It was found that a protein concentration of at least 2.5 mg/ml resulted in efficient conjugation and labeling. A low protein concentration of 0.5 mg/ml appeared to be too low for efficient conjugation. Protein concentrations as high as 50 mg/ml (*3*) and 20 mg/ml (*11*) have been reported. Schwartz et al. (*10*) varied IgG concentrations from 4.6 mg/ml up to 37 mg/ml. Increasing concentrations resulted in increasing efficiencies of the conjugation reaction. Our study with small proteins demonstrated no substantial gains at protein concentrations exceeding 5 mg/ml.

The effect of the duration of the reaction was studied with the leukocyte receptor binding proteins: longer reaction time resulted in higher labeling efficiency. The addition of an excess of glycine to stop the conjugation reaction was highly effective. The biological characteristics of IL-8, IL-1α and IL-1ra were clearly affected by the conjugation conditions. Preservation of receptor binding capacity was obtained only at low conjugation ratios and/or short reaction times. A possible explanation for the loss of receptor binding capacity might be that the most susceptible lysine ε-amino groups for reaction with S-HYNIC are not located in the receptor binding region of the

molecule. The results of our experiments in conjugating, labeling and receptor binding of IL-8, IL-1α and IL-1ra present a dilemma: optimal labeling efficiency can be obtained only at the expense of receptor binding. If, on the other hand, receptor binding is to be preserved, labeling efficiency will be lower. A careful balancing of reaction conditions will result in acceptable, be it suboptimal, labeling efficiencies and receptor binding.

In conclusion, labeling proteins with ^{99m}Tc using S-HYNIC is easy, rapid and efficient and preparations with high specific activity can be obtained. However, if biological activity has to be preserved, the conjugation conditions will need to be fine-tuned in case lysine-residues critical for biological activity are affected by conjugation with S-HYNIC.

REFERENCES

1. Hnatowich DJ. Recent developments in the radiolabeling of antibodies with iodine, indium, and technetium. *Semin Nucl Med.* 1990;20:80-91.
2. Srivastava SC, Mease RC. Progress in research on ligands, nuclides and techniques for labeling monoclonal antibodies. *Int J Rad Appl Instrum B.* 1991;18:589-603.
3. Abrams MJ, Juweid M, tenKate CI, Schwartz DA, Hauser MM, Gaul FE, Fuccello AJ, Rubin RH, Strauss HW, Fischman AJ. Technetium-99m-human polyclonal IgG radiolabeled via the hydrazino nicotinamide derivative for imaging focal sites of infection in rats. *J Nucl Med.* 1990;31:2022-2028.
4. Liu S, Edwards DS, Looby RJ, Harris AR, Poirier MJ, Barrett JA, Heminway SJ, Carroll TR. Labeling a hydrazino nicotinamide-modified cyclic IIb/IIIa receptor antagonist with 99mTc using aminocarboxylates as coligands. *Bioconjug Chem.* 1996;7:63-71.
5. van der Laken CJ, Boerman OC, Oyen WJ, van de Ven MT, Claessens RA, van der Meer JW, Corstens FH. Different behaviour of radioiodinated human recombinant interleukin-1 and its receptor antagonist in an animal model of infection. *Eur J Nucl Med.* 1996;23:1531-1535.
6. Rennen HJ, Boerman OC, Oyen WJ, van der Meer JW, Corstens FH. Specific and rapid scintigraphic detection of infection with 99mTc- labeled interleukin-8. *J Nucl Med.* 2001;42:117-123.
7. Bridger GJ, Abrams MJ, Padmanabhan S, Gaul F, Larsen S, Henson GW, Schwartz DA, Longley CB, Burton CA, Ultee ME. A comparison of cleavable and noncleavable hydrazinopyridine linkers for the 99mTc labeling of Fab' monoclonal antibody fragments. *Bioconjug Chem.* 1996;7:255-264.
8. Lindmo T, Boven E, Cuttitta F, Fedorko J, Bunn PA, Jr. Determination of the immunoreactive fraction of radiolabeled monoclonal antibodies by linear extrapolation to binding at infinite antigen excess. *J Immunol Methods.* 1984;72:77-89.
9. Zubler RH, Erard F, Lees RK, Van Laer M, Mingari C, Moretta L, MacDonald HR. Mutant EL-4 thymoma cells polyclonally activate murine and human B cells via direct cell interaction. *J Immunol.* 1985;134:3662-3668.
10. Schwartz DA, Abrams MJ, Hauser MM, Gaul FE, Larsen SK, Rauh D, Zubieta JA. Preparation of hydrazino-modified proteins and their use for the synthesis of 99mTc-protein conjugates. *Bioconjug Chem.* 1991;2:333-336.
11. Verbeke K, Hjelstuen O, Debrock E, Cleynhens B, De Roo M, Verbruggen A. Comparative evaluation of 99Tcm-Hynic-HSA and 99Tcm-MAG3-HSA as possible blood pool agents. *Nucl Med Commun.* 1995;16:942-957.

Chapter 3

The effect of molecular weight on nonspecific accumulation of ^{99m}Tc-labeled proteins in inflammatory foci

Huub J.J.M. Rennen, Jacek Makarewicz, Wim J.G. Oyen,
Peter Laverman, Frans H.M. Corstens, Otto C. Boerman

ABSTRACT

Although several proteins have been proposed and tested for scintigraphic detection of infection, the most optimal characteristics of a protein for this application have not yet been determined. Molecular weight (MW) of the protein, its charge, shape, carbohydrate content, characteristics of the radionuclide and receptor interactions are factors that could affect the in vivo behavior of the infection imaging agent. The effect of molecular weight on nonspecific accumulation of ^{99m}Tc-labeled proteins in inflammatory foci was studied in a rat model.

Methods: Eleven proteins whose MWs ranged from 2.5 kDa up to 800 kDa were labeled with ^{99m}Tc using the hydrazinonicotinamide (HYNIC) chelator. Rats with *S. aureus* infection were injected i.v. with 15 MBq ^{99m}Tc-labeled protein. Gamma camera images were acquired and biodistribution of the radiolabel was determined *ex vivo*.

Results: From biodistribution data no significant correlation was found between abscess uptake and molecular size of the ^{99m}Tc-labeled proteins that were studied. Fast blood clearance with predominant uptake in liver and spleen was found for the largest proteins (MW 669 kDa - 800 kDA). For proteins of intermediate size (MW 66 kDa – 206 kDa) we found relatively slow blood clearance with relatively moderate uptake in liver and spleen. For smaller proteins (MW 2.5 kDa – 29 kDa) rapid blood clearance with predominant kidney uptake was observed. The abscess uptake of the ^{99m}Tc-labeled proteins (%ID/g, 24 h p.i.) was highest for serum proteins IgG and BSA. Abscess uptake correlated well with blood levels: r=0.95 and 0.84 at 4 and 24 h respectively (P<0.005). The abscess-to-muscle ratios varied from 2.1 to 17.8 at 24 h p.i. with highest values for α-2 macroglobulin (MW 725 kDa) and the intermediate sized proteins (MW 66-206 kDa). Gamma camera imaging showed localization of all radiotracers at the site of infection with abscess-to-background ratios (A/B) ranging from 1.4 to 7.0 (IgG) at 20 h p.i. The serum proteins IgG and BSA showed highest blood levels and best infection imaging characteristics.

Conclusion: Not molecular weight but blood residence time is the principal factor that determines localization of a nonspecific tracer protein in infectious foci. The ideal nonspecific infection imaging agent is a protein with a long circulatory half-life. From the proteins tested here IgG and albumin showed the best characteristics for an infection imaging agent.

INTRODUCTION

Localization of radiolabeled proteins in infectious and inflammatory foci is driven by specific and/or nonspecific interactions. At present, multiple new agents are under study for infection imaging and the main interest is focussed on proteins that are easy to prepare and bind specifically to receptors or antigens present in inflammatory foci (*1-5*). Small molecules, like chemotactic peptides, have been shown to localize rapidly in infectious foci, but their absolute uptake in infectious foci is low (*6*). In addition, these molecules are biologically active and can evoke undesirable side-effects. Therefore, biologically inert compounds have some advantages. It is now well established that the preferential localization of proteins without specific receptor interaction in infectious and inflammatory foci is mainly the result of locally enhanced vascular permeability (*7-9*). Such proteins, labeled with In-111 or Tc-99m have been applied successfully for the scintigraphic detection of infection and inflammation (*10-12*).

In this study we focussed on radiolabeled proteins with no known interaction with receptors at the site of infection. The most optimal characteristics of these proteins for infection imaging have not yet been determined. Molecular weight (MW) of the protein involved, pI (*13;14*), shape (*15*), carbohydrate content (*16;17*) and characteristics of the chelating system and radionuclide (*18*) are factors that could affect the *in vivo* behavior of the infection imaging agent.

We studied the effect of molecular weight on nonspecific accumulation of ^{99m}Tc-labeled proteins in inflammatory foci in a rat model of infection. To our knowledge, this has not been studied systematically yet. Eleven ^{99m}Tc-labeled proteins in a broad MW range from 2.5 kDa up to 800 kDa were tested. In order to eliminate the effect of glycosylation, a series of nonglycosylated proteins was selected for these studies. The pI values of these proteins ranged from 4.5 to 7.2. Polyclonal human IgG, a clinically used infection imaging agent, was included in the study as a reference.

MATERIALS AND METHODS

Radiopharmaceuticals

Eleven proteins and peptides were selected for these studies. All proteins were obtained from Sigma Chemical Company (St. Louis, Mo) unless stated otherwise: α-crystallin molecular weight (MW) 800 kDa (a kind gift of Prof. Dr. W.W. de Jong, Dept of Biochemistry, University Hospital Nijmegen, The Netherlands), α-2 macro-globulin MW 725 kDa (ICN, Costa Mesa, CA), thyroglobulin MW 669 kDa, amylase

(sweet potatoes) MW 206 kDa, aldolase (rabbit muscle) MW 158 kDa (Boehringer, Mannheim, Germany), human polyclonal immunoglobulin G (IgG) MW 150 kDa (Baxter/Hyland Gammagard S/D, Lessines, Belgium), phosphorylase b (rabbit muscle) MW 97 kDa, bovine serum albumin (BSA) MW 66 kDa, carbonic anhydrase MW 29 kDa, myoglobin MW 17 kDa and insulin-A-chain MW 2.5 kDa. None of these proteins (with the possible exception of IgG) has any known specific interaction at the site of infection. To exclude the effects of carbohydrate groups, only non-glycosylated proteins were selected for these studies. The proteins had pI-values ranging from 4.5 to 7.2.

The proteins were conjugated with S-HYNIC, essentially as described by Abrams et al. (*19*). Briefly; a 3-60 fold molar excess of freshly dissolved succinimidyl 6-hydrazino nicotinate hydrochloride (in dry DMSO) was added dropwise to a solution of each protein (5-10 mg/ml in 0.1 M NaHCO$_3$ buffer, pH 8.2) under constant stirring. The added volume did not exceed 10% of the total reaction volume. The solution was incubated for 30 min at room temperature, protected from light. The reaction was stopped by adding 100 µl of precooled phosphate buffered saline (PBS), pH 7.4 (4°C). Following extensive dialysis (Slide-A-Lyser Cassette; molecular weight cut-off 3.5 kDa, Pierce, Rockford, IL) against PBS (overnight, 4°C, protected from light, four buffer changes) the mixture was diluted with PBS to a final concentration of 1 mg/ml, divided into 0.2 – 1 ml aliquots and stored at -20°C.

For ^{99m}Tc-labeling of HYNIC conjugated proteins, tricine (N-[Tris(hydroxymethyl)-methyl]glycine, Fluka, Buchs, Switzerland) was used as co-ligand. Twenty milligrams of tricine and 10 µg of stannous chloride in 0.2 ml PBS were added to vials containing HYNIC-protein. Subsequently, ^{99m}TcO$_4^-$ was added and the mixture was incubated at room temperature for 15 min. Following the labeling reaction the reaction mixture was applied on a Sephadex G-25 column (PD-10; Pharmacia, Uppsala, Sweden) and eluted with 0.5% BSA in PBS to remove unbound ^{99m}Tc-pertechnetate.

Radiochemical purity and *in vitro* stability

The radiochemical purity of the preparations was determined by instant thin-layer chromatography (ITLC) on Gelman ITLC-SG strips (Gelman Laboratories, Ann Arbour, MI) with 0.15 M sodium citrate (pH 6.0) as mobile phase. In addition, samples of ^{99m}Tc-labeled proteins and peptides (except insulin A-chain) were analyzed by size exclusion FPLC using Biosep SEC S-3000 (300x7.8 mm, Phenomenex, Torrance, CA), Superdex 75 HR 10/30 (Pharmacia, Uppsala, Sweden) or Shodex Protein KW 802.5 (300x8 mm, Showa Denko, Japan) columns. ^{99m}Tc-HYNIC-insulin-

A-chain was analyzed on a reversed phase chromatography column (Zorbax Rx-C18, 250x4.6 mm, Atas, Veldhoven, The Netherlands).

The *in vitro* stability of the radiolabeled proteins was monitored in rat serum. A sample of 0.2 ml ^{99m}Tc-HYNIC-protein solution (15 MBq, 20-100 µg protein) was diluted 1:5 in rat serum and incubated for 4 hours at 37°C. After 1, 2 and 4 hours aliquots of the mixture were diluted 5x with PBS and analyzed by ITLC as described above.

Animal studies

Abscesses were induced under ether anaesthesia in male Wistar rats (weighing 200-240 g) by intramuscular injection of $2x10^9$ colony forming units of *Staphylococcus aureus* in 100 µl 50:50% suspension of autologous blood and saline in the left calf muscle. Twenty-four hours after inoculation of bacteria the radiolabeled proteins were injected via the tail vein (0.2 ml of solution, 15 MBq, 20-100 µg protein).

Biodistribution

Four and twenty-four hours after injection, groups of five animals were killed by carbon dioxide suffocation. Blood was collected by cardiac puncture. Samples of normal muscle, abscess, lung, spleen, kidney, liver and small intestine were dissected and weighed. The radioactivity in the tissues was measured in a shielded well-type gammacounter (Gamma-Wizard, Pharmacia LKB, Uppsala, Sweden). To correct for radioactive decay and permit calculation of the uptake of the radiopharmaceuticals in each organ as fraction of the injected dose, aliquots of the injected doses were counted simultaneously. The activity in the tissues was expressed as percentage of injected dose per gram of tissue.

Gamma camera imaging

Separate sets of three animals with *S. aureus* infection were injected with each of the ^{99m}Tc-labeled proteins (0.2 ml, 15 MBq, 20-100 µg per rat). Scintigraphic images of anaesthetized rats (oxygen/nitrous oxide/enflurane) were obtained with a Siemens Orbiter γ-camera connected to an ICON computer system (Siemens Inc., Hoffman Estates, IL). Rats were imaged immediately after injection and 1, 2, 4, 8 and 20 h p.i. All images were acquired with a LEAP-collimator and 15% symmetric window centered on the 140 keV ^{99m}Tc γ-radiation peak and stored in 256x256 matrix. Regions of interest were drawn over the infectious focus and a symmetrical region over the contralateral muscle. Abscess-to-background ratios were calculated.

Statistical analysis

The biodistribution and imaging data are presented as the mean ± SD. Correlation was tested using the nonparametric Spearman rank correlation test. r and P values were computed for biodistribution data at four and twenty-four hours post injection for every pair of the following variables: Activity in the infect as percentage of injected dose per gram of tissue (%ID/g), molecular weight of the radiolabeled protein, activity in the blood (%ID/g), kidney uptake (%ID/g) and liver uptake (%ID/g).

RESULTS

Radiopharmaceuticals

Radiochemical purity of all preparations exceeded 92%. FPLC analysis revealed monomeric radioactivity peaks concordant with protein peaks measured at 280 nm for all preparations except BSA which showed two peaks with approximately 11% of activity in a higher MW peak. All preparations were stable up to 4 h in rat serum as determined by ITLC. In no preparation the percentage of free pertechnetate during incubation increased by more than 2%.

Biodistribution

The biodistribution data of the ^{99m}Tc-HYNIC-proteins for liver, abscess, blood and kidneys at 4 and 24 h post injection are depicted in Figure 1. Relatively high hepatic uptake was observed with proteins of molecular weight greater than that of BSA, especially the very large proteins α-crystallin and thyroglobulin. Relatively high renal uptake was observed with proteins of molecular weight smaller than that of BSA. Proteins of intermediate size like aldolase, IgG, phosphorylase and BSA showed moderate hepatic and renal uptake.

^{99m}Tc-HYNIC-IgG had the highest abscess uptake (1.29 ± 0.13 and 1.39 ± 0.32 %ID/g at 4 and 24 h p.i. respectively). Abscess uptake of all other ^{99m}Tc-HYNIC-proteins (except aldolase) decreased from 4 to 24 hrs. There was no significant correlation between abscess uptake and MW within the agents studied. In contrast, there was a highly significant correlation between abscess uptake and blood level of tested proteins as illustrated in figure 2 (r=0.95 and 0.84 at 4 and 24 h, respectively; P<0.005). Significant correlation was found between muscle uptake and blood level at 4 h (r=0.76; P<0.01). No significant correlations were found between blood level and renal or hepatic uptake (P>0.05 at all time points). In addition, there was a highly significant correlation between MW and hepatic uptake (r=0.89 and 0.94 at 4 and 24 h; P<0.005) but no significant correlation between MW and renal uptake.
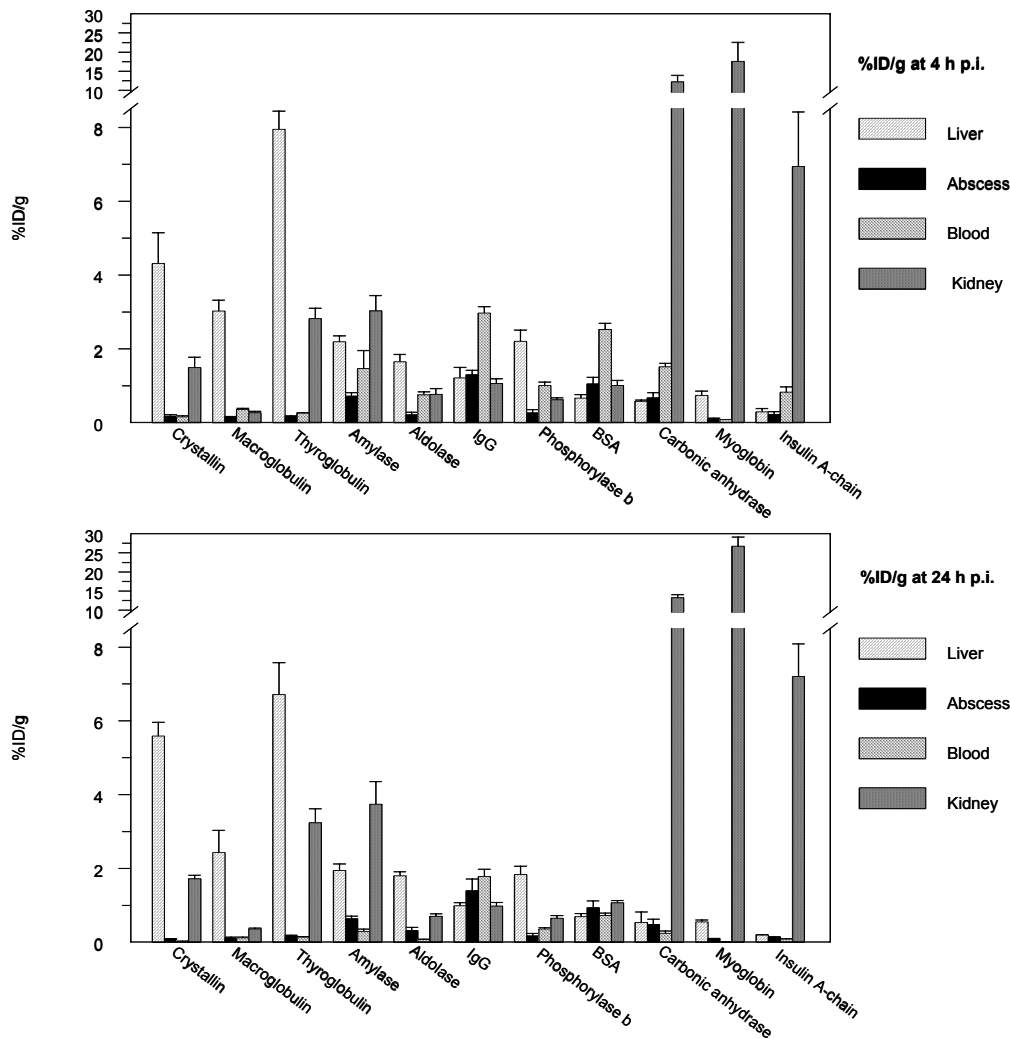
Figure 1. *Selected data from the biodistribution of* ^{99m}*Tc-labeled protein in rats with S. aureus infection at 4 and 24 h p.i. in diagram form (%ID/g, mean of 5 values per protein per time point, error bars indicate SD).*

Scintigraphy

The scintigraphic images obtained with each ^{99m}Tc-labeled protein at 20 h p.i. are shown in figure 3. Figure 4 presents data from quantitative analysis of the scintigraphic images of groups of three rats at 0, 1, 2, 4, 8 and 20 h p.i. The 20 h p.i. scintigrams show relatively high hepatic uptake for proteins of molecular weight ≥ 66 kDa. However, there is no linear relationship between molecular weight and hepatic uptake: for instance ^{99m}Tc-HYNIC-phosphorylase b (97 kDa) cleared predominantly via the hepatobiliary route whereas similarly sized proteins like IgG (150 kDa) and BSA (66 kDa) showed only moderate uptake in the liver. Proteins smaller than BSA showed high kidney uptake as is clearly demonstrated in the scintigrams of ^{99m}Tc-HYNIC-carbonic anhydrase, myoglobin and insulin-A-chain.
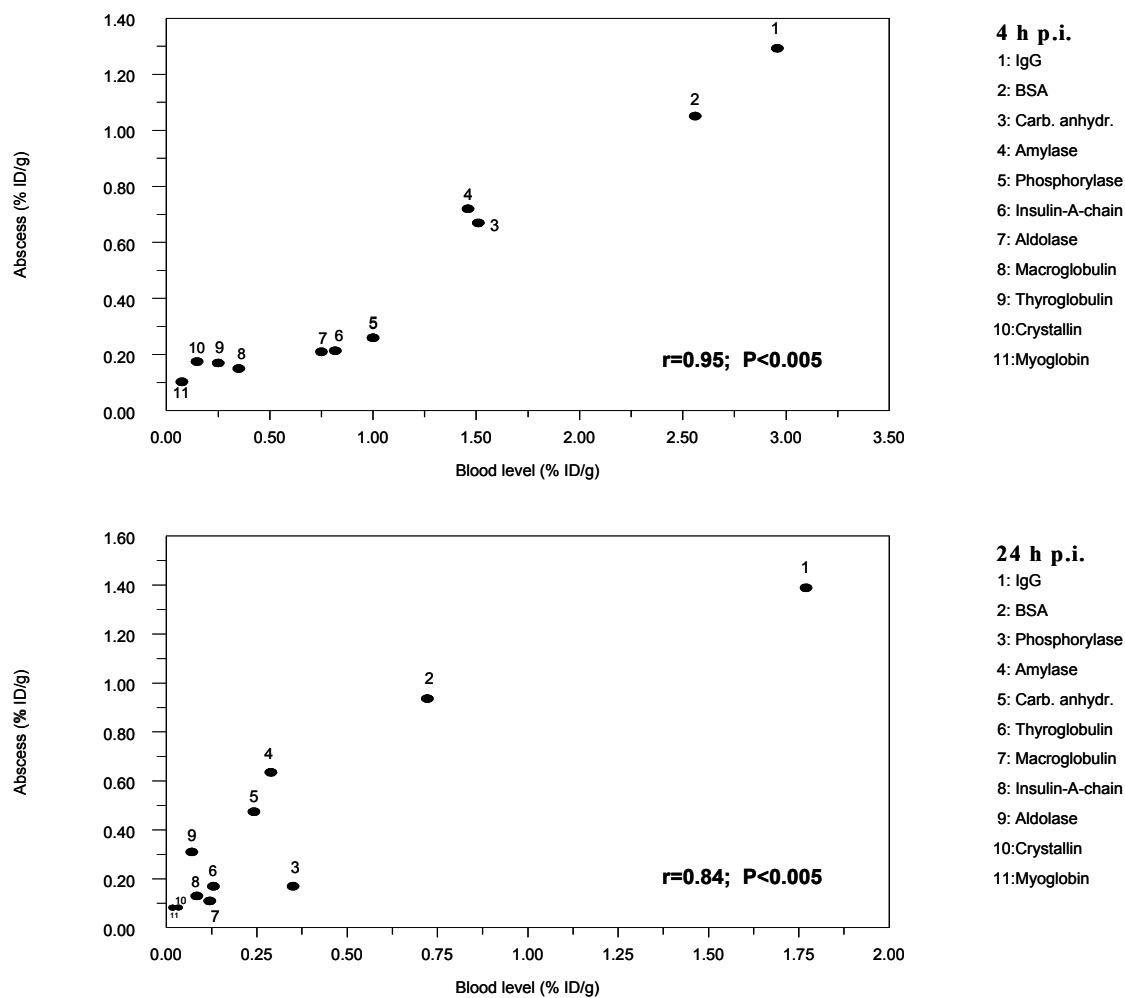
Figure 2. *Correlation between blood level (%ID/g) and abscess uptake (%ID/g) of* ^{99m}*Tc-labeled protein in rats with S. aureus infection at 4 and 24 h p.i.*

Inflammatory foci were well visualized with all proteins except ^{99m}Tc-HYNIC-α-crystallin, thyroglobulin, myoglobin and insulin-A-chain. Furthermore, the abscess visualization did not correlate with molecular weight: for instance ^{99m}Tc-HYNIC-α-crystallin, α-2-macroglobulin and thyroglobulin are proteins of similar weight; only α-2-macroglobulin showed good visualization of the abscess, whereas the other proteins did not. Quantitative analysis of the scintigrams revealed that particularly the small peptide ^{99m}Tc-HYNIC-insulin-A-chain cleared rapidly from the body (data not shown). Retention of the radiolabel at the site of infection increased with time for ^{99m}Tc-HYNIC-amylase, aldolase, IgG, phosporylase b, BSA and carbonic anhydrase. Highest percentage of residual activity retained in the abscess was obtained with ^{99m}Tc-HYNIC-IgG: up to $13.3 \pm 1.5\%$ of the whole body activity was found in the abscess at 20 h p.i.
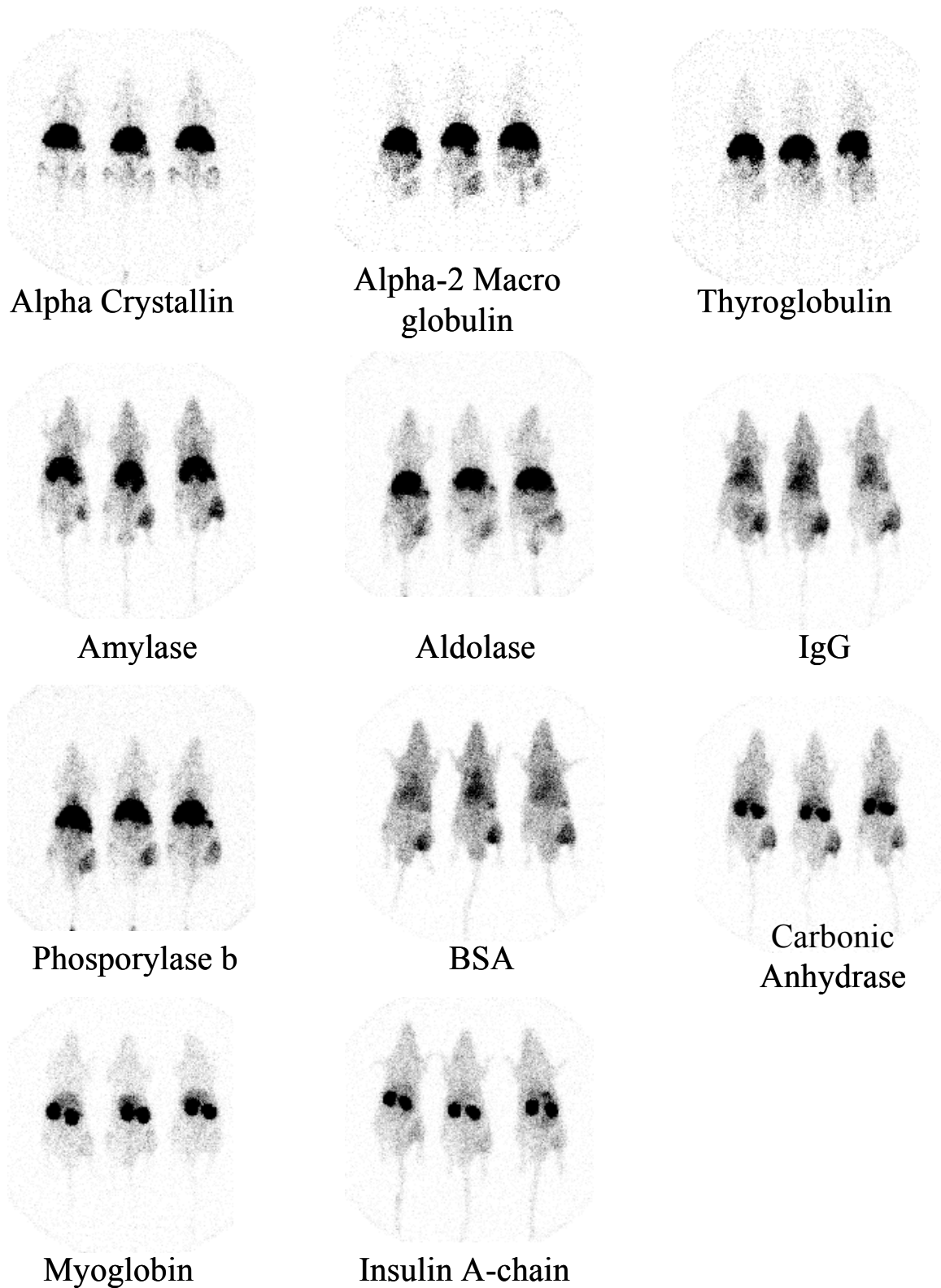
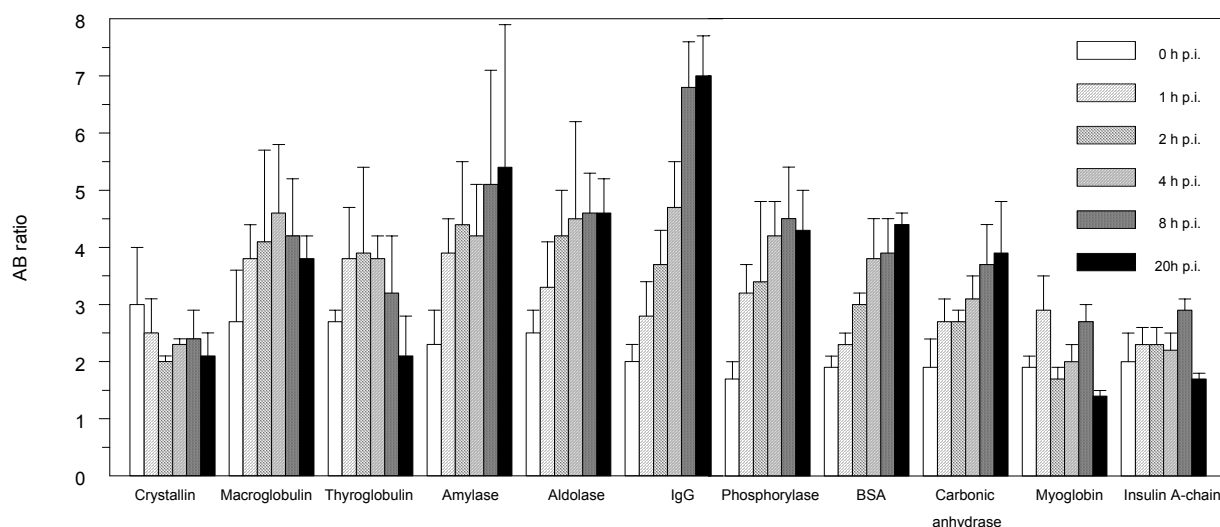**Figure 3.** *Images of rats with S. aureus infection at 20 h post injection of ^{99m}Tc-labeled protein*

Figure 4. *Abscess-to-background ratios as determined by quantitative analysis of the images of rats with S. aureus infection injected with* ^{99m}*Tc-labeled protein (mean of 3 values per protein per time point, error bars indicate SD).*

DISCUSSION

In the present study, the effect of molecular size of proteins with no known specific receptor interactions on accumulation in foci of acute inflammation was investigated. No significant correlation was found between abscess uptake and molecular size for the eleven ^{99m}Tc-labeled proteins in this study. Data from biodistribution and γ-camera imaging demonstrated fast blood clearance with predominant uptake in liver and spleen for the largest proteins in study (MW 669 kDa - 800 kDa). Proteins of intermediate size (MW 66 kDa – 206 kDa) had relatively slow blood clearance with relatively moderate uptake in liver and spleen. For smaller proteins (MW 2.5 kDa – 29 kDa) rapid blood clearance with predominant renal uptake was observed. Serum proteins IgG and BSA revealed the highest abscess uptake (%ID/g, 24 h p.i.). These proteins showed the best infection imaging characteristics. Interestingly, there was a highly significant correlation between abscess uptake and blood level. This finding suggests that the process of abscess accumulation of non receptor binding proteins is mainly driven by sustained blood levels. However, there was no significant correlation between molecular weight and circulatory half-life: for instance, IgG and aldolase have similar molecular weights (150, 158 kDa respectively), but IgG had much higher blood levels at both time points (4 and 24 h p.i.), whereas aldolase cleared from the blood very rapidly. There are similarities in blood clearance patterns of non-protein polymeric molecules as compared to those of the proteins presented here. Molecular weight dependent tissue accumulation has been systematically investigated for dextrans (*20*) and polyethyleneglycols (PEGs) (*21*). For PEGs it was found that the

circulatory half-life of PEG increased from 18 min to 1 day as the PEG MW increased from 6 to 190 kDa. Renal clearance decreased and hepatic clearance increased with increasing PEG MW. For dextrans in a MW range of 4 to 150 kDa, it was found that renal clearance decreased with increasing MW. However, hepatic clearance of dextrans showed a maximum for the 70 kDa species: a further increase in MW resulted in a decrease of liver uptake.

Whether IgG accumulates in infections in a specific or nonspecific way has been a matter of debate for a long time. Accumulation has been ascribed to a process of increased vascular permeability (nonspecific) (*7;8*), the chemical nature of the radiolabel (nonspecific) (*22;23*), binding to bacteria (*24*) and specific trapping of IgG by Fc-receptors on inflammatory cells (*25*). However, assignment of a major role for Fc-receptor binding was rejected later (*10;16;23*). The results reported in this study indicate that the superior characteristics of IgG for infection imaging are most likely due to a long circulatory half-life of the radiolabel and increased vascular permeability at the site of infection. The present results are in line with the hypothesis that accumulation of radiolabeled IgG is nonspecific due to nonspecific leakage through the leaky capillaries near infectious foci. The data in the present study suggest that no mechanisms including specific interactions are required to explain focal accumulation. The effect of blood retention time on abscess uptake of nonspecific agents was noticed already in studies with radiolabeled liposomes (*26*) and supposed to play a role in the accumulation of immunoglobulins at the site of infection (*12*).

In conclusion, molecular weight of a nonspecific tracer protein is not the principal determinant in targeting infections. Blood residence time has a more profound effect on abscess uptake of nonspecific tracers. The ideal nonspecific infection imaging agent is a protein with a long circulatory half-life. From the proteins tested here IgG and serum albumin showed the best characteristics for an infection imaging agent.

REFERENCES

1. Babich JW, Graham W, Barrow SA, Dragotakes SC, Tompkins RG, Rubin RH, Fischman AJ. Technetium-99m-labeled chemotactic peptides: comparison with indium-111-labeled white blood cells for localizing acute bacterial infection in the rabbit. J Nucl Med. 1993;34:2176-2181.
2. Becker W, Bair J, Behr T, Repp R, Streckenbach H, Beck H, Gramatzki M, Winship MJ, Goldenberg DM, Wolf F. Detection of soft-tissue infections and osteomyelitis using a technetium-99m-labeled anti-granulocyte monoclonal antibody fragment. J Nucl Med. 1994;35:1436-1443.
3. Hay RV, Skinner RS, Newman OC, Kunkel SL, Lyle LR, Shapiro B, Gross MD. Scintigraphy of acute inflammatory lesions in rats with radiolabelled recombinant human interleukin-8. Nucl Med Commun. 1997;18:367-378.
4. Signore A, Chianelli M, Toscano A, et al. A radiopharmaceutical for imaging areas of lymphocytic infiltration: 123I-interleukin-2. Labelling procedure and animal studies. Nucl Med Commun. 1992;13:713-722.

5. van der Laken CJ, Boerman OC, Oyen WJ, van de Ven MT, Claessens RA, van der Meer JW, Corstens FH. Specific targeting of infectious foci with radioiodinated human recombinant interleukin-1 in an experimental model. Eur J Nucl Med. 1995;22:1249-1255.

6. Fischman AJ, Pike MC, Kroon D, et al. Imaging focal sites of bacterial infection in rats with indium-111-labeled chemotactic peptide analogs. J Nucl Med. 1991;32:483-491.

7. Juweid M, Strauss HW, Yaoita H, Rubin RH, Fischman AJ. Accumulation of immunoglobulin G at focal sites of inflammation. Eur J Nucl Med. 1992;19:159-165.

8. Morrell EM, Tompkins RG, Fischman AJ, Wilkinson RA, Burke JF, Rubin RH, Strauss HW, Yarmush ML. Autoradiographic method for quantitation of radiolabeled proteins in tissues using indium-111. J Nucl Med. 1989;30:1538-1545.

9. Oyen WJ, Boerman OC, van der Laken CJ, Claessens RA, van der Meer JW, Corstens FH. The uptake mechanisms of inflammation- and infection-localizing agents. Eur J Nucl Med. 1996;23:459-465.

10. Oyen WJ, Claessens RA, Raemaekers JM, de Pauw BE, van der Meer JW, Corstens FH. Diagnosing infection in febrile granulocytopenic patients with indium-111-labeled human immunoglobulin G. J Clin Oncol. 1992;10:61-68.

11. Rubin RH, Fischman AJ, Needleman M, Wilkinson R, Callahan RJ, Khaw BA, Hansen WP, Kramer PB, Strauss HW. Radiolabeled, nonspecific, polyclonal human immunoglobulin in the detection of focal inflammation by scintigraphy: comparison with gallium-67 citrate and technetium-99m-labeled albumin. J Nucl Med. 1989;30:385-389.

12. Subramanian R, Vallabhajoshula S, Lipszyc H, Zhao Q, Murray J, Shaban S, Machac J, Hanna MG, Jr. Preclinical studies of indium-111-labeled IgM: a human monoclonal antibody for infection imaging. J Nucl Med. 1997;38:1054-1059.

13. ten Kate CI, Fischman AJ, Rubin RH, Fucello AJ, Riexinger D, Wilkinson RA, Du L, Khaw BA, Strauss HW. Effect of isoelectric point on biodistribution and inflammation: imaging with indium-111-labelled IgG. Eur J Nucl Med. 1990;17:305-309.

14. Welling M, Feitsma HI, Calame W, Ensing GJ, Goedemans W, Pauwels EK. Optimized localization of bacterial infections with technetium-99m labelled human immunoglobulin after protein charge selection. Eur J Nucl Med. 1994;21:1135-1140.

15. Lindstrom KE, Blom A, Johnsson E, Haraldsson B, Fries E. High glomerular permeability of bikunin despite similarity in charge and hydrodynamic size to serum albumin. Kidney Int. 1997;51:1053-1058.

16. Fischman AJ, Fucello AJ, Pellegrino-Gensey JL, Geltofsky J, Yarmush ML, Rubin RH, Strauss HW. Effect of carbohydrate modification on the localization of human polyclonal IgG at focal sites of bacterial infection. J Nucl Med. 1992;33:1378-1382.

17. Staud F, Nishikawa M, Takakura Y, Hashida M. Liver uptake and hepato-biliary transfer of galactosylated proteins in rats are determined by the extent of galactosylation. Biochim Biophys Acta. 1999;1427:183-192.

18. Verbeke K, Hjelstuen O, Debrock E, Cleynhens B, De Roo M, Verbruggen A. Comparative evaluation of 99Tcm-Hynic-HSA and 99Tcm-MAG3-HSA as possible blood pool agents. Nucl Med Commun. 1995;16:942-957.

19. Abrams MJ, Juweid M, tenKate CI, Schwartz DA, Hauser MM, Gaul FE, Fuccello AJ, Rubin RH, Strauss HW, Fischman AJ. Technetium-99m-human polyclonal IgG radiolabeled via the hydrazino nicotinamide derivative for imaging focal sites of infection in rats. J Nucl Med. 1990;31:2022-2028.

20. Mehvar R, Robinson MA, Reynolds JM. Molecular weight dependent tissue accumulation of dextrans: in vivo studies in rats. J Pharm Sci. 1994;83:1495-1499.

21. Yamaoka T, Tabata Y, Ikada Y. Distribution and tissue uptake of poly(ethylene glycol) with different molecular weights after intravenous administration to mice. J Pharm Sci. 1994;83:601-606.

22. Claessens RA, Koenders EB, Boerman OC, Oyen WJ, Borm GF, van der Meer JW, Corstens FH. Dissociation of indium from indium-111-labelled diethylene triamine penta-acetic acid conjugated non-specific polyclonal human immunoglobulin G in inflammatory foci. Eur J Nucl Med. 1995;22:212-219.

23. Oyen WJ, Claessens RA, van der Meer JW, Corstens FH. Biodistribution and kinetics of radiolabeled proteins in rats with focal infection. J Nucl Med. 1992;33:388-394.

24. Calame W, Feitsma HI, Ensing GJ, Arndt JW, van Furth R, Pauwels EK. Binding of 99mTc-labelled polyclonal human immunoglobulin to bacteria as a mechanism for scintigraphic detection of infection. Eur J Nucl Med. 1991;18:396-400.

25. Fischman AJ, Rubin RH, White JA, Locke E, Wilkinson RA, Nedelman M, Callahan RJ, Khaw BA, Strauss HW. Localization of Fc and Fab fragments of nonspecific polyclonal IgG at focal sites of inflammation. J Nucl Med. 1990;31:1199-1205.

26. Boerman OC, Oyen WJ, van Bloois L, Koenders EB, van der Meer JW, Corstens FH, Storm G. Optimization of technetium-99m-labeled PEG liposomes to image focal infection: effects of particle size and circulation time. J Nucl Med. 1997;38:489-493.

Chapter 4

Specific and rapid scintigraphic detection of infection with ^{99m}Tc-labeled interleukin-8

Huub J.J.M. Rennen, Otto C. Boerman, Wim J.G. Oyen,
Jos W.M. van der Meer, Frans H.M. Corstens

ABSTRACT

Interleukin-8 (IL-8) is a chemotactic cytokine involved in activation and recruitment of neutrophils to areas of infection. In our previous studies in rabbits we tested ^{123}I-labeled IL-8 for its potential to image infections and showed that IL-8 rapidly and efficiently accumulated in infectious foci. However, labeling of IL-8 with ^{123}I is costly, laborious and the specific activity of the preparation was low. In the present study IL-8 was labeled with ^{99m}Tc via the hydrazinonicotinamide (HYNIC) chelator.

Methods: The leukocyte receptor binding capacity of the preparation was determined in vitro. Rabbits with E. coli abscesses were i.v. injected with 7 MBq ^{99m}Tc-HYNIC-IL-8. Biodistribution of the radiolabel was determined by γ-camera imaging and tissue counting at 8 h p.i. ^{99m}Tc-HYNIC-Lysozyme was used as a size-matched control.

Results: The leukocyte receptor binding capacity of the ^{99m}Tc-HYNIC-IL-8 preparation was preserved as determined in vitro, but labeling efficiency was modest with a specific activity of 3 MBq/μg. ^{99m}Tc-HYNIC-IL-8 accumulated rapidly in the abscess up to 0.33 ± 0.06 %ID/g at 8 h p.i (versus 0.025 ± 0.003 %ID/g for ^{99m}Tc-HYNIC-Lysozyme). Total uptake in the abscess was 4.9 ± 0.7 %ID (versus 0.44 ± 0.05 %ID for ^{99m}Tc-HYNIC-Lysozyme). Abscess-to-contralateral muscle ratios increased up to 127 ± 23 (compared to 6.7 ± 1.1 for ^{99m}Tc-HYNIC-Lysozyme) and abscess-blood ratios to 11.9 ± 2.2 (0.24 ± 0.03 for ^{99m}Tc-HYNIC-Lysozyme). The radiolabel was excreted renally, with a retention in the kidneys of 28 %ID. Gamma camera imaging rapidly visualized the abscess from 1 h p.i. onwards, with abscess-to-background ratios improving with time up to 22 at 8 h p.i. (vs 2.7 for ^{99m}Tc-HYNIC-Lysozyme), as determined by quantitative analysis of the images. Most importantly, only a transient (30 min) moderate drop of leukocyte counts and no leukocytosis was observed after injection of an imaging dose of ^{99m}Tc-HYNIC-IL-8.

Conclusion: IL-8 can be labeled with ^{99m}Tc using HYNIC as a chelator. By this method the leukocyte receptor binding capacity is preserved. The preparation allows rapid visualization of infection in a rabbit model with high target-to-background ratios. The mild transient drop of leukocyte counts and the absence of leukocytosis suggest that ^{99m}Tc-HYNIC-IL-8 may be used as an imaging agent with only mild and transient side-effects.

INTRODUCTION

A wide range of radiopharmaceuticals has been proposed to visualize infections and inflammations scintigraphically. Autologous leukocytes, labeled with ^{111}In or ^{99m}Tc, is still considered the 'gold standard' nuclear medicine technique to image infection and inflammation. With regard to diagnostic accuracy there is no need for a better imaging agent than labeled autologous leukocytes. However, the labeling procedure is time-consuming, complex and could be hazardous. Therefore, there is a need for a radiopharmaceutical with at least similar clinical performance, that can be prepared rapidly and easily. In the search for new agents to image infections and inflammations, the development of new radiopharmaceuticals has gradually shifted during the past decades: from large proteins with aspecific uptake mechanisms (e.g. IgG (*1-3*)) via receptor-specific proteins of large size (e.g. anti-granulocyte (*4;5*) and anti-E-selectin antibodies (*6*)) and moderate size (antibody fragments (*7*)) to small receptor-binding proteins and peptides (e.g. cytokines).

Labeled cytokines such as interleukin-1, interleukin-2 and interleukin-8 are a promising class of protein radiopharmaceuticals of small molecular weight (<20 kDa). Cytokines act through an interaction with specific cell-surface receptors expressed on known cell populations. Binding affinities are usually high (nanomolar range).

Interleukin-1 (IL-1) binds receptors as expressed mainly on granulocytes, monocytes and lymphocytes, with high affinity. Studies in mice with focal *Staphylococcus aureus* infections showed specific uptake of radioiodinated IL-1 at the site of infection (infection-to-background ratios exceeded 40, 48 h p.i.) (*8*). Unfortunately, the biologic effects (e.g., hypotension, headache) of IL-1 even at very low doses (10 ng/kg) precluded clinical application of radiolabeled IL-1.

Chronic inflammation is characterized by infiltration of the target tissue by lymphocytes. It was successfully targeted with radiolabeled Interleukin-2 (IL-2) via specific binding to IL-2 receptors, expressed on activated T-lymphocytes. A method was developed that allowed the preparation of a ^{99m}Tc-IL-2 preparation with a high specific activity (*9*). Studies in patients with insulin-dependent diabetes, Hashimoto thyroiditis, Graves' disease, Crohn's disease or coeliac disease demonstrated localization of ^{123}I- or ^{99m}Tc-labeled IL-2 at the site of lymphocytic infiltration (*10*).

Interleukin-8 (IL-8) is a member of the CXC subfamily of the chemokines, or chemotactic cytokines, in which the first two cysteine residues are separated by one aminoacid residue. IL-8 binds the CXC type I (=IL-8 type A) and CXC type II (= IL-8 type B) receptors expressed on neutrophils and monocytes with high affinity (0.3 – 4 nM) (*11;12*). Hay and collegues (*13*) studied the in vivo behaviour of radioiodinated IL-8 in a rat model with carrageenan-induced sterile inflammations. The uptake

peaked at 1-3 hours after injection and declined thereafter. Target-to-background ratios did not exceed 2.5. In a pilot study in 8 patients these investigators showed that a ^{123}I-IL-8 could visualize inflammatory foci (*14*). We investigated the behaviour and kinetics of radioiodonated IL-8 in various models of infection and sterile inflammation in rabbits (*15;16*). These studies showed that particularly IL-8 labeled according to the Bolton-Hunter method showed superior imaging characteristics. In rabbits with focal *E. coli* infection, accumulation of ^{123}I-labeled IL-8 in the abscess was rapid and high (0.85 ± 0.1 %ID, 8 h p.i.). Abscess-to-contralateral muscle ratios exceeded 100 in this model within 8 h postinjection. The specific activity of this IL-8 preparations was relatively low; the imaging dose of ^{123}I-IL-8 (25 µg/kg) caused a transient drop of peripheral leukocyte counts to 45%, followed by a leukocytosis (170 % of preinjection level) during several hours.

For clinical imaging ^{123}I is not a very suitable radionuclide: it is expensive and the Bolton-Hunter labeling method is rather laborious. For clinical application, a simple and rapid labeling procedure of IL-8, using the radionuclide ^{99m}Tc, would be preferable. In the present study we investigated the potential of ^{99m}Tc-labeled IL-8 to image infections in a rabbit model. We aimed to develop a labeling technique that would result in a radiopharmaceutical with a high specific activity in order to reduce the IL-8 dose, thus reducing biologic activity. At the same time the leukocyte receptor binding capacity ought to be conserved. In order to accomplish this we used the bifunctional chelator hydrazino-nicotinamide (HYNIC). ^{99m}Tc-labeled Lysozyme (MW 14.3 kDa), with no specific receptor interaction, was used as a size-matched control in this study.

MATERIALS AND METHODS

Preparation of HYNIC-conjugates with IL-8

Human recombinant IL-8 was kindly provided by Dr I. Lindley (Novartis, Vienna, Austria). Lysozyme was purchased from Sigma (St. Louis, MO). IL-8 was conjugated to hydrazino-nicotinamide (HYNIC) essentially as described by Abrams et al. (*17*). Briefly, in a 1.5 ml vial 1.5 µl 1 M $NaHCO_3$, pH 8.2 was added to 15 µl of IL-8 (5.7 mg/ml). Subsequently succinimidyl-hydrazinonicotinamide (S-HYNIC) in 5 µl dry DMSO was added dropwise to the mixture. A series of conjugates was prepared by using different molar conjugation ratios IL-8 : S-HYNIC (1:1 - 1:10) and different reaction times (3 - 60 min.). After incubation at room temperature, the reaction was stopped by adding an excess of 1.0 M glycine. Subsequently, precooled PBS was added to a total volume of 170 µl. To remove excess unbound S-HYNIC the mixture

was extensively dialyzed against PBS (0.1-0.5 ml dialysis cell 3.5 MWCO, Pierce, Rockford, IL). Dialyzed samples of circa 7 µg IL-8-HYNIC were stored at –20 ^{0}C. The preparation of the Lysozyme-HYNIC-conjugate was similar; a three-fold molar excess of S-HYNIC was used and the reaction was stopped after 3, 10 or 30 minutes.

^{99m}Tc-labeling of HYNIC conjugated IL-8

Tricine-SnSO$_4$-kits (0.2 ml) were prepared containing 20 mg tricine (N-[Tris(hydroxymethyl)-methyl]glycine, Fluka, Buchs, Switzerland) and 0.01 mg SnSO$_4$ (Merck, Darmstadt, Germany) in 0.2 ml PBS pH 7.0. To prevent precipitation of stannous, SnSO$_4$ dissolved in 2 M HCl was added to a solution of tricine in PBS and the pH was subsequently adjusted to 7.0 with 1.0 M NaOH.

For receptor binding assays the HYNIC-conjugated IL-8 preparations with different molar conjugation ratios and different conjugation reaction times were labeled and tested. For animal studies the HYNIC-IL-8 preparation which showed the best leukocyte receptor binding capacity was selected for labeling and i.v. administration. As control a HYNIC-Lysozyme preparation with the same reaction conditions was chosen. For receptor binding assays a 0.2 ml tricine-SnSO$_4$-kit and 0.1 - 0.3 ml 20 - 30 MBq ^{99m}TcO$_4^-$ in saline were added to 5 µg thawed HYNIC-IL-8 and incubated at room temperature for 30 minutes. For animal studies a 0.2 ml tricine-SnSO$_4$-kit and 0.5 ml 500 MBq ^{99m}TcO$_4^-$ in saline were added to 20 µg thawed HYNIC-IL-8 or HYNIC-Lysozyme and incubated at room temperature for 30 minutes. The radiochemical purity was determined by instant thin-layer chromatography (ITLC) on ITLC-SG strips (Gelman Laboratories, Ann Arbor, MI) with 0.1 M citrate, pH 6.0, as the mobile phase.

Following the labeling reaction the reaction mixture was applied to a Sephadex G-25 column (PD-10; Pharmacia, Uppsala, Sweden) and eluted with 0.5 % BSA in PBS to purify the radiolabeled IL-8 or Lysozyme conjugate.

Receptor binding assay

Human neutrophils were isolated from heparinized whole blood obtained from healthy donors. Receptor binding assays were performed essentially as described previously (*16*), using ^{99m}Tc-labeled IL-8 instead of radioiodinated IL-8.

Animal studies

Animal studies were performed essentially as described previously (*16*). The experiments were carried out in accordance with the guidelines of the local animal welfare committee. Abscesses were induced in the left thigh muscle of ten female New Zealand rabbits (2.4-2.7 kg) with 4 x 10^{10} colony forming units (cfu) of *Escherichia coli* in 0.5 ml. During the

procedure, the rabbits were sedated with a subcutaneous injection of a 0.6 ml mixture of fentanyl 0.315 mg/ml and fluanisone 10 mg/ml (Hypnorm, Janssens Pharmaceutical, Buckinghamshire, UK). After 24 hours, when swelling of the muscle was apparent, six rabbits were injected with 7 MBq ^{99m}Tc-HYNIC-IL-8 (protein dose 2.5 μg) via the ear vein. Three of them were used for gamma camera imaging (0, 1, 2, 4 and 8 h p.i.), while the other three were used to determine the pharmacokinetics and monitor white blood cell counts. A control group of five rabbits was injected with 18 MBq ^{99m}Tc-HYNIC-Lysozyme (protein dose 2.5 μg). Two of these animals were imaged with a gamma camera (0, 1, 2, 4 and 8 h p.i.).

For imaging, rabbits were immobilized, placed prone on the gamma camera and injected with either ^{99m}Tc-HYNIC-IL-8 or ^{99m}Tc-HYNIC-Lysozyme in the lateral ear vein. Images were recorded at 1 min, 1, 2, 4 and 8 hr p.i. with a single-head gamma camera (Orbiter, Siemens Medical Systems Inc., Hoffman Estates, IL) equipped with a parallel-hole low-energy all purpose collimator. Images (100,000-200,000 counts per image) were obtained and digitally stored in a 256 x 256 matrix.

The scintigraphic results were analyzed quantitatively by drawing regions of interest (ROI) over the abscess and the uninfected contralateral thigh muscle (background). Abscess-to-background ratios were calculated.

Pharmacokinetics and white blood cell counts were determined in a group of three rabbits injected with 7 MBq 2.5 μg ^{99m}Tc-HYNIC-IL-8. Blood samples were collected at −1, 1, 3, 5, 10, 30, 60, 120, 240 and 480 minutes after injection. Blood samples were weighed, their activity was measured and their uptake expressed as %ID/g and as %ID in the blood pool based on an estimated total blood volume of 6% of the total body weight of the rabbit (*18*). White blood cell counts were measured in the same blood samples and expressed as percentage of the pre-injection value.

After completion of the final imaging and blood sampling (8 h p.i.), the rabbits were killed with a lethal dose of sodium phenobarbital. Samples of blood, infected thigh muscle, uninfected contralateral thigh muscle, lung, spleen, liver, kidneys and intestines were collected. The dissected tissues were weighed and counted in a gamma counter. Injection standards were counted simultaneously to correct for radioactive decay. The measured activity in samples was expressed as percentage of injected dose per gram tissue (%ID/g). Additionally, total uptake of the radiopharmaceutical (%ID) was measured for kidneys and abscesses. Abscess-to-contralateral muscle ratios and abscess-to-blood ratios were calculated.

Statistical analysis
All mean values are given as %ID/g or ratios ± one standard error of the mean (s.e.m.). The data were analyzed statistically using the one-way analysis of variance (ANOVA).

RESULTS

Radiolabeling and characterization of ^{99m}Tc-HYNIC-IL-8

The labeling efficiencies (%) and receptor binding fractions RBF (%) of various ^{99m}Tc-HYNIC-IL-8 and ^{99m}Tc-HYNIC-Lysozyme preparations are shown in Table 1. There is an inverse relationship between labeling efficiency and leukocyte receptor binding capacity (RBF). For animal studies the most mildly modified HYNIC-IL-8-preparation with the highest receptor binding capacity was chosen, i.e. the preparation with molar conjugation protein:S-HYNIC of 1:3 and a conjugation reaction time of 3 min. The conventional binding plot for this preparation is presented in figure 1. As control the HYNIC-Lysozyme preparation with the same molar conjugation ratio 1:3 and conjugation time 3 minutes was chosen. The specific activity was 2.8 MBq/µg for the ^{99m}Tc-HYNIC-IL-8 preparation and 7.2 MBq/µg for the ^{99m}Tc-HYNIC-Lysozyme preparation. The radiochemical purity of all radiopharmaceuticals was higher than 95% after gel filtration as determined by ITLC. In other experiments we used a more rigorously conjugated IL-8 preparation (molar conjugation ratio protein:S-HYNIC 1:10; conjugation reaction time 60 min.) (*19*). This preparation showed a labeling efficiency of 97% with specific activities as high as 75 MBq/µg. However, the leukocyte receptor binding capacity was greatly reduced (RBF=16%), indicating that the conjugation conditions were too aggresive and modifications occurred in regions of the protein that are critical for receptor binding.

Table 1. *Labeling efficiencies (%) and receptor binding fractions RBF (%) of various ^{99m}Tc-HYNIC-IL-8 and ^{99m}Tc-HYNIC-Lysozyme preparations.*[*]

Protein	Molar conjugation ratio Protein : S-HYNIC	Reaction time (min)	Labeling Efficiency (%)	RBF (%)
IL-8	1 : 1	3	15	65
IL-8	1 : 1	60	87	31
IL-8	1 : 2	60	94	24
IL-8	1 : 3	3	20	65
IL-8	1 : 3	10	71	37
IL-8	1 : 3	30	83	30
IL-8	1 : 3	60	95	21
IL-8	1 : 10	60	97	16
Lysozyme	1 : 3	3	69	n.d.
Lysozyme	1 : 3	10	90	n.d.
Lysozyme	1 : 3	30	95	n.d.

[*]*For determination of labeling efficiencies, 5 µg of HYNIC-conjugated protein was used with 20 - 30 MBq ^{99m}Tc. (n.d. = not determined)*
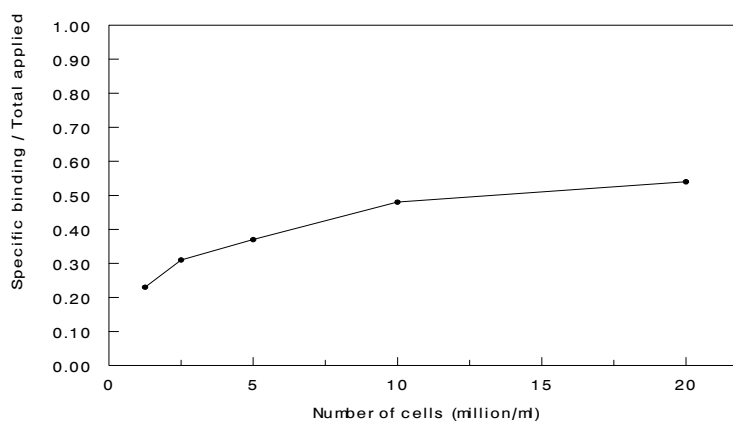
Figure 1. *The conventional binding plot of* ^{99m}*Tc-HYNIC-IL-8 as determined on isolated human granulocytes. The specific binding over total applied radioactivity is plotted as a function of increasing cell concentration.*

^{99m}Tc-HYNIC-IL-8 in rabbits with *E. coli* infection

Immediately after injection of ^{99m}Tc-HYNIC-IL-8 (1 µg/kg body weight), a transient reduction of peripheral leukocyte levels to 54% was observed (Fig. 2). The white blood cell count returned to base levels within 30 minutes. No subsequent leukocytosis was observed. The blood clearance pattern fitted a two-phase model with a half-life (t½α) of 4.2 min during the distribution phase and a half-life (t½β) of 5.1 h during the elimination phase (Fig. 3).

The abscesses were clearly delineated on the images recorded from 1 h onwards (Fig. 4). ^{99m}Tc-HYNIC-IL-8 rapidly accumulated at the site of infection. Quantitative analysis of the images indicated that the abscess-to-background ratios improved with time up to 21.8 ± 1.0 at 8 h p.i. (Fig. 5). Immediately after injection high kidney uptake was observed; kidney uptake remained high during the 8 h p.i. In addition, activity was found in bladder, liver and lungs. The control agent ^{99m}Tc-HYNIC-Lysozyme showed a similar kidney uptake pattern, but failed to accumulate significantly at the site of infection. Abscess-to-background ratios did not exceed 2.7 (Fig. 5).

Tissue biodistribution of the radiolabel determined at 8 h p.i. is summarized in table 2. Except for the kidneys and the spleen, the highest uptake of ^{99m}Tc-HYNIC-IL-8 was found in the abscess: 0.33 ± 0.06 %ID/g, versus 0.025 ± 0.003 %ID/g for ^{99m}Tc-HYNIC-Lysozyme (p=0.0001). Total uptake in the infected tissue was 4.9 ± 0.7 %ID versus 0.44 ± 0.05 %ID for ^{99m}Tc-HYNIC-Lysozyme (p=0.0001), indicating preferential retention of IL-8 in infected tissue. Abscess-to-contralateral muscle ratios reached a value as high as 127 ± 23 at 8 h p.i. versus 6.7 ± 1.1 for ^{99m}Tc-HYNIC-Lysozyme (p<0.001). The abscess-to-blood ratio was 11.9 ± 2.2 at 8 h p.i. compared to 0.24 ± 0.03 for ^{99m}Tc-HYNIC-Lysozyme (p=0.0001). Kidney retention was high: at 8 h p.i. 28 ± 1 %ID was found in the kidneys (35 ± 1 %ID for ^{99m}Tc-HYNIC-Lysozyme).
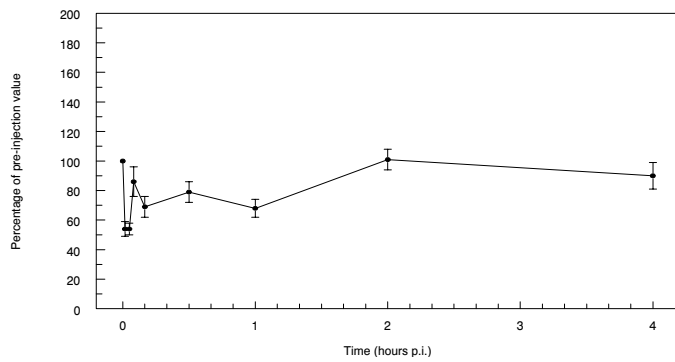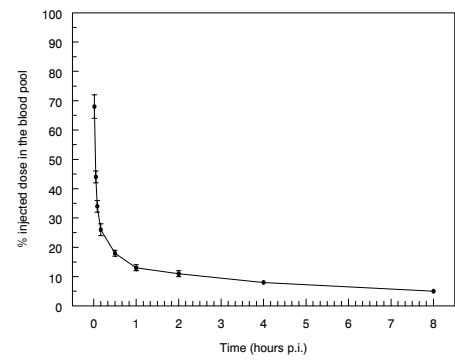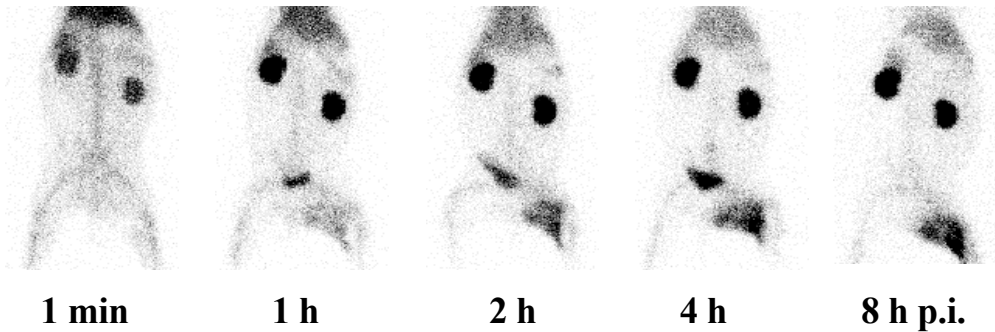
Figure 2

Figure 3

Figure 2 (left). *White blood cell counts in blood of E. coli infected New Zealand rabbits after intravenous injection of 2.5 μg ^{99m}Tc-HYNIC-IL-8, expressed as percentage of the pre-injection value. The error bars indicate s.e.m*

Figure 3 (right). *Blood clearance of ^{99m}Tc-HYNIC-IL-8 determined in rabbits with E. coli infection. Data are expressed as percentage of the injected dose in the blood pool. The error bars indicate s.e.m.*

Interleukin-8

1 min   **1 h**   **2 h**   **4 h**   **8 h p.i.**

Lysozyme

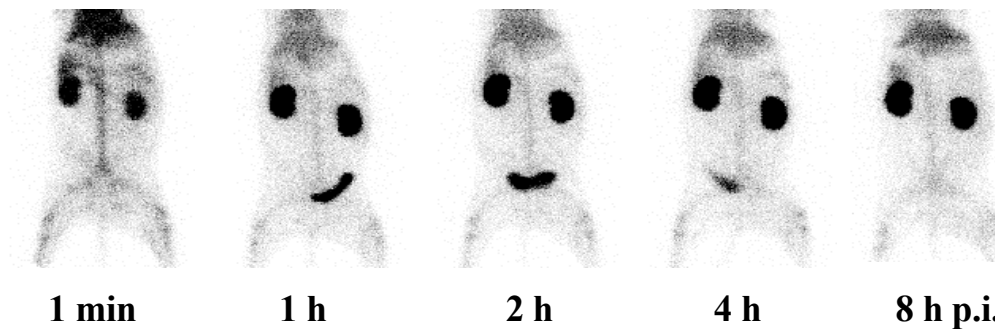**1 min**   **1 h**   **2 h**   **4 h**   **8 h p.i.**

Figure 4. *Images of rabbits with an E. coli abscess in the left thigh muscle at 1 min, 1, 2, 4 and 8 hr after injection of ^{99m}Tc-HYNIC-IL-8 (upper panel) or ^{99m}Tc-HYNIC-Lysozyme (lower panel). All photographs were produced with the same image contrast.*
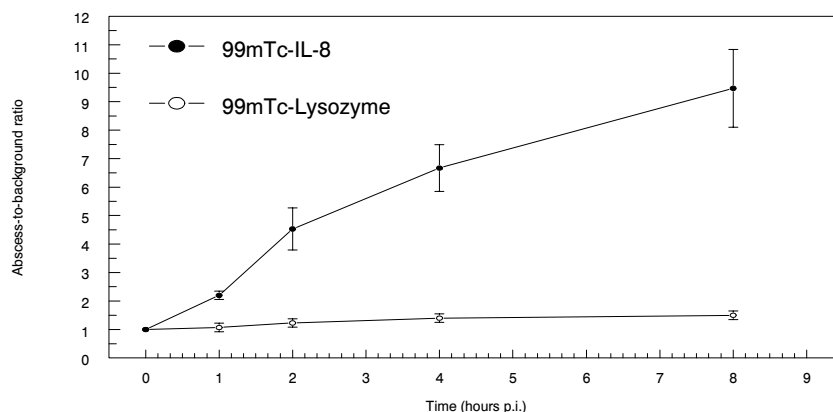
Figure 5. *The abscess-to-background ratios as determined by quantitative analysis of the images of rabbits with E. coli infection injected with ^{99m}Tc-HYNIC-IL-8 or ^{99m}Tc-HYNIC-Lysozyme. The error bars indicate s.e.m.*

Table 2. *Biodistribution of ^{99m}Tc-HYNIC-IL-8 and ^{99m}Tc-HYNIC-Lysozyme in rabbits with E. coli infections at 8 h p.i. (%ID/g, mean values ± s.e.m.)*

Organ	^{99m}Tc-IL-8 n=6	^{99m}Tc-Lysozyme n=5
Blood	0.028 ± 0.001	0.105 ± 0.006
Abscess	0.33 ± 0.06	0.025 ± 0.003
Muscle	0.0026 ± 0.0001	0.0041 ± 0.0008
Lung	0.19 ± 0.04	0.077 ± 0.011
Spleen	0.64 ± 0.06	0.119 ± 0.005
Kidney	1.47 ± 0.06	1.77 ± 0.06
Liver	0.14 ± 0.01	0.124 ± 0.006
Intestine	0.025 ± 0.002	0.028 ± 0.001
Abscess/muscle	127 ± 23	6.7 ± 1.1
Abscess/blood	11.9 ± 2.2	0.24 ± 0.03
Total uptake infected tissue (%ID)	4.9 ± 0.7	0.44 ± 0.05
Total uptake in kidneys (%ID)	28 ± 1	35 ± 1

DISCUSSION

Based on results with radioiodinated IL-8 previously obtained in our laboratory, we explored here the potential of ^{99m}Tc-labeled IL-8 to image infection and inflammation in rabbits with E. coli infection. The present study showed that IL-8 can be labeled with ^{99m}Tc using HYNIC as a chelator with preservation of its leukocyte receptor binding capacity. The preparation allows rapid visualization of infection within a few hours after injection and high target-to-background ratios. The mild transient drop of leukocyte counts and the absence of leukocytosis suggest that ^{99m}Tc-HYNIC-IL-8 may be applied as a clinically useful imaging agent.

The labeling efficiency and leukocyte receptor binding capacity of various ^{99m}Tc-HYNIC-IL-8 preparations was tested. Mildly modified ^{99m}Tc-HYNIC-IL-8 preparations showed good receptor binding but modest ^{99m}Tc binding, with a relatively low specific activity of nearly 3 MBq/μg. On the other hand, higher substitution of the protein with S-HYNIC resulted in ^{99m}Tc-HYNIC-IL-8 preparations with high specific activities (as high as 75 MBq/μg), but with a severe loss of receptor binding capacity. The best infection imaging characteristics were obtained with the mildly modified ^{99m}Tc-HYNIC-IL-8 preparation presented in this study. This was demonstrated for instance by an abscess-muscle ratio at 8 h p.i. of 127 as compared to 36 for a more rigorously conjugated IL-8 preparation formerly used (*19*).

The observation that infection uptake of ^{99m}Tc-HYNIC-IL-8 was more than ten times higher than the uptake of ^{99m}Tc-HYNIC-Lysozyme suggested that abscess uptake was a result of the interaction of IL-8 with its receptors in the infectious foci. Specific uptake was shown also by an abscess-muscle ratio of 127 as compared to 6.7 for the control peptide. Uptake in the kidneys was high for both peptides which is a common phenomenom for radiolabeled peptides (*20-24*). The mechanism of renal uptake and retention of proteins is believed to involve glomerular filtration and subsequent reabsorption and catabolism in the proximal tubular cells (*25;26*). This process is dependent on molecular weight and charge of the proteins. Proteins exceeding a molecular weight of approximately 60 kDa are too large to pass the glomerular basement membrane and are thus not retained in the kidneys. Cationic proteins, as compared to anionic ones, are preferably retained in the kidneys. Several investigators have lowered renal uptake by infusing basic amino acids such as lysine and arginine (for a Review see *26*). Other strategies involve chemical modification of the protein. A substantial reduction of renal uptake has been achieved by glycolation of free amino groups (lysine side chains) (*27-28*).

In previous studies IL-8 has been investigated for scintigraphic detection of infection and inflammation by Hay et al. (*13*) and in our laboratory by Van der Laken et al. (*15;16*). In these studies IL-8 was radioiodonated according to the chloramine-T, the iodogen or the Bolton-Hunter method. The last method was found to be superior. With preparations of iodonated IL-8 via the Bolton-Hunter method (^{123}I-BH-IL-8) abscess-muscle and abscess-blood ratios of 115 and 12 respectively (8 h p.i.) were obtained in a rabbit model, similar to the ratios obtained in the present study. With both preparations, abscesses were visualized as early as 1 h p.i. Uptake of activity in the kidneys was high with both preparations, although it was less pronounced for ^{123}I-BH-IL-8. The difference is caused by clearance of the radioiodonated label from the tubular cells after degradation in the lysosomes, whereas radiometal chelates remain trapped within lysosomes (*21,26-28*). Labeling IL-8 with ^{99m}Tc via HYNIC offers great advantages over the Bolton-Hunter iodonation method. In the first place, the preparation of ^{99m}Tc-HYNIC-IL-8 as compared to ^{123}I-BH-IL-8 is easy, fast and suitable for instant kit formulations for routine use. Secondly, a formulation with ^{99m}Tc is inexpensive and always available, compared to [123]I. Most importantly, a preparation with much higher specific activity could be obtained. In this way the amount of biologically active material injected is reduced 25-fold: 1 µg/kg ^{99m}Tc-HYNIC-IL-8 versus 25 µg/kg ^{123}I-BH-IL-8. Using a dose of 25 µg/kg, IL-8 induced transient leukopenia followed by a leukocytosis lasting for several hours (*15*), while at a dose level of 1 µg/kg only a mild transient drop of leukocyte counts without subsequent leukocytosis was observed. This suggests that ^{99m}Tc-HYNIC-IL-8 can be used as an imaging agent potentially without clinically significant side-effects.

Besides IL-8 several small ^{99m}Tc-labeled peptides capable of binding to leukocytes in vivo have been developed and tested for their imaging qualities. [99m]Tc labeled N-formyl-methionyl-leucyl-phenylalanyl-lysine (fMLFK) (*29*) and Platelet Factor 4 derived peptide P483H (*30*) are effective infection-seeking agents. However, in the same animal model abscess-muscle ratios obtained with these agents were only a quarter of those obtained with IL-8. In addition, fMLFK showed relatively high activity in bowel and liver resulting in high background activity, making this imaging agent less suitable for detection of infections in the abdomen.

Future experiments with ^{99m}Tc labeled IL-8 will focus on improvement of the labeling efficiency without compromising the receptor binding activity and infection localizing capacity of the agent. Site specific attachment of a bifunctional chelating group in a region of IL-8 not critical for receptor binding will be the proper solution.

CONCLUSION

The present study showed that ^{99m}Tc-labeled IL-8 has excellent characteristics as an infection imaging agent: it rapidly accumulated in infectious foci, while it rapidly cleared from nontarget tissues. The technetium chemistry allowed labeling of IL-8 with preservation of its leukocyte receptor binding capacity. The mild transient drop of leukocyte counts without subsequent leukocytosis suggest that ^{99m}Tc-HYNIC-IL-8 may be used as a clinically useful imaging agent without significant side-effects. These results warrant further development of an IL-8 based radiopharmaceutical for infection imaging.

ACKNOWLEDGMENTS

REFERENCES

1. Oyen WJG, Claessens RAMJ, van der Meer JWM, Corstens FHM. Biodistribution and kinetics of radiolabelled proteins in rats with focal infection. *J Nucl Med.* 1992; 33:388-394.
2. Buscombe JR, Oyen WJG, Grant A, et al. Indium-111-labeled human polyclonal immunoglobulin: identifying focal infection in patients positive for human immunodeficiency virus (HIV). *J Nucl Med.* 1993;34:1621-1625.
3. Babich JW, Graham W, Barrow SA, Fischman AJ. Comparison of the infection imaging properties of a ^{99m}Tc labeled chemotactic peptide with ^{111}In IgG. *Nucl Med Biol.* 1995;22:643-648.
4. Becker W, Goldenberg DM, Wolf F. The use of monoclonal antibodies and antibody fragments in the imaging of infectious lesions. *Semin Nucl Med.* 1994;24:142-153.
5. Thakur ML, Marcus CS, Henneman P et al. Imaging inflammatory diseases with neutrophil-specific technetium-99m-labeled monoclonal antibody anti-SSEA-1. *J Nucl Med.* 1996;37:1789-1795.
6. Keelan E, Chapman P, Binns R, Peters A, Haskard D. Imaging vascular endothelial activation: An approach using radiolabeled monoclonal antibodies against the endothelial cell adhesion molecule E-selectin. *J Nucl Med.* 1994;35:276-281.
7. Becker W, Palestro CJ, Winship J, Feld T, Pinsky CM, Wolf F, Goldenberg DM. Rapid imaging of infections with a monoclonal antibody fragment (Leukoscan). *Clin Orthopeadics.* 1996;329:263-272.
8. Van der Laken CJ, Boerman OC, Oyen WJG, et al. Specific targeting of infectious foci with radioiodinated human recombinant interleukin-1 in an experimental model. *Eur J Nucl Med.* 1995;22:1249-1255.
9. Chianelli M, Signore A, Fritzberg AR, Mather SJ. The development of technetium-99m-labelled interleukin-2: a new radiopharmaceutical for the in vivo detection of mononuclear cell infiltrates in immune-mediated diseases. *Nucl Med Biol.* 1997;24:579-586.
10. Signore A. Interleukin-2 scintigraphy: An overview [Abstract]. *Nucl Med Commun.* 1999;20:938.
11. Lee J, Horuk R, Rice GC, Bennett GL, Camerato T, Wood WI. Characterization of two high affinity human interleukin-8 receptors. *J Biol Chem.* 1992;267:16283-16287.
12. Cerretti DP, Kozlosky CJ, VandenBos T, Nelson N, Gearing DP, Beckmann MP. Molecular characterization of receptors for human interleukin-8, GRO/melanoma growth-stimulatory activity and neutrophil activating peptide-2. *Mol Immunol.* 1993;30:359-367.
13. Hay RV, Skinner RS, Newman OC, et al. Scintigraphy of acute inflammatory lesions in rats with radiolabelled recombinant human interleukin-8. *Nucl Med Commun.* 1997;18:367-378.

14. Gross MD, Shapiro B, Skinner RS, Shreve P, Fig LM, Hay RV. Scintigraphy of osteomyelitis in man with human recombinant interleukin-8 [Abstract]. *J Nucl Med*. 1996;37:25P.

15. Van der Laken CJ, Boerman OC, Oyen WJ, Van de Ven MT, Ven der Meer JW, Corstens FH. The kinetics of radiolabelled interleukin-8 in infection and sterile inflammation. *Nucl Med Commun*. 1998;19:271-281.

16. Van der Laken CJ, Boerman OC, Oyen WJ, Van de Ven MT, Van der Meer JW, Corstens FH. Radiolabeled interleukin-8: specific scintigraphic detection of infection within a few hours. *J Nucl Med*. 2000;41:463-469.

17. Abrams MJ, Juweid M, tenKate CI, et al. Technetium-99m-human polyclonal IgG radiolabeled via the hydrazino nicotinamide derivative for imaging focal sites of infection in rats. *J Nucl Med*. 1990;31:2022-2028.

18. Jain NC. Chapter 3: Blood volume and water balance. In: Jain NC, ed. *Schalm's veterinary hematology*. 4th ed. Philadelphia, PA: Lea & Febiger; 1986:87-102.

19. Rennen HJJM, Boerman OC, Oyen WJG, Van der Laken CJ, Corstens FHM. Specific and rapid scintigraphic detection of infection with Tc-99m-labeled Interleukin-8 [Abstract]. *Eur J Nucl Med*. 1999;26:1005.

20. Maack T, Park CH, Camargo MJF. Renal filtration, transport, and metabolism of proteins. In: Seldin DW, Giebisch G, eds. *The Kidney: Physiology and Pathophysiology*. 2nd ed. New York, NY: Raven Press; 1992:3005-3038.

21. Behr TM, Sharkey RM, Sgouros G, et al. Overcoming the nephrotoxicity of radiometal-labeled immuno-conjugates: improved cancer therapy administered to a nude mouse model in relation to the internal radiation dosimetry. *Cancer*. 1997;80:2591-2610.

22. Kobayashi H, Nhat Le, Kim IS, et al. The pharmacokinetic characteristics of glycolated humanized anti-Tac Fabs are determined by their isoelectric points. *Cancer Res*. 1999;59:422-430.

23. Kobayashi H, Kim IS, Drumm D, et al. Favorable effects of glycolate conjugation on the biodistribution of humanized antiTac Fab fragment. *J Nucl Med*. 1999;40:837-845.

24. Kim IS, Yoo TM, Kobayashi H, et al. Chemical modification to reduce renal uptake of disulfide-bonded variable region fragment of anti-Tac monoclonal antibody labeled with 99m-Tc. *Bioconjugate Chem*. 1999;10:447-453.

25. Sumpio BE and Maack T. Kinetics, competition and selectivity of tubular absorption of proteins. *Am J Physiol*. 1982;243:F379-F392.

26. Behr TM, Goldenberg DM and Becker W. Reducing the renal uptake of radiolabeled antibody fragments and peptides for diagnosis and therapy: present status, future prospects and limitations. *Eur J Nucl Med*. 1998;25:201-212.

27. Naruki Y, Carrasquillo JA, Reynolds JC, et al. Differential cellular catabolism of 111-In, 90-Y and 125-I radiolabeled T101 anti-CD5 monoclonal antibody. *Int J Radiat Appl Instr*. 1990;17:201-207.

28. Sakahara H, Saga T, Endo K, et al. In vivo instability of reduction-mediated 99m-Tc-labeled monoclonal antibody. *Nucl Med Biol*. 1993;20:617-623.

29. Van der Laken CJ, Boerman OC, Oyen WJ, et al. Technetium-99m-labeled chemotactic peptides in acute infection and sterile inflammation. *J Nucl Med*. 1997;38:1310-1315.

30. Moyer BR, Vallabhajosula S, Lister-James J, et al. Technetium-99m-white blood cell-specific imaging agent developed from platelet factor 4 to detect infection. *J Nucl Med*. 1996;37:673-679.

Chapter 5

Effects of coligand variation on the in-vivo characteristics of ^{99m}Tc-labeled interleukin-8 in detection of infection

Huub J.J.M. Rennen, Julliëtte E. van Eerd, Wim J.G. Oyen,
Frans H.M. Corstens, D. Scott Edwards, Otto C. Boerman

ABSTRACT

In our previous studies interleukin-8 (IL-8) was labeled with [99mTc] using hydrazino-nicotinamide (HYNIC) as bifunctional coupling agent and tricine as coligand. This preparation showed excellent characteristics for imaging of infection in a rabbit model of soft-tissue infection. In the present study the propylaldehyde hydrazone formulation of HYNIC was introduced to stabilize HYNIC-IL-8. [99mTc]-HYNIC-IL-8 was prepared using 5 different coligand formulations. The effect of these coligand formulations on the *in vitro* characteristics and *in vivo* behavior of [99mTc]-HYNIC-IL-8 was investigated.

Methods: HYNIC-conjugated IL-8 was labeled with [99mTc] in the presence of either (A) Tricine, (B) ethylenediaminediacetic acid (EDDA), (C) Tricine and trisodium triphenylphosphinetrisulfonate (TPPTS), (D) Tricine and nicotinic acid (NIC) or (E) Tricine and isonicotinic acid (ISONIC). These preparations were characterized *in vitro* by RP-HPLC, determination of the octanol/water partition coefficient, stability studies and by receptor binding assays. The *in vivo* biodistribution of the radiolabel in rabbits with *E.coli* induced soft-tissue infection was determined both by γ-camera imaging as well as by tissue counting at 6 h p.i.

Results: Specific activity (MBq/μg) was highest for (ISO)NIC (up to 80) > TPPTS (40) > Tricine (15) > EDDA (7). RP-HPLC and octanol/water partition coefficients showed a shift toward higher lipophilicity for the TPPTS preparation. The leukocyte receptor binding fractions were around 40-55% for all preparations except for TPPTS, which showed predominantly nonspecific binding. All preparations were stabilized in serum, but the stability in PBS was highest for NIC and TPPTS > EDDA > ISONIC > Tricine. The *in vivo* biodistribution showed highest abscess/muscle for NIC and ISONIC (>200) > EDDA and Tricine (~100) > TPPTS (<40). Gamma camera imaging rapidly visualized the abscess from 2 h p.i. onwards for all formulations. The abscess/background (A/B) at 6 h p.i. for ISONIC was significantly higher ($P<0.05$) than that of Tricine and the A/B of TPPTS was significantly lower ($P<0.05$).

Conclusion: IL-8 can be rapidly and easily labeled with [99mTc] using HYNIC as a chelator in combination with various coligands. The most optimal infection imaging characteristics were found for formulations using Nicotinic acid/tricine as coligand system combining a high specific activity and high *in vitro* stability with high abscess/muscle ratios (>200) and high abscess/background ratios (>20). Protein doses to be administered were as low as 70 ng/kg bodyweight. At these low protein doses side effects are not to be expected in the human system. This paves the way for infection imaging studies in patients.

INTRODUCTION

Scintigraphic imaging of infectious and noninfectious inflammation is a powerful diagnostic tool in the management of patients with inflammatory disorders. Most inflammatory foci can be visualized accurately with *ex vivo* radiolabeled autologous leukocytes. However, preparation of this radiopharmaceutical is laborious and requires the handling of potentially contaminated blood with inherent risks for both personnel and patients.

There is an ongoing search for radiolabeling small molecules that bind to circulating leukocytes (*in vivo* labeling of leukocytes) after the relatively poor results obtained with large size monoclonal antibodies directed against leukocytes. These small molecules include chemotactic peptides (analogues of formyl-Met-Leu-Phe) and cytokines (e.g., the interleukins, platelet factor 4 derivatives) [for a review: (*1*)]. We have actively pursued a research program to explore the potential of radiolabeled formyl-Met-Leu-Phe-Lys, interleukin-1, interleukin-8 and other cytokines for imaging inflammation.

Radiolabeled interleukin-8 (IL-8) proved to be the most promising candidate so far. IL-8 is a member of the CXC subfamily of chemokines, or chemotactic cytokines, in which the first two cysteine residues are separated by one aminoacid residue. This cytokine binds the CXC type l (= IL-8 type A) and CXC type ll (= IL-8 type B) receptors expressed on neutrophils and monocytes with high affinity (0.3-4 nM) (*2,3*). Hay and colleagues (*4*) studied the *in vivo* behavior of radioiodinated IL-8 in a rat model with carrageenan-induced sterile inflammations and found only modest target-to-background ratios of 2.5. In a pilot study in eight patients these investigators showed that a ^{123}I-IL-8 could visualize inflammatory foci (*5*).

We investigated the *in vivo* behavior of radiolabeled IL-8 in various models of infection and sterile inflammation in rabbits (*6-10*). Studies with ^{123}I-labeled IL-8 in rabbits with focal *E. coli* infection showed rapid accumulation of the radiopharmaceutical in the abscess (*6,7*). Abscess-to-contralateral muscle ratios exceeded 100 in this model within 8 h postinjection. A drawback of this preparation was its relatively low specific activity; the imaging dose of ^{123}I-IL-8 (25 μg/kg) caused a transient drop of peripheral leukocyte counts to 45%, followed by a leukocytosis (170% of preinjection level) during several hours. Moreover, ^{123}I is not a very suitable radionuclide for clinical imaging: it is expensive and the Bolton-Hunter labeling method used for preparing ^{123}I-labeled IL-8 is rather laborious.

For clinical application, a simple and rapid labeling procedure of IL-8, using the radionuclide ^{99m}Tc, is preferable. [99m]Tc combines highly favorable physical characteristics ($t_{1/2} = 6$ h, $E_{max} = 140$ keV) with easy availability and low cost. In a

subsequent study IL-8 was labeled with ^{99m}Tc using hydrazinonicotinamide (HYNIC) as bifunctional coupling agent (*8*). HYNIC has been introduced by Abrams and co-workers (*11*) for labeling polyclonal IgG with ^{99m}Tc to image infections. Since the HYNIC group can only occupy one or two coordination sites in the technetium coordination sphere, an additional coligand is required. For labeling HYNIC conjugated IL-8 with ^{99m}Tc tricine was chosen as coligand, because specific activities obtained with this coligand are much higher than with e.g. glucoheptonate (*12*). The specific activity of the ^{99m}Tc-labeled IL-8 preparation was found to be 25x higher than the specific activity of the ^{123}I-labeled IL-8 preparation. In rabbits with *E.coli* induced softtissue infection abscess to contralateral muscle ratios and abscess to blood ratios obtained with the ^{99m}Tc- and the ^{123}I-labeled preparation were similar. Preparing ^{99m}Tc-labeled IL-8 is easy and fast, offering a major advantage over the radioiodination procedure.

The aim of the present study was to improve the characteristics for imaging infection of a ^{99m}Tc-labeled IL-8 preparation together with a further increase in specific activity of the preparation, thus reducing the required IL-8 protein dose. Two aspects of the labeling procedure were further optimized.

First, a modified form of HYNIC was synthesized. To improve long term stability Schwartz and coworkers introduced the use of a propylaldehyde hydrazone formulation to stabilize HYNIC modified proteins (*13,14*). This protection of the hydrazine moiety of HYNIC ensures greater stability in aqueous solutions and the hydrazone retains the capacity to produce enough free hydrazine for successful labeling with ^{99m}Tc.

Second, different coligand formulations were adopted in labeling HYNIC conjugated IL-8 with ^{99m}Tc. Babich and Fischman (*15*) were the first to show that the nature of the coligand has a distinctive influence on the biologic properties of the radioconjugate. Liu and Edwards et al. have performed systematic studies on labeling a HYNIC-conjugated platelet glycoprotein receptor antagonist with ^{99m}Tc using various coligand formulations: tricine; ethylenediaminediacetic acid (EDDA) (*16*); tricine in combination with water soluble phosphines (*17*); tricine in combination with imine-N-containing heterocycles (*18*).

In the present study HYNIC conjugated IL-8 was labeled with ^{99m}Tc using five different coligand systems: i) tricine; ii) EDDA; iii) tricine in combination with trisodium triphenyl-phosphine-3,3',3''-trisulfonate (TPPTS); iv) tricine in combination with nicotinic acid; and v) tricine in combination with isonicotinic acid (see Fig. 1). The proposed structures (*16-18*) of the resulting binary technetium complexes [^{99m}Tc(IL-8-HYNIC)(tricine)$_2$] and [^{99m}Tc(IL-8-HYNIC)(EDDA)] and ternary technetium complexes [^{99m}Tc(IL-8-HYNIC)(tricine)(L)] (L = TPPTS or nicotinic acid or isonicotinic

acid) are depicted in Fig. 2. The effect of the coligand on the *in vivo* behavior of ^{99m}Tc-labeled IL-8 was investigated in a rabbit model of *E.coli* induced soft tissue infection.
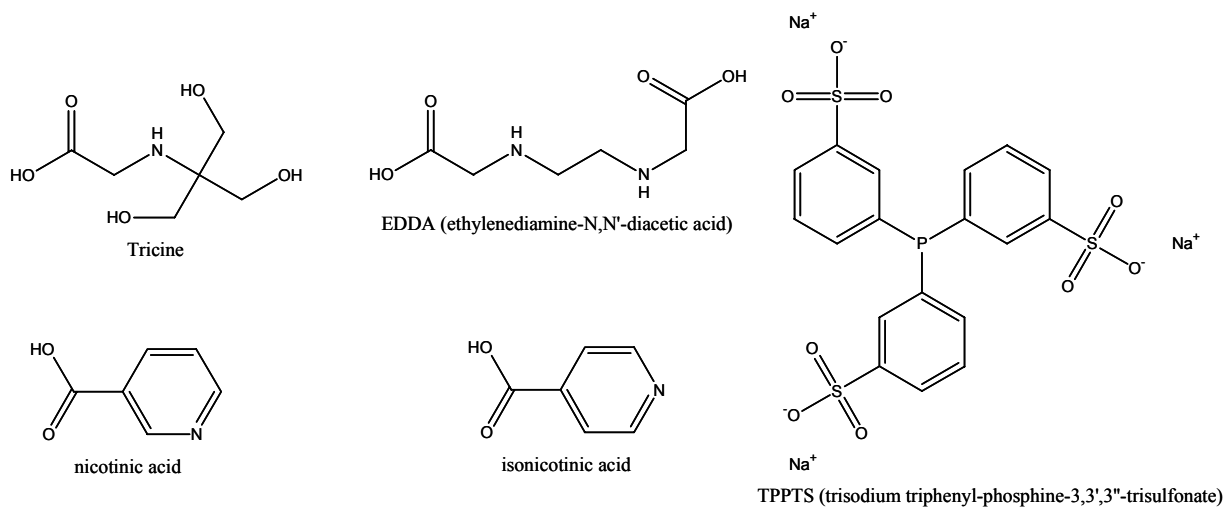
Figure 1. *Structures of coligands used in this study.*
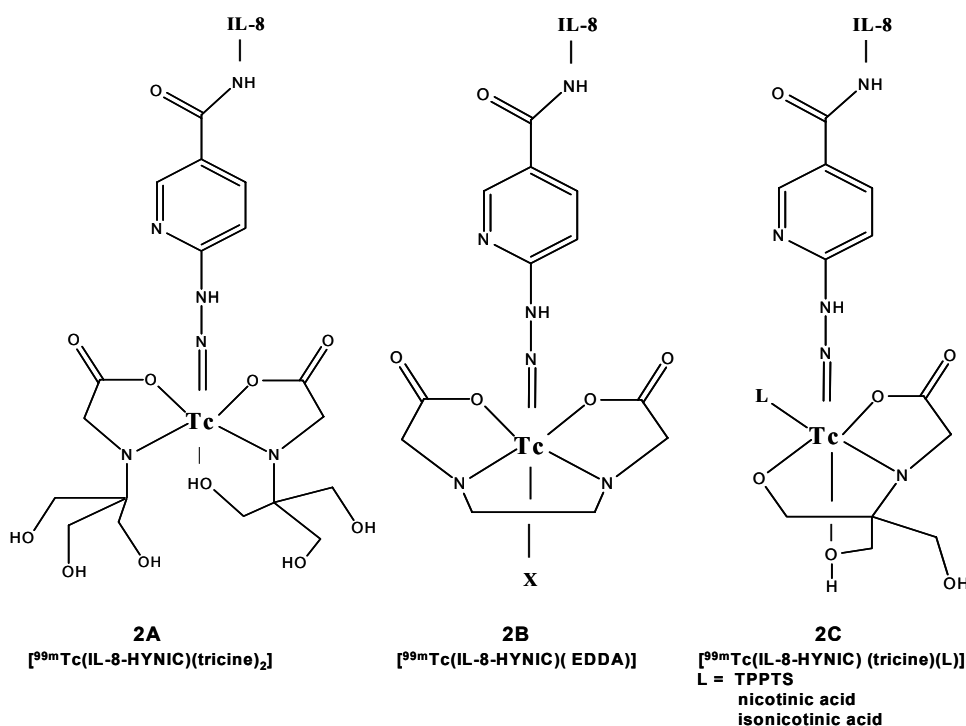
Figure 2. *Binary technetium complexes [^{99m}Tc(IL-8-HYNIC)(tricine)$_2$] [Fig. 2A] and [^{99m}Tc(IL-8-HYNIC)(EDDA)] [Fig. 2B]. The exact nature of the bonding between the IL-8-HYNIC-^{99m}Tc core and EDDA is unclear. X is a supposed additional monodentate ligand, such as Cl$^-$ (16). Ternary technetium complexes [^{99m}Tc(IL-8-HYNIC)(tricine)(L)] (L = TPPTS or nicotinic acid or isonicotinic acid) [Fig 2C].*

MATERIALS AND METHODS

Human recombinant IL-8 was kindly provided by Dr I. Lindley (Novartis, Vienna, Austria). Tricine (N-[Tris(hydroxymethyl)-methyl]glycine was purchased from Fluka, Buchs, Switzerland. EDDA (ethylenediaminediacetic acid), TPPTS (trisodium triphenyl-phosphine-3,3',3''-trisulfonate), nicotinic acid and isonicotinic acid were obtained from Sigma-Aldrich (St. Louis, MO).

Conjugation of HYNIC to IL-8

The propylaldehyde hydrazone of succinimidyl-hydrazinonicotinamide (HYNIC) was synthesized essentially as described by Abrams, Schwartz et al. (*11,13*). The IL-8-HYNIC conjugate was prepared as described previously (*8*). Briefly, in a 1.5 ml vial 4 µl 1 M $NaHCO_3$, pH 8.2 was added to 35 µl of IL-8 (4.8 mg/ml). Subsequently, a three-fold molar excess of HYNIC in 5 µl dry DMSO was added dropwise to the mixture. After incubation for five minutes at room temperature, the reaction was stopped by adding an excess of 200 µl 1 M glycine in PBS. To remove excess unbound HYNIC the mixture was extensively dialyzed against PBS (0.1-0.5 ml dialysis cell 3.5 MWCO, Pierce, Rockford, IL). Dialyzed samples of circa 5 µg IL-8-HYNIC were stored at –20 ^{0}C.

^{99m}Tc-labeling of HYNIC conjugated IL-8

i)Tricine as coligand

Tricine-$SnSO_4$-kits (0.2 ml) were prepared containing 20 mg tricine and 0.01 mg $SnSO_4$ in 0.2 ml PBS, pH 7.0. To prevent precipitation of stannous, $SnSO_4$ dissolved in 2 M HCl was added to a solution of tricine in PBS and the pH was adjusted to 7.0 with 1.0 M NaOH. A 0.2 ml tricine-$SnSO_4$-kit and 100 - 350 MBq $^{99m}TcO_4^-$ in saline were added to 5 µg thawed HYNIC-IL-8 and incubated at room temperature for 30 minutes.

ii) EDDA as coligand

10 µg thawed HYNIC-IL-8 was incubated with 0.5 ml of solution of EDDA (10 mg/ml in PBS), 100 - 350 MBq $^{99m}TcO_4^-$ in saline, and 10 µl of tin(II)solution (1.0 mg/ml $SnSO_4$ in nitrogen purged 0.1 N HCl) for 30 minutes at 70 ^{0}C.

iii) TPPTS/tricine as coligands

5 µg thawed HYNIC-IL-8 was incubated with 0.1 ml of solution of TPPTS (10 mg/ml in 25 mM benzoate buffer, pH 5.0), 0.3 ml of a tricine solution (100 mg/ml in 25 mM benzoate buffer, pH 5.0), 100 - 350 MBq $^{99m}TcO_4^-$ in saline, and 25 µl of tin(II)solution (1.0 mg/ml $SnSO_4$ in nitrogen purged 0.1 N HCl) for 30 minutes at 70 ^{0}C.

iv) Nicotinic acid/tricine as coligands

5 µg thawed HYNIC-IL-8 was incubated with 0.1 ml of solution of nicotinic acid (20 mg/ml in 25 mM benzoate buffer, pH 5.0), 0.4 ml of a tricine solution (100 mg/ml in 25

mM benzoate buffer, pH 5.0), 100 - 350 MBq $^{99m}TcO_4^-$ in saline, and 25 µl of tin(II)solution (1.0 mg/ml $SnSO_4$ in nitrogen purged 0.1 N HCl) for 30 minutes at 70 ^{0}C.

v) Isonicotinic acid/tricine as coligands

The labeling procedure was identical to the one above, using isonicotinic acid instead of nicotinic acid.

Chemical characterization of ^{99m}Tc-labeled IL-8 preparations

i) Radiochemical purity by ITLC

The radiochemical purity was determined by instant thin-layer chromatography (ITLC) on ITLC-SG strips (Gelman Laboratories, Ann Arbor, MI) with 0.1 M citrate, pH 6.0, as the mobile phase.

ii) Purification

Following the labeling reaction the reaction mixture was applied to a Sephadex G-25 column (PD-10; Pharmacia, Uppsala, Sweden) and eluted with PBS, 0.5% BSA to purify the radiolabeled IL-8 conjugate.

iii) Octanol/water partition coefficient as a measure of lipophilicity

In order to determine the lipophilicity of the various ^{99m}Tc-HYNIC-IL-8 preparations, approximately 100,000 cpm of a purified preparation was diluted with PBS to a total volume of three mL. An equal volume of octanol was added and the resulting biphasic system was mixed vigorously for one minute and gently for another ten minutes. The two phases were separated by centrifugation (10 min 2000 g) and 0.2 mL aliquots were taken from each layer. The partition coefficient was expressed as the ratio of cpm in the octanol phase to the cpm in the PBS phase.

iv) Stability in PBS and in serum

Following the labeling reactions, the five ^{99m}Tc-labeled IL-8 preparations were purified on a Sephadex G-25 column eluted with PBS without BSA. The stability of the purified preparations was monitored in PBS at room temperature and in human serum (1:5) at 37 ^{0}C for six hours. At several time points post incubation (0, 2, 4 and 6 h), samples were analyzed for the amount of free radiolabel using ITLC. Samples of the serum incubated preparations were diluted 1:5 in PBS with 0.5% BSA before applying to the ITLC-strip in order to prevent protein overload of the strips by serum proteins.

v) Analytical RP-HPLC

The radiochemical purity was determined by reversed phase high-performance liquid chromatography (RP-HPLC) (HP 1100 series, Hewlett Packard, Palo Alto, CA) using an Agilent Zorbax Stable Bond Analytical 4.6x250mm column (300SB-C8) at a flow rate of 1 mL/min. The radioactivity of the eluate was monitored using an in-line radiodetector (Flo-one Beta series A-100, Radiomatic, Meriden, CT).

Method 1: Solvents used: A) 0.01% TFA in water; B) 90% acetonitrile (ACN), 10% solution A. Gradient: from 70% A and 30% B to 45% A and 55% B in 30 minutes.
Method 2: Solvents used: A) 10 mM phosphate buffer pH 6.0; B) 100% ACN. Gradient: 0-3 min 0% B, 3-18 min 0%-30% B, 18-23 min 30% B, 23-33 min 30%-75% B, 33-34 min 70%-0% B.

Receptor binding assays

The receptor binding fraction (RBF) of the various ^{99m}Tc-HYNIC-IL-8 preparations was determined in receptor binding assays essentially as described by Lindmo et al. (*19*). The *in vitro* receptor binding assays were performed using Jurkat cells transfected with either IL-8 receptor 1 (CXCR1) or IL-8 receptor 2 (CXCR2), a kind gift of Drs. Loetscher and Baggiolini (Theodor Kocher Institute, University of Bern, Bern, Switzerland). The two cell lines were cultured at 37 °C in a humidified atmosphere of air/CO_2 (95:5) in RPMI 1640 medium (GIBCO, Gaithersburg, MD) containing 10% fetal calf serum and 1% glutamine, amino acids and pyruvate. The medium also contained Pen/Strep, 5×10^{-5} M of β-mercaptoethanol and 1.5 μg/ml puromycin for selection. Live Jurkat cells were centrifuged (5 min, 2000xg) and washed once with assay buffer (RPMI 1640, 0.5% BSA, 0.05% NaN_3). A series of serially diluted cell suspensions ($0.125-2 \times 10^8$ cells/ml) of cells bearing CXCR1 and a second series bearing CXCR2 were incubated with 10,000 cpm of a ^{99m}Tc-labeled IL-8 preparation in assay buffer. For each series, a duplicate of the lowest cell concentration was incubated in the presence of at least a 100-fold molar excess of unlabeled IL-8 to correct for nonspecific binding. After 30 minutes incubation at 37 °C, cells were centrifuged (5 min, 2000xg) and the radioactivity in the pellet (total bound radioactivity) was measured in a shielded well-type gamma counter (Wizard; Pharmacia, Uppsala, Sweden). The data were graphically analyzed in a modified Lineweaver-Burk plot: a double inverse plot of the conventional binding plot (specifically bound fraction versus cell concentration). The receptor-binding fraction at infinite cell excess was calculated by linear extrapolation to the ordinate.

Animal studies

Abscesses were induced in the left thigh muscle of 25 female New Zealand rabbits (2.4-2.7 kg) with $1-2 \times 10^{11}$ colony forming units (cfu) of *Escherichia coli* in 0.5 ml. During the procedure, rabbits were anaesthetized with a subcutaneous injection of a 0.6 ml mixture of fentanyl 0.315 mg/ml and fluanisone 10 mg/ml (Hypnorm, Janssens Pharmaceutical, Buckinghamshire, UK). The rabbits were divided into five groups of five animals (five animals per ^{99m}Tc-HYNIC-IL-8 coligand formulation). After 24 hours, when swelling of the muscle was apparent, the rabbits were injected with 10-40 MBq ^{99m}Tc-HYNIC-IL-8 (protein dose 0.2-2 μg) via the ear vein. Three rabbits out of each

group were used for gamma camera imaging. These rabbits were immobilized, placed prone on the gamma camera and images were recorded at 0, 2, 4 and 6 h p.i. with a single-head gamma camera (Orbiter, Siemens Medical Systems Inc., Hoffman Estates, IL) equipped with a parallel-hole low-energy all purpose collimator. Images were obtained with a 15% symmetrical window over the 140 keV energy peak of ^{99m}Tc. After acquisition of 100,000-300,000 counts, the images were digitally stored in a 256 x 256 matrix.

Scintigraphic images were analyzed quantitatively by drawing regions of interest (ROI) over the abscess and the uninfected contralateral thigh muscle (background). Abscess-to-background ratios were calculated.

After completion of the final imaging (6 h p.i.), all rabbits were killed with a lethal dose of sodium phenobarbital. Samples of blood, infected thigh muscle, uninfected contralateral thigh muscle, lung, spleen, liver, kidneys and intestines were collected. The dissected tissues were weighed and counted in a gamma counter. To correct for radioactive decay injection standards were counted simultaneously. The measured activity in samples was expressed as percentage of injected dose per gram tissue (%ID/g). Additionally, total uptake of the radiopharmaceutical (%ID) was determined for kidneys and abscesses. Abscess-to-contralateral muscle ratios and abscess-to-blood ratios were calculated.

Statistical analysis

All mean values are given as %ID/g, %ID or ratios ± 1 standard error of the mean (s.e.m.). The data were analyzed statistically using the one-way ANOVA with Dunnett's posttest (GraphPad Instat 3.00 Win 95, San Diego, CA, USA) comparing data for the EDDA, the TPPTS, the nicotinic and the isonicotinic preparation with data for the tricine preparation.

RESULTS

Radiolabeling and characterization of ^{99m}Tc-labeled IL-8 preparations

Table 1 shows the specific activities (MBq/μg), the octanol/water partition coefficients, the receptor binding fractions RBF for CXCR1 and CXCR2 receptors and the stability of the preparations in PBS and in serum. The five preparations will be denoted here by their main discriminating component: tricine, EDDA, TPPTS, nicotinic acid and isonicotinic acid.

Radiolabeling of each of the five HYNIC-IL-8 coligand formulations was rapid and straightforward, resulting in high specific activities of four out of five formulations.

With EDDA only a modest specific activity could be obtained (7 MBq/μg) as compared to tricine (15 MBq/μg), TPPTS (40 MBq/μg), nicotinic acid and isonicotinic acid (up to 80 MBq/μg). In our experience, the protection of the hydrazine moiety with propylaldehyde resulted in a HYNIC-conjugated IL-8 product with increased stability (at –20 ^{0}C): it could be labeled with high labeling efficiency over longer time periods (several months). Using the same tricine coligand formulation, the specific activity of ^{99m}Tc-labeled hydrazine protected HYNIC-IL-8 was found to be 15 MBq/μg as compared to 3 MBq/μg for ^{99m}Tc-labeled free hydrazine HYNIC-IL-8 previously reported (*8*). Both products started at similar labeling efficiencies but the free hydrazine HYNIC-IL-8 product showed a gradual decrease in labeling efficiency over 3 months even when stored at –20 ^{0}C.

The lipophilicity as reflected in the octanol/water partition coefficient was highest for the TPPTS preparation. This is in line with the HPLC-analyses (Fig. 3) and a significantly higher liver uptake of the TPPTS preparation as found in the biodistribution (Table 2) (see below).

All the formulations with the exception of TPPTS showed similar RBF-values for both receptors: between 45% and 55% for CXCR1 and between 36% and 45% for CXCR2. The TPPTS preparation showed predominantly nonspecific binding to the cells.

All radiolabeled IL-8 preparations were stable in human serum: after six hours of incubation at 37 ^{0}C the amount of free radiolabel was less than 10% as determined by ITLC. However, the same preparations diluted in PBS showed a large variation in stability: after six hours of incubation at room temperature the amount of free radiolabel was less than 10% for TPPTS and nicotinic acid only. For EDDA between 35 and 45% of the radiolabel was released, for isonicotinic acid between 55 and 60% and for tricine around 80%.

Table 1. *In vitro characteristics of five different ^{99m}Tc-labeled IL-8 coligand preparations.*

Coligand system	Specific activity	Octanol/water partition	RBF:		Stability:	
			CXCR1	CXCR2	PBS	serum
Tricine	15 MBq/μg	0.017	50-55%	40-45%	15-20%	>90%
EDDA	7 MBq/μg	0.0053	45-50%	36-42%	55-65%	>90%
TPPTS / tricine	40 MBq/μg	0.033	n.s.	n.s.	>90%	>90%
Nicotinic acid / tricine	80 MBq/μg	0.0046	46-50%	42-45%	>90%	>90%
Isonicotinic acid / tricine	80 MBq/μg	0.0049	50-54%	40-45%	40-45%	>90%

Specific activities (MBq/μg), octanol/water partition coefficients, receptor binding fractions RBF (%) to Jurkat cells transfected with either IL-8 receptor 1 (CXCR1) or IL-8 receptor 2 (CXCR2) and stabilities in PBS and in serum (labeling efficiencies after six hours of incubation). n.s. = predominantly non-specific cellbinding.
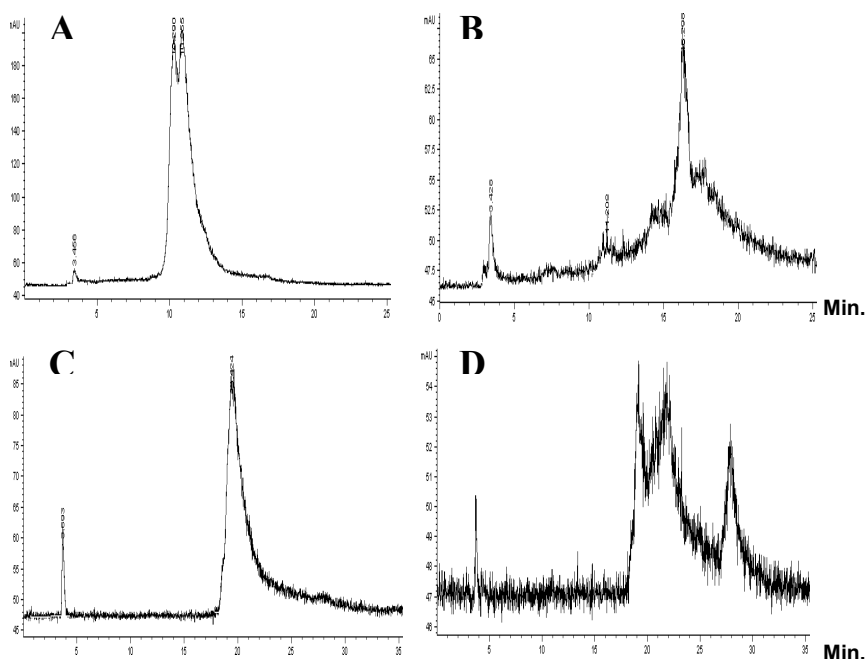
Figure 3. *Radio-HPLC chromatograms of ^{99m}Tc-labeled IL-8 with coligand tricine (Fig. 3A) and coligand TPPTS/tricine (Fig. 3B) using HPLC method 1. Radio-HPLC chromatograms of ^{99m}Tc-labeled IL-8 with coligand nicotinic acid/tricine (Fig. 3C) and coligand TPPTS/tricine (Fig. 3D) using HPLC method 2.*

The radio-HPLC chromatograms (method 1) of tricine and of TPPTS are presented in Figure 3A and 3B. The tricine chromatogram shows a pertechnetate peak with retention time of 3.5 minutes (<1.5%) and a doublet peak of [^{99m}Tc(IL-8-HYNIC)(tricine)$_2$] with retention times of 10.3 and 10.9 minutes. The radiochromatograms of the EDDA, the nicotinic acid and isonicotinic acid preparations showed essentially the same profile. Retention times of the doublet peak were found at 10.3 and 10.9 minutes for EDDA, at 10.3 and 11.0 minutes for nicotinic and at 10.4 and 11.1 minutes for isonicotic. The radiochromatogram of TPPTS turned out to be completely different: the major peak eluted much later (16.3 min) indicating the higher lipophilicity of the preparation. It might be the case that TPPTS interacts with the protein outside the protein-HYNIC-core. For instance, triaryl phosphines like TPPTS can reduce disulfide linkages, whereas maintenance of the disulfide structure is critical for IL-8 activity. The possibility of interaction of TPPTS with IL-8 outside the protein-HYNIC-core was investigated in an additional experiment. The radiochromatograms of a iodinated IL-8 preparation and the same preparation incubated at 70 ^{0}C for 30 minutes in the presence of an excess of TPPTS were compared (not shown). The ^{125}I-IL-8 radiochromatogram showed a profile similar to that of [^{99m}Tc(IL-8-HYNIC)(tricine)$_2$] with a doublet at 11.2 and 11.9 minutes. The radiochromatogram of ^{125}I-IL-8 incubated with TPPTS was similar, indicating that (chemical) interaction of TPPTS with IL-8 is not the principal determinant for the

aberrant *in vitro* behavior of [^{99m}Tc(IL-8-HYNIC)(tricine)(TPPTS)]. The characteristics of the mobile phase itself may explain the chromatographic behavior of TPPTS. The acidic sulfonate groups of TPPTS are partly protonated/deprotonated using the acidic TFA/ACN mobile phase of method 1. A mix of protonation states might be responsible for the broad and multispecies chromatogram of TPPTS. To investigate this, the acidic mobile phase of HPLC method 1 (diluted TFA/ACN) was replaced by a more pH neutral mobile phase in HPLC method 2 (phosphate buffer pH 6.0/ACN) in an additional experiment. The radio-HPLC chromatograms (method 2) of nicotinic acid (representative for tricine, EDDA and isonicotinic acid) and of TPPTS are presented in Figure 3C and 3D. The nicotinic acid chromatogram showed a pertechnetate peak with a retention time of 3.7 minutes and a single peak of [^{99m}Tc(IL-8-HYNIC)(tricine)(nicotinic acid)] with a retention time of 19.4 minutes. The chromatogram of TPPTS showed a pertechnetate peak with a retention time of 3.7 minutes and, again, a multispecies pattern with peaks at 19.0, 21.8 and 27.8 minutes, indicating a higher lipophilicity of the TPPTS preparation.

Table 2. *Biodistribution of five different ^{99m}Tc-labeled IL-8 coligand preparations in rabbits with E. coli infections at 6 h p.i. (% ID/g, % ID or ratios, mean values ±s.e.m.).*

%ID/g	tricine	EDDA	TPPTS/tricine	nicotinic/tricine	isonicotinic/tricine
blood	0.045±0.005	0.024±0.005	0.010±0.001	0.030±0.007	0.032±0.003
muscle	0.0044±0.0007	0.0037±0.0001	0.0022±0.0002	0.0024±0.0003	0.0027±0.0003
abscess	0.39±0.02	0.42±0.04	0.075±0.004	0.55±0.13	0.53±0.07
lung	0.36±0.03	0.39±0.03	0.17±0.04	0.31±0.07	0.33±0.02
spleen	0.86±0.10	1.00±0.15	1.01±0.04	0.83±0.20	0.98±0.13
kidney	2.59±0.14	2.86±0.17	2.69±0.11	1.75±0.14	1.91±0.13
liver	0.10±0.01	0.12±0.01	0.28±0.01	0.10±0.02	0.10±0.02
intestine	0.030±0.003	0.030±0.001	0.019±0.002	0.017±0.002	0.019±0.002
abscess/muscle	94±12	116±14	36±5	248±69	204±24
abscess/blood	9.6±2.0	22.3±5.6	7.6±0.8	18.6±3.5	17.0±2.3
%ID abscess	5.6±0.2	6.0±0.3	1.1±0.1	6.5±1.3	7.8±0.5
%ID kidneys	43±2	44±1	48±1	29±2	34±1

Animal studies

The coligand system clearly affected the biodistribution of ^{99m}Tc-labeled IL-8-HYNIC as showed in Table 2. Figure 4 summarizes the main *in vivo* characteristics: abscesss/muscle and abscess/blood ratios and the principal routes of clearance (renally and/or hepatobiliary) of the five preparations. As compared to tricine, the EDDA preparation cleared faster from the blood, resulting in a significantly lower percentage of residual activity in the blood (P<0.05) and (in combination with a similar muscle uptake) in a significantly higher abscess/blood ratio (P<0.05) (Fig. 4b). The biodistribution pattern of TPPTS was very different from the other ones. This preparation had a significantly reduced uptake in the abscess as well as in muscles, lungs and intestines (P<0.05). Blood clearance was much faster (P<0.001), presumably due to a more than twofold higher uptake by the liver (P<0.001). Lower lung uptake might suggest that there was less interaction of this preparation with leukocytes. The nicotinic acid and isonicotinic acid preparation had almost identical *in vivo* characteristics. In comparison to the tricine preparation a significantly lower percentage residual activity in the muscles (P<0.001 and P<0.05 resp.) and intestines (P<0.001) was found. Abscess/muscle ratio of the nicotinic acid preparation was significantly higher (P<0.05) (Fig. 4a). At 6 h p.i. kidney uptake was significantly lower for nicotinic and isonicotinic acid (P<0.001) (Fig. 4c). All preparations were excreted renally except for the TPPTS preparation which partly cleared via the hepatobiliary route (Fig. 4c and 4d).

The abscesses were clearly delineated on the images recorded from 2 h onwards for all preparations with the exception of TPPTS (Fig. 5). Quantitative analysis of the images indicated that the abscess/background ratios (A/B) improved with time for all preparations (Fig. 6). The A/B at 6 h p.i. of isonicotinic acid was significantly higher (P<0.05) than that of tricine and the A/B of TPPTS was significantly lower (P<0.05). Immediately after injection high kidney uptake was observed for all preparations, remaining prominent during the 6 h p.i. In addition to this, high liver uptake was seen on all the TPPTS images.
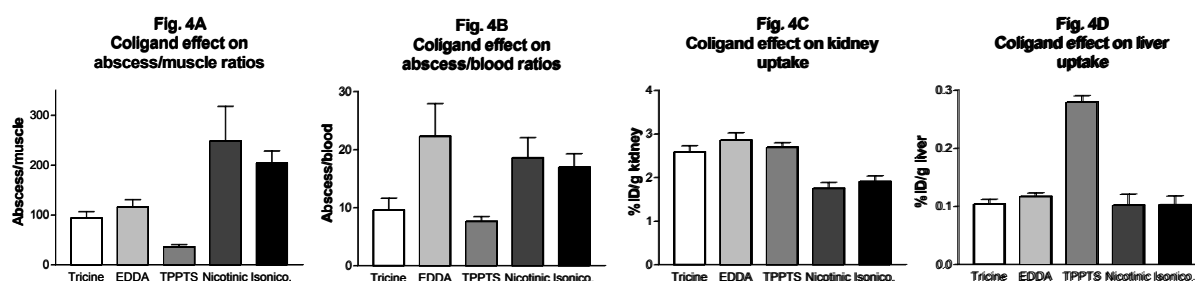

Figure 4. *Biodistribution ratios: Abscess/muscle (4A) and abscess/blood (4B). Principal routes of clearance: Renal (4C) and hepatobiliar (4D). The five different ^{99m}Tc-labeled IL-8 coligand preparations are named by their discriminating component (Nicotinic = nicotinic acid; Isonico. = isonicotinic acid). Data are taken from Table 2. The error bars indicate s.e.m.*

Figure 5. *Images of rabbits with an E.coli abscess in the left thigh muscle at 1 min, 2, 4 and 6 hr after injection of five different ^{99m}Tc-HYNIC-IL-8 coligand preparations.*

Figure 6. *The abscess/background ratios as determined by quantitative analysis of the images of rabbits with E.coli infection injected with five different ^{99m}Tc-HYNIC-IL-8 coligand preparations. The coligand preparations are named by their discriminating component (Nicotinic = nicotinic acid; Isonico. = isonicotinic acid). The error bars indicate s.e.m.*

DISCUSSION

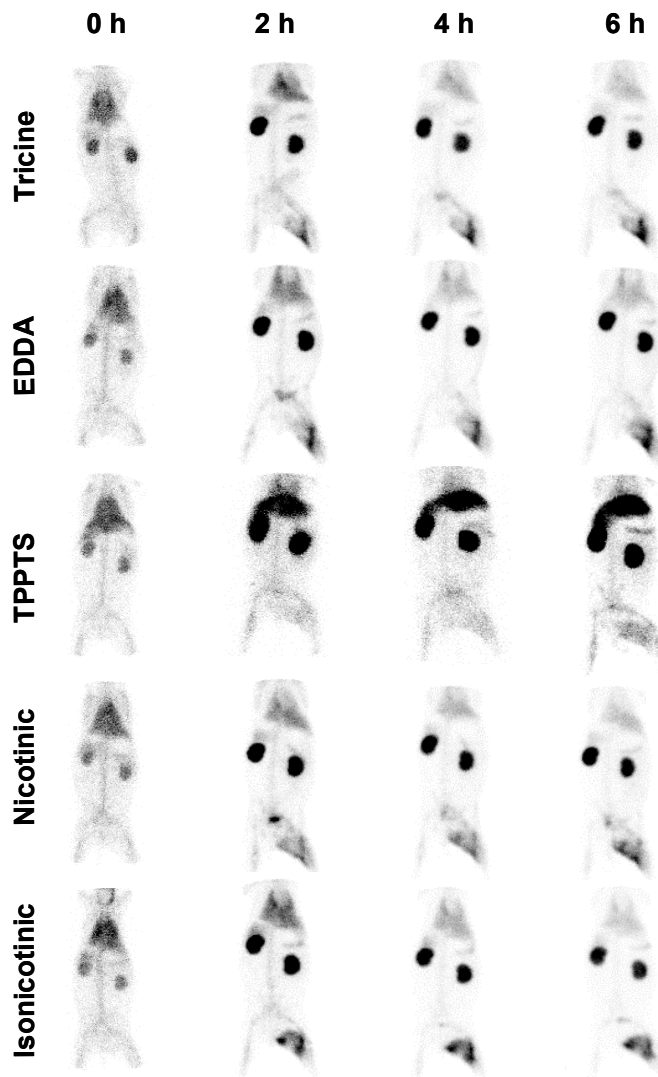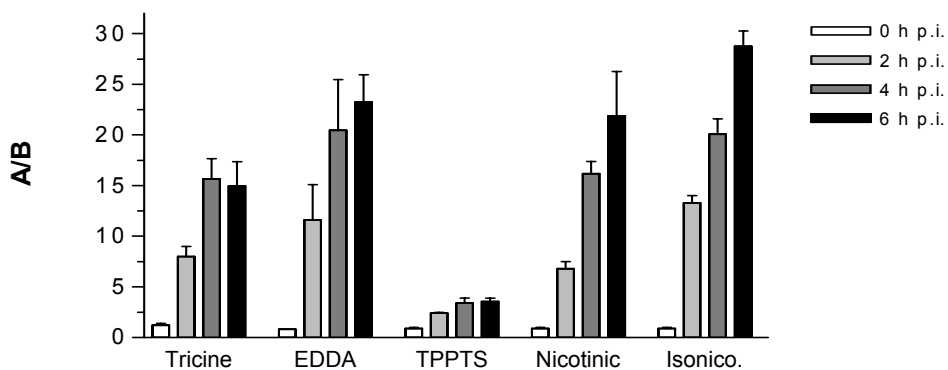In our previous study IL-8 was conjugated with HYNIC and subsequently labeled with ^{99m}Tc using tricine as coligand (*8*). This preparation showed excellent characteristics as an infection imaging agent, approaching the characteristics of the ideal radiopharmaceutical for infection imaging: rapid and high accumulation in infectious foci together with rapid clearance from the blood and the nontarget tissues. The leukocyte receptor binding capacity was still largely preserved.

The primary concern in using IL-8 *in vivo* is that it is a highly potent activator of neutrophils. Administration doses of micrograms of IL-8 per kg of body-weight in healthy rabbits caused a serious but transient neutropenia followed by a leukocytosis lasting several hours (*6*). These side-effects are undesirable for a diagnostic utility in routine clinical practice. Our research program focussed on increasing the specific activity of a radiolabeled IL-8 preparation in combination with preservation of the leukocyte receptor binding capacity. A first and most important reduction of the amount of biologically active material to be injected was achieved with ^{99m}Tc-HYNIC-IL-8 (with coligand tricine) as compared to radioiodinated IL-8: 1 μg/kg ^{99m}Tc-HYNIC-IL-8 versus 25 μg/kg ^{123}I-IL-8 (*8*).

In the present study the bifunctional coupling agent HYNIC was adopted again for labeling IL-8 with technetium. A decisive improvement was obtained with a slightly modified HYNIC formulation: the propylaldehyde hydrazone formulation instead of the free hydrazine formulation (*13*). Protection of the hydrazine group of HYNIC in HYNIC-conjugated IL-8 resulted in a product with improved long-term stability resulting in an increased labeling efficiency using the same coligand tricine as in previous studies.

Further improvement was sought in the exploration of various coligands. Liu and Edwards et al. have performed systematic studies on labeling a HYNIC-conjugated platelet glycoprotein receptor antagonist with ^{99m}Tc using various alternative coligand systems. The formulation with tricine was found to be unstable in solution, particularly under dilute conditions, and to exist in many isomeric forms (*16*). Increased stability of the complex and reduction of the number of isomers could be achieved by replacing tricine by other coligand systems like EDDA (16), tricine/TPPTS (*17*), tricine/(iso)nicotinic acid (*18*). High specific activities were obtained with all these preparations, though the labeling efficiency using EDDA as coligand was not as high as that using the other coligand systems. Decristoforo and Mather described the preclinical evaluation of ^{99m}Tc-labeled HYNIC-conjugated somatostatin analogues using tricine, EDDA and tricine in combination with nicotinic acid as coligands (*20-22*). These preparations showed preserved binding affinity for the somatostatin receptor. Again, reduced *in vitro* stability was found for the complex

using tricine only as coligand, resulting in higher blood levels. The preparation using tricine/nicotinic acid produced significant levels of activity in the gastrointestinal tract. The preparation using EDDA showed the most promising overall biodistribution profile, though labeling efficiency was considerably lower. Consequently, a first clinical study was performed with this EDDA formulation (*23*).

Our findings concerning stability of the coligand complexes are in line with the above reported results. The tricine formulation was found to be unstable *in vitro* under diluted conditions (PBS). Alternative coligand systems offered a solution towards more stable *in vitro* complexes, especially the TPPTS and the nicotinic acid preparations. In contrast, in serum all preparations proved to be equally stable. In a recent study Ono and coworkers have demonstrated that plasma proteins can stabilize ^{99m}Tc-labeled HYNIC conjugated Fab-fragments when tricine is used as coligand (*24*). The authors proposed that one of the tricine coligands is replaced by a plasma protein to generate higher molecular weight species that exhibit a slower blood clearance. This could explain not only the stability of the $[^{99m}$Tc(IL-8-HYNIC)(tricine)$_2$] complex in serum, but also the relatively slow blood clearance of the $[^{99m}$Tc(IL-8-HYNIC)(tricine)$_2$] complex. In addition, Ono et al. found that replacement of one tricine molecule by a nicotinic acid molecule in the reported complexes resulted in a stabilized ternary ligand system which demonstrated a significantly faster blood clearance. We arrived at similar conclusions for $[^{99m}$Tc(IL-8-HYNIC)(tricine)(nicotinic)].

It is rather surprising that the *in vitro* and *in vivo* properties of a 72 aminoacid protein as IL-8 could be greatly affected by a coligand. Introduction of the bulky coligand TPPTS resulted in a severe reduction of *in vitro* receptor binding affinity, a shift in lipophilicity of the total complex, significant lower abscess uptake and lower blood levels, and a much higher liver uptake. Quality of the images was poor as compared to the other coligand systems. Several explanations can be given for the marked change in biodistribution pattern of TPPTS. First, TPPTS is considerably larger than the other coligands (Fig. 1). TPPTS equals the size of approximately four aminoacid residues, whereas the other coligands have the size of just one aminoacid residue. Steric hindrance of the relatively bulky TPPTS group might, at least in part, explain the major impact on binding affinity towards the IL-8 receptors. Second, the charge of the complex is affected by the three TPPTS sulfonato groups. These sulfonato groups are expected to be deprotonated under physiologic conditions (*17*), which has a definite impact on the (local) electron distribution. We investigated the possibility of interaction of TPPTS with IL-8 outside the protein-HYNIC-core and compared the radiochromatograms of a iodinated IL-8 preparation with the same preparation incubated at 70 ^{0}C for 30 minutes in the presence of an excess of TPPTS. In this experiment the dramatic changes in RP-HPLC patterns were not seen as with the

^{99m}Tc-labeled IL-8 TPPTS preparation. Apparently, interaction of TPPTS with IL-8 outside the protein-HYNIC-core does not play a major role in explaining the aberrant *in vitro* and *in vivo* behavior of the TPPTS preparation.

The ^{99m}Tc-HYNIC-IL-8 EDDA preparation showed highly favorable characteristics for infection imaging. The preparation cleared relatively rapidly from the blood. EDDA is, however, not the coligand of choice for IL-8 for two reasons. First, the formulations using (iso)nicotinic acid generated higher abscess/muscle (and A/B) ratios. Second, the EDDA preparation had a relatively low specific activity. The specific activity of the tricine formulation was twice as high as that of EDDA, and with (iso)nicotinic acid specific activities were up to ten times higher (Table 1).

The most optimal characteristics for infection imaging were obtained with formulations using nicotinic acid or isonicotinic acid as coligands. With these coligands specific activities 20-fold higher than those previously reported with the unprotected hydrazine and with tricine as coligand could be achieved, without compromising the receptor binding capacity. Administration of doses as low as 70 ng/kg ^{99m}Tc-HYNIC-IL-8 (versus 1 μg/kg previously reported) will suffice for imaging procedures. Moreover, (iso)nicotinic acid showed the most favorable *in vivo* characteristics with abscess/muscle, abscess/blood and ROI derived abscess /background ratios being twice as high as those obtained with tricine. Its higher *in vitro* stability makes nicotinic acid the preferred coligand. Future experiments with ^{99m}Tc-HYNIC-IL-8 will exploit the advantages of the nicotinic acid/tricine coligand formulations. At low IL-8 protein doses of 70 ng/kg side effects are not to be expected in the human system. This opens the way to infection imaging studies in patients.

In conclusion, IL-8 can be rapidly, easily and efficiently labeled with ^{99m}Tc using (hydrazine protected) HYNIC as chelator and using various coligands. The most optimal infection imaging characteristics were found for formulations using nicotinic acid/tricine as coligands combining a high specific activity (up to 80 MBq/μg) and high *in vitro* stability with high abscess/muscle ratios (>200) and high abscess/background ratios (>20) *in vivo*. High quality images with clear delineation of infectious foci could be obtained within two hours after injection of the radiopharmaceutical. The low administration doses of 70 ng/kg ^{99m}Tc-HYNIC-IL-8 paves the way for infection imaging studies in patients.

ACKNOWLEDGMENTS

REFERENCES

1. Rennen HJ, Boerman OC, Oyen WJ, Corstens FH. Imaging infection/inflammation in the new millennium. *Eur J Nucl Med*. 2001;28:241-252.
2. Lee J, Horuk R, Rice GC, Bennett GL, Camerato T, Wood WI. Characterization of two high affinity human interleukin-8 receptors. *J Biol Chem*. 1992;267:16283-16287.
3. Cerretti DP, Kozlosky CJ, VandenBos T, Nelson N, Gearing DP, Beckmann MP. Molecular characterization of receptors for human interleukin-8, GRO/melanoma growth-stimulatory activity and neutrophil activating peptide-2. *Mol Immunol*. 1993;30:359-367.
4. Hay RV, Skinner RS, Newman OC, et al. Scintigraphy of acute inflammatory lesions in rats with radiolabelled recombinant human interleukin-8. *Nucl Med Commun*. 1997;18:367-378.
5. Gross MD, Shapiro B, Skinner RS, Shreve P, Fig LM, Hay RV. Scintigraphy of osteomyelitis in man with human recombinant interleukin-8. *J Nucl Med* 1996;37:25P.
6. Van der Laken CJ, Boerman OC, Oyen WJ, Van de Ven MT, Van der Meer JW, Corstens FH. The kinetics of radiolabelled interleukin-8 in infection and sterile inflammation. *Nucl Med Commun*. 1998;19:271-281.
7. Van der Laken CJ, Boerman OC, Oyen WJ, Van de Ven MT, Van der Meer JW, Corstens FH. Radiolabeled interleukin-8: specific scintigraphic detection of infection within a few hours. *J Nucl Med*. 2000;41:463-469.
8. Rennen HJ, Boerman OC, Oyen WJ, van der Meer JW and Corstens FH. Specific and rapid scintigraphic detection of infection with ^{99m}Tc-labeled Interleukin-8. *J Nucl Med*. 2001;42:117-123.
9. Gratz S, Rennen HJ, Boerman OC, Oyen WJ, Corstens FH. Rapid imaging of experimental colitis with ^{99m}Tc-Interleukin-8 in rabbits. *J Nucl Med*. 2001;42:917-923.
10. Gratz S, Rennen HJ, Boerman OC, Oyen WJ, Burma P, Corstens FH. ^{99m}Tc-Interleukin-8 for imaging acute osteomyelitis. *J Nucl Med*. 2001;42:1257-1264.
11. Abrams MJ, Juweid M, tenKate CI, et al. Technetium-99m-human polyclonal IgG radiolabeled via the hydrazino nicotinamide derivative for imaging focal sites of infection in rats. *J Nucl Med*. 1990;31:2022-2028.
12. Larsen SK, Solomon HF, Caldwell G, Abrams MJ. [99mTc]tricine: a useful precursor complex for the radio-labeling of hydrazinonicotinate protein conjugates. *Bioconjug Chem*. 1995;6:635-638.
13. Schwartz DA, Abrams MJ, Gladomenico CM and Zubieta JA. Certain pyridyl hydrazines and hydrazides useful for protein labeling. 1993; U.S. Patent 5,206,370.
14. Edwards DS, Liu S, Harris AR, Poirier MJ, Ewels BA. 99mTc-labeling of hydrazones of a hydrazinonico-tinamide conjugated cyclic peptide. *Bioconjug Chem*. 1999;10:803-807.
15. Babich JW, Fischman AJ. Effect of "co-ligand" on the biodistribution of 99mTc-labeled hydrazinonicotinic acid derivatized chemotactic peptides. *Nucl Med Biol*. 1995;22:25-30.
16. Liu S, Edwards DS, Looby RJ, Harris AR, Poirier MJ, Barrett JA, Heminway SJ, Carroll TR. Labeling a hydrazino nicotinamide-modified cyclic IIb/IIIa receptor antagonist with 99mTc using aminocarboxylates as coligands. *Bioconjug Chem*. 1996;7:63-71.
17. Edwards DS, Liu S, Barrett JA, Harris AR, Looby RJ, Ziegler MC, Heminway SJ, Carroll TR. New and versatile ternary ligand system for technetium radiopharmaceuticals: water soluble phosphines and tricine as coligands in labeling a hydrazinonicotinamide-modified cyclic glycoprotein IIb/IIIa receptor antagonist with 99mTc. *Bioconjug Chem*. 1997;8:146-154.
18. Liu S, Edwards DS, Harris AR. A novel ternary ligand system for 99mTc-labeling of hydrazinonicotinamide modified biologically active molecules using imine-N-containing heterocycles as coligands. *Bioconjug Chem*. 1998;9:583-595.
19. Lindmo T, Boven E, Cuttitta F, Fedorko J, Bunn PA. Determination of the immunoreactive fraction of radio-labeled monoclonal antibodies by linear extrapolation to binding at infinite antigen excess. *J Immunol Methods* 1984;72:77-89.
20. Decristoforo C, Mather SJ. Preparation, (99m)Tc-labeling, and in vitro characterization of hynic and N(3)S modified RC-160 and [Tyr3]-octreotide. *Bioconjug Chem*. 1999;10:701-702.
21. Decristoforo C, Mather SJ. Technetium-99m somatostatin analogues: effect of labelling methods and peptide sequence. *Eur J Nucl Med*. 1999;26:869-876.
22. Decristoforo C, Melendez-Alafort L, Sosabowski JK, Mather SJ. 99mTc-HYNIC-[Tyr3]-octreotide for imaging somatostatin-receptor-positive tumors: preclinical evaluation and comparison with 111In-octreotide. *J Nucl Med*. 2000;41:1114-1119.
23. Decristoforo C, Mather SJ, Cholewinski W, et al. 99mTc-EDDA/HYNIC-TOC: a new 99mTc-labelled radio-pharmaceutical for imaging somatostatin receptor-positive tumours; first clinical results and intra-patient comparison with 111In-labelled octreotide derivatives. *Eur J Nucl Med*. 2000;27:1318-1325.
24. Ono M, Arano Y, Mukai T, Uehara T, Fujioka Y, Ogawa K, Namba S, Nakayama M, Saga T, Konishi J, Horiuchi K, Yokoyama A, Saji H. Plasma protein binding of (99m)Tc-labeled hydrazino nicotinamide derivatized polypeptides and peptides. *Nucl Med Biol* 2001;28:155-164.

Addendum

Labeling method largely affects the imaging potential of interleukin-8

Huub J.J.M. Rennen, Otto C. Boerman,
Wim J.G. Oyen, Frans H.M. Corstens

We read with interest the paper by Gross et al. entitled "Imaging of human infection with ^{131}I-labeled recombinant human Interleukin-8" (1). The authors conducted a pilot study with ^{131}I-labeled IL-8 for detection of infection in patients. The data nicely showed that this IL-8 preparation could visualize infectious foci in patients with osteomyelitis and cellulitis. Furthermore, the agent appeared to be safe, since no significant side effects were observed upon i.v. administration. Apparently, the study was performed years prior to the present publication (2). In the meantime we studied several aspects related to labeling IL-8 for detection of infection.

We have shown that the labeling method used in this study is rather suboptimal for IL-8 and that substantial improvements can be obtained by using alternative labeling strategies. IL-8 was radioiodinated according to the chloramine-T method (3). This method results in iodination of the tyrosine residues similar to the iodogen method. We pointed out that the radioiodination method clearly affected the in vivo biodistribution of IL-8 (4). IL-8 radioiodinated via the Bolton-Hunter method, showed superior characteristics for infection imaging as compared to IL-8 radioiodinated via the iodogen method. In a rabbit model of E.coli induced soft tissue infection, abscess-to-background ratios as determined by ROI analysis of the images were 3 for ^{123}I-IL-8 (iodogen method) versus 13 for ^{123}I-IL-8 (Bolton-Hunter method) at 8 h p.i.. As pointed out by the authors themselves, labeling IL-8 with ^{123}I would have been a better choice instead of labeling with [131]I. The physical properties of ^{131}I limit spatial resolution.

The authors made the suggestion that IL-8 labeled with a radiometal instead of iodine may be preferable as infection imaging agent. Indeed, preclinical studies in our laboratory with ^{99m}Tc-labeled IL-8 showed excellent imaging characteristics for this preparation with abscess-to-background ratios up to 22 at 8 h p.i. (5). Studies in patients using ^{99m}Tc-labeled IL-8 are planned to evaluate the efficacy of this particular preparation to visualize inflammatory foci in humans.

REFERENCES

1. Gross MD, Shapiro B, Fig LM, Steventon R, Skinner RWS, Hay RV. Imaging of human infection with ^{131}I-labeled recombinant human Interleukin-8. *J Nucl Med* 2001;42:1656-1659.
2. Gross MD, Shapiro B, Skinner RS, Shreve P, Fig LM, Hay RV. Scintigraphy of osteomyelitis in man with human recombinant interleukin-8. *J Nucl Med* 1996;37:25P.
3. Hay RV, Skinner RS, Newman DC, Kunkel SL, Lyle LR, Shapiro B, Gross MD. Scintigraphy of acute inflammatory lesions in rats with radiolabelled recombinant human interleukin-8. *Nucl Med Commun* 1997;18:367-378.
4. Van der Laken CJ, Boerman OC, Oyen WJG, van de Ven MTP, van der Meer JWM, Corstens FHM. Radiolabeled interleukin-8: scintigraphic detection of infection within a few hours. *J Nucl Med* 2000;41:463-469.
5. Rennen HJJM, Boerman OC, Oyen WJG, van der Laken CJ, Corstens FHM. Specific and rapid scintigraphic detection of infection with Tc-99m-labeled interleukin-8. *J Nucl Med* 2001;42: 117-123.

Chapter 6

Rapid imaging of experimental colitis with
^{99m}Tc-interleukin-8 in rabbits

Stefan Gratz, Huub J. J. M. Rennen,
Otto C. Boerman, Wim J.G. Oyen, Frans H.M. Corstens

ABSTRACT

Radiolabeled autologous leukocytes (WBC) are the gold standard for imaging inflammatory bowel disease (IBD). For the rapid and adequate management of patients with IBD, there is need for a new agent, which is at least as good as radiolabeled WBC, but easier to prepare and without its inherent risks. In the present study, the potential of Interleukin-8 labeled with ^{99m}Tc via hydrazinonicotinamide (HYNIC) to image IBD was investigated in a rabbit model of acute colitis and compared to that of ^{99m}Tc-HMPAO-labeled granulocytes.

Methods: In rabbits with chemically-induced acute colitis, inflammatory lesions were scintigraphically visualized following injection of either IL-8 or purified granulocytes both labeled with ^{99m}Tc. Gamma camera images were acquired at 2 min, 1, 2 and 4 hrs p.i.. At 4 h p.i. the rabbits were killed, and the uptake of the radiolabel in the dissected tissues was determined. Furthermore, the dissected colon was imaged and the inflammatory lesions were scored macroscopically. For each affected colon segment, the colitis index (CI, affected colon-to-normal colon uptake ratio) was calculated and correlated to the macroscopically scored severity of inflammation.

Results: ^{99m}Tc-HYNIC-IL-8 visualized the colitis within 1 h p.i.. ^{99m}Tc-HYNIC-IL-8 images of the colonic abnormalities were more accurate, the intensity of uptake in the affected colon continously increased until 4 h p.i., whereas no further increase after 1 h p.i. was noticed scintigraphically for ^{99m}Tc-HMPAO-granulocytes. The uptake in the affected colon was much higher for IL-8 than for the radiolabeled granulocytes with the percentage injected dose per gram (%ID/g) 0.41 ± 0.04 and 0.09 ± 0.05 at 4 h p.i., respectively. With increasing severity, the CI at 4 h p.i. for ^{99m}Tc-HYNIC-IL-8 was 4.4 ± 0.6, 13.5 ± 0.5 and 25.8 ± 1.0; for granulocytes, the CI at 4 h p.i. was 1.5 ± 0.1, 3.4 ± 0.2 and 6.4 ± 0.5, respectively. The CI correlated with the severity of the inflammation (r=0.95, p<0.0001 for IL-8 and r=0.95, p<0.0001 for granulocytes).

Conclusion: Already within 1 h p.i. visualization of the extent of colonic inflammation in vivo was possible with ^{99m}Tc-HYNIC-IL-8. Within 2 h p.i. ^{99m}Tc-IL-8 allowed a good and at 4 h p.i. a meticulous evaluation of the severity of IBD. ^{99m}Tc-HMPAO-granulocytes were able to delineate the extent of IBD within 2 h p.i., whereas an accurate estimation of severity of inflammation was not possible. ^{99m}Tc-HYNIC-IL-8 is an inflammation imaging agent that showed promising results in this study. ^{99m}Tc-IL-8 can be prepared off-the-shelf and yields excellent imaging with high target / background ratios.

INTRODUCTION

The degree of activity of inflammatory bowel disease (IBD) may be difficult to evaluate because of the fluctuating episodes of relapses and remissions of acute colitis. A noninvasive method for monitoring the disease is needed to allow accurate therapeutic management of the patients during exacerbations of IBD. Various nuclear medicine diagnostic procedures have become available for evaluating the status of the diseased colon. The advantage of nuclear medicine procedures over conventional diagnostic modalities, such as planar radiography with barium is their ability to provide functional information and to allow an estimation of the degree of inflammatory activity in affected areas in the intestine, rather than to give more morphologically orientated information. The radiopharmaceutical of choice for imaging IBD at present is radiolabeled leukocytes. Unfortunately, the preparation has several disadvantages limiting its application (laborious, handling of possibly contaminated blood). Therefore, search for an agent, that is at least as good as radiolabeled-WBC, but easier to prepare, is needed.

IBDs with chronic character such as Crohn's disease are characterized by a high intestinal mononuclear cell infiltration (*1*). More acute IBDs, such as ulcerative colitis, are characterized by a strong neutrophil infiltration to the extracellular matrix of the colonic wall. Proinflammatory cytokines play an important role in the neutrophil recruitement of neutrophils into the colonic mucosa. Levels of these cytokines (IL-1β, IL-6, IL-8, and TNF-α) as well as neutrophils expressing receptors for these cytokines are markedly increased in active ulcerative colitis as compared to the normal noninflamed bowel tissue (*2*). In acute IBD, chemotactic factors generated in the mucosa attract neutrophils from the circulation into the inflammatory site and induce infiltration of neutrophils in the interstitial tissue, thus contributing to accumulation and activation of neutrophils in the infected mucosa (*3*). Since neutrophils express high affinity IL–8 receptors (0.3-4 nM) (*4-7*), radiolabeled IL-8 might prove useful for the imaging of acute IBD.

The scintigraphic imaging characteristics of radiolabeled IL-8 strongly depend on the procedure of labeling. Van der Laken et al. showed that ¹²³I-IL-8 labeled via the Bolton-Hunter method was clearly superior to ¹²³I-IL-8 labeled via the iodogen method, despite similar in vitro cell binding characteristics (*8*). Recently, we described the development of a ⁹⁹ᵐTc-labeled IL-8 preparation using HYNIC as a chelator (*9*). In rabbits with E. coli infection, absolute uptake of ⁹⁹ᵐTc-HYNIC-IL-8 in the soft tissue abscess was more rapid and higher than that obtained with the radioiodinated preparation, while abscess-to-muscle ratios reached values over 100 at 8 h p.i.(*9*). Furthermore, ⁹⁹ᵐTc-HYNIC-IL-8 showed a remarkably fast clearance from nontarget tissues.

We studied the performance of ^{99m}Tc-HYNIC-IL-8 in a well established animal model of acute inflammatory bowel disease (*10, 11*). ^{99m}Tc-HMPAO-labeled purified granulocytes were used as a reference agent in this study. The in vivo characteristics of ^{99m}Tc-HYNIC-IL-8 were compared in rabbits with chemically-induced colitis (*11*) to those obtained after administration of ^{99m}Tc-HMPAO-labeled purified granulocytes.

The aim of this study was twofold: a.) to determine the potential of ^{99m}Tc-HYNIC-IL-8 to visualize acute colitis in rabbits, and b.) to find the earliest imaging time point, that allows accurate diagnosis of acute colitis using this agent.

MATERIAL AND METHODS

Animal Model

In 10 female New Zealand white rabbits (weight 2.5 - 3 kg), acute colitis was induced as described previously with minor modifications (*12-14*). Briefly, animals were anesthetized with an intramuscular injection of a 0.7-ml mixture of fentanyl 0.315 mg/ml and fluanisone 10 mg/ml (Hypnorm, Janssen Pharmaceutical, Oxford, UK). After retrograde insertion of a flexible silicone tube, first 1 ml 50% ethanol followed by 1 ml 25 mg trinitrobenzene sulfonic acid (TNBS; Sigma Chemicals, St. Louis, MO) in 50% ethanol, and 3 ml 50% ethanol flush, was instilled in the colon at a 25 cm proximally of the anal sphincter. Forty-eight hours after induction of the colitis, the respective radiopharmaceuticals were injected via the ear vein. Experiments were performed in accordance with the guidelines of the local animal welfare committee. During the experiment, the rabbits were fasted. Water was provided ad libitum.

Radiopharmaceuticals

Preparation of HYNIC-conjugated IL-8: Human recombinant IL-8 was kindly provided by Dr I. Lindley (Novartis, Vienna, Austria). IL-8 was conjugated to hydrazino-nicotinamide (HYNIC) essentially as described by Abrams et al. (*15*). Briefly, in a 1.5 ml vial 1.5 µl 1 M NaHCO$_3$, pH 8.2 was added to 15 µl of IL-8 (5.7 mg/ml). Subsequently a three-fold excess of succinimidyl-hydrazinonicotinamide (S-HYNIC) in 5 µl dry DMSO was added dropwise to the IL-8 solution. After incubation at room temperature for 10 minutes, the reaction was stopped by adding 115 µl of 1.0 M glycine solution in PBS. Subsequently, 30 µl precooled PBS was added to a total volume of 170 µl. To remove excess unconjugated S-HYNIC, the mixture was extensively dialyzed against PBS (0.1-0.5 ml dialysis cell 3.5 MWCO, Pierce, Rockford, IL). Dialyzed samples of circa 7 µg IL-8-HYNIC were stored at –20 ^{0}C.

^{99m}Tc-labeling of HYNIC conjugated IL-8: Tricine-SnSO$_4$-kits (0.2 ml) were prepared containing 20 mg tricine (N-[Tris(hydroxymethyl)-methyl]glycine, Fluka, Buchs, Switzerland) and 0.01 mg SnSO$_4$ (Merck, Darmstadt, Germany) in 0.2 ml PBS pH 7.0. To prevent precipitation of stannous, SnSO$_4$ dissolved in 2 M HCl was added to a solution of tricine in PBS pH was subsequently adjusted with 1.0 M NaOH to 7.0.

For animal studies a 0.2 ml tricine-SnSO$_4$-kit and 0.5 ml 400 MBq ^{99m}TcO$_4^-$ in saline were added to 7 µg thawed HYNIC-IL-8 and incubated at room temperature for 30 minutes. Following the labeling reaction the reaction mixture was applied on a Sephadex G-25 column (PD-10; Pharmacia, Uppsala, Sweden) and eluted with 0.5 % BSA in PBS to purify the radiolabeled IL-8. The radiochemical purity was determined by instant thin-layer chromatography (ITLC) on ITLC-SG strips (Gelman Laboratories, Ann Arbor, MI) with 0.1 M citrate, pH 6.0, as the mobile phase. Each animal was injected with 18.5 MBq ^{99m}Tc labeled to 0.5 ml IL-8 solution.

Receptor binding assay

As previously described by Rennen et al. (9) the leukocyte receptor binding fraction of the ^{99m}Tc-IL-8 preparation was determined in an in vitro receptor binding assay. For this assay heparinized human whole blood (10 ml) was mixed with 2.5 ml 5% Dextran (Sigma, St. Louis, MO). After sedimentation of the red blood cell bulk during 1 h at room temperature, the remainder of the blood sample was washed in incubation buffer (1 mM NaH$_2$PO$_4$, 5 mM Na$_2$HPO$_4$, 140 mM NaCL, 0.5 mM MgCL$_2$, 0.15 mM CaCl$_2$, 0.5% HSA, pH 7.4) and centrifuged at 500xg for 20 min. The cell pellet was then resuspended in 7 ml incubation buffer and layered on 5 ml Ficoll-Hypaque (Pharmacia, Uppsala, Sweden), followed by centrifugation at 500xg for 20 min. The pellet was washed once and subsequently resuspended in incubation buffer. Afterwards, a series of serially diluted PMN suspensions (0.5 - 8 x 10^6 PMN/0.5ml) was incubated with 10,000 cpm of ^{99m}Tc-labeled IL-8 during 2 h at 37^0 C. A duplicate of the lowest cell concentration was incubated in the presence of a 100-fold molar excess of unlabeled IL-8 to determine the nonspecific binding. The radioactivity in the cell pellet (total bound activity) was measured in a shielded well-type gamma counter (Wizard, Pharmacia-LKB, Sweden).

The specific activity of ^{99m}Tc-IL-8 was 20 MBq/µg. The radiochemical purity of the radiopharmaceutical was higher than 95% after gel filtration as determined by ITLC. The receptor binding fraction of the ^{99m}Tc-IL-8 preparation was 65%.

^{99m}Tc-HMPAO-granulocytes

Carotid artery canulation was performed in one anesthetized donor rabbit. A total amount of 100 ml blood was carefully drawn into acid citrate dextrose-tubes (containing 7 ml acid citrate dextrose per 35 ml blood). The total leukocyte count of the donor rabbits was 7.1 x 10^9/L with approximately 50% granulocytes. Purification of granulocytes was performed according to the method described by Lillevang et al. (*16*) with minor modifications (*17*). Briefly, the blood was mixed with 0.1 volume of 6% dextran (Dextran 500, Pharmacia, Uppsala, Sweden) solution in 0.9% NaCl and allowed to settle for 1 h at room temperature. The leukocyte-rich supernatant was layered carefully on 1/3 volume of Nycoprep density medium (14.1% Nycodenz, 0.3% NaCl, 5 mM Tricine / NaOH pH 7.2, density = 1.077 g/ml, osmolality = 265 mOsm: Nycomed, Oslo, Norway) and centrifuged for 15 min at 600x g. The plasma above the mononuclear cells, the mononuclear band and the density medium above the granulocyte pellet were carefully removed. The pellet was washed with 5 ml of Hank's balanced salt solution (HBSS) with 10% autologous plasma and centrifuged for 10 min at 50xg. The cell pellet was resuspended in 1.5 ml HBSS, 10% rabbit plasma. Following this purification procedure the granulocyte purity was > 90% (*11*). 0.5 GBq freshly prepared ^{99m}Tc-HMPAO was added to the cell suspension. The cells were incubated at room temperature for 30 min and centrifuged for 10 min at 50xg. The pellet was resuspended in 5 ml of cell free autologous plasma. Labeling efficiency (Cell associated activity / total activity added) exceeded 80%. Functional integrity of labeled granulocytes was evaluated by their in vivo performance, including transit through the lungs, hepatic- and splenic uptake. A dose of 18.5 MBq ^{99m}Tc-labeled granulocytes was administered intravenously in each rabbit.

Gamma camera image acquisition and data analysis

Fourty-eight hours after induction of the colitis, five rabbits were intravenously injected through the ear vein with ^{99m}Tc-HYNIC-IL-8. Another group of five rabbits was injected with ^{99m}Tc-HMPAO-WBC. The rabbits were immobilized in a mold and placed prone on a gamma camera equipped with a parrallel-hole, low-energy all purpose collimator (Orbiter; Siemens Inc., Hoffman Estate, IL). Each rabbit was imaged at 2 min, 1 h, 2 h, and 4 h after injection. Images with 300,000 counts were acquired and stored in a 256 x 256 matrix.

After acquiring the final images, the rabbits were killed with an overdose of sodium phenobarbital and biodistribution of the radiolabeled radiopharmaceuticals was determined. After dissection, an image of the entire dissected colon was acquired (100,000 counts per image) using the same collimator and matrix. Blood was obtained by cardiac puncture. Tissues [lung, liver, spleen, kidney, small intestine, normal (ascending) colon and affected (transverse and descending) colon] were obtained. The

affected colon was divided in seven consecutive colonic segments of 5 cm each. The degree of inflammation of the colonic segments was scored macroscopically on an arbitrary scale (0= no visible abnormalities, 1= redness and wall thickening, 2= ulcers). The tissue samples were weighed and the radioactivity was measured in a shielded well-type scintillation gamma counter (Wizard, Pharmacia-LKB, Sweden). The stool and the intestinal wall of the inflamed and the noninflamed colon were separately analyzed and their average uptake was assessed. To correct for decay and to permit calculation of the uptake of the radiolabeled radiopharmaceuticals in each organ as a fraction of the injected dose, aliquots of 1% of the injected dose were counted simultaneously. The results were expressed as percent injected dose per gram (%ID/g). From these results, the colitis index (CI, affected-to-normal colon ratio) for each of the radiopharmaceuticals was calculated for each segment.

Statistical Analysis

All mean uptake values are given as %ID/g $\pm$ 1 s.e.m. For statistical analysis the Mann-Whitney test was performed and correlations were calculated by linear regression analysis: Spearman Rank correlation (GraphPad InStat 3.00 Win 95, GraphPad Software, San Diego, CA., USA). The level of significance was set at p < 0.05.

RESULTS

Two days after the retrograde installation of TNBS in all 10 rabbits severe mucosal alterations in the colon transversum and colon descendens were observed.

The scintigraphic images of the two radiotracers at 1, 2 and 4 h p.i. as well as the respective image of the dissected colon 4 h p.i. are shown in Figure 1. Both radiotracers showed focally increased uptake in the inflamed colon. Quantitative analysis of the scintigrams of ^{99m}Tc-HMPAO-granulocytes showed that the lung uptake decreased from 39 %ID to 17 %ID between 5 min and 1 h p.i.and that the hepatic uptake did not exceed 17 %ID at 2 h p.i., indicating that the ^{99m}Tc-labeling procedure had not compromised granulocyte function.

^{99m}Tc-HYNIC-IL-8 nicely delineated the inflamed colon as early as 1 h p.i. With ^{99m}Tc-HYNIC-IL-8 the extent of the inflammation in the colon was clearly visualized at 2 h p.i., while a further increase of uptake in the inflamed colon was observed until 4 h p.i. Whole-body images of the rabbit and images of the dissected colon clearly showed the focal ulcerations and the extent of the colonic inflammation .

1 h   2 h   4 h

^{99m}**Tc-HYNIC-IL-8**

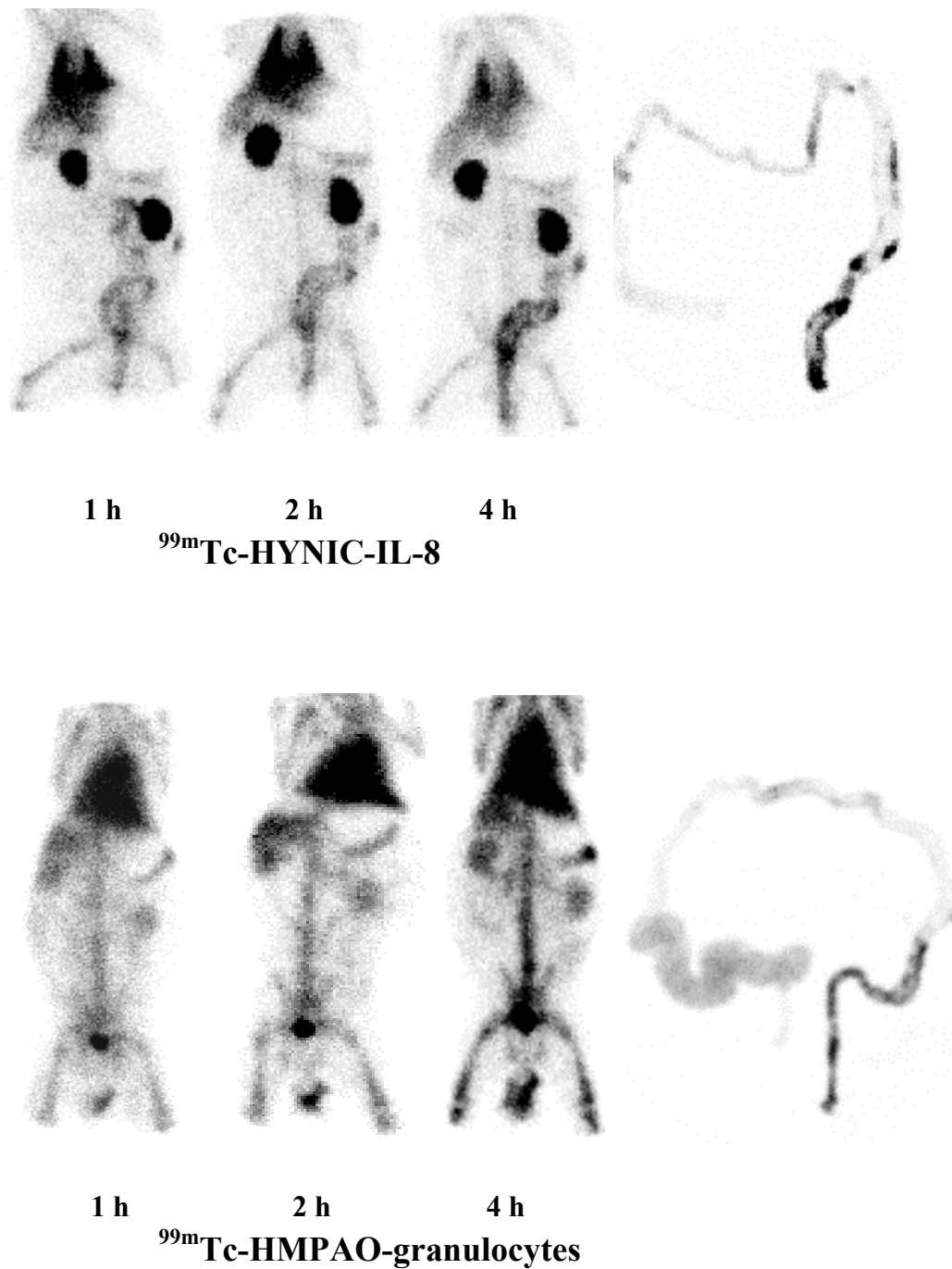**1 h   2 h   4 h**

^{99m}**Tc-HMPAO-granulocytes**

Figure 1: *Scintigraphic images of rabbits with experimental colitis, imaged at 1, 2, and 4 h after injection of ^{99m}Tc-HYNIC-IL-8 (upper panel) or ^{99m}Tc-HMPAO-granulocytes (lower panel) together with separate images of the dissected colons.*

Using ^{99m}Tc-HMPAO-granulocytes, images were less precise since uptake in the inflammatory foci was much lower at 2 h and 4 h p.i.. No nonspecific bowel uptake was apparent with either of the radiotracers until 4 h p.i.

The biodistribution data of ^{99m}Tc-HYNIC-IL-8 and ^{99m}Tc-HMPAO-granulocytes at 4 h p.i. are shown in Table 1. The uptake of ^{99m}Tc-HYNIC-IL-8 in the affected colon exceeded that of ^{99m}Tc-HMPAO-WBC by a factor of 4.5 (%ID/g 0.41 ± 0.04 for ^{99m}Tc-IL-8 and 0.091 ± 0.05 for ^{99m}Tc-HMPAO-WBC respectively) (p < 0.01). ^{99m}Tc-HYNIC-IL-8 showed higher CIs at 4 h p.i. compared to ^{99m}Tc-HMPAO-granulocytes (p<0.008 each grade) (Figure 2). The uptake of both radiotracers in the nonaffected colon was similarly low. Consequently, the affected colon / nonaffected colon uptake was much higher for ^{99m}Tc-HYNIC-IL-8 with 18.5±4.1 compared to 4.1±1.4 for ^{99m}Tc-HMPAO-granulocytes (p<0.01). With both radiotracers the CIs increased with the severity of inflammation. When evaluating the relative uptake in the affected segments for both radiopharmaceuticals, a positive correlation was observed between CIs and the severity of the macroscopic abnormalities (Figure 3). For ^{99m}Tc-HYNIC-IL-8 the correlation ($r^2 = 0.95$, p< 0.0001) was as strong as for ^{99m}Tc-HMPAO-WBC ($r^2 = 0.95$, p< 0.0001).

^{99m}Tc-IL-8 and ^{99m}Tc-HMPAO-granulocytes showed similar low uptake in the stool of the affected colon and the nonaffected colon as well as in the nonaffected colonic wall. The total uptake in the stool of the inflamed colon and the total uptake in the inflamed colonic wall and the ratios of the uptake in the inflamed colon and the nonaffected colon are shown in Table 1. The 4.5 fold higher %ID/g uptake of ^{99m}Tc-IL-8 compared with ^{99m}Tc-HMPAO in the affected colonic wall led to a affected colonic wall / affected stool ratio of 31:1 for ^{99m}Tc-IL-8 compared with a ratio of 4:1 for ^{99m}Tc-HMPAO-WBC, respectively.

Regarding the uptake at 4 h p.i. ^{99m}Tc-HYNIC-IL-8 showed significantly higher uptake for the different grades of inflammation (p<0.008) compared to those after injection of ^{99m}Tc-HMPAO-granulocytes. Focal uptake in the inflamed colon 4 h p.i. allowed a point-by-point comparison with macroscopic ulcerations at inflammatory sites. Furthermore, ^{99m}Tc-HYNIC-IL-8 had significantly lower blood levels than ^{99m}Tc-HMPAO-WBC (p<0.01) resulting in a lower uptake in background tissues (muscle, small intestine). In the kidneys, the uptake of the ^{99m}Tc-IL-8 was higher, probably due to tubular reabsorption of the peptide (*18, 19*). The uptake of both radiotracers in most other tissue samples was remarkably similar. Hepatic uptake of ^{99m}Tc-HYNIC-IL-8 was relatively low, reflecting the predominantly renal excretion of the tracer.

Table 1. *Biodistribution at 4 h p.i. of ^{99m}Tc-HYNIC-IL-8 and ^{99m}Tc-HMPAO-granulocytes in two groups of 5 rabbits with experimental colitis (%ID/g or %ID or ratios; mean ± s.e.m.)*

	^{99m}Tc-HYNIC-IL-8		^{99m}Tc-HMPAO-granulocytes
	%ID/g	**p***	**%ID/g**
Blood	0.044±0.001	<0.01	0.30±0.03
Lung	0.27 ±0.09		0.18 ±0.01
Spleen	0.67 ±0.22		0.83 ±0.12
Kidney	1.86 ±0.28	<0.01	0.20 ±0.01
Liver	0.091±0.005	<0.01	0.21 ±0.03
Small Intestine	0.032±0.003		0.024±0.003
Nonaffected colon tissue	0.025±0.004		0.023±0.008
Affected colon tissue	0.41 ±0.04	<0.01	0.091±0.055
Feces nonaffected colon	0.005±0.001	<0.05	0.015±0.003
Feces affected colon	0.013±0.002		0.022±0.007
	Ratio	**p***	**Ratio**
Affected/Nonaffected colon tissue	18.5±4.1	<0.01	4.1±1.4
	%ID	**(as % of total uptake in stool + colonic wall)**	**%ID** **(as % of total uptake in stool + colonic wall)**
Total uptake inflamed colonic wall	5.18	(87.3%)	1.70 (80.1%)
Total uptake stool in inflamed colon	1.07	(12.6%)	0.38 (19.8%)
Total uptake in stool + colonic wall	6.25	(100%)	2.08 (100%)

Mann-Whitney test =^{99m}Tc-HYNIC-IL-8 versus ^{99m}Tc-HMPAO-granulocytes. Biodistribution of 2 groups of 5 rabbits is shown at 4 h after injection. The level of significance was set at p < 0.05.
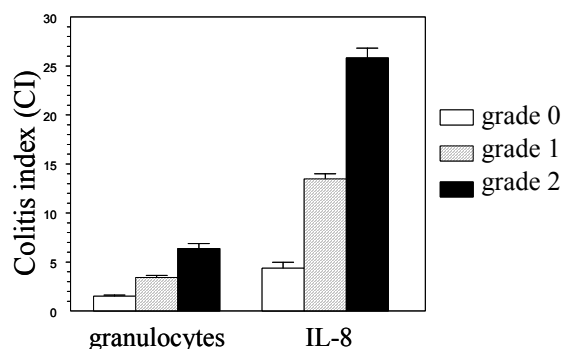
Figure 2.
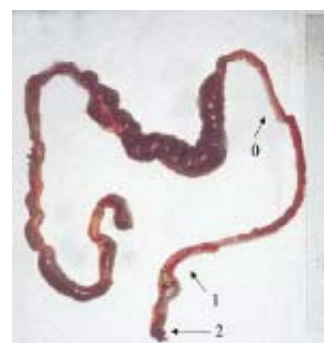
Figure 3.

Figure 2 (left): *Colitis Indices (affected-to-normal-colon-uptake ratio) of both radiotracers at 4 h p.i., compared with the severity of macroscopic inflammation (grade 0 = normal, grade 1 = inflammation, grade 2 = ulceration). Error bars represent s.e.m.*

Figure 3 (right):   *Macroscopic aspect of colonic mucosa in trinitrobenzene sulfonic acid induced acute colitis. Scoring of inflammation is shown: 0 = normal (colon descending), 1 = inflammation (sigmoide colon), 2 = ulceration (rectum).*

DISCUSSION

For nuclear medicine imaging of IBD, the use of radiolabeled leukocytes still is the "gold standard", because an accurate diagnosis of the extent and severity of IBD is possible. Several reports documented superior performance of ^{99m}Tc-HMPAO labeled white blood cells (WBC) compared with ^{111}In-labeled-WBC for the evaluation of colitis (*20-22*). When ^{99m}Tc-HMPAO-WBC are used, only early 2 h p.i. images (*23*) will allow specific imaging of IBD, because at later images nonspecific bowel uptake occurs. However, preparation of labeled autologous leukocytes is rather laborious and time consuming. Furthermore, there is a small but definite risk of personnel contamination or even inadvertent cross-contamination between patients (*24*). Therefore, there is an urgent need for a sensitive and specific imaging agent which can be prepared relatively easy.

Recently, we introduced ^{99m}Tc-HYNIC-IL-8 as such a new agent for scintigraphy. In a rabbit animal model with E. coli infection, ^{99m}Tc-HYNIC-IL-8 allowed rapid visualization of the abscess as early as 1 h p.i. with high and rapid accretion of the radiolabel in the abscess.

The present study was designed to test this new ^{99m}Tc-HYNIC-IL-8 agent for its potential to visualize inflammatory lesions in a more clinically relevant animal model and to determine the earliest time point for diagnosis of IBD. Diagnostic imaging was done until 4 h p.i., since no further increase of uptake in the affected colon can be expected with ^{99m}Tc-HMPAO-granulocytes (*11*). In the present study we demonstrated, that the ^{99m}Tc-HYNIC-IL-8 preparation already at 1 h p.i. visualized the affected colon. The images of ^{99m}Tc-HYNIC-IL-8 were superior to those of ^{99m}Tc-HMPAO-granulocytes at all time points. Uptake in the affected colon increased to a level of 4.5-fold higher than with ^{99m}Tc-HMPAO-granulocytes at 4 h p.i.. ^{99m}Tc-HYNIC-IL-8 scintigraphically allowed a visual differentiation between mild (grade 1 = inflammation) and severe (grade2 = ulceration) inflammation within 2 h postinjection. In addition, image quality improved even further from 2 h to 4 h p.i. (Figure 1). Such a differentiation between mild and severe inflammation was not possible with ^{99m}Tc-HMPAO-granulocytes. Ex vivo, very mild nonspecific uptake in the nonaffected colon was observed with ^{99m}Tc-HMPAO-granulocytes after dissection, whereas this was not seen with ^{99m}Tc-HYNIC-IL-8, apparently due to specific binding. The higher uptake in the affected colon for ^{99m}Tc-HYNIC-IL-8 was mainly due to an increased uptake of ^{99m}Tc-IL-8 in the inflamed colonic wall. This led to a more accurate visual differentiation between inflamed colon and noninflamed colon for ^{99m}Tc-HYNIC-IL-8 compared with ^{99m}Tc-HMPAO-granulocytes. Furthermore, in favor of the excellent performance of ^{99m}Tc-HYNIC-IL-8 was its low uptake in the cell

wall of the nonaffected colon and the low uptake in the stool of the affected colon. Apparently this seems to be an important reason for the dramatically better performance of ^{99m}Tc-HYNIC-IL-8 compared with ^{99m}Tc-HMPAO-granulocytes in scintigraphic imaging of chemically induced colitis. The CI index of ^{99m}Tc-HYNIC-IL-8 was fourfold higher than that of ^{99m}Tc-HMPAO-granulocytes, almost allowing a point-by-point comparison between whole-body images and macroscopical observations. In addition, as compared to labeled-granulocytes, labeled HYNIC-IL-8 has the important advantage of an easier preparation without the need for blood manipulation.

The moderate performance of ^{99m}Tc-HMPAO-granulocytes compared with ^{99m}Tc-HYNIC-IL-8 is remarkable (*23, 8*). This could be due to the longer circulating time and slower background clearance of labeled white blood cells or, more probable, to additional specific uptake of IL-8 in inflammatory cells. Since quantitative analysis of the scintigrams of ^{99m}Tc-HMPAO-labeled granulocytes demonstrated rapid initial lung transit and low hepatic uptake, there was no indication of deterioration of granulocyte function due to the labeling procedure.

Previous studies showed that ^{99m}Tc-HYNIC-IL-8 induced a transient neutropenia in rabbits (*8,9*). Actually, we aim to further increase the specific activity of the ^{99m}Tc-HYNIC-IL-8 preparation and to decrease the biological activity of the agent. Until now, going from ^{123}I to ^{99m}Tc as radiolabel, a 25-fold reduction of protein dose was achieved (*9*).

CONCLUSION

In this rabbit model the imaging performance of ^{99m}Tc-HYNIC-IL-8 appeared superior to that of ^{99m}Tc-HMPAO-labeled white blood cells in the evaluation of experimental colitis at all time points after injection of the respective radiotracers. Due to its high uptake in inflammatory foci in combination with minimal nonspecific bowel uptake, ^{99m}Tc-HYNIC-IL-8 allowed a point-by-point correlation with the macroscopical observation at 4 h p.i.. These results suggest that ^{99m}Tc-HYNIC-IL-8 potentially is an ideal imaging agent for accurate diagnosis of IBD, provided that the problem related to the biologic activity can be circumvented.

ACKNOWLEDGMENTS

REFERENCES

1. Signore A, Chianelli M, Annovazzi A et al.. 123I-interleukin-2 scintigraphy for in vivo assessment of intestinal mononuclear cell infiltration in Crohn's disease. J Nucl Med. 2000;41:242-249.
2. Murata Y, Ishiguro Y, Itoh J, Munakata A, Yoshida Y.The role of proinflammatory and immunoregulatory cytokines in the pathogenesis of ulcerative colitis. J Gastroenterol. 1995;30 Suppl 8:56-60.
3. Ina K, Kusugami K, Yamaguchi T et al.. Mucosal interleukin-8 is involved in neutrophil migration and binding to extracellular matrix in inflammatory bowel disease. Am J Gastroenterol. 1997;92:1342-1346.
4. Holmes WE, Lee J, Kuang WJ, Rice GC, Wood WI. Structure and functional expression of a human interleukin-8 receptor. Science. 1991;253:1278-1280.
5. Murphy PM, Tiffany HL. Cloning of complementary DNA encoding a functional human interleukin-8 receptor. Science. 1991;253:1280-1283.
6. Lee J, Horuk R, Rice GC, Bennett GL, Camerato T, Wood WI. Characterization of two high affinity human interleukin-8 receptors. J Biol Chem. 1992;267:16283-16287.
7. Cerretti DP, Kozlosky CJ, VandenBos T, Nelson N, Gearing DP, Beckmann MP. Molecular characterization of receptors for human interleukin-8, GRO/melanoma growth-stimulatory activity and neutrophil activating peptide-2. Mol Immunol. 1993;30:359-367.
8. Van der Laken CJ, Boerman OC, Oyen WJG, van de Ven MTP, van der Meer JWM, Corstens FHM. Radiolabeled interleukin-8: scintigraphic detection of infection within a few hours. J Nucl Med. 2000; 41: 463-469.
9. Rennen HJJM, Boerman OC, Oyen WJG, van der Meer JWM, Corstens FHM. Specific and rapid scintigraphic detection of infection with Tc-99m-labeled interleukin-8. J Nucl Med. 2001; 42: 117-123.
10. Oyen WJ, Boerman OC, Dams ET et al.. Scintigraphic evaluation of experimental colitis in rabbits. J Nucl Med. 1997;38:1596-1600.
11. Dams ET, Oyen WJ, Boerman OC et al.. Technetium-99m-labeled liposomes to image experimental colitis in rabbits: comparison with technetium-99m-HMPAO-granulocytes and technetium-99m-HYNIC-IgG. J Nucl Med. 1998;39:2172-2178.
12. Allgayer H, Deschryver K, Stenson WF. Treatment with 16,16'-dimethyl prostaglandin E2 before and after induction of colitis with trinitrobenzenesulfonic acid in rats decreases inflammation. Gastroenterology. 1989;96: 1290-1300
13. Percy WH, Burton MB, Rose K, Donovan V, Burakoff R. In vitro changes in the properties of rabbit colonic muscularis mucosae in colitis. Gastroenterology. 1993; 104: 369-376.
14. Kim HS, Berstad A. Experimental colitis in animal models. Scand J Gastroenterol. 1992; 27: 529-537.
15. Abrams MJ, Juweid M, tenKate CI, et al. Technetium-99m-human polyclonal IgG radiolabeled via the hydrazino nicotinamide derivative for imaging focal sites of infection in rats. J Nucl Med. 1990;31:2022-2028.
16. Lillevang ST, Toft P, Nilsen B. A method for isolating granulocytes from rabbit blood without causing activation. J Immunol Methods. 1994; 28;169:137-138.
17. Böyum A, Lövhaug D, Tresland L, Nordlie EM. Separation of leucocytes: improved cell purity by fine adjustments of gradient medium density and osmolality. Scand J Immunol. 1991; 34: 697-712.
18. Behr TM, Becker WS, Sharkey RM, Juweid ME, Dunn RM, Bair HJ, Wolf FG, Goldenberg DM. Reduction of renal uptake of monoclonal antibody fragments by amino acid infusion J-Nucl-Med. 1996; 37: 829-833.

19. Behr TM, Sharkey RM, Sgouros G et al.. Overcoming the nephrotoxicity of radiometal-labeled immuno-conjugates: improved cancer therapy administered to a nude mouse model in relation to the internal radiation dosimetry. Cancer. 1997; 80(12 Suppl): 2591-2610

20. Mansfield JC, Giaffer MH, Tindale WB, Holdsworth CD. Quantitative assessment of overall inflammatory bowel disease activity using labelled leucocytes: a direct comparison between indium-111 and technetium-99m HMPAO methods. Gut. 1995;37: 679-683.

21. Allan RA, Sladen GE, Bassingham S, Lazarus C, Clarke SE, Fogelman I.Comparison of simultaneous 99mTc-HMPAO and 111In oxine labelled white cell scansin the assessment of inflammatory bowel disease. Eur J Nucl Med. 1993;20:195-200.

22. Arndt JW, van der Sluys Veer A, Blok D et al.. Prospective comparative study of technetium-99m-WBCs and indium-111-granulocytes for the examination of patients with inflammatory bowel disease. J Nucl Med. 1993;34:1052-1057.

23. Lantto EH, Lantto TJ, Vorne M.Fast diagnosis of abdominal infections and inflammations with technetium-99m-HMPAO labeled leukocytes. J Nucl Med. 1991; 32: 2029-2034.

24. Lange JM, Boucher CA, Hollak CE et al.. Failure of zidovudine prophylaxis after accidental exposure to HIV-1. N Engl J Med 1990: 10;322:1375-1377.

Chapter 7

*^{99m}Tc-labeled IL-8 for scintigraphic
detection of pulmonary infections*

Huub J.J.M. Rennen, Chantal P. Bleeker-Rovers, Julliëtte E.M. van Eerd,
Cathelijne Frielink, Wim J.G. Oyen, Frans H.M. Corstens, Otto C. Boerman

ABSTRACT

Interleukin-8 (IL-8) is a chemotactic cytokine that binds with high affinity to receptors on neutrophils. Previously we showed that ^{99m}Tc-labeled IL-8 is highly suitable for scintigraphic imaging in rabbit models of intramuscular infection and of colitis. Here, ^{99m}Tc-labeled IL-8 was tested for its potential to image pulmonary infection in three experimental rabbit models: aspergillosis in immunocompromized rabbits, pneumococcal (gram-positive) pneumonia and *E.coli*-induced (gram-negative) pneumonia in immunocompetent rabbits.

Methods: A derivative of hydrazinonicotinamide (HYNIC) was used as bifunctional coupling agent to label IL-8 with ^{99m}Tc. Biodistribution of ^{99m}Tc-IL-8 was determined both by γ-camera imaging and by counting dissected tissues at 6 h after injection.

Results: ^{99m}Tc-IL-8 enabled early (within 2h after injection) and excellent visualization of localization and extent of pulmonary infection in each of the three experimental models of pulmonary infection. Uptake of ^{99m}Tc-IL-8 in the infected lung and the contralateral lung was (in percentage of the injected dose per gram of tissue ± SEM) at 6h after injection 0.63±0.12 and 0.12±0.02 (aspergillosis), 0.89±0.04 and 0.44±0.04 (pneumococcal pneumonia) 1.53±0.12 and 0.36±0.06 (*E.coli* pneumonia), respectively. In the *E.coli* model, uptake of ^{99m}Tc-IL-8 in the focus of infection even exceeded uptake in the kidneys, the main clearing organs.

Discussion: ^{99m}Tc-IL-8 offers many advantages over the conventionally used radiopharmaceuticals to image pulmonary infection, ^{67}Ga-citrate and radiolabeled leukocytes, i.e.: rapid and easy preparation, short time span between injection and imaging, low radiation burden and most importantly: clear delineation of the infectious foci.

INTRODUCTION

Adequate diagnosis of infection presents a major challenge to the clinician. Early and accurate detection of infection is crucial to enable adequate treatment. In cases suspected of pulmonary infection, chest X-ray and computed tomograpy (CT) provide high-quality anatomic information. However, early stages of pulmonary infection, in the absence of structural changes in the lungs, are difficult to diagnose by these methods. Moreover, scar tissue formation may complicate the interpretation of the images. Also, in immunosuppressed patients with pneumonia, chest X-ray findings are often minimal or even absent. An alternative approach for detection of pulmonary infection is radionuclide imaging. Scintigraphic imaging does not depend on structural

changes in the lung induced by the presence of the invaded microorganisms, but on physiologic changes in the lung as induced by these microorganisms. Therefore, radionuclide imaging can be complementary to the conventional anatomic imaging modalities.

In the United States, ^{67}Ga-citrate, ^{111}In- and ^{99m}Tc-labeled leukocytes are the only approved radiopharmaceuticals for imaging of infection. ^{67}Ga-citrate binds, once injected intravenously, to circulating transferrin. This complex extravasates at the site of infection due to the locally enhanced vascular permeability (1). There are several shortcomings in the use of ^{67}Ga-citrate that limit its clinical application. For instance, this radiopharmaceutical has unfavorable imaging characteristics (long physical half-life and high energy gamma photons), causing poor image quality and high radiation absorbed doses (2). Moreover, the interval between injection and imaging is relatively long (several days).

Techniques using isolated leukocytes, labeled either with ^{111}In or ^{99m}Tc, have been introduced in the seventies and eighties of the past century (3-6) and are generally adopted in nuclear medicine as techniques for infection imaging. Ex vivo labeling requires the withdrawal of blood from the patient, purification of leukocytes, labeling and reinjection of the radiolabeled cells. Radiolabeled leukocytes can be used to image infection due to the fact that leukocytes, even after ex-vivo labeling, have the capacity to migrate to the inflamed area. Disadvantages of this approach are, among others, a laborious preparation (3 hours) and handling of potentially contaminated blood (7). These have stimulated investigators to search for alternative methods that would allow labeling of leukocytes in the circulation. Instead of isolating the white blood cells from a patient and labeling the cells ex vivo, new methods now aim to label white blood cells in vivo.

Radiolabeled Interleukin-8 (IL-8) is an interesting candidate to replace radiolabeled leukocytes by in vivo labeling of neutrophils. Neutrophilic granulocytes are known to express two types of Interleukin-8 (IL-8) receptors, CXCR1 and CXCR2, abundantly (8). IL-8 binds these receptors with high affinity (0.3-4 nM) (9-12). Recently, we described the development of a ^{99m}Tc-labeled IL-8 preparation using hydrazino-nicotinamide (HYNIC) as a bifunctional coupling agent (13). This preparation showed good characteristics for imaging of infection and inflammation (13-15).

In the present study, ^{99m}Tc-labeled IL-8 was tested for its potential to image pulmonary infection. Three different experimental rabbit models were introduced in order to simulate a broad range of clinically relevant applications: aspergillosis in immunocompromized rabbits, Pneumococcal pneumonia and *E.coli*-induced pneumonia in immunocompetent rabbits. Invasive pulmonary aspergillosis is an

important cause of infectious morbidity and mortality in patients with granulocytopenia following chemotherapy. *Streptococcus pneumoniae* is a representative of the group of gram-positive bacteria and is the leading cause of community-acquired pneumonia. *E.coli*-induced pneumonia is an example of a pneumonia caused by gram-negative bacteria and is frequently encountered as a nosocomial infection. Severe *S.pneumoniae* and *E.coli* pneumonia infections have significant morbidity and mortality rates.

METHODS

Human recombinant IL-8 was kindly provided by Dr I. Lindley (Novartis, Vienna, Austria). Tricine (N-(Tris(hydroxymethyl)-methyl)glycine was purchased from Fluka (Buchs, Switzerland), nicotinic acid from Sigma-Aldrich (St. Louis, MO).

Conjugation of HYNIC to IL-8

The propylaldehyde hydrazone of succinimidyl-hydrazinonicotinamide (HYNIC) was synthesized essentially as described previously (16,17). The IL-8-HYNIC conjugate was prepared as described previously (13,18). Briefly, in a 1.5 ml vial 5 μl 1 M NaHCO$_3$, pH 8.2 was added to 35 μl of IL-8 (5 mg/ml). Subsequently, a three-fold molar excess of HYNIC in 5 μl dry DMSO was added dropwise to the mixture. After incubation for five minutes at room temperature, the reaction was stopped by adding an excess of glycine (200 μl, 1 M in PBS). To remove excess unbound HYNIC the mixture was extensively dialyzed against PBS (0.1-0.5 ml dialysis cell 3,500 molecular weight cut-off, Pierce, Rockford, IL). Dialyzed samples of circa 8 μg IL-8-HYNIC were stored at –0020 ^{0}C.

Technetium-99m labeling of HYNIC conjugated IL-8

To a thawed sample of 8 μg IL-8-HYNIC was added 0.2 ml of a solution of tricine and nicotinic acid (125 mg/ml and 12.5 mg/ml respectively, in PBS, adjusted to pH 7.0 with 2M NaOH), 20 μL of a freshly prepared tin (II) solution (10 mg SnSO$_4$ in 10 ml nitrogen-purged 0.1 N HCl) and 400 MBq ^{99m}TcO$_4^-$ in saline. The mixture was incubated at 70 ^{0}C for 30 minutes. The radiochemical purity was determined by instant thin-layer chromatography (ITLC) on ITLC-SG strips (Gelman Laboratories, Ann Arbor, MI) with 0.1 M citrate, pH 6.0, as the mobile phase. Following the labeling reaction the reaction mixture was diluted with PBS, 0.5% BSA to a concentration of 40 MBq/ml, ready for i.v. administration in the rabbits. A description of an extensive in vitro characterization (HPLC, stability, receptor binding assays) has been given elsewhere (18).

Animal studies

All animal experiments were carried out in accordance with the guidelines of the local animal welfare committee. Female New Zealand White rabbits weighing 2.3-2.8 kg were used in these experiments. Animals were housed individually and fed standard laboratory chow and water ad libitum.

Pulmonary infection models

Pulmonary aspergillosis.

Induction of aspergillosis was based on the animal model described by Groll *et al.* with a few modifications (19). Four female New Zealand White rabbits received injections of Cytarabine (Onco-Tain®, Faulding Pharmaceuticals, Brussels, Belgium) to reduce their neutrophil counts. Cytarabine was administered daily intravenously (25 mg/kg ~ 525 mg/m^2) on day –4 through –1 prior to the injection of ^{99m}Tc-IL-8. At day –3, after the second dose of cytarabine, the inoculation of *Aspergillus fumigatus* was performed. *A. fumigatus* was isolated from an immunocompromized patient positively diagnosed with aspergillosis. Before inoculation animals were sedated with a subcutaneous injection of 0.7 ml Hypnorm® (Fentanyl 0.315 mg/ml + Fluanisone 10 mg/ml) (Janssen Pharmaceutical, Buckinghamshire, UK). The rabbits were anesthetized with a mixture of isoflurane, nitrous oxide and oxygen and placed on the surgical table. The inoculum of $1x10^8$ conidia in 250 µL of phosphate buffered saline (PBS) was given intra-tracheally into the left lung, together with 50 µL of 5% Evans blue dye (Sigma-Aldrich, Zwijndrecht, Netherlands) via a syringe attached to a polyethyleen 0.76*1.22 mm catheter (Maxxim Medical, Oss, Netherlands).

Pneumococcal pneumonia and E.coli induced pneumonia.

Pneumonia was installed in female New Zealand White rabbits one day before injection of ^{99m}Tc-IL-8. The animals were sedated and anesthetized as described above. Four rabbits were inoculated intra-tracheally with $1x10^9$ CFU of *Streptococcus pneumoniae* and four rabbits with $1x10^9$ *E.coli* together with 50 µL of 5% Evans blue dye as described above.

Scintigraphic imaging of rabbits with pulmonary infection

20 MBq ^{99m}Tc-labeled IL-8 (0.4 µg protein, 0.5 ml) was injected via the ear vein in rabbits with aspergillosis two days after installation of pulmonary aspergillosis and in rabbits with *S.pneumoniae* and *E.coli* pulmonary infection one day after induction of pulmonary infection (four rabbits in each group). Three rabbits out of each group were randomly selected and used for gamma camera imaging. These rabbits were immobilized in a mold, placed prone on the gamma camera and images were acquired at 1-5 min, 2, 4 and 6 h p.i. with a single-head gamma camera (Orbiter, Siemens Medical

Systems Inc., Hoffman Estates, IL) equipped with a parallel-hole low-energy all purpose collimator. Images were obtained with a 15% symmetrical window over the 140 keV energy peak of ^{99m}Tc. After acquisition of 200,000-300,000 counts, the images were digitally stored in a 256 x 256 matrix. Scintigraphic images were analyzed quantitatively by drawing regions of interest (ROI) over the affected region of the left lung (=target, T) and a similar region over the contralateral unaffected right lung (=background, BGr). Target-to-background ratios (T/BGr) were calculated.

After completion of the final imaging session (6 h p.i.), all rabbits were killed with a lethal dose of pentobarbital (Euthesate®, Ceva Sante Animale, Naaldwijk, The Netherlands). Samples of blood, muscle, affected lung, unaffected contralateral lung, spleen, liver, kidneys and intestines were collected. The dissected tissues were weighed and the activity in the samples was measured in a gamma counter. To correct for radioactive decay injection standards were counted simultaneously. The measured activity in samples was expressed as percentage of injected dose per gram tissue (%ID/g). Affected-lung-to-control-lung ratios and affected-lung-to-blood ratios were calculated.

For comparison, two rabbits with pneumococcal pneumonia were imaged with ^{67}Ga-citrate (Mallinckrodt, Petten, Netherlands), using the same gamma camera as above equipped with a parallel-hole medium energy collimator. Images were acquired at 1-5 min, 2, 4, 6 and, additionally, 24 h after injection of 18 MBq of ^{67}Ga-citrate.

For histological examination, samples of affected and unaffected lung were fixed in formalin and embedded in paraffin. 5 μm sections were cut and stained with hematoxylin-eosin (HE) and/or Grocott's methenamine silver (aspergillosis only) for light microscopic examination.

Statistical analysis

All mean values are expressed as %ID/g, %ID or ratios ± 1 standard error of the mean (SEM). Data were analyzed statistically using the one-way ANOVA test with Tukey-Kramer multiple comparisons posttest (GraphPad Instat 3.00 Win 95, San Diego, CA, USA).

RESULTS

99mTc-labeling of IL-8

The radiochemical purity of the 99mTc-IL-8 preparation exceeded 98%, as determined by instant thin-layer chromatography, excluding the need for further purification, in line with our previous findings (18). The specific activity of the 99mTc-IL-8 preparations used in these studies was high, approximately 50 MBq per microgram IL-8.

Animal studies

Pulmonary infection models.

Cytarabine treatment of rabbits in the aspergillosis group resulted in an average reduction of total white blood cell counts of 61% ± 7%. Histological examination revealed the presence of abundant A.fumigatus conidia in lung tissue and a moderate leukocyte infiltration similar to what was found in our rat aspergillosis model (20). Massive leukocyte infiltration in infected lung tissue in both pneumococcal pneumonia and *E.coli* induced pneumonia was observed.

Scintigraphic imaging of pulmonary infection in rabbits.

Figure 1 shows the scintigrams acquired between 0 and 6 h after injection of 99mTc-IL-8. The pulmonary infections were clearly delineated in all three models. Images acquired immediately after injection occasionally showed the affected lung area as a photopenic area: High uptake of 99mTc-IL-8 in the contralateral unaffected lung and relatively low uptake in the affected part of the lung, resulting in a photopenic area (see arrow, figure 1), suggesting that the affected area is less well perfused and accumulation of 99mTc-IL-8 in the focus of infection occurs in the first hours after injection.

Quantitative analysis of the images as shown in Figure 2 showed that the Target-to-Background (T/Bgr: affected lung to nonaffected lung) ratios improved with time in all models of pulmonary infection up to 3.4 ± 0.3 in the aspergillosis model, 3.2 ± 0.5 in the *S.pneumoniae* model and 4.5 ± 0.25 in the *E.coli* model. These values were not significantly different.

The biodistribution of 99mTc-IL-8 in the three rabbit models of pulmonary infection is presented in Table 1. 99mTc-IL-8 cleared faster from the blood in rabbits with aspergillosis as compared to rabbits with *S.pneumoniae* or *E.coli* infection, resulting in a significantly lower percentage of residual activity in the blood at 6 h p.i. (P<0.01). Uptake of 99mTc-IL-8 in the contralateral healthy lung lobe was lowest in the aspergillosis model (P<0.01). Uptake of the radiolabel in the infected lung was similar in the aspergillosis and the *S.pneumoniae* model. The uptake in the infected lung in the

	1-5 min	2 h	4 h	6 h after injection
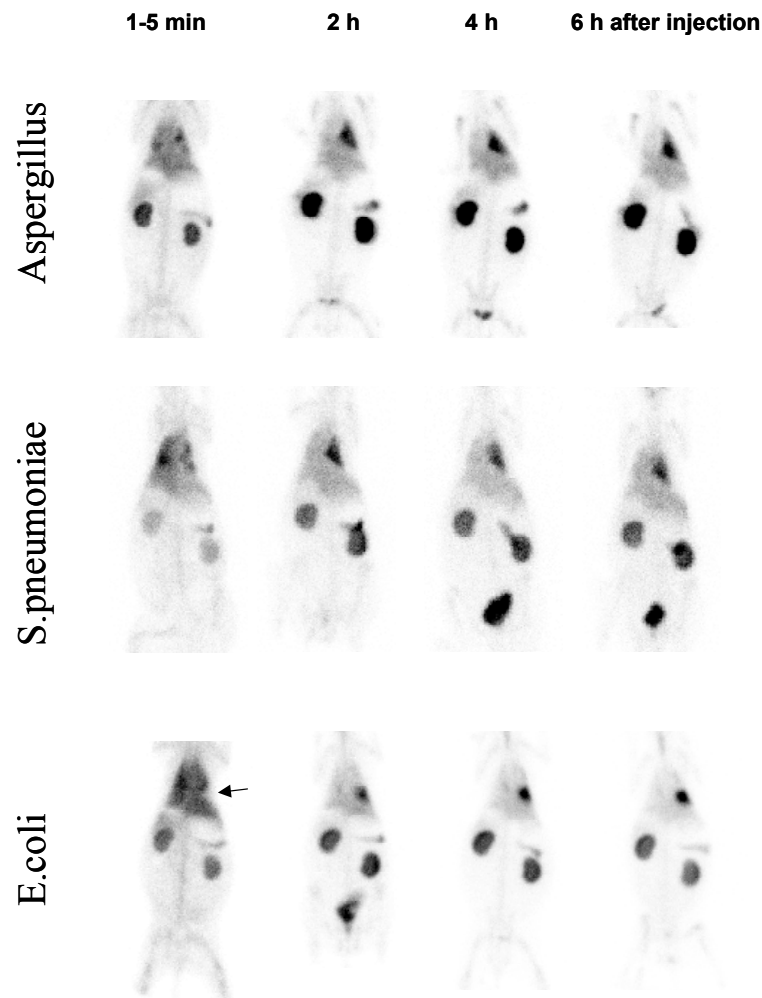
Figure 1. *Images of rabbits with pulmonary infection in the left lung at 1-5 min, 2, 4 and 6 h after injection of 99mTc-IL-8. Typical example of aspergillosis (upper row), pneumococcal pneumonia (second row) and E.coli induced pneumonia (third row). An arrow in the 1-5 min E.coli infection image indicates a remarkable photopenic area in the affected part of the lung.*

E.coli model surpassed the uptake in the other models in this area (P<0.01). In the aspergillosis model the uptake in the spleen was significantly lower than in the *S.pneumoniae* model (P<0.05). Kidneys were the main clearing organs in all three models and kidney uptake was highest in the aspergillosis model (P<0.05). In the *E.coli* model, the uptake in the infected lung was even higher than uptake in the kidneys. Figure 3 summarizes uptake of ^{99m}Tc-IL-8 in (affected and nonaffected) lungs and spleen. Physiologic uptake of ^{99m}Tc-IL-8 in nonaffected lungs was threefold lower in immunocompromized rabbits with aspergillosis than in immunocompetent rabbits with *S.pneumoniae* or *E.coli* infection. Spleen uptake was twofold higher in immunocompetent rabbits.

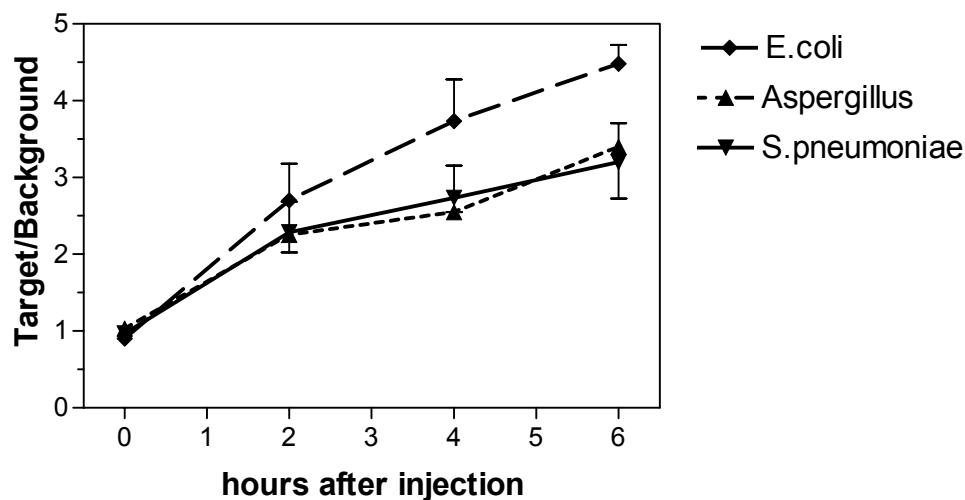***Figure 2.*** *Target-to-Background (affected lung to nonaffected lung) ratios from quantitative analysis of the images of rabbits with pulmonary infection at 1-5 min, 2, 4 and 6 h after injection of ^{99m}Tc-IL-8.*

Table 1. *Biodistribution of ^{99m}Tc-IL-8 in three rabbit models of pulmonary infection (four rabbits per model) at six hours after injection. Values are expressed as percentages of the injected dose per gram tissue (%ID/g) ± one standard error of the mean or as ratios thereof.*

	Aspergillosis	**S.pneumoniae**	**E.coli**
blood	**0.0069** ± 0.0022	**0.041** ± 0.008	**0.035** ± 0.007
muscle	**0.0010** ± 0.0002	**0.0032** ± 0.0009	**0.0020** ± 0.0001
lung abscess	**0.63** ± 0.12	**0.89** ± 0.04	**1.53** ± 0.12
lung control	**0.12** ± 0.02	**0.44** ± 0.04	**0.36** ± 0.06
spleen	**0.56** ± 0.18	**1.31** ± 0.18	**1.16** ± 0.20
kidney	**1.56** ± 0.08	**1.09** ± 0.09	**1.25** ± 0.04
liver	**0.059** ± 0.006	**0.069** ± 0.013	**0.083** ± 0.012
intestine	**0.010** ± 0.001	**0.013** ± 0.001	**0.015** ± 0.001
lung abscess/control	**5.5** ± 1.6	**2.1** ± 0.2	**4.4** ± 0.4
lung abscess/blood	**66** ± 11	**26** ± 8	**50** ± 10
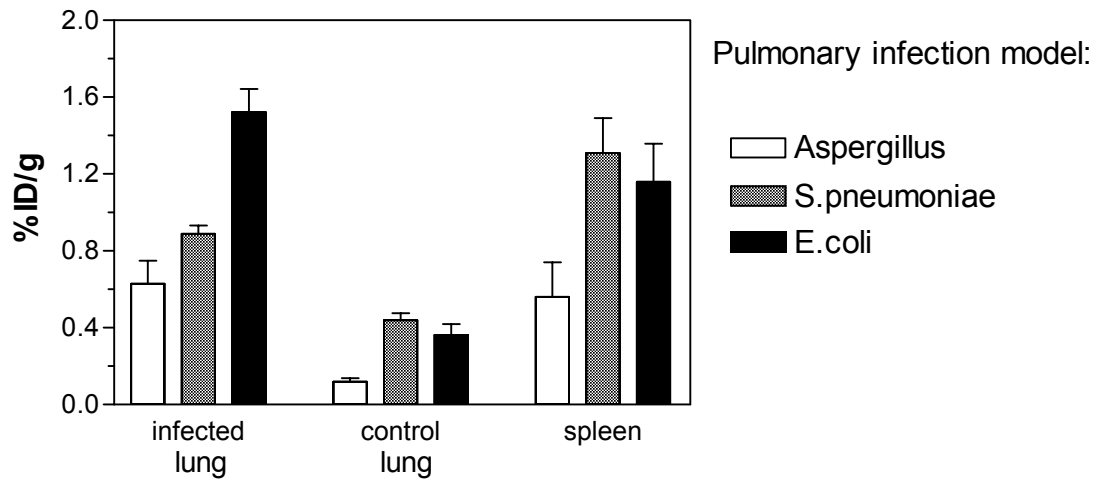
Figure 3. *Uptake of* ^{99m}Tc*-IL-8 at six hours after injection in tissues with a high natural abundancy of neutrophils lung (infected and control non-infected) and spleen in three different rabbit models of pulmonary infection. Values are expressed as percentages of the injected dose per gram tissue (%ID/g) ± one standard error of the mean.*

Figure 4 shows for comparison scintigraphic images of a rabbit with pneumococcal pneumonia after injection of ^{67}Ga-citrate, illustrating the rather suboptimal characteristics of this radiopharmaceutical.

Figure 4. *Scintigraphic images of a rabbit with pneumococcal pneumonia in the left lung at 1-5 min, 2, 4, 6 and 24 h after injection of* ^{67}*Ga-citrate.*

DISCUSSION

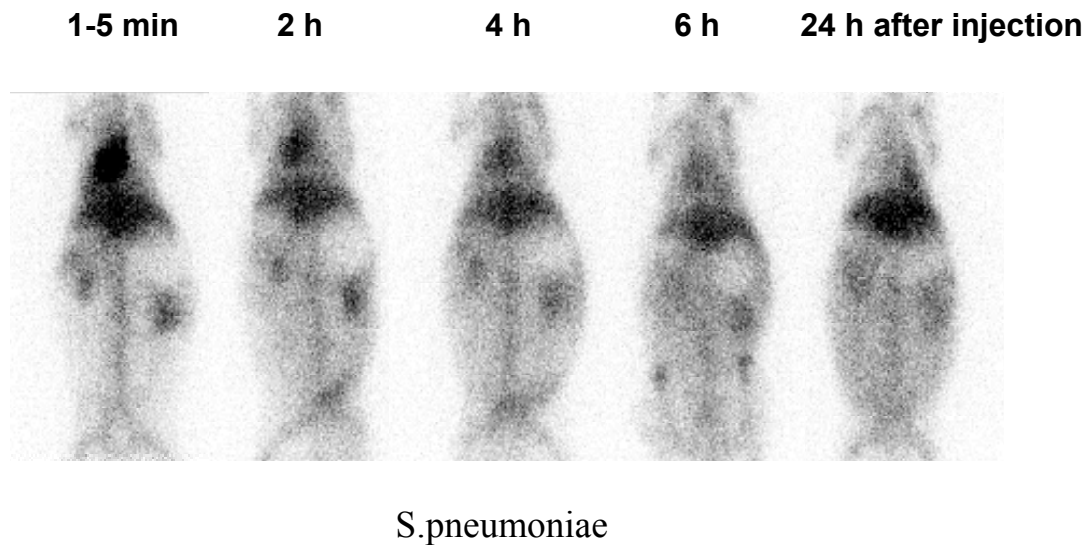^{99m}Tc-IL-8 has favorable characteristics as an infection imaging agent: rapid accumulation in target tissue and rapid clearance from blood and non-target tissues. The activity is mainly cleared via the kidneys, which is an advantage over hepatobiliary clearance: high activity in liver and bowel would have made this agent less suitable for imaging of the abdominal region. This study in particular showed the suitability of ^{99m}Tc-IL-8 to delineate infectious foci in rabbits with pulmonary infection.

In previous studies with ^{99m}Tc-IL-8 (13,18) and with radioiodinated IL-8 (21), a diffuse and initially high physiologic uptake of radiolabeled IL-8 was seen in the lungs. Therefore there was concern about the suitability of ^{99m}Tc-IL-8 to image foci of infection in the chest. High uptake in the lungs, immediately after i.v. administration of ^{99m}Tc-IL-8, has been ascribed to the biologic, agonistic effects of IL-8 on neutrophils (22-25). Circulating neutrophils pass through the narrow pulmonary capillary bed. Under nonstimulating conditions, there is already a delay in the pulmonary microvascular transit of neutrophils, relative to erythrocyte transit (26,27). Cell deformability plays a crucial role in transit time. IL-8 treated neutrophils showed a transient increase in F-actin, which reduces cell deformability. A marked and rapid reduction of cell deformability could result in immediate retention of the neutrophils in the microvasculature of the lungs. It has been shown that cell deformability recovers within minutes following exposure to IL-8.

The initially high physiologic uptake of ^{99m}Tc-IL-8 in the lungs did not hamper the visualization of infectious foci in the lungs, for two reasons. In the first place, clearance of radioactivity from the lungs was relatively fast. Secondly, ^{99m}Tc-IL-8 accumulated in the infected lung to a relatively high degree. The uptake in the lungs changed dramatically in the first hours after injection of ^{99m}Tc-IL-8. Immediately after injection of ^{99m}Tc-IL-8, uptake in the noninfected lung was often higher than in the infected lung, resulting in a relatively photopenic area in the affected part of the lung on the scintigrams. In contrast, images acquired at 2 h after injection showed a reversal: a clearly positive image of the affected area and a strongly reduced uptake in noninfected lung tissue. Although the activity in the background was higher in the pulmonary infection models than in our previous studies in the muscular infection model, this is compensated by a stronger signal from the target. Residual activity (as expressed in percentage of the injected dose per gram of tissue) in infected tissue ranged from 0.63 ± 0.12 to 1.53 ± 0.12 in pulmonary infection, as compared to 0.55 ± 0.13 in intramuscular infection (18). In the aspergillosis model, the relatively modest uptake in the affected lung was balanced by low uptake of the radiolabel in the unaffected lung, being about one third of the lung background activity in the other pulmonary infection models and the models of intramuscular infection as well.

We have selected three different experimental models of pulmonary infection in order to cover a broad range of (clinical) applications of ^{99m}Tc-IL-8 in detection of pulmonary infection. First, we studied a rabbit model of invasive pulmonary aspergillosis that would reflect conditions encountered in patients with profound granulocytopenia after e.g. chemotherapeutic treatment. Even if the underlying disorder (e.g., tumor) has resolved completely, the aspergillosis may persist. Despite aggressive antifungal therapy, the mortality from pulmonary aspergillosis in these patients remains high, illustrating the need for early and accurate diagnosis. In this study, ^{99m}Tc-IL-8 proved to be a useful diagnostic tool for pulmonary aspergillosis. As ^{99m}Tc-IL-8 binds to receptors expressed on neutrophils, the use of this radiopharmaceutical might encounter its limitations in diagnosing pulmonary aspergillosis in deeply neutropenic conditions. We found in our aspergillosis model lower physiologic uptake of ^{99m}Tc-IL-8 in neutrophil abundant organs such as lung and spleen as compared to infection models with normal neutrophil counts. A significant reduction of background signal in unaffected lung tissue resulted in a good visualization of the infectious foci in the affected lung. However, in persistent, deeply neutropenic conditions, i.e., in a severe paucity of target cells for ^{99m}Tc-IL-8, this new tool may meet its limitations as an infection imaging agent. Clinical trials with this new radiopharmaceutical are planned and will reveal whether ^{99m}Tc-IL-8 can be used to image patients with deep neutropenia.

Two more experimental models of pulmonary infection were included in this study. Pneumococcal and also *E.coli*-induced pneumonia in previously healthy individuals is in most cases easily detected by chest X-ray. Diagnosing these infections in patients with pre-existent lung disease is more difficult. Conventional techniques such as chest X-ray and CT have difficulty in distinguishing residual anatomic changes due to cured processes from active infection. Since IL-8 scintigraphy shows physiologic changes only, it should be able to differentiate scar tissue from active infection in such patients. Early diagnosis and prompt treatment of active infection, especially in patients with pre-existent lung disease, will result in earlier recovery and may reduce mortality in these patients. ^{99m}Tc-IL-8 showed to be very efficacious in visualizing foci of pulmonary infection in experimental models of Pneumococcal and *E.coli* induced pneumonia. Uptake of ^{99m}Tc-IL-8 in affected and nonaffected lungs and in the spleen was higher in immunocompetent rabbits in these two models than in immunocompromized rabbits in the aspergillosis model. These results strongly suggest a relationship between numbers of neutrophils in spleen and lung tissue and uptake of ^{99m}Tc-IL-8. IL-8-receptors are preferentially expressed on neutrophils and high uptake of ^{99m}Tc-IL-8 is seen in neutrophil abundant organs as lung and spleen. As a result, in immunocompromized rabbits, with lower levels of IL-8-receptor expressing cells, physiologic uptake of ^{99m}Tc-IL-8 in these organs is lower. Higher uptake of ^{99m}Tc-IL-8 by the kidneys and a lower level of residual activity in the blood might be explained by the fact that a larger percentage of ^{99m}Tc-IL-8 in immunocompromized rabbits is not

bound to target cells (neutrophils) and unbound ^{99m}Tc-IL-8 is fastly cleared by the kidneys.

^{99m}Tc-IL-8 offers several advantages over the most commonly used radiopharmaceuticals for infection imaging, ^{67}Ga-citrate and radiolabeled leukocytes (28). The radionuclide ^{99m}Tc is preferred over ^{67}Ga because of its virtually ideal physical characteristics (short half life, ideal energy, low radiation burden), its cost-effectiveness and general availability (2). [67]Ga has a longer physical half-life and high energy gamma radiations, causing high radiation absorbed doses and generating images of lower resolution. Generally, ^{67}Ga-citrate shows relatively slow pharmacokinetics. As a consequence, a long interval between injection of the radiopharmaceutical and imaging is required. Typically, ^{67}Ga-imaging is performed between 48 and 72 h p.i. In imaging rabbits using ^{99m}Tc-IL-8, a 2 h interval between injection and imaging was sufficient. In humans, slower pharmacokinetics can be expected, but diagnostic images within 4 h after injection in patients should be possible.

^{99m}Tc-IL-8 offers many advantages over radiolabeled leukocytes. Preparation of ^{99m}Tc-IL-8 is easy and rapid, ready within 30 minutes and with no need for further purification, whereas preparation of labeled leukocytes, be it with either ^{111}In or ^{99m}Tc, is cumbersome, time-consuming and not possible in granulocytopenic patients (2). The procedure of taking blood from a patient, purification of the leukocytes and labeling of these cells takes a trained technician approximately 3 hours. Cells should be handled cautiously in order to preserve their capacity to migrate to the inflamed area upon reinjection. In addition, the need to handle potentially contaminated blood could lead to transmission of blood-born pathogens such as HIV (7) and presents serious risks to both personnel and patient. The convenient method of labeling leukocytes in vivo with ^{99m}Tc-IL-8 reflects the traditional method of labeling leukocytes ex vivo, with all the advantages of the new method mentioned above.

CONCLUSION

Imaging of a variety of pulmonary infections with ^{99m}Tc-IL-8 proved to be feasible and offers many advantages over the conventionally used tools in nuclear medicine, ^{67}Ga-citrate and radiolabeled leukocytes. ^{99m}Tc-IL-8 allowed excellent visualization of localization and extent of pulmonary infection in three experimental models simulating immunocompromized conditions (aspergillosis) as well as models simulating immunocompetent conditions with gram-positive (*S.pneumoniae*) as well as gram-negative (*E.coli*) bacterial infections.

REFERENCES

1. Tsan MF. Mechanism of gallium-67 accumulation in inflammatory lesions. *J Nucl Med* 1985;26:88-92.
2. Palestro CJ, Love C, Tronco GG, Tomas MB. Role of radionuclide imaging in the diagnosis of postoperative infection. *Radiographics* 2000;20:1649-60.
3. McAfee JG, Thakur ML. Survey of radioactive agents for in vitro labeling of phagocytic leukocytes. I. Soluble agents. *J Nucl Med* 1976;17:480-7.
4. McAfee JG, Thakur ML. Survey of radioactive agents for in vitro labeling of phagocytic leukocytes. II. Particles. *J Nucl Med* 1976;17:488-92.
5. Peters AM, Danpure HJ, Osman S et al. Clinical experience with 99mTc-hexamethylpropylene-amineoxime for labelling leucocytes and imaging inflammation. *Lancet* 1986;2:946-9.
6. Peters AM. The utility of ^{99m}TcHMPAO-leukocytes for imaging infection. *Semin Nucl Med* 1994;24:110-27.
7. Lange JM, Boucher CA, Hollak CE et al. Failure of zidovudine prophylaxis after accidental exposure to HIV-1. *N Engl J Med* 1990;322:1375-7.
8. Patel L, Charlton SJ, Chambers JK, Macphee CH. Expression and functional analysis of chemokine receptors in human peripheral blood leukocyte populations. *Cytokine* 2001;14:27-36.
9. Holmes WE, Lee J, Kuang WJ, Rice GC, Wood WI. Structure and functional expression of a human interleukin-8 receptor. *Science* 1991;253:1278-80.
10. Murphy PM, Tiffany HL. Cloning of complementary DNA encoding a functional human interleukin-8 receptor. *Science* 1991;253:1280-3.
11. Lee J, Horuk R, Rice GC, Bennett GL, Camerato T, Wood WI. Characterization of two high affinity human interleukin-8 receptors. *J Biol Chem* 1992;267:16283-7.
12. Cerretti DP, Kozlosky CJ, Vanden Bos T, Nelson N, Gearing DP, Beckmann MP. Molecular characterization of receptors for human interleukin-8, GRO/melanoma growth-stimulatory activity and neutrophil activating peptide-2. *Mol Immunol* 1993;30:359-67.
13. Rennen HJ, Boerman OC, Oyen WJ, van der Meer JW, Corstens FH. Specific and rapid scintigraphic detection of infection with 99mTc- labeled interleukin-8. *J Nucl Med* 2001;42:117-23.
14. Gratz S, Rennen HJ, Boerman OC, Oyen WJ, Corstens FH. Rapid imaging of experimental colitis with (99m)Tc-interleukin-8 in rabbits. *J Nucl Med* 2001;42:917-23.
15. Gratz S, Rennen HJ, Boerman OC, Oyen WJ, Burma P, Corstens FH. (99m)Tc-interleukin-8 for imaging acute osteomyelitis. *J Nucl Med* 2001;42:1257-64.
16. Abrams MJ, Juweid M, tenKate CI et al. Technetium-99m-human polyclonal IgG radiolabeled via the hydrazino nicotinamide derivative for imaging focal sites of infection in rats. *J Nucl Med* 1990;31:2022-8.
17. Schwartz DA, Abrams MJ, Giadomenico CM, Zubieta JA. Certain pyridyl hydrazines and hydrazides useful for protein labeling. USA patent bo. 5,206,370. 27-4-1993.
18. Rennen HJ, van Eerd JE, Oyen WJ, Corstens FH, Edwards DS, Boerman OC. Effects of coligand variation on the in vivo characteristics of Tc-99m- labeled interleukin-8 in detection of infection. *Bioconjug Chem* 2002;13:370-7.
19. Groll AH, Gonzalez CE, Giri N et al. Liposomal nystatin against experimental pulmonary aspergillosis in persistently neutropenic rabbits: efficacy, safety and non- compartmental pharmacokinetics. *J Antimicrob Chemother* 1999;43:95-103.
20. Dams ET, Becker MJ, Oyen WJ et al. Scintigraphic imaging of bacterial and fungal infection in granulocytopenic rats. *J Nucl Med* 1999;40:2066-72.
21. van der Laken CJ, Boerman OC, Oyen WJ, van de Ven MT, van der Meer JW, Corstens FH. Radiolabeled interleukin-8: specific scintigraphic detection of infection within a few hours. *J Nucl Med* 2000;41:463-9.
22. Worthen GS, Schwab B, III, Elson EL, Downey GP. Mechanics of stimulated neutrophils: cell stiffening induces retention in capillaries. *Science* 1989;245:183-6.
23. Aoki T, Suzuki Y, Nishio K et al. Role of CD18-ICAM-1 in the entrapment of stimulated leukocytes in alveolar capillaries of perfused rat lungs. *Am J Physiol* 1997;273:H2361-H2371.
24. Drost EM, MacNee W. Potential role of IL-8, platelet-activating factor and TNF-alpha in the sequestration of neutrophils in the lung: effects on neutrophil deformability, adhesion receptor expression, and chemotaxis. *Eur J Immunol* 2002;32:393-403.
25. Rennen HJ, Boerman OC, Oyen WJ, Corstens FH. Kinetics of Tc-99m-labeled Interleukin-8 in experimental inflammation and infection. J.Nucl.Med. 2003;44:1502-1509.
26. Selby C, Drost E, Wraith PK, MacNee W. In vivo neutrophil sequestration within lungs of humans is determined by in vitro "filterability". *J Appl Physiol* 1991;71:1996-2003.
27. Selby C, MacNee W. Factors affecting neutrophil transit during acute pulmonary inflammation: minireview. *Exp Lung Res* 1993;19:407-28.
28. Palestro CJ. The current role of gallium imaging in infection. *Semin Nucl Med* 1994;24:128-41.

Chapter 8

Kinetics of ^{99m}Tc-labeled interleukin-8 in experimental inflammation and infection

Huub J.J.M. Rennen, Otto C. Boerman, Wim J.G. Oyen, Frans H.M. Corstens

ABSTRACT

The cytokine interleukin-8 (IL-8) binds with high affinity to the CXCR1 and CXCR2 receptors on neutrophils. In previous studies we showed that ^{99m}Tc-IL-8 could rapidly and effectively delineate foci of infection and inflammation in rabbit models of intramuscular infection, colitis and osteomyelitis. Here, the *in vivo* kinetics and pharmacodynamics of ^{99m}Tc-IL-8 are studied in detail. A derivative of hydrazinonicotinamide (HYNIC) was used as bifunctional coupling agent to label the protein with ^{99m}Tc.

Methods: i) To address specificity of uptake of ^{99m}Tc-IL-8 in the abscess, uptake in turpentine-induced abscesses in neutropenic rabbits was compared to uptake in turpentine-induced abscesses in normal rabbits. ii) The pharmacokinetics of ^{99m}Tc-IL-8 were studied in neutropenic rabbits and compared to those in normal rabbits. To investigate the interaction of ^{99m}Tc-IL-8 with blood cells in circulation in normal rabbits, the distribution of the radiolabel over circulating white and red blood cells and plasma was determined. iii) The *in vivo* kinetics of ^{99m}Tc-IL-8 were studied by quantitative analysis of whole body images acquired between 0 and 6 h p.i. The results of this analysis (*in vivo* biodistribution) were validated by *ex vivo* counting of radioactivity in dissected tissues.

Results: i) Abscess uptake (%ID/g ± s.e.m.) in immunocompetent rabbits (0.41 ± 0.05) was ten times higher than in neutropenic rabbits (0.038 ± 0.014), demonstrating specificity of the target uptake of ^{99m}Tc-IL-8. Abscess-to-muscle ratios (± s.e.m.) were also ten times higher (110 ± 10 vs 10 ± 5). Lung and spleen uptake in normal rabbits was three times higher than in neutropenic rabbits. ii) The blood clearance of the radiolabel in neutropenic rabbits was similar to that in normal rabbits. In circulation, most of ^{99m}Tc-IL-8 (70%) was found in the plasma fraction. Less than one third was associated with red blood cells, and only a very low percentage (<2.5%) with white blood cells. iii) Image analysis revealed a gradually increasing abscess uptake over time up to over 15% ID, which was confirmed by *ex vivo* gamma counting of the infected muscle. Highest increase in uptake in the abscess was observed after 2 h p.i., when most of ^{99m}Tc-IL-8 was cleared from the blood, suggesting specific neutrophil-mediated accumulation of ^{99m}Tc-IL-8 in the abscess. Furthermore, region-of-interest analysis revealed that gradual accumulation of ^{99m}Tc-IL-8 in the abscess was accompanied by a simultaneous clearance of activity from the lungs, suggesting that neutrophil associated ^{99m}Tc-IL-8 that was initially trapped in the lungs migrates to the abscess at later time-points, favoring neutrophil-bound transportation from the lungs to the abscess.

Conclusion: Substantial support is given for the hypothesis that ^{99m}Tc-IL-8 localizes in the abscess mainly as bound to peripheral neutrophils. Accumulation in the abscess is a highly specific, neutrophil-driven process. As assessed by *in vivo* and *ex vivo* analysis, the total fraction that accumulates in the inflamed tissue is extremely high (up to over 15% ID), compared to other agents used for imaging infection and inflammation.

INTRODUCTION

Neutrophils are known to express two types of interleukin-8 (IL-8) receptors, CXCR1 and CXCR2, abundantly (*1*). IL-8 binds these receptors with high affinity (0.3-4 nmol/L) (*2-5*). The *in vivo* behavior of radioiodinated IL-8 has been studied in rat (*6*) and rabbit (*7,8*) models of infection. Gross et al. showed in a pilot study that ^{131}I-labeled IL-8 could visualize osteomyelitic lesions in patients (*9*). We have pointed out that the radioiodination method clearly affected the *in vivo* biodistribution of IL-8 (*10*). For clinical applications, a labeling procedure using the radiometal ^{99m}Tc is to be preferred over iodine (*10*). Recently, we described the development of a ^{99m}Tc-labeled IL-8 preparation using hydrazinonicotinamide (HYNIC) as a bifunctional coupling agent (*11*). This preparation showed excellent characteristics for imaging infection in three different models of infection and inflammation in rabbits (*11-13*). In rabbits with intramuscular infection induced by *E.coli*, uptake of ^{99m}Tc-IL-8 in the abscess was rapid and high (*11*). Moreover, ^{99m}Tc-IL-8 showed a remarkably fast clearance from nontarget tissues. Abscess-to-muscle ratios exceeded 100 at 8 h after injection.

In rabbits with chemically induced acute colitis, inflammatory lesions were scintigraphically visualized after injection of either IL-8 or purified granulocytes, both labeled with ^{99m}Tc (*13*). Within a few hours after injection, ^{99m}Tc-IL-8 allowed an adequate evaluation of the inflamed colon. Absolute uptake in the inflamed foci in the colon was much higher for ^{99m}Tc-IL-8 than for ^{99m}Tc-labeled granulocytes.

In a third study, the performance of ^{99m}Tc-IL-8 was evaluated in an experimental model of acute osteomyelitis in rabbits (*12*). The results were compared with those obtained using the conventional and well-established agents ^{111}In-granulocytes, ^{67}Ga-citrate and ^{99m}Tc-MDP. In this rabbit model of osteomyelitis, ^{99m}Tc-IL-8 clearly delineated the osteomyelitic lesions. Although absolute uptake in the osteomyelitic area was lower than that obtained with ^{67}Ga-citrate and ^{99m}Tc-MDP, the target-to-background ratios were significantly higher for ^{99m}Tc-IL-8.

IL-8 is a proinflammatory chemotactic cytokine. For scintigraphic purposes protein doses to be administered should be below levels that generate side-effects. We

showed that a preparation with a high specific activity (80 MBq/µg) and high in vitro stability could be prepared when nicotinic acid was used as a coligand (*14*). Imaging doses as low as 70 ng/kg ^{99m}Tc-IL-8 open the way to infection imaging studies in patients.

In the present study three fundamental aspects of the *in vivo* behavior of ^{99m}Tc-IL-8 were investigated: a) Specificity of uptake of ^{99m}Tc-IL-8 in the abscess; b) Mechanism of migration of ^{99m}Tc-IL-8 from the circulation to the inflammatory focus; c) Kinetics of ^{99m}Tc-IL-8 *in vivo*.

MATERIALS AND METHODS

Human recombinant IL-8 was kindly provided by Dr I. Lindley (Novartis, Vienna, Austria). Tricine (N-[Tris(hydroxymethyl)-methyl]glycine was purchased from Fluka (Buchs, Switzerland), nicotinic acid from Sigma-Aldrich (St. Louis, MO).

Conjugation of HYNIC to IL-8

The propylaldehyde hydrazone of succinimidyl-hydrazinonicotinamide (HYNIC) was synthesized essentially as described previously (*15,16*). The IL-8-HYNIC conjugate was prepared as described previously (*8*). Briefly, in a 1.5 ml vial 4 µl 1 M NaHCO$_3$, pH 8.2 was added to 35 µl of IL-8 (4.8 mg/ml). Subsequently, a three-fold molar excess of HYNIC in 5 µl dry DMSO was added dropwise to the mixture. After incubation for five minutes at room temperature, the reaction was stopped by adding an excess of glycine (200 µl, 1 M in PBS). To remove excess unbound HYNIC the mixture was extensively dialyzed against PBS (0.1-0.5 ml dialysis cell 3.5 MWCO, Pierce, Rockford, IL). Dialyzed samples of circa 5 µg IL-8-HYNIC were stored at –20 ^{0}C.

Technetium-99m Labeling of HYNIC Conjugated IL-8

5 micrograms IL-8-HYNIC were incubated with 0.2 ml of tricine solution (100 mg/ml in PBS), 25 µL of a freshly prepared tin (II) solution (10 mg SnSO$_4$ in 10 ml nitrogen-purged 0.1 N HCl) and 150 - 350 MBq ^{99m}TcO$_4$$^-$ in saline at room temperature for 30 minutes. The radiochemical purity was determined by instant thin-layer chromatography (ITLC) on ITLC-SG strips (Gelman Laboratories, Ann Arbor, MI) with 0.1 M citrate, pH 6.0, as the mobile phase. Following the labeling reaction the reaction mixture was applied to a Sephadex G-25 column (PD-10; Pharmacia, Uppsala, Sweden) and eluted with PBS, 0.5% BSA to purify radiolabeled IL-8. A description of an extensive in vitro characterization (HPLC, stability, receptor binding assays) has been given elsewhere (*14*).

Animal Studies

All animal experiments were carried out in accordance with the guidelines of the local animal welfare committee.

Specificity of Uptake of ^{99m}Tc-*IL-8 in the Abscess.* Neutropenia was induced in five female New Zealand rabbits (2.4-2.7 kg) by i.v. administration of cytarabine (David Bull Laboratories, Mulgrave, Victoria, Australia) (50 mg per rabbit per day during 7 days). Routinely a rabbit model of intramuscular infection induced by *Escherichia coli* is used, because it generates a strong leukocytic response and it is a good reflection of a common bacterial infection. In neutropenic rabbits the immune system is seriously troubled and an infection induced by *Escherichia coli* could have a fatal effect on these animals. For that reason a sterile turpentine inflammation rather than a bacterial infection was installed. On day 8, a sterile inflammation was induced in the left thigh muscle of these five neutropenic rabbits and in a control group of four immunocompetent rabbits (0.5 ml of turpentine i.m.). During the procedure, rabbits were anaesthetized with a subcutaneous injection of a 0.6 ml mixture of fentanyl 0.315 mg/ml and fluanisone 10 mg/ml (Hypnorm, Janssens Pharmaceutical, Buckinghamshire, UK). On day 9, blood samples of 1 ml were taken from the rabbits and a manual differential leukocyte count of these samples was performed. Then, both groups of rabbits received 20 MBq ^{99m}Tc-IL-8 (protein dose 0.5 µg) via the ear vein. Three rabbits out of each group were used for gamma camera imaging. These rabbits were immobilized in a mold, placed prone on the gamma camera and images were acquired at 0, 1, 2 and 4 h p.i. with a single-head gamma camera (Orbiter, Siemens Medical Systems Inc., Hoffman Estates, IL) equipped with a parallel-hole low-energy all purpose collimator. Images were obtained with a 15% symmetrical window over the 140 keV energy peak of ^{99m}Tc. After acquisition of 100,000-300,000 counts, the images were digitally stored in a 256 x 256 matrix. Scintigraphic images were analyzed quantitatively by drawing regions of interest (ROI) over the abscess and the contralateral thigh muscle (background). Abscess-to-background ratios were calculated.

After completion of the final imaging session (4 h p.i.), all rabbits were killed with a lethal dose of sodium phenobarbital. Samples of blood, infected thigh muscle, uninfected contralateral thigh muscle, lung, spleen, liver, kidneys and intestines were collected. The dissected tissues were weighed and the activity in the samples was measured in a gamma counter. To correct for radioactive decay injection standards were counted simultaneously. The measured activity in samples was expressed as percentage of injected dose per gram tissue (%ID/g). Abscess-to-contralateral muscle ratios and abscess-to-blood ratios were calculated.

For histological examination, samples of infected thigh muscle of neutropenic as well as normal rabbits were fixed in formalin and embedded in paraffin. 5 μm sections were cut and stained with hematoxylin-eosin for lightmicroscopic examination.

Mechanism of Migration of ^{99m}*Tc-IL-8 from the Circulation to the Inflammatory Focus.* Pharmacokinetics of ^{99m}Tc-IL-8 were determined in neutropenic as well as normal rabbits with turpentine-induced abscesses (three rabbits per group). Multiple blood samples were collected between one minute and four hours after injection. Blood samples were weighed, their activity was measured and their uptake expressed as %ID/g and as %ID in the blood pool based on an estimated total blood volume of 6% of the total body weight of the rabbit (*17*).

The association of ^{99m}Tc-IL-8 with blood cells in circulation was studied following intravenous injection of radiolabeled IL-8. Blood samples of 3 ml (in heparinized tubes) of three normal rabbits with turpentine induced inflammation were taken at five minutes, two hours and four hours after injection of the radiolabel. The blood was mixed with 1/4 dextran (dextran 500, Pharmacia, Uppsala, Sweden) 6% solution in 0.9% NaCl, and allowed to sediment for one hour at room temperature. The leukocyte-rich supernatant was carefully removed. The leukocyte-rich layer and the erythrocyte-rich layer were centrifuged for 15 minutes at 500xg. The supernatants of both layers were removed and retained. The leukocyte pellet and the erythrocyte pellet were washed three times with 5 ml of Hank's balanced salt solution (HBSS) and centrifuged for 10 minutes at 500xg. The supernatants of all washing steps were retained. Radioactivity of the leukocyte pellet, the erythrocyte pellet, the plasma layer and the supernatants of the washing steps was counted in a gamma-counter. All radioactivity in plasma layer and supernatants of the washing steps were taken together and designated as "plasma".

Kinetics of ^{99m}*Tc-IL-8 In Vivo.* Soft-tissue infections were induced in the left thigh muscle of four female New Zealand rabbits (2.5-3.0 kg) with 1-2 x 10^{11} colony forming units (cfu) of *Escherichia coli* in 0.5 ml. After 24 hours the rabbits were injected i.v. with ^{99m}Tc-labeled IL-8. Scintigraphic images were obtained with a dual head Siemens MultiSpect 2 gamma-camera connected to a Scintiview image processor and ICON computersystem (Siemens Inc., Hoffman Estates, IL). All images were collected in digital format in a 256x256 matrix. Low-energy parallel-hole collimators were used (140 keV photopeak, 15% symmetric window). Three rabbits were imaged alternately at a preset time of 10 minutes per image, one set of three images taking approximately 35-40 minutes. In this way, 10 sets of whole-body images were generated between 0 and 6 h p.i. The animals were killed after completion of the last image and tissue samples were collected, weighed and counted in a gamma counter. Scintigraphic images were analyzed quantitatively by drawing regions of interest (ROI) over the abscess, the contralateral

thigh muscle, kidneys, bladder, liver, spleen, lungs and heart, spine. In addition, regions were drawn near the organs for background correction.

Results of quantitative analysis of the images (*in vivo* biodistribution) were compared to results of counting radioactivity in dissected tissues (*ex vivo* biodistribution) in an additional experiment. To ascertain whether *in vivo* biodistribution data are in accordance with *ex vivo* biodistribution data, one rabbit with intramuscular infection was imaged on the dual headed Siemens MultiSpect 2 gamma-camera as described above. After finishing the last image at 6 h p.i., the animal was killed and dissected. Radioactivity was counted in whole organs on a NaI-crystal connected to a multichannel analyzer. Appropriate standards of injected dose (1%, 3%, 6%, 10%, 20% and 30% ID) were counted as well. Special attention was paid to the analysis of radioactivity uptake in the infected hindleg. After counting radioactivity in the whole infected leg (similarly to drawing a ROI over the total high-uptake region), the leg was dissected stepwise in the direction of the central part of the abscess. The various dissected parts were weighed and counted. In this way, total percentages of the injected dose (%ID) and %ID per gram of tissue could be determined (*ex vivo* data). Similarly, abscess uptake was analyzed on the whole body image, by drawing concentric regions around the central focus of the abscess (*in vivo* data). *Ex vivo* data were compared to *in vivo* data.

Statistical Analysis

All mean values are expressed as %ID/g, %ID or ratios ± 1 standard error of the mean (s.e.m.). Data were analyzed statistically using the unpaired t-test (GraphPad Instat 3.00 Win 95, San Diego, CA, USA).

RESULTS

Specificity of Uptake of ^{99m}Tc-IL-8 in the Abscess

Hematoxylin-eosin stained 5-μm sections of the abscess of a normal, immunocompetent rabbit and a neutropenic rabbit are shown in Figure 1. Microscopic examination revealed a massive influx of predominantly polymorphonuclear cells (neutrophils) in the abscesses of normal rabbits (Figure 1a). Remarkably, in neutropenic rabbits the abscesses were also characterized by high numbers of infiltrating cells. However, in these animals the invading leukocytes were predominantly mononuclear, i.e. lymphocytes and/or monocytes (Figure 1b).

The reduction of neutrophil counts markedly affected the biodistribution of ^{99m}Tc-IL-8 in these rabbits as shown in Table 1 and Figure 2. Two cytarabine-treated rabbits were designated as "semineutropenic rabbits" because of higher neutrophil levels as

compared to three deeply neutropenic rabbits (8% and 19% versus 4%, 0% and 1% respectively). These "semineutropenic" rabbits showed higher abscess uptakes than the deeply neutropenic rabbits. Abscess uptake correlated well with neutrophil counts in the cytarabine-treated and non-treated animals (r=0.90, data not shown).
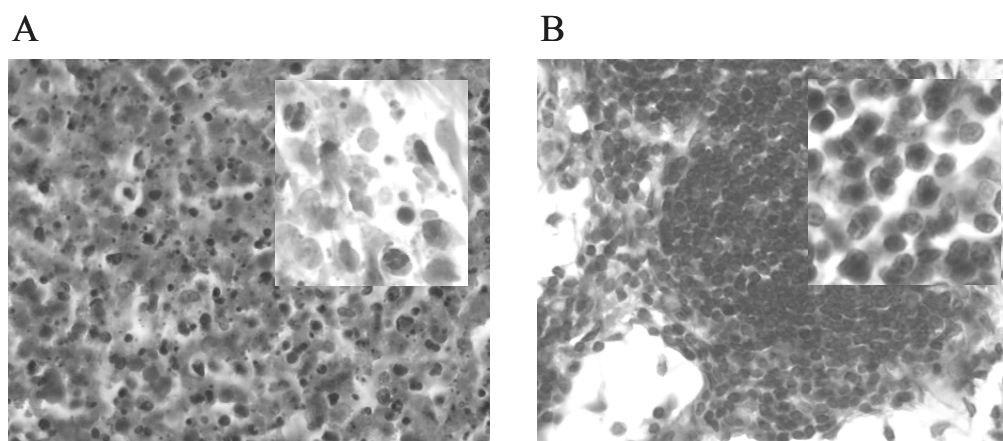
A   B

Figure 1. Hematoxylin-eosin stained tissues of turpentine induced abscesses in a normal, immunocompetent rabbit (A) and a neutropenic rabbit (B). Note the massive infiltration of polymorphonuclear cells (neutrophils) in A and mononuclear cells in B. Magnification 400x and 1000x (inset).

Table 1. Biodistribution of ^{99m}Tc-IL-8 in neutropenic and normal rabbits with turpentine-induced abscesses. Uptake is given as %ID/g. Values are expressed as mean ± 1 SEM.

	Neutropenic rabbit (n=3)	Normal rabbits (n=4)
Blood	0.073 ± 0.004	0.069 ± 0.004
Muscle	0.005 ± 0.001	0.004 ± 0.001
Abscess	0.038 ± 0.014	0.41 ± 0.05
Lung	0.10 ± 0.02	0.34 ± 0.04
Spleen	0.38 ± 0.04	0.90 ± 0.08
Kidney	2.32 ± 0.30	2.13 ± 0.22
Liver	0.110 ± 0.024	0.080 ± 0.006
Intestine	0.044 ± 0.008	0.025 ± 0.002
Ratios		
Abscess/Blood	0.5 ± 0.2	5.9 ± 0.7
Abscess/Muscle	10 ± 5	110 ± 10
Target/Background	1.2 ± 0.1	15 ± 1

Figure 2 illustrates the dramatic impact of neutrophil reduction on uptake of ^{99m}Tc-IL-8 in the abscess: Low abscess uptake in a neutropenic rabbit, moderate uptake in a "semineutropenic" rabbit and high uptake in a normal rabbit. Association of ^{99m}Tc-IL-8 with neutrophils is demonstrated in Table 1: (i) abscess uptake is significantly higher ($P<0.01$) in normal rabbits as compared to neutropenic rabbits; (ii) lung uptake is significantly higher ($P<0.01$) in normal rabbits (0.34 ± 0.04 %ID/g vs 0.10 ± 0.02 %ID/g); (iii) uptake in spleen is also significantly higher ($P<0.01$) in normal rabbits (0.90 ± 0.08 %ID/g vs 0.38 ± 0.04 %ID/g). These organs are known for accommodating high concentrations of neutrophils. Remarkably, uptake in intestinal tissue was significantly higher ($P<0.05$) in neutropenic rabbits (0.044 ± 0.008 %ID/g vs 0.025 ± 0.002 %ID/g). The ratios Abscess/Blood, Abscess/Muscle and Target/Background from analysis of the images were significantly higher ($P<0.01$, $P<0.001$, $P=0.0001$ respectively) for normal rabbits as compared to the neutropenic ones.
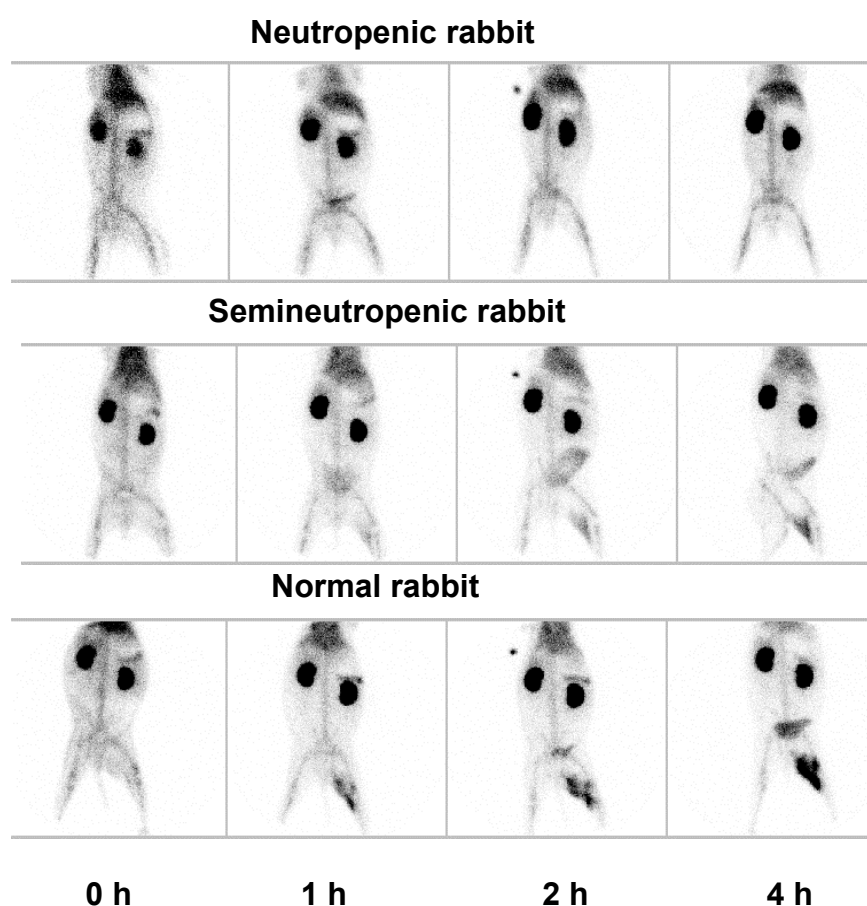

Figure 2. *Images of rabbits with turpentine induced abscesses in the left thigh muscle at 5 minutes, 1, 2 and 4 hour after injection of ^{99m}Tc-IL-8. Neutrophil counts varied from very low levels (Neutropenic rabbit) via low levels (Semineutropenic rabbit) to normal levels (Normal rabbit).*

Mechanism of Migration of ^{99m}Tc-IL-8 from the Circulation to the Inflammatory Focus

The blood clearance patterns of ^{99m}Tc-IL-8 in normal versus neutropenic rabbits with turpentine-induced soft-tissue abscesses were essentially congruent (Figure 3), demonstrating that there is no major effect of the reduction of the number of neutrophils in circulation on the blood clearance of ^{99m}Tc-IL-8. The association of ^{99m}Tc-IL-8 with blood cells in samples of normal rabbits with turpentine-induced abscesses is shown in Table 2. The major fraction of the radiolabel was found in the plasma fraction, ranging from 68% immediately after injection, to 76% at the last time point. Less than one third of the radiolabel was associated with red blood cells, and only a very low percentage (<2.5%) with white blood cells.
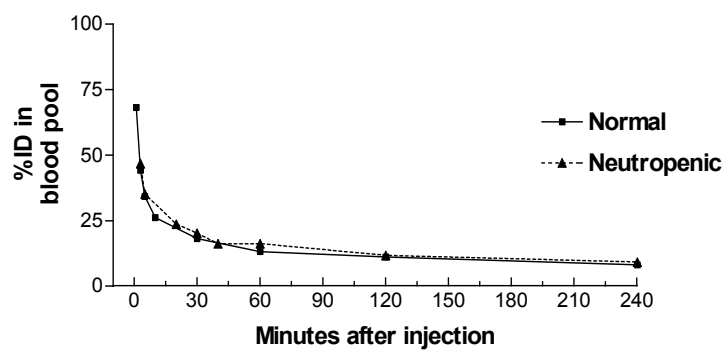
Figure 3. Blood clearance of ^{99m}Tc-IL-8 in immunocompetent, normal rabbits and in neutropenic rabbits with turpentine induced inflammation. Data are expressed as percentage of the injected dose (%ID) in the blood pool.

Table 2. Distribution of ^{99m}Tc-IL-8 over red blood cells, white blood cells, and plasma in normal rabbits with turpentine-induced abscesses.

	%plasma	%RBC	%WBC
T=5'	68 ± 2	31 ± 2	0.3 ± 0.02
T=2h	68 ± 4	30 ± 4	2.3 ± 0.2
T=5h	76 ± 4	23 ± 4	0.8 ± 0.2

RBC = red blood cells; WBC = white blood cells. From plasma blood samples at 3 different time points. Values are expressed as mean ± 1 SEM.

Kinetics of ^{99m}Tc-IL-8 In Vivo

The kinetics of the *in vivo* distribution of ^{99m}Tc-IL-8 in rabbits with *E.coli*-induced infection are summarized in Figure 4. The whole body activity (corrected for physical decay) did not decrease. Ergo, during the experiment radioactivity was not excreted from the body. An example of a posterior image with regions of interest (ROI) drawn is given in Figure 5. Analysis of the images showed a gradual increase in abscess uptake up to 15 ± 1 % of whole body activity (WBA) at 5.5 h p.i. At that time maximum uptake was not reached yet. Kidney uptake reached high levels immediately after injection of the radiolabel and remained stable from one hour onwards at a level of approximately 30 %WBA. Uptake in the lungs showed a gradual decrease from a high level of uptake immediately after injection (23 ± 0.5 %WBA) towards a moderate level at 5.5 h p.i. (13 ± 1 %WBA). Liver uptake was nearly stable over time at approximately 10 %WBA. Spleen uptake appeared to be marginal in this experiment; <1 %WBA at all time points. Activity in the bladder was low and did not exceed 3 ± 1 %WBA at 5.5 h p.i. In addition, ROI's of spine and corresponding background areas were drawn, revealing only marginal uptake in the spine area (data not shown). A substantial amount of uptake was observed in the head and forelegs region, declining from 15 ± 1 %WBA at the start to 9 ± 1 %WBA at the end (not shown in Figure 4). The major shifts in radioactivity distribution over time involved a clearance from the lungs (-10 %WBA), the head/forelegs (-6 %WBA) and the trunk (minus organs) in favor of kidney (+9 %WBA) and the abscess (+12 %WBA).
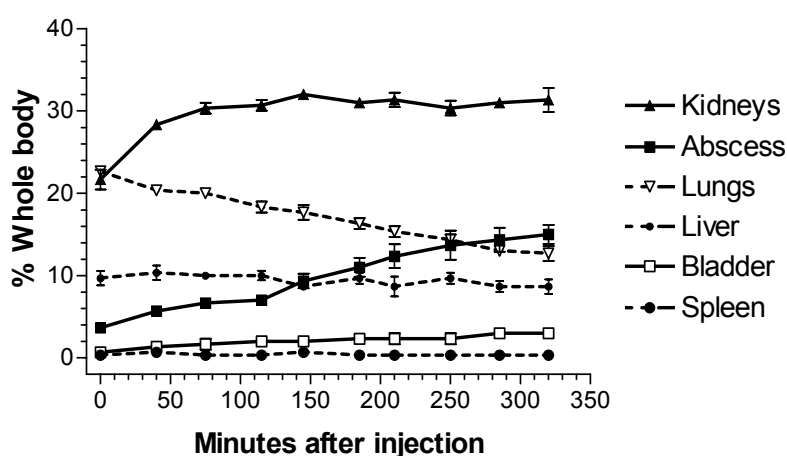

Figure 4. *Kinetics of the in vivo distribution of ^{99m}Tc-IL-8 in rabbits with E.coli induced infection as determined by quantitative analysis of the images. Uptake is quantified as percentage of whole body activity. The error bars indicate $\pm$ SEM.*
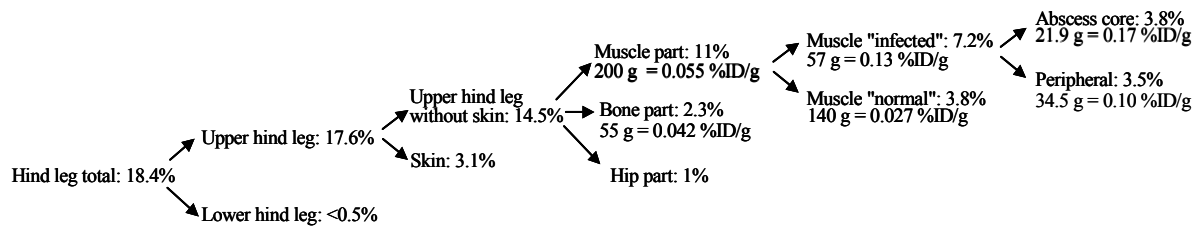
Abscess core: 3.8%
21.9 g = 0.17 %ID/g

Muscle "infected": 7.2%
57 g = 0.13 %ID/g

Peripheral: 3.5%
34.5 g = 0.10 %ID/g

Muscle part: 11%
200 g = 0.055 %ID/g

Muscle "normal": 3.8%
140 g = 0.027 %ID/g

Upper hind leg without skin: 14.5%

Bone part: 2.3%
55 g = 0.042 %ID/g

Skin: 3.1%

Upper hind leg: 17.6%

Hip part: 1%

Hind leg total: 18.4%

Lower hind leg: <0.5%

Figure 5. *Detailed ex vivo analysis of uptake of* ^{99m}*Tc-IL-8 in the E.coli infected hind leg of a New Zealand white rabbit at 6 h after injection. Uptake is given as percentage of the injected dose (%ID) and as %ID per gram for the central parts of the affected muscle (see also in vivo analysis data of Table 3).*

Table 3. *Detailed analysis of uptake of* ^{99m}*Tc-IL-8 in E. coli-infected hindleg of a New Zealand white rabbit. Comparison of radioactivity uptake in whole unfragmented organs and abscess parts (ex vivo analysis; Fig. 5) with uptake as determined by quantitative analysis of images at 6 h after injection. Ex vivo data are expressed as %ID; in vivo data are expressed as percentage of whole body activity (WBA).*

	ex vivo data		*in vivo* data
dissected parts	% injected dose	regions of interest	% whole body
abscess core	3.8%	abscess core	4.5%
muscle part	11%	abscess peripheral	12.2%
upper hindleg	17.6%	abscess total	18.5%
kidney left	14.4%	kidney left	13.2%
kidney right	15.4%	kidney right	15.1%
liver	8.6%	liver	9.7%
spleen	0.75%	spleen	0.60%
lungs	4.4%	lungs	3.9%

The results of a detailed analysis (both *ex vivo* and *in vivo*) of uptake of ^{99m}Tc-IL-8 in one rabbit are presented in Table 3 and Figure 5. Regions of interest were drawn as in Figure 6. Data of *ex vivo* and *in vivo* analysis showed a fair congruency. *Ex vivo* analysis displayed a gradual increase in radioactivity concentration (%ID/g) towards the core of the abscess. Taking into account considerably large uptakes in concentric areas around this abscess core, a total uptake in the affected leg of 17.6% ID was determined. Similarly, *in vivo* analysis displayed a gradual increase in Target-to-Background ratios towards the center of inflammation, from 8.1 (abscess total), 14.2 (abscess periphery) up to 20.0 (abscess core). Total uptake in the affected leg (designated as abscess total) amounted to 18.5 %WBA, based on ROI analysis, as compared to 17.6 %ID from the *ex vivo* analysis.
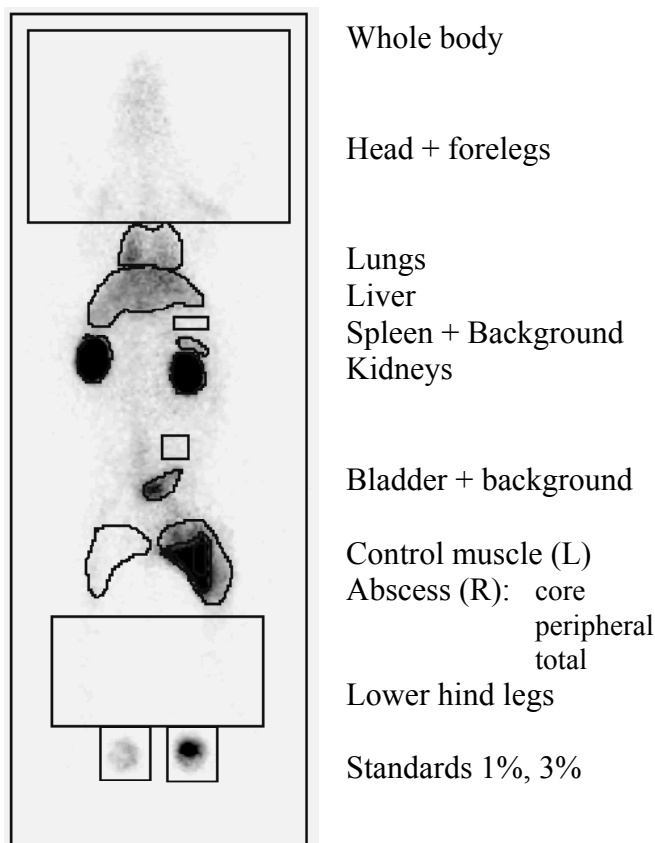
Whole body

Head + forelegs

Lungs
Liver
Spleen + Background
Kidneys

Bladder + background

Control muscle (L)
Abscess (R):   core
                   peripheral
                   total
Lower hind legs

Standards 1%, 3%

Figure 6. *Typical example of regions of interest (ROI) in an image of a rabbit with an E.coli induced intramuscular infection injected with* ^{99m}*Tc-IL-8.*

DISCUSSION

Specific uptake of ^{99m}Tc-IL-8 in inflamed tissue is assumed to be based on high-affinity binding to IL-8 receptors on neutrophils. Neutrophil-driven specificity can be demonstrated in various ways. Firstly, by studying the behavior of a control protein with similar size and charge but with no specific interaction with receptors on neutrophils. The observation in a previous study that abscess uptake of ^{99m}Tc-IL-8 was more than ten times higher than abscess uptake of ^{99m}Tc-Lysozyme suggested that abscess uptake was a result of the interaction of IL-8 with its receptors in inflammatory foci (*11*). An alternative way to demonstrate specific uptake is *in vivo* receptor blocking using an excess of unlabeled IL-8 or an excess of receptor blocking monoclonal antibodies. However, saturation of receptors before injection of ^{99m}Tc-IL-8 is not feasible because excessive amounts of unlabeled IL-8 will generate unacceptable biological effects or would require excessive amounts of costly monoclonal antibodies. In the present study an alternative approach was chosen: Comparing abscess uptake of ^{99m}Tc-IL-8 in neutropenic rabbits with that in rabbits with normal numbers of neutrophils. Microscopic examination of inflamed muscular

tissue samples showed a shift in infiltrating leukocyte populations from predominantly polymorphonuclear cells (i.e., neutrophils) in normal rabbits to mononuclear cells (lymphocytes, monocytes) in cytarabine-pretreated rabbits. Patel et al. demonstrated that activated neutrophils express high numbers of CXCR1 and CXCR2 receptors (10^4/cell), whereas activated mononuclear cells express low numbers of these receptors (<10^2/cell)(*1*). As a consequence, the number of available receptors for ^{99m}Tc-IL-8 is greatly reduced in neutrophil-depleted rabbits. Accordingly, the uptake of ^{99m}Tc-IL-8 in the abscess was dramatically reduced in neutrophil-depleted rabbits. More precisely, a good correlation between neutrophil counts and abscess uptake was found (r=0.90). Specific involvement of ^{99m}Tc-IL-8 with neutrophils was also reflected in high uptake in neutrophil abundant organs such as lungs and spleen. Low uptake in neutrophil-depleted animals in these organs and in the abscess strongly suggests that accumulation of ^{99m}Tc-IL-8 is a neutrophil-driven process. Only a minor fraction of ^{99m}Tc-IL-8 localizes in the abscess nonspecifically. In neutropenic rabbits, uptake of ^{99m}Tc-IL-8 in the abscess is only 10% as compared to abscess uptake in normal rabbits (Table 1), but is still ten times as high as uptake in contralateral muscle. A similar uptake pattern was seen for ^{99m}Tc-Lysozyme in a previous study (*11*), suggesting again that some 10% of uptake of the radiolabel in the abscess could be ascribed to nonspecific uptake.

The mechanism of migration of ^{99m}Tc-IL-8 from the circulation to the focus of inflammation was the second issue of investigation. Several mechanisms of transportation can be conceived, grossly divided into neutrophil-bound transportation and non-neutrophil-bound transportation. Neutrophil-bound transportation involves high affinity binding of ^{99m}Tc-IL-8 to receptors on peripheral neutrophils, followed by migration of the labeled cells to the inflamed tissue and passage through the endothelium. Non-neutrophil-bound transportation involves freely circulating ^{99m}Tc-IL-8 which extravasates and is subsequently trapped by receptors on infiltrated neutrophils. In addition, it has been shown that ^{99m}Tc-IL-8 can bind to some degree to receptors on red blood cells with low affinity (*18*). The present study pointed out that some 30% of the injected ^{99m}Tc-IL-8 was bound to red blood cells. The binding to red blood cells is rapidly reversible and dissociation of ^{99m}Tc-IL-8 from the binding site on red blood cells is supposed to take place at the site of inflammation where ^{99m}Tc-IL-8 is exposed to massive numbers of high affinity binding sites on neutrophils (*8,18*).

Only a very low percentage of ^{99m}Tc-IL-8 in blood samples was associated with white blood cells. This observation is in favor of a non-neutrophil-bound transportation mechanism. On the other hand, several observations do support the concept of neutrophil-bound transportation. Blood clearance of ^{99m}Tc-IL-8 in rabbits with turpentine-induced soft-tissue abscess showed a fast initial clearance (Fig. 3)

within the first hour after injection, whereas the time period of highest increase in uptake of ^{99m}Tc-IL-8 in the abscess was between 2 and 5 h p.i. (Fig. 4). Uptake during that time period increased from some 7 to approximately 15 percent of the injected dose. This observation, that the major part of ^{99m}Tc-IL-8 accumulates in the abscess in the time period that ^{99m}Tc-IL-8 has cleared (almost) completely from the blood, argues against non-neutrophil-bound transportation of ^{99m}Tc-IL-8 to the abscess. Furthermore, quantitative analysis of the images at various timepoints revealed that the accumulation of ^{99m}Tc-IL-8 in the abscess is accompanied by a simultaneous clearance of activity from the lungs, suggesting that neutrophil associated ^{99m}Tc-IL-8 that is trapped in the lungs initially migrates to the abscess at later timepoints, favoring neutrophil-bound transportation from the lungs to the abscess. It has been shown that IL-8 can induce stiffening of neutrophils by reorganisation of intracellular actin, and this could explain the leukosequestration in the lungs. These cells loose their flexibility and consequently can not pass the narrow microcapillaries of the lungs anymore (*19,20*). As leukosequestration is a transient phenomenon, neutrophils (with radiolabel adhered) gradually re-enter circulation and subsequently migrate to the inflamed tissue due to their enhanced chemotactic status induced by IL-8. Between injection and the final imaging, the lung uptake decreased by 10%, while the abscess uptake increased by 12%. It is tempting to speculate that increasing abscess uptake could (partly) be ascribed to a continuous supply of radiolabeled neutrophils from the lungs.

Furthermore, several studies have shown that infiltrated (phagocytosing) neutrophils (*21*) in inflamed tissue in an environment of high concentrations of chemotactic cytokines (*22*) (and micro-organisms (*23*) or products thereof (*24*)) have downregulated their CXCR1 and CXCR2 expression and express relatively low numbers of these receptors, further arguing against direct targeting of infiltrated neutrophils by ^{99m}Tc-IL-8. It is most plausible that ^{99m}Tc-IL-8 targets predominantly peripheral neutrophils and not neutrophils within the inflammatory lesion.

Based on these considerations, we would propose the following hypothesis. Upon intravenous injection ^{99m}Tc-IL-8 is partly bound to peripheral neutrophils and the major fraction of ^{99m}Tc-IL-8 remains unbound. The fast blood clearance of the radiolabel is mainly reflecting the fast pharmacokinetics of the unbound ^{99m}Tc-IL-8 fraction. Unbound ^{99m}Tc-IL-8 is rapidly cleared predominantly by the kidneys. Not surprisingly, the blood clearance patterns in normal versus neutropenic rabbits are essentially congruent, as these are both reflecting unbound ^{99m}Tc-IL-8. The neutrophils that bind ^{99m}Tc-IL-8 stiffen and are trapped in the microcapillaries of the lungs. Following release from the lungs, these cells migrate to the inflamed tissue and extravasate at the site of infection in a highly selective way. As the release of the cells from the lungs is a gradual process, the analysis of blood samples reveals only a low

percentage of the radiolabel attached to white blood cells. Analysis of blood samples mainly reflects unbound ^{99m}Tc-IL-8. Quantitative analysis of images reveals the comparitively slow pharmacokinetics of the cell-bound ^{99m}Tc-IL-8 fraction.

Accumulation of ^{99m}Tc-IL-8 in the abscess is a neutrophil-driven gradual process, highly specific and efficient. ^{99m}Tc-IL-8 accumulated in abscesses of immunocompetent rabbits to a very high degree as determined by quantitative analysis of images and *ex vivo* quantification. *In vivo* biodistribution data did not conflict with *ex vivo* biodistribution data, showing the reliability of both approaches. The results showed that in previous studies (*11,14*) the total *ex vivo* abscess uptake of ^{99m}Tc-IL-8 was underestimated. Apparently, in the earlier studies only a part of the inflamed tissue was dissected and analyzed.

CONCLUSION

In this study substantial support is provided in favor of the hypothesis that ^{99m}Tc-IL-8 localizes in the abscess mainly due to neutrophil-bound transportation. Accumulation of ^{99m}Tc-IL-8 in the abscess is a neutrophil-driven process, highly specific and efficient: Abscess uptake in immunocompetent rabbits with intramuscular infection is extremely high (up to over 15% ID) as confirmed by *in vivo* and *ex vivo* analysis. Based on experimental data, ^{99m}Tc-IL-8 meets virtually all desiderata for successful imaging of infection and inflammation: High and highly specific uptake in abscesses, fast clearance from non-target tissues and low protein doses are promising features for the introduction of ^{99m}Tc-IL-8 into the clinic.

ACKNOWLEDGMENT

REFERENCES

1. Patel L, Charlton SJ, Chambers JK, Macphee CH. Expression and functional analysis of chemokine receptors in human peripheral blood leukocyte populations. *Cytokine.* 2001;14:27-36.
2. Holmes WE, Lee J, Kuang WJ, Rice GC, Wood WI. Structure and functional expression of a human interleukin-8 receptor. *Science.* 1991;253:1278-1280.
3. Murphy PM, Tiffany HL. Cloning of complementary DNA encoding a functional human interleukin-8 receptor. *Science.* 1991;253:1280-1283.
4. Lee J, Horuk R, Rice GC, Bennett GL, Camerato T, Wood WI. Characterization of two high affinity human interleukin-8 receptors. *J Biol Chem.* 1992;267:16283-16287.
5. Cerretti DP, Kozlosky CJ, Vanden Bos T, Nelson N, Gearing DP, Beckmann MP. Molecular characterization of receptors for human interleukin-8, GRO/melanoma growth-stimulatory activity and neutrophil activating peptide-2. *Mol Immunol.* 1993;30:359-367.
6. Hay RV, Skinner RS, Newman OC, *et al.* Scintigraphy of acute inflammatory lesions in rats with radiolabelled recombinant human interleukin-8. *Nucl Med Commun.* 1997;18:367-378.
7. van der Laken CJ, Boerman OC, Oyen WJ, van de Ven MT, van der Meer JW, Corstens FH. Radiolabeled interleukin-8: specific scintigraphic detection of infection within a few hours. *J Nucl Med.* 2000;41:463-469.
8. van der Laken CJ, Boerman OC, Oyen WJ, van de Ven MT, Ven der Meer JW, Corstens FH. The kinetics of radiolabelled interleukin-8 in infection and sterile inflammation. *Nucl Med Commun.* 1998;19:271-281.
9. Gross MD, Shapiro B, Fig LM, Steventon R, Skinner RW, Hay RV. Imaging of human infection with (131)I-labeled recombinant human interleukin-8. *J Nucl Med.* 2001;42:1656-1659.
10. Rennen H, Boerman O, Oyen W, Corstens F. Labeling method largely affects the imaging potential of interleukin-8 [letter]. *J Nucl Med.* 2002;43:1128.
11. Rennen HJ, Boerman OC, Oyen WJ, van der Meer JW, Corstens FH. Specific and rapid scintigraphic detection of infection with 99mTc-labeled interleukin-8. *J Nucl Med.* 2001;42:117-123.
12. Gratz S, Rennen HJ, Boerman OC, Oyen WJ, Burma P, Corstens FH. 99mTc-interleukin-8 for imaging acute osteomyelitis. *J Nucl Med.* 2001;42:1257-1264.
13. Gratz S, Rennen HJ, Boerman OC, Oyen WJ, Corstens FH. Rapid imaging of experimental colitis with (99m)Tc-interleukin-8 in rabbits. *J Nucl Med.* 2001;42:917-923.
14. Rennen HJ, van Eerd JE, Oyen WJ, Corstens FH, Edwards DS, Boerman OC. Effects of coligand variation on the in vivo characteristics of Tc-99m- labeled interleukin-8 in detection of infection. *Bioconjug Chem.* 2002;13:370-377.
15. Abrams MJ, Juweid M, tenKate CI, *et al.* Technetium-99m-human polyclonal IgG radiolabeled via the hydrazino nicotinamide derivative for imaging focal sites of infection in rats. *J Nucl Med.* 1990;31:2022-2028.
16. Schwartz DA, Abrams MJ, Giadomenico CM, Zubieta JA. Certain pyridyl hydrazines and hydrazides useful for protein labeling. US patent number 5,206,370. 27-4-1993
17. Jain NC. Blood volume and water balance. In: Jain NC, ed. *Schalm's Veterinary Hematology.* Philadelphia: Lea & Febiger, 1986:87-102.
18. Darbonne WC, Rice GC, Mohler MA, *et al.* Red blood cells are a sink for interleukin 8, a leukocyte chemotaxin. *J Clin Invest.* 1991;88:1362-1369.
19. Worthen GS, Schwab B, III, Elson EL, Downey GP. Mechanics of stimulated neutrophils: cell stiffening induces retention in capillaries. *Science.* 1989;245:183-186.
20. Drost EM, MacNee W. Potential role of IL-8, platelet-activating factor and TNF-alpha in the sequestration of neutrophils in the lung: effects on neutrophil deformability, adhesion receptor expression, and chemotaxis. *Eur J Immunol.* 2002;32:393-403.
21. Doroshenko T, Chaly Y, Savitskiy V *et al.* Phagocytosing neutrophils down-regulate the expression of chemokine receptors CXCR1 and CXCR2. *Blood.* 2002;100:2668-2671.
22. Feniger-Barish R, Belkin D, Zaslaver A *et al.* GCP-2-induced internalization of IL-8 receptors: hierarchical relationships between GCP-2 and other ELR(+)-CXC chemokines and mechanisms regulating CXCR2 internalization and recycling. *Blood.* 2000;95:1551-1559.
23. Tikhonov I, Doroshenko T, Chaly Y, Smolnikova V, Pauza CD, Voitenok N. Down-regulation of CXCR1 and CXCR2 expression on human neutrophils upon activation of whole blood by S. aureus is mediated by TNF-alpha. *Clin Exp Immunol.* 2001;125:414-422.
24. Khandaker MH, Xu L, Rahimpour R, *et al.* CXCR1 and CXCR2 are rapidly down-modulated by bacterial endotoxin through a unique agonist-independent, tyrosine kinase-dependent mechanism. *J Immunol.* 1998;161:1930-1938.

Chapter 9

^{99m}*Tc-labeled C5a and C5a des Arg^{74} for infection imaging*

Huub J.J.M. Rennen, Wim J.G. Oyen, Stuart. A. Cain,
Peter N. Monk, Frans H.M. Corstens, Otto C. Boerman

ABSTRACT

The complement anaphylatoxin C5a and its natural metabolite C5a des Arg^{74} (C5adR) are involved in several stages of the inflammatory process. Both act on a common receptor expressed on different cell types, including neutrophils and monocytes. The receptor binding affinity of C5a is in the nanomolar range and exceeds that of C5adR by 1-2 orders of magnitude. The biologic potency of C5a is considerably higher than that of C5adR. Here we tested both proteins labeled with ^{99m}Tc for imaging of infection.

Methods: The proteins were labeled with ^{99m}Tc via the hydrazinonicotinamide (HYNIC) chelator. The preparations were tested for imaging of infection in a rabbit model of intramuscular infection. Biodistribution of the radiolabel was determined by γ-camera imaging and by counting dissected tissues at 5 h p.i..

Results: C5a and C5adR showed in vivo abscess uptakes of 0.12 and 0.025 %ID/g, abscess/muscle ratios of 76 and 14, abscess/blood ratios of 9.1 and 2.6, and ROI derived target-to-background ratios of 5.9 and 2.1, respectively at 5 h p.i..

Conclusion: For infection imaging ^{99m}Tc-labeled C5a showed excellent in vivo characteristics. However, C5a is a very bioactive protein, impeding its clinical use as an infection imaging agent. The naturally occurring partial agonist C5adR has less biological effect but showed suboptimal imaging characteristics. The present study showed that for adequate localization of a receptor binding ligand affinities for the receptor in the nanomolar range are required.

INTRODUCTION

Leukocytes, particularly neutrophils and monocytes, accumulate in high numbers at sites of infection. They function as the primary line of defense in the destruction of microorganisms and initiate the repair of tissue. Leukocytes preferentially target infection by chemotaxis and can therefore be used to transport radionuclides to the infected area. Scintigraphic detection of infection can be accomplished by direct labeling of leukocytes (*ex vivo* labeling) or by labeling leukocytes indirectly, i.e. *in vivo* (for a recent review: (*1*)).

Ex vivo labeling requires withdrawal of blood from the patient, purification of leukocytes, labeling and reinjection of the radiolabeled cells. The *ex vivo* leukocyte labeling approach has been developed in the seventies and eighties of the previous century and is still considered the "gold standard" nuclear medicine technique for infection imaging, but is time-consuming and bears the risk of cross contamination.

In vivo labeling of leukocytes can be based on antibody-antigen interactions (e.g. radiolabeled antigranulocyte antibodies) and on leukocyte receptor binding. Recent studies in our laboratory focussed on the use of small leukocyte receptor binding peptides such as chemotactic peptides (formyl-Met-Leu-Phe) (*2*) and cytokines (interleukin-1 and interleukin-8 (*3-5*)). Especially ^{99m}Tc-labeled interleukin-8 appeared to be a highly promising candidate for infection imaging in several preclinical studies (*3;6-8*).

The present study investigated the potential of two selected components of the complement system, C5a and its natural metabolite C5a des Arg[74] (C5adR), for infection imaging. C5a is involved in several stages of the inflammatory response to tissue injury (for a review: (*9;10*)). C5a is a highly potent activator of a wide variety of cell types, including mast cells, neutrophils, monocytes, endothelial and epithelial cells. C5a causes chemotaxis and degranulation of neutrophils, enhances vascular permeability and stimulates the release of cytokines from macrophages and monocytes. *In vivo*, the C-terminal Arginine-residue of C5a is rapidly degraded by serum carboxypeptidase resulting in C5adR. The des-Arg form of C5a has a different pattern of activity as compared to intact C5a, being less active in general and having little spasmogenic or anaphylactic activity. Both C5a and its one aminoacid shortened version C5adR act on a common receptor on neutrophils, monocytes and other cell types, but the receptor affinity of C5a is in the nanomolar range, whereas the receptor affinity of C5adR is considerably lower (*11*). Yancey and coworkers reported monocyte binding affinities of 1.2 nM and 30 nM and neutrophil binding affinities of 2.6 nM and 68 nM for fluorescein-conjugated C5a and C5adR, respectively (*12*). In the present study C5a and C5adR were labeled with ^{99m}Tc via the hydrazinonicotinamide (HYNIC) coupling agent. The preparations were compared for their potential to image infections in a rabbit model of soft-tissue infection.

MATERIALS AND METHODS

Preparation of proteins and of HYNIC-protein-conjugates

Human recombinant C5a and human C5adR were produced in *E. coli* and purified by the methods described by Bubeck et al (*13*). The propylaldehyde hydrazone derivative of succinimidyl-hydrazinonicotinamide (HYNIC) was synthesized essentially as described by Abrams, Schwartz et al. (*14;15*). The C5a-HYNIC and C5adR-HYNIC conjugates were prepared as described previously (*3*). Briefly, in a 1.5 ml vial 4 μl 1 M NaHCO$_3$, pH 8.2 was added to 35-40 μl of protein (4-5 mg/ml). Subsequently, a three-fold molar excess of HYNIC in 5 μl dry DMSO was added dropwise to the

mixture. After incubation for five minutes at room temperature, the reaction was stopped by adding an excess of 200 µl 1 M glycine in PBS. To remove excess unbound HYNIC the mixture was extensively dialyzed against PBS (0.1-0.5 ml dialysis cell 3.5 MWCO, Pierce, Rockford, IL). Dialyzed samples of circa 5 µg protein-HYNIC were stored at –20 ^{0}C.

Technetium-99m labeling of HYNIC conjugated proteins

20 mg tricine (N-[Tris(hydroxymethyl)-methyl]glycine, Fluka, Buchs, Switzerland) in 0.2 ml PBS, 20 µl of a solution containing $SnSO_4$ (1 mg/ml in 0.1M HCl) and 0.5 ml 200-300 MBq $^{99m}TcO_4^-$ in saline were added to 5 µg thawed HYNIC-C5a or HYNIC-C5adR and incubated at room temperature for 30 minutes. The radiochemical purity was determined by instant thin-layer chromatography (ITLC) on ITLC-SG strips (Gelman Laboratories, Ann Arbor, MI) with 0.1 M citrate, pH 6.0, as the mobile phase. Following the labeling reaction the reaction mixture was applied to a Sephadex G-25 column (PD-10; Pharmacia, Uppsala, Sweden) and eluted with 0.5 % BSA in PBS to purify the radiolabeled conjugates.

Receptor binding assay

Human neutrophils were isolated from heparinized whole blood obtained from healthy donors. Receptor binding assays were performed essentially as described previously (*4*). Briefly, heparinized human whole blood (20 ml) was mixed with 2.5 ml 5% Dextran (Sigma, St. Louis, MO). After removing the red blood cell bulk by sedimentation during 1 hr at room temperature, the remainder of the blood sample was washed in incubation buffer (1 mM NaH_2PO_4, 5 mM Na_2HPO_4, 140 mM NaCl, 0.5 mM $MgCl_2$, 0.15 mM $CaCl_2$, 0.5% HSA, pH 7.4) and centrifuged at 500xg for 20 min. The cell pellet was then resuspended in 7 ml incubation buffer and layered on 5 ml Ficoll-Hypaque (Pharmacia, Uppsala, Sweden), followed by centrifugation at 500xg for 20 min. The pellet, rich of polymorphonuclear cells (PMNs), was washed once and subsequently resuspended in incubation buffer. A series of serially diluted PMN suspensions (0.5 - 8 x 10^6 PMN/ml) was incubated with 10,000 cpm of ^{99m}Tc-labeled C5a and another series similarly with ^{99m}Tc-labeled C5adR. Duplicates of the lowest cell concentration were incubated in the presence of a 100-fold molar excess of unlabeled C5a to correct for nonspecific binding. After 3 h incubation at 4 ^{0}C, PMNs were centrifuged (5 min, 2000xg) and the radioactivity in the pellet (total bound activity) was measured in a shielded well-type gamma counter (Wizard, Pharmacia-LKB, Sweden). The data were graphically analyzed in a modified Lineweaver-Burk plot: a double inverse plot of the conventional binding plot (specifically bound fraction

versus cell concentration) (*16*). The receptor-binding fraction at infinite cell excess was calculated by linear extrapolation to the ordinate.

Animal studies

Animal studies were carried out in accordance with the guidelines of the local animal welfare committee. Abscesses were induced in the left thigh muscle of ten female New Zealand white rabbits (2.4-2.7 kg) with 10^{11} colony forming units (cfu) of *Escherichia coli* in 0.5 ml. During the procedure, the rabbits were sedated with a subcutaneous injection of a 0.6 ml mixture of fentanyl 0.315 mg/ml and fluanisone 10 mg/ml (Hypnorm, Janssens Pharmaceutical, Buckinghamshire, UK). After 24 hours, when swelling of the muscle was apparent, five rabbits were injected with 18 MBq ^{99m}Tc-HYNIC-C5a (protein dose 2 µg) via the ear vein. The five other rabbits received 16 MBq ^{99m}Tc-HYNIC-C5adR (protein dose 2 µg) intravenously. Three rabbits of each group were used for gamma camera imaging. For imaging, rabbits were immobilized, placed prone on the gamma camera and injected with either ^{99m}Tc-HYNIC-C5a or ^{99m}Tc-HYNIC-C5adR in the lateral ear vein. Images were recorded at 1 min, 1, 3 and 5 h p.i. with a single-head gamma camera (Orbiter, Siemens Medical Systems Inc., Hoffman Estates, IL) equipped with a parallel-hole low-energy all purpose collimator. Images (100,000-200,000 counts per image) were obtained and digitally stored in a 256 x 256 matrix.

The scintigraphic results were analyzed quantitatively by drawing regions of interest (ROI) over the abscess and the uninfected contralateral thigh muscle (background). Abscess-to-background ratios were calculated.

After completion of the final imaging and blood sampling (5 h p.i.), the rabbits were killed with a lethal dose of sodium phenobarbital. Samples of blood, infected thigh muscle, uninfected contralateral thigh muscle, lung, spleen, liver, kidneys and intestines were collected. The dissected tissues were weighed and counted in a gamma counter. Injection standards were counted simultaneously to correct for radioactive decay. The measured activity in samples was expressed as percentage of injected dose per gram tissue (%ID/g). Abscess-to-contralateral muscle ratios and abscess-to-blood ratios were calculated.

Statistical analysis

All mean values are given as %ID/g or ratios ± one standard error of the mean (s.e.m.). The data were analyzed statistically using unpaired two-tailed t tests (GraphPad Instat 3.00 Win 95, San Diego, CA, USA).

RESULTS

Radiolabeling and characterization of ^{99m}Tc-HYNIC-C5a and ^{99m}Tc-HYNIC-C5adR
The specific activities of the radiolabeled purified C5a and C5adR preparations were 9 MBq/μg and 8 MBq/μg, respectively. The radiochemical purity of both preparations was higher than 95% after gel filtration as determined by ITLC. The fraction of the radiolabeled preparation binding to receptors on granulocytes was 40% for ^{99m}Tc-HYNIC-C5a and 50% for ^{99m}Tc-HYNIC-C5adR.

Animal studies in rabbits with *E. coli* infection

Table 1 shows the biodistribution of ^{99m}Tc-HYNIC-C5a and ^{99m}Tc-HYNIC-C5adR in rabbits with *E. coli* infections at 5 h p.i. For C5a significantly higher values were observed for radioactivity uptake in the abscess (P<0.01), lungs (P<0.01) and spleen (P<0.001). Kidney uptake of C5a was significantly lower as compared to C5adR (P<0.05). Abscess/muscle and abscess/blood ratios were significantly higher for C5a (P<0.05, P<0.01 resp.): 75 ± 24 and 9.1 ± 1.8 vs 14 ± 2 and 2.6 ± 0.3 for C5adR resp. For both preparations the radiolabel was excreted almost exclusively via the kidneys. Gamma camera imaging rapidly visualized the abscesses in the thigh muscles from 1 h p.i. onwards for C5a (Fig. 1). The C5adR preparation showed only modest results in delineating infectious foci from 3 h p.i. onwards. Quantitative analysis of the images revealed abscess/background ratios improving with time up to 5.9 ± 1.0 for C5a vs 2.1 ± 0.1 for C5adR at 5 h p.i. (Fig. 2). Abscess/background ratios were significantly higher for C5a as compared to C5adR from 1 h p.i. onwards (P<0.05). Immediately after injection high kidney uptake was observed for both preparations, remaining prominent throughout the study.

Table 1. *Biodistribution of ^{99m}Tc-HYNIC-C5a and ^{99m}Tc-HYNIC-C5adR in rabbits with E. coli infections at 5 h p.i. (mean values ± s.e.m.). * P<0.05, ** P<0.01, *** P<0.001 (unpaired two-tailed t tests).*

%ID/g	^{99m}Tc-C5a N=5	P	^{99m}Tc-C5adR N=5
blood	0.013 ± 0.001		0.010 ± 0.001
muscle	0.002 ± 0.0004		0.002 ± 0.0004
abscess	0.12 ± 0.02	**	0.025 ± 0.003
lung	0.13 ± 0.02	**	0.032 ± 0.005
spleen	0.26 ± 0.03	***	0.093 ± 0.010
kidney	1.88 ± 0.09	*	2.44 ± 0.19
liver	0.046 ± 0.004		0.045 ± 0.006
intestine	0.028 ± 0.002		0.029 ± 0.002
abscess/muscle	75 ± 24	*	14 ± 2
abscess/blood	9.1 ± 1.8	**	2.6 ± 0.3
%ID kidneys	33 ± 1	**	40 ± 1
%ID abscess	1.63 ± 0.22	***	0.37 ± 0.06
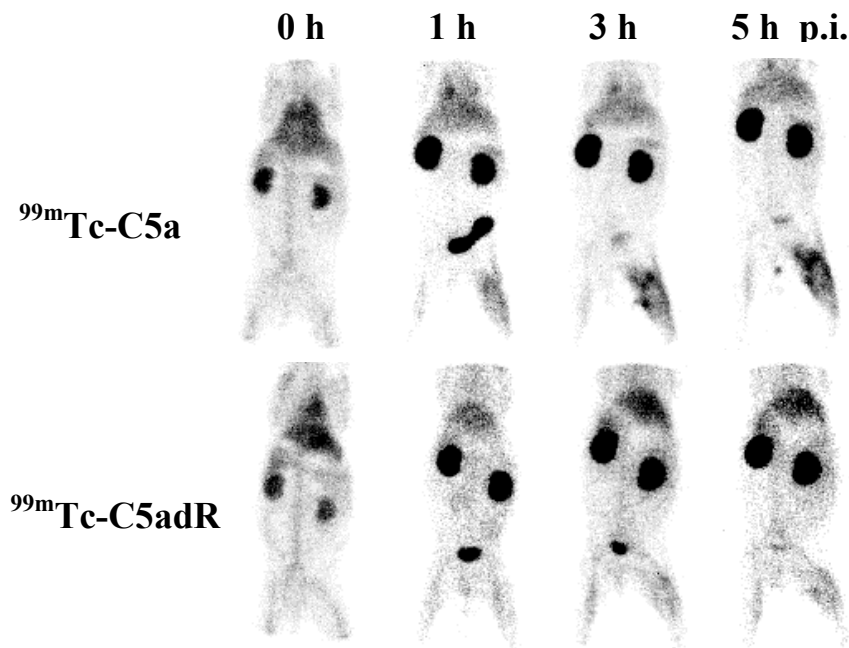
Figure 1. *Scintigraphic images of rabbits with an E. coli abscess in the left thigh muscle at 1 min, 1, 3 and 5 h after injection of ^{99m}Tc-HYNIC-C5a (upper panel) or ^{99m}Tc-HYNIC-C5adR (lower panel).*

Figure 2. *The abscess-to-background ratios as determined by quantitative analysis of the images of rabbits with E. coli infection injected with ^{99m}Tc-HYNIC-C5a or ^{99m}Tc-HYNIC-C5adR. The error bars indicate s.e.m. * P<0.05 (unpaired two-tailed t tests).*

DISCUSSION

In this study the imaging potential of two small leukocyte receptor binding proteins was explored: The complement factor C5a and its natural metabolite C5adR. The difference between the two proteins is that C5a has just one additional C-terminal aminoacid r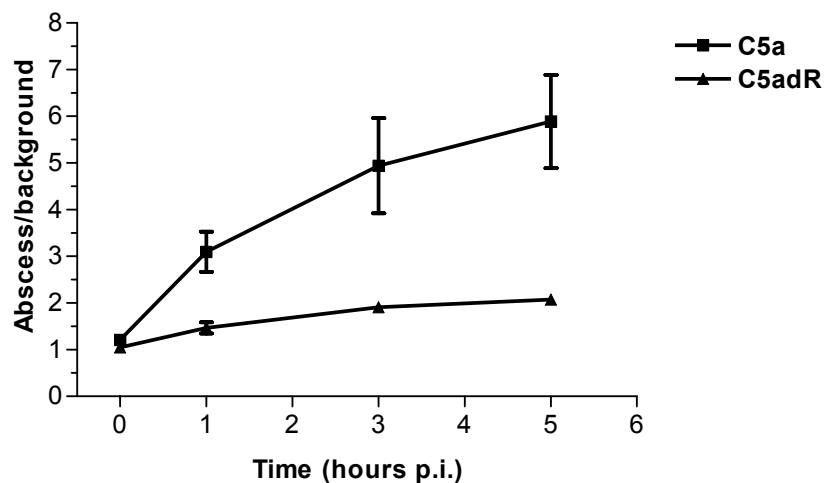esidue but the *in vivo* behavior of the peptides in the rabbit model was totally different. Theoretically, for infection imaging one would prefer a protein that binds its receptor with high affinity, while inducing marginal biologic effects. C5a has a relatively high affinity for its receptor (in the nanomolar range) resulting in superior image quality of ^{99m}Tc-labeled C5a over C5adR. However, the spasmogenic and anaphylactic potencies of C5a make it unsuitable for use as a clinical diagnostic agent. C5adR has less undesirable biological effect, but the characteristics for infection imaging are far from optimal, presumably due to the lower binding affinity for the C5a-receptor. In fact, we investigated two other C5a receptor antagonists: the C5adR mutant with Lys[68] substituted by Glu[68] (C5adR E68) (*17*) and a C5adR mutant with a C-terminus heptapeptide substitution (*18*). Like C5adR, these low affinity antagonists also showed relatively low uptake in the abscess and thus are unsuitable for infection imaging (data not shown).

In order to block inappropriate activation of the complement system in human disease numerous C5a receptor antagonists have been developed. Such agents include high molecular weight C5a receptor antagonists derived from C5a (*18;19*) and low molecular weight (<1000 Da) cyclic and linear peptides (*20-29*). Some of these antagonists have been shown to be potentially valuable complement therapeutics showing potent anti-inflammatory antagonist properties. In general, however, these antagonists bind with lower affinity to the C5a-receptor (affinities one to two orders of magnitude lower than C5a). The present study showed that for adequate localization of a receptor binding ligand an affinitiy for the receptor in the nanomolar range is required. However, the only C5a derivative meeting this demand is C5a itself. A C5a protein dose of 1 µg/kg of body weight as used in this study is reported to induce a serious but transient neutropenia followed by a prolonged neutrophilia (*30*). Theoretically, biological effects could be avoided by reducing the C5a administration doses below the biological threshold. In order to decrease protein doses, the specific activity of radiolabeled C5a (as expressed in MBq/µg) should be increased. By adopting alternative labeling strategies, specific activities could be substantially increased as demonstrated by our studies with ^{99m}Tc-labeled interleukin-8 (*8*). In the case of labeling interleukin-8 with ^{99m}Tc, different coligand formulations were used to enhance the specific activity of the preparation. The use of (iso-)nicotinic acid as coligand resulted in a dramatic improvement of the specific activity of the [99m]Tc-

labeled interleukin-8 preparation. However, in case of labeling C5a with ^{99m}Tc we did not succeed in generating specific activities that were high enough to exclude potential biological effects.

In conclusion, as an infection imaging agent ^{99m}Tc-labeled C5a is an excellent agent yielding high target-to-background ratios and is clearly better than C5adR, but its use in the clinic is impeded due to its biological activity. C5adR is less bioactive but its imaging quality is inferior. Binding affinities for the receptor in the nanomolar range appeared to be critical for effective accumulation in receptor rich tissue. To our knowledge no C5a receptor antagonist exists which combines high binding affinity with low biological activity. In the absence of such an antagonist the only solution to circumvent biological effects on i.v. administration of labeled C5a is to reduce protein doses by enhancing the specific activity of ^{99m}Tc-labeled C5a (in MBq/µg). So far, the applied radiolabeling procedures could not put C5a protein doses below the biological threshold.

REFERENCES

1. Rennen HJ, Boerman OC, Oyen WJ, Corstens FH. Imaging infection/inflammation in the new millennium. *Eur J Nucl Med.* 2001;28:241-252.
2. van der Laken CJ, Boerman OC, Oyen WJ, van de Ven MT, Edwards DS, Barrett JA, van der Meer JW, Corstens FH. Technetium-99m-labeled chemotactic peptides in acute infection and sterile inflammation. *J Nucl Med.* 1997;38:1310-1315.
3. Rennen HJ, Boerman OC, Oyen WJ, van der Meer JW, Corstens FH. Specific and rapid scintigraphic detection of infection with 99mTc- labeled interleukin-8. *J Nucl Med.* 2001;42:117-123.
4. van der Laken CJ, Boerman OC, Oyen WJ, van de Ven MT, Claessens RA, van der Meer JW, Corstens FH. Specific targeting of infectious foci with radioiodinated human recombinant interleukin-1 in an experimental model. *Eur J Nucl Med.* 1995;22:1249-1255.
5. van der Laken CJ, Boerman OC, Oyen WJ, van de Ven MT, van der Meer JW, Corstens FH. Radiolabeled interleukin-8: specific scintigraphic detection of infection within a few hours. *J Nucl Med.* 2000;41:463-469.
6. Gratz S, Rennen HJ, Boerman OC, Oyen WJ, Burma P, Corstens FH. (99m)Tc-interleukin-8 for imaging acute osteomyelitis. *J Nucl Med.* 2001;42:1257-1264.
7. Gratz S, Rennen HJ, Boerman OC, Oyen WJ, Corstens FH. Rapid imaging of experimental colitis with (99m)Tc-interleukin-8 in rabbits. *J Nucl Med.* 2001;42:917-923.
8. Rennen HJ, van Eerd JE, Oyen WJ, Corstens FH, Edwards DS, Boerman OC. Effects of coligand variation on the in vivo characteristics of ^{99m}Tc-labeled interleukin-8 in detection of infection. *Bioconjug Chem.* 2002;13:370-377.
9. Makrides SC. Therapeutic inhibition of the complement system. *Pharmacol Rev.* 1998;50:59-87.
10. Pellas TC, Wennogle LP. C5a receptor antagonists. *Curr Pharm Des.* 1999;5:737-755.
11. Marder SR, Chenoweth DE, Goldstein IM, Perez HD. Chemotactic responses of human peripheral blood monocytes to the complement-derived peptides C5a and C5a des Arg. *J Immunol.* 1985;134:3325-3331.
12. Yancey KB, Lawley TJ, Dersookian M, Harvath L. Analysis of the interaction of human C5a and C5a des Arg with human monocytes and neutrophils: flow cytometric and chemotaxis studies. *J Invest Dermatol.* 1989;92:184-189.
13. Bubeck P, Grotzinger J, Winkler M, Kohl J, Wollmer A, Klos A, Bautsch W. Site-specific mutagenesis of residues in the human C5a anaphylatoxin which are involved in possible interaction with the C5a receptor. *Eur J Biochem.* 1994;219:897-904.
14. Abrams MJ, Juweid M, tenKate CI, Schwartz DA, Hauser MM, Gaul FE, Fuccello AJ, Rubin RH, Strauss HW, Fischman AJ. Technetium-99m-human polyclonal IgG radiolabeled via the hydrazino nicotinamide derivative for imaging focal sites of infection in rats. *J Nucl Med.* 1990;31:2022-2028.
15. Schwartz DA, Abrams MJ, Giadomenico CM, Zubieta JA. Certain pyridyl hydrazines and hydrazides useful for protein labeling. US patent nr 5,206,370. Apr 1993.

16. Lindmo T, Boven E, Cuttitta F, Fedorko J, Bunn PA, Jr. Determination of the immunoreactive fraction of radiolabeled monoclonal antibodies by linear extrapolation to binding at infinite antigen excess. *J Immunol Methods.* 1984;72:77-89.

17. Cain SA, Williams DM, Harris V, Monk PN. Selection of novel ligands from a whole-molecule randomly mutated C5a library. *Protein Eng.* 2001;14:189-193.

18. Heller T, Hennecke M, Baumann U, Gessner JE, zu Vilsendorf AM, Baensch M, Boulay F, Kola A, Klos A, Bautsch W, Kohl J. Selection of a C5a receptor antagonist from phage libraries attenuating the inflammatory response in immune complex disease and ischemia/reperfusion injury. *J Immunol.* 1999;163:985-994.

19. Pellas TC, Boyar W, van Oostrum J, Wasvary J, Fryer LR, Pastor G, Sills M, et al. Novel C5a receptor antagonists regulate neutrophil functions in vitro and in vivo. *J Immunol.* 1998;160:5616-5621.

20. Finch AM, Wong AK, Paczkowski NJ, Wadi SK, Craik DJ, Fairlie DP, Taylor SM. Low-molecular-weight peptidic and cyclic antagonists of the receptor for the complement factor C5a. *J Med Chem.* 1999;42:1965-1974.

21. Haynes DR, Harkin DG, Bignold LP, Hutchens MJ, Taylor SM, Fairlie DP. Inhibition of C5a-induced neutrophil chemotaxis and macrophage cytokine production in vitro by a new C5a receptor antagonist. *Biochem Pharmacol.* 2000;60:729-733.

22. Paczkowski NJ, Finch AM, Whitmore JB, Short AJ, Wong AK, Monk PN, Cain SA, Fairlie DP, Taylor SM. Pharmacological characterization of antagonists of the C5a receptor. *Br J Pharmacol.* 1999;128:1461-1466.

23. Short A, Wong AK, Finch AM, Haaima G, Shiels IA, Fairlie DP, Taylor SM. Effects of a new C5a receptor antagonist on C5a- and endotoxin-induced neutropenia in the rat. *Br J Pharmacol.* 1999;126:551-554.

24. Short AJ, Paczkowski NJ, Vogen SM, Sanderson SD, Taylor SM. Response-selective C5a agonists: differential effects on neutropenia and hypotension in the rat. *Br J Pharmacol.* 1999;128:511-514.

25. Strachan AJ, Shiels IA, Reid RC, Fairlie DP, Taylor SM. Inhibition of immune-complex mediated dermal inflammation in rats following either oral or topical administration of a small molecule C5a receptor antagonist. *Br J Pharmacol.* 2001;134:1778-1786.

26. Strachan AJ, Woodruff TM, Haaima G, Fairlie DP, Taylor SM. A new small molecule C5a receptor antagonist inhibits the reverse- passive Arthus reaction and endotoxic shock in rats. *J Immunol.* 2000;164:6560-6565.

27. Tempero RM, Hollingsworth MA, Burdick MD, Finch AM, Taylor SM, Vogen SM, et al. Molecular adjuvant effects of a conformationally biased agonist of human C5a anaphylatoxin. *J Immunol.* 1997;158:1377-1382.

28. Ulrich JT, Cieplak W, Paczkowski NJ, Taylor SM, Sanderson SD. Induction of an antigen-specific CTL response by a conformationally biased agonist of human C5a anaphylatoxin as a molecular adjuvant. *J Immunol.* 2000;164:5492-5498.

29. Vogen SM, Prakash O, Kirnarsky L, Sanderson SD, Sherman SA. Determination of structural elements related to the biological activities of a potent decapeptide agonist of human C5a anaphylatoxin. *J Pept Res.* 1999;54:74-84.

30. Kajita T, Hugli TE. C5a-induced neutrophilia. A primary humoral mechanism for recruitment of neutrophils. *Am J Pathol.* 1990;137:467-477.

Chapter 10

Relationship between neutrophil binding affinity and suitability for infection imaging: Comparison of ^{99m}Tc-labeled NAP-2 (CXCL-7) and three C-terminally truncated isoforms

Huub J.J.M. Rennen, Cathelijne Frielink, Ernst Brandt, Sebastiaan A.J. Zaat, Otto C. Boerman, Wim J.G. Oyen, Frans H.M. Corstens

ABSTRACT

The CXC-chemokines are a family of closely related chemoattractant cytokines, which bind to, attract and activate neutrophils to variable degrees. In this study the relationship between neutrophil binding affinity and suitability for infection imaging was investigated in a selected group of CXC-chemokines. Neutrophil-activating-peptide-2 (NAP-2, 70 residues, also called CXCL7) binds with high affinity to the CXCR2 receptor on neutrophils. Recently, C-terminally truncated NAP-2-variants have been described that have enhanced neutrophil binding affinity and neutrophil-stimulating capacity. Here, NAP-2 and its C-terminal shortened variants NAP-2(1-68), NAP-2(1-66) and NAP-2(1-63) were labeled with ^{99m}Tc via the hydrazinonicotinamide (HYNIC) chelator and their potential for imaging of infection was investigated in a rabbit model of infection. The CXC-chemokine interleukin-8 (IL-8) was used as a reference. In addition, a series of ^{99m}Tc-labeled CXC-chemokines were screened for their potential to image infection including CTAP-III, GCP-2, ENA-78, PF-4 and IP-10.

Methods: The receptor binding affinity of HYNIC-conjugated NAP-2 and its analogues was compared in competitive binding assays on Jurkat cells transfected with the CXCR2 receptor gene. Biodistribution of labeled NAP-2 (analogues) and other CXC-chemokines in rabbits with intramuscular *E.coli* infections was determined both by γ-camera imaging and by counting dissected tissues at 6 h p.i.

Results: The CXCR2 binding affinity of the HYNIC-conjugated NAP-2 analogues relative to NAP-2 was: NAP-2(1-68) 2.5-fold, NAP-2 (1-66) 10-fold and NAP-2(1-63) 3-fold. In the rabbit model, uptake in the abscess (in %ID/g ± s.e.m.) was for NAP-2 0.084 ± 0.015, for NAP-2(1-68) 0.098 ± 0.010, for NAP-2(1-66) 0.189 ± 0.044 and for NAP-2(1-63) 0.114 ± 0.017 at 6 h p.i. respectively. In comparison, higher uptake in the abscess was found for labeled IL-8, a modest uptake for GCP-2 and ENA-78, and a low uptake for CTAP-III, PF-4 and IP-10.

Conclusion: This study showed a clear relationship between affinity to receptors on neutrophils and suitability for infection imaging. Of the NAP-2 variants, NAP-2(1-66) combined highest affinity to CXCR2 with best characteristics for imaging. IL-8 binds to both CXCR1 and CXCR2 with high affinity and showed a superior imaging quality. The other CXC-chemokines tested bind to neutrophils with lower affinity and showed to be less suitable for infection imaging in this study.

INTRODUCTION

White blood cells, particularly neutrophils and monocytes, accumulate in high numbers at sites of infection. They function as the primary line of defense in the destruction of microorganisms and initiate the repair of tissue. A variety of chemotactic peptides and proteins orchestrate the directed migration of leukocytes to inflammatory sites. Potentially these leukocyte-binding proteins can be used as an infection imaging agent, labeled either in their original natural form or in the sophisticated disguise of a receptor antagonist (for a review see (*1*)). This study focusses on a selection of chemokines for infection imaging.

The "chemokines" (short for *chemo*attractant cyto*kines*) are a superfamily of closely related and conserved cytokines. Most of the chemokines are small, with molecular weights in the range of 8 to 12 kDa. The chemokine superfamily is divided into subfamilies depending on the position of the highly conserved cysteines (*2*). One major subfamily is designated "CXC" because the two cysteines (C) nearest the N-termini of these proteins are separated by a single, nonconserved amino acid residue (X). The other major subfamily is called "CC" because these two cysteines are adjacent. The CXC-chemokines act predominantly on neutrophils, whereas the CC-chemokines act on lymphocytes, monocytes, mastcells and eosinophils (*3*). The CXC chemokine subfamily can be further divided into ELR$^+$ and ELR$^-$ CXC chemokines depending on the presence or absence of a Glu-Leu-Arg (ELR) motif, respectively. This motif is positioned in the NH$_2$-terminal region just in front of the first cysteine of the CXC-motif. The ELR$^+$ CXC chemokines are the most selective chemotactic factors for neutrophil migration. Interleukin-8 (IL-8, recently renamed CXC chemokine ligand 8 (CXCL8) (*4*)) is the prototype of this group and is the most potent neutrophil activating protein of the CXC chemokines in the human system. Other members of this group include growth regulated oncogene (GROα (CXCL1), GROβ (CXCL2) and GROγ (CXCL3)), connective tissue activating peptide-III (CTAP-III), neutrophil activating protein-2 (NAP-2 (CXCL7)), epithelial cell derived neutrophil attractant-78 (ENA-78 (CXCL5)) and granulocyte chemotactic protein-2 (GCP-2 (CXCL6)). The ELR$^-$ CXC chemokines include platelet factor-4 (PF-4 (CXCL4)) and interferon γ-inducible protein (IP-10 (CXCL10)). There are two high affinity G protein-coupled CXC chemokine receptors on neutrophils: CXC chemokine receptor 1 (CXCR1) and CXCR2 (*5*). IL-8 and GCP-2 bind to both CXCR1 and CXCR2, whereas the other ELR$^+$ CXC chemokines are specific ligands for CXCR2 (*6;7*). The ELR$^-$ CXC chemokines PF-4 and IP-10 lack significant CXCR1 and CXCR2 binding (*8;9*). PF-4 is reported to be active on many different cell types, including neutrophils (*10*), but no G protein-coupled receptor has been identified for PF-4 so far.

In this study we aimed to select the most promising candidates within the family of the CXC-chemokines. Is there a clear relationship between biological properties such as neutrophil chemoattractant activity (as can be assessed in Boyden chamber assays), neutrophil activating properties (e.g., elastase release) and neutrophil binding affinity on the one side and suitability for infection imaging on the other side? We hypothesize that neutrophil binding affinity is a useful criterion for selecting the most suitable CXC-chemokine for infection imaging. This study focusses on NAP-2 and three C-terminally truncated NAP-2 variants. NAP-2 is a member of a group of CXC-chemokines collectively termed β-thromboglobulins (*10*). These are platelet α-granule-derived proteins, which differ only in the length of the termini. Platelet basic protein (PBP, 94 residues) and CTAP-III (85 residues) were shown to become converted into NAP-2 (70 residues) by N-terminal truncation through limited proteolysis (*11;12*). Although structurally closely related, the β-thromboglobulins PBP and CTAP-III do not exhibit neutrophil-stimulatory activity in contrast to their proteolytic daughter compound NAP-2. Recently, C-terminally truncated NAP-2-variants have been described that have enhanced affinity for receptors on neutrophils and enhanced neutrophil-stimulating capacity (*13;14*). NAP-2(1-68) is also named thrombocidin-1 (TC-1) and has bactericidal properties (*15*). Here, NAP-2 and its C-terminally shortened variants NAP-2(1-68), NAP-2(1-66) and NAP-2(1-63) were labeled with ^{99m}Tc and their potential for imaging of infection was investigated in rabbits with intramuscular *E.coli* infection. IL-8, binding to both CXCR1 and CXCR2 with high affinity, has already been studied in detail for infection imaging purposes and was used as a reference (*16-18*).

In addition, a broad inventarisation of the CXC-chemokines for infection imaging was made. CTAP-III, GCP-2, ENA-78 (ELR$^+$ CXC-chemokines) and PF-4, IP-10 (ELR$^-$ CXC-chemokines) are a representative selection of the CXC-chemokines and were tested in our laboratory using the same rabbit model of intramuscular infection as used above.

MATERIALS AND METHODS

Chemokines

The following human recombinant proteins were used: NAP-2 was purchased from RDI (Flanders, NJ, USA). NAP-2(1-68) (also named thrombocidin-1 (TC-1)), NAP-2(1-66) and NAP-2(1-63) were produced by recombinant methods as described previously (*12*). IL-8 was kindly provided by Dr I. Lindley (Novartis, Vienna, Austria). GCP-2, ENA-78 and IP-10 were purchased from RDI (Flanders, NJ, USA). CTAP-III and PF-4 were

kindly provided by Dr A. Waltz (Theodor-Kocher Institute, University of Bern, Bern, Switzerland).

Conjugation of HYNIC to chemokine

The propylaldehyde hydrazone of succinimidyl-hydrazinonicotinamide (HYNIC) was synthesized essentially as described previously (*3;19*). The HYNIC-chemokine conjugate was prepared as described previously (*16*). Briefly, in a 1.5 ml vial 5 μl 1 M NaHCO$_3$, pH 8.2 was added to 35 μl of chemokine (5 mg/ml). Subsequently, a three-fold molar excess of HYNIC in 5 μl dry DMSO was added dropwise to the mixture. After incubation for ten to thirty minutes at room temperature, the reaction was stopped by adding an excess of glycine (200 μl, 1 M in PBS). To remove excess unbound HYNIC the mixture was extensively dialyzed against PBS (0.1-0.5 ml dialysis cell 3.5 MWCO, Pierce, Rockford, IL). Dialyzed samples of circa 8 μg HYNIC-conjugated chemokine were stored at –20 ^{0}C.

Technetium-99m labeling of HYNIC conjugated chemokine

Tricine (N-[Tris(hydroxymethyl)-methyl]glycine) was purchased from Fluka (Buchs, Switzerland), nicotinic acid from Sigma-Aldrich (St. Louis, MO). For labeling of the HYNIC-conjugated chemokines with ^{99m}Tc, tricine and nicotinic acid were used as coligands as described previously (*17*). To a thawed sample of 8 μg HYNIC-chemokine was added 0.2 ml of a solution of tricine and nicotinic acid (125 mg/ml and 12.5 mg/ml respectively, in PBS, adjusted to pH 7.0 with 2M NaOH), 20 μL of a freshly prepared tin (II) solution (10 mg SnSO$_4$ in 10 ml nitrogen-purged 0.1 N HCl) and 300-400 MBq $^{99m}TcO_4^-$ in saline. The mixture was incubated at 70 ^{0}C for 30 minutes.

The radiochemical purity was determined by instant thin-layer chromatography (ITLC) on ITLC-SG strips (Gelman Laboratories, Ann Arbor, MI) with 0.1 M citrate, pH 6.0, as the mobile phase. In case of a labeling-efficiency smaller than 96%, the reaction mixture was applied to a Sephadex G-25 column (PD-10; Pharmacia, Uppsala, Sweden) and eluted with PBS, 0.5% BSA to purify the radiolabeled chemokine. For animal experiments, the reaction mixture was diluted with PBS, 0.5% BSA to a concentration of 40 MBq/mL, ready for i.v. administration in the rabbits.

Receptor binding competition assays

The interaction of HYNIC conjugated NAP-2, its variants and IL-8 with chemokine receptor CXCR2 was investigated in binding competition assays using ^{99m}Tc-labeled IL-8 as a tracer. These assays were performed using Jurkat cells transfected with the CXCR2 receptor, a kind gift of Drs. Loetscher and Baggiolini (Theodor Kocher

Institute, University of Bern, Bern, Switserland) (*20*). The Jurkat cells were cultured at 37 $^{\circ}$C in a humidified atmosphere of air/CO$_2$ (95:5) in RPMI 1640 medium (GIBCO, Gaithersburg, MD) containing 10% fetal calf serum and 1% glutamine, amino acids and pyruvate. The medium also contained Pen/Strep, 5 x 10^{-5} M of β-mercaptoethanol and 1.5 μg/ml puromycin for selection. Live Jurkat cells were centrifuged (5 min, 2000xg) and washed once with assay buffer (RPMI 1640, 0.5% BSA, 0.05% NaN$_3$). For the receptor binding competition assays CXCR2 bearing Jurkat cells were suspended at ~4x10^8 cells/ml (final concentration) in RPMI 1640 medium containing 0.5% BSA. Duplicate samples of ~2x10^8 cells were incubated on ice for 3 h with a constant amount of ^{99m}Tc-labeled IL-8 (~0.014 nM IL-8, ~50,000 counts of radioactivity) as a tracer, in the presence or absence of increasing concentrations (0.25 nM – 400 nM) of HYNIC-conjugated NAP-2, its variants and IL-8 in a total volume of 0.5 ml. To correct for nonspecific binding of ^{99m}Tc-labeled IL-8 a sample was incubated in the presence of a 30,000 fold excess of native IL-8. After an incubation of 3 h on ice, cells were centrifuged (5 min, 2000xg), washed twice with incubation buffer and the radioactivity in the pellet (total bound radioactivity) was measured in a shielded well-type gamma counter (Wizard; Pharmacia, Uppsala, Sweden). Nonspecific binding of ^{99m}Tc-labeled IL-8 was subtracted. Each assay was performed in duplo. The concentration of HYNIC-conjugated NAP-2 that caused 50% displacement was set at 1 and the IC50 concentrations of the HYNIC-conjugated NAP-2 variants and IL-8 were expressed relative to that of HYNIC-conjugated NAP-2.

Animal studies

For a direct comparison between ^{99m}Tc-labeled NAP-2, its three C-terminally truncated variants and IL-8 in imaging intramuscular infection, abscesses were induced in the left thigh muscle of 25 female New Zealand rabbits (2.4-2.7 kg) with 1-2 x 10^{11} colony forming units (cfu) of *Escherichia coli* in 0.5 ml. During the procedure, rabbits were anaesthetized with a subcutaneous injection of a 0.6 ml mixture of fentanyl 0.315 mg/ml and fluanisone 10 mg/ml (Hypnorm, Janssens Pharmaceutical, Buckinghamshire, UK). The rabbits were divided into five groups of five animals (five animals per ^{99m}Tc-labeled chemokine). After 24 hours, when swelling of the muscle was apparent, the rabbits were injected with 20 MBq ^{99m}Tc-labeled chemokine (protein dose 0.5 μg) via the ear vein. Three rabbits out of each group were used for gamma camera imaging. These rabbits were immobilized, placed prone on the gamma camera and images were recorded at 1-5 min, 1½, 3, 4½ and 6 h p.i. with a single-head gamma camera (Orbiter, Siemens Medical Systems Inc., Hoffman Estates, IL) equipped with a parallel-hole low-energy all purpose collimator. Images were obtained with a 15% symmetrical window over the 140 keV energy peak

of ^{99m}Tc. After acquisition of 200,000-300,000 counts, the images were digitally stored in a 256 x 256 matrix. Scintigraphic images were analyzed quantitatively by drawing regions of interest (ROI) over the abscess and the uninfected contralateral thigh muscle (background). Abscess-to-background ratios were calculated.

After completion of the final imaging session (6 h p.i.), all rabbits were killed with a lethal dose of pentobarbital (euthesate®, Ceva Sante Animale, Naaldwijk, The Netherlands). Samples of blood, infected thigh muscle, uninfected contralateral thigh muscle, lung, spleen, liver, kidneys and intestines were collected. The dissected tissues were weighed and counted in a gamma counter. To correct for radioactive decay injection standards were counted simultaneously. The measured activity in samples was expressed as percentage of injected dose per gram tissue (%ID/g). Abscess-to-contralateral muscle ratios and abscess-to-blood ratios were calculated.

Using the same rabbit model of intramuscular infection, the ^{99m}Tc-labeled CXC-chemokines CTAP-III, GCP-2, ENA-78, PF-4 and IP-10 were tested for infection imaging at a smaller scale.

Statistical analysis

All mean values are given as %ID/g, %ID or ratios ± 1 standard error of the mean (s.e.m.). The data were analyzed statistically using the one-way ANOVA with Dunnett's posttest (GraphPad Instat 3.00 Win 95, San Diego, CA, USA) comparing data for the ^{99m}Tc-labeled NAP-2 derivatives with data for ^{99m}Tc-labeled NAP-2.

RESULTS

^{99m}Tc-labeling of the chemokines

The radiochemical purities of ^{99m}Tc-labeled NAP-2, its variants and IL-8 exceeded 98% in all cases, as determined by instant thin-layer chromatography, excluding the need for further purification. This is in line with our previous findings for IL-8, where the same labeling strategy using tricine and nicotinic acid as coligands was adopted (*17*). The specific activities of the preparations of ^{99m}Tc-labeled NAP-2, its variants and IL-8 were high, approximately 40-50 MBq per microgram of protein. The specific activities of the preparations of ^{99m}Tc-labeled CTAP-III, GCP-2, ENA-78, PF-4 and IP-10 ranged from 20-40 MBq per microgram of protein.

Receptor binding competition assays

The receptor binding competition assays involved a direct comparison in binding to the CXCR2 receptor between HYNIC-conjugated proteins, i.e., chemically modified

proteins. The relative potencies of HYNIC-conjugated NAP-2 and its three C-terminally truncated variants for binding to CXCR2 receptors transfected on Jurkat cells is depicted in figure 1. A two to three fold higher binding potency was found for the HYNIC-conjugated forms of NAP-2(1-68) and NAP-2(1-63) as compared to NAP-2. HYNIC-conjugated NAP-2(1-66) showed a ten-fold higher binding potency relative to NAP-2. For comparison, the binding potency of HYNIC-conjugated IL-8 was seventy-five fold higher.
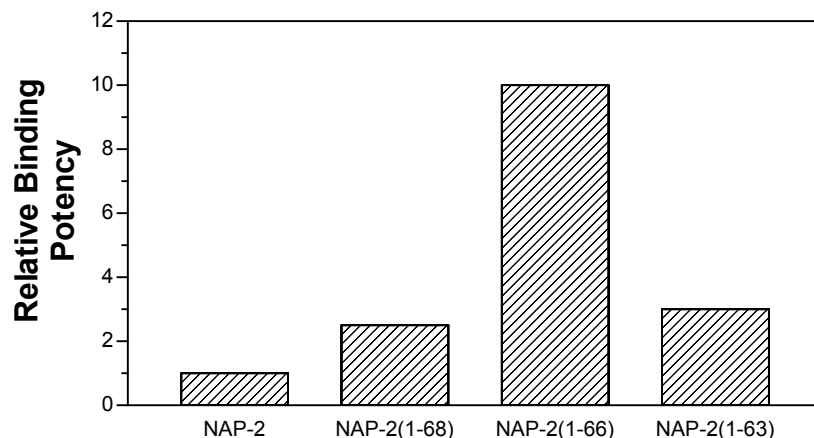

Figure 1. Relative potencies of HYNIC-conjugated NAP-2 and three C-terminally truncated variants to compete with ^{99m}Tc-labeled IL-8 for binding to Jurkat cells transfected with the CXCR2 receptor. The potency of HYNIC-conjugated NAP-2 is set at 1.

Animal studies

Table 1 summarizes the biodistribution results of the four radiolabeled chemokine preparations in rabbits with an *E.coli* infection at 6 h p.i. Figure 2 presents uptake of the four radiolabeled chemokines in neutrophil-rich tissues, i.e., the abscess, the lungs and the spleen. ^{99m}Tc-labeled NAP-2(1-66) showed higher uptake in the abscess ($P<0.05$) as compared to ^{99m}Tc-labeled NAP-2. Physiologic uptake in the lungs was significantly higher for ^{99m}Tc-labeled NAP-2(1-66) as well ($P<0.01$). Abscess/muscle and abscess/blood ratios showed no significant differences. The agents cleared predominantly via the kidneys and the residual amount of radioactivity in the kidneys was significantly lower ($P<0.01$) for the two shortest labeled NAP-2 variants, NAP-2(1-66) and NAP-2(1-63) as compared to NAP-2. In comparison to ^{99m}Tc-labeled NAP-2, IL-8 showed significantly higher uptake in the abscess (0.39 ± 0.09 %ID/g), the lungs (0.12 ± 0.01 %ID/g), the spleen (0.55 ± 0.13 %ID/g) and higher ratios of abscess/muscle (215 ± 90) and abscess/blood (24 ± 4).

Table 1. *Biodistribution of ^{99m}Tc-labeled NAP-2 and three C-terminally truncated variants in rabbits with E.coli induced intramuscular infection. Rabbits were injected with 20 MBq ^{99m}Tc-labeled chemokine, sacrificed at six hours after injection and dissected. Tissue samples were weighed and counted in a gamma counter. Values are expressed as percentages of the injected dose per gram tissue (%ID/g) ± one standard error of the mean or as ratios thereof.*

|	^{99m}Tc-NAP-2	^{99m}Tc-NAP-2(1-68)	^{99m}Tc-NAP-2(1-66)	^{99m}Tc-NAP-2(1-63)
blood	**0.015** ± 0.001	**0.013** ± 0.002	**0.017** ± 0.003	**0.013** ± 0.002
muscle	**0.0017** ± 0.0002	**0.0016** ± 0.0002	**0.0024** ± 0.0001	**0.0018** ± 0.0003
abscess	**0.084** ± 0.015	**0.098** ± 0.010	**0.189** ± 0.044	**0.114** ± 0.017
lung	**0.057** ± 0.005	**0.081** ± 0.015	**0.171** ± 0.026	**0.074** ± 0.016
spleen	**0.15** ± 0.02	**0.20** ± 0.05	**0.30** ± 0.06	**0.17** ± 0.03
kidney	**3.1** ± 0.1	**3.0** ± 0.1	**1.9** ± 0.1	**2.3** ± 0.1
liver	**0.032** ± 0.001	**0.035** ± 0.001	**0.048** ± 0.006	**0.043** ± 0.007
intestine	**0.011** ± 0.001	**0.012** ± 0.001	**0.016** ± 0.002	**0.014** ± 0.001
abscess/muscle	**52** ± 11	**65** ± 11	**80** ± 23	**66** ± 14
abscess/blood	**5.7** ± 1.3	**8.0** ± 1.1	**12** ± 3	**8.8** ± 1.2
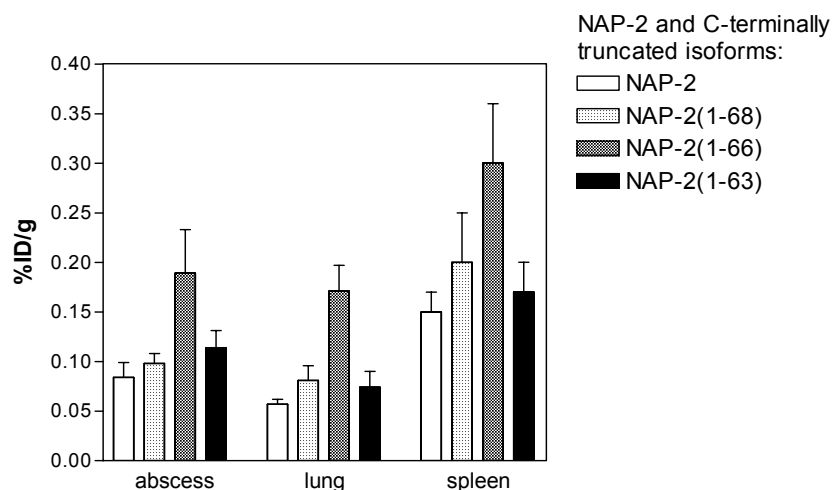
Figure 2. *Uptake of ^{99m}Tc-labeled NAP-2 and three C-terminally truncated variants at six hours after injection in tissues with a high natural abundancy of neutrophils: abscess, lungs and spleen. Values are expressed as percentages of the injected dose per gram tissue (%ID/g) ± one standard error of the mean.*

Figure 3 shows the scintigrams acquired between 0 and 6 h after injection of ^{99m}Tc-labeled NAP-2 and its three C-terminally truncated variants. Gamma camera imaging rapidly visualized the abscess from a few h p.i. onwards for all preparations. Quantitative analysis of the images revealed that the abscess-to-background ratios improved with time for all labeled chemokines up to 9 ± 1 for NAP-2, 9 ± 2 for NAP-2(1-68), 13 ± 1 for NAP-2(1-66) and 10 ± 1 for NAP-2(1-63) at 6 h p.i.. For comparison, ^{99m}Tc-IL-8 generated an abscess-to-background ratio of 20 ± 4 in the same animal model. Immediately after injection high kidney uptake was observed for all preparations, remaining prominent throughout the study.
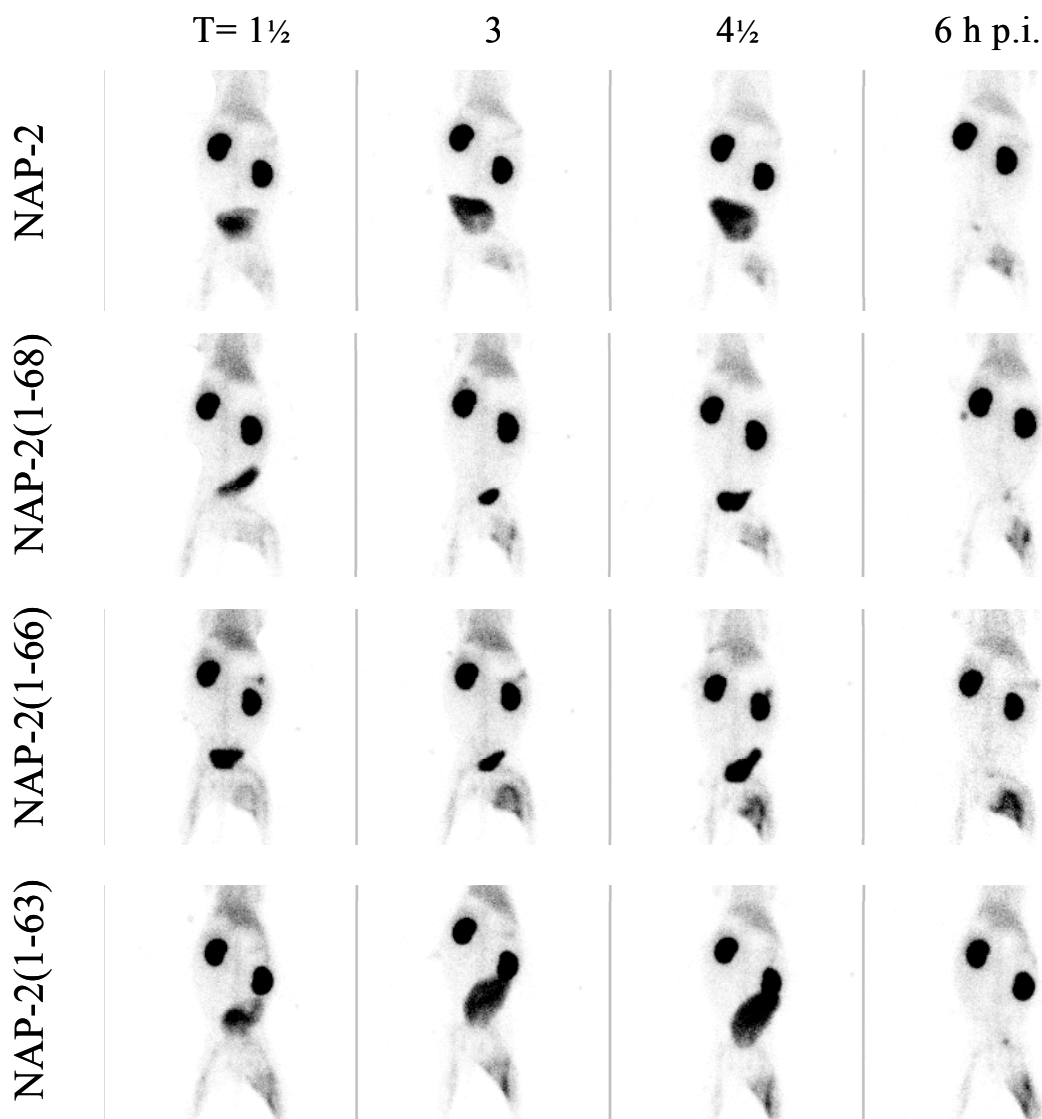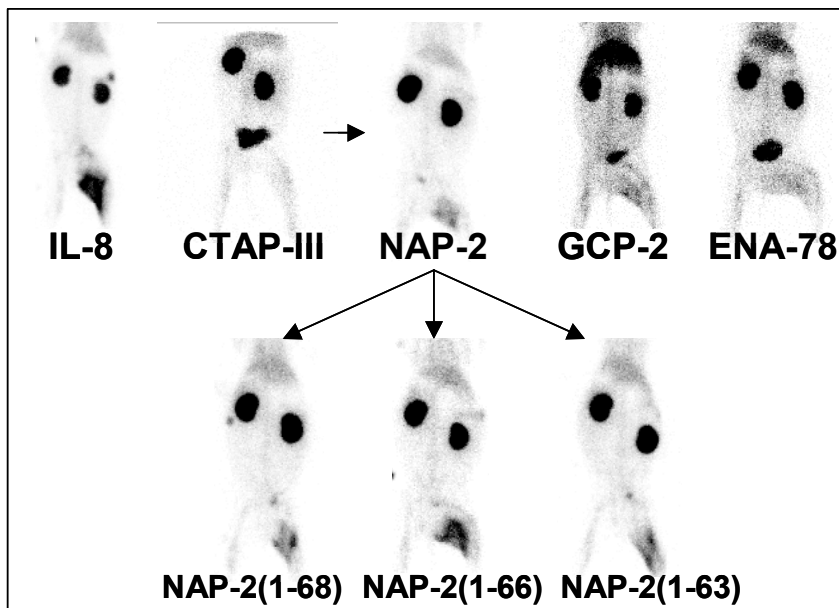

Figure 3. Images of rabbits with an E.coli induced abscess in the left thigh muscle (at the right side on the image) at 1½, 3, 4½ and 6 hour after injection of ^{99m}Tc-labeled NAP-2 and three C-terminally truncated variants.

An overview of the various radiolabeled CXC-chemokines studied in the same rabbit model of intramuscular infection is presented in Figure 4. This figure contains representative images of ^{99m}Tc-labeled IL-8 (high affinity for both CXCR1 and CXCR2), CTAP-III (no binding to CXCR2), NAP-2 and its variants (various affinities for CXCR2), GCP-2 (acts via both CXCR1 and CXCR2) and ENA-78 (high affinity for CXCR2). Two examples of ELR⁻ CXC-chemokines with poor neutrophil attractant capacity and no binding to CXCR1 and CXCR2 are PF-4 and IP-10. This figure illustrates the good characteristics for infection imaging of various ^{99m}Tc-labeled ELR⁺ CXC-chemokines, especially for NAP-2(1-66) and IL-8. In comparison to abscess uptake of NAP-2(1-66) (0.189 %ID/g) and IL-8 (0.39 %ID/g), only modest uptake was found for GCP-2 (0.081 %ID/g) and ENA-78 (0.056 %ID/g), and low uptake for CTAP-III (0.016 %ID/g), PF-4 (0.016 %ID/g) and IP-10 (0.0052 %ID/g).
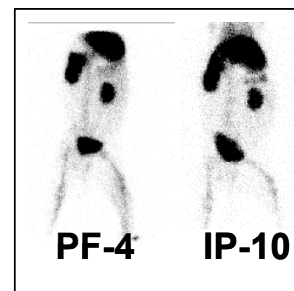

Figure 4. *Overview of images of rabbits with E.coli induced intramuscular infection obtained 6 h after injection of various ^{99m}Tc-labeled CXC-chemokines: ELR⁺ CXC-chemokines IL-8, CTAP-III, the NAP-2 analogues, GCP-2 and ENA-78; and ELR⁻ CXC-chemokines PF-4 and IP-10.*

DISCUSSION

In order to select the most suitable candidate for infection imaging within the family of CXC-chemokines, we screened a series of ^{99m}Tc-labeled CXC-chemokines for infection imaging. In this study we focussed on the relationship between binding affinity towards the CXCR2 receptor and suitability for infection imaging in a selected group of CXC-chemokines: NAP-2 (70 residues) and three C-terminally truncated variants NAP-2(1-68), NAP-2(1-66) and NAP-2(1-63). It was previously shown that limited and defined truncation at the C-terminus of native NAP-2 enhances receptor binding and degranulation activity (*13;14*). A most prominent increase in potency to stimulate neutrophil degranulation and to bind neutrophils was observed for isoforms of NAP-2 with a C-terminal deletion of four (NAP-2(1-66)) and seven amino acids (NAP-2(1-63)). Here, NAP-2 and its three variants were conjugated with the bifunctional chelator HYNIC which links ^{99m}Tc to protein via primary aminogroups within the protein. In receptor binding competition assays the relative binding affinities of the HYNIC-conjugated (i.e., chemically modified) proteins were determined and the highest binding potency for the CXCR2 receptor was found for NAP-2(1-66). This finding correlated well with the findings of the infection imaging experiments with ^{99m}Tc-labeled NAP-2 and its variants. ^{99m}Tc-labeled NAP-2(1-66) showed highest uptake in the abscess and highest physiologic uptake in the lungs, an organ that accomodates large numbers of neutrophils. HYNIC-conjugated IL-8 had a higher affinity for the CXCR2 receptor and ^{99m}Tc-labeled IL-8 displayed the highest uptake in the abscess. However, it can not be excluded that NAP-2 and its variants might be more vulnerable to loose receptor binding affinity due to the conjugation procedure than IL-8. This (hypothetical) situation might explain, at least in part, the differences in affinity for the CXCR2 receptor of the various HYNIC-conjugated chemokines.

A survey of the ^{99m}Tc-labeled CXC-chemokines PF-4, IP-10, CTAP-III, ENA-78 and GCP-2 in infection imaging provided additional evidence for the close relationship between neutrophil binding affinity and suitability for infection imaging. The presence of an ELR sequence within the CXC-chemokine was associated with effective imaging of infection. The ^{99m}Tc-labeled non-ELR CXC-chemokines studied in this paper, PF-4 and IP-10, lack significant binding to the CXCR1 and the CXCR2 receptor (*8;9*) and showed a very low uptake in the abscess. The presence of an ELR-sequence may be a prerequisite, but does not guarantee effective infection imaging. The radiolabeled ELR^{+} CXC-chemokine CTAP-III showed very low uptake in the abscess as well. CTAP-III is an N-terminally extended precursor of NAP-2 . CTAP-III neither binds to nor activates neutrophils in sharp contrast to NAP-2. NAP-2 has one amino acid residue preceeding the ELR-sequence and CTAP-III has sixteen residues preceeding the ELR-sequence. It is

suggested that the fraying N-terminal end of CTAP-III is interfering with the binding (*21*). In this way the ELR-sequence is masked and functionally not present. The radiolabeled ELR$^+$ CXC-chemokines ENA-78 and GCP-2 showed only a modest uptake in the abscess. ENA-78 has high affinity towards the CXCR2 receptor only, but this affinity was found to be lower than that of GCP-2 and considerably lower than that of IL-8. GCP-2 is reported to be efficient in binding the CXCR1 receptor as well (*7*). In the present study ^{99m}Tc-labeled GCP-2 more clearly delineated infectious foci than ENA-78. In accordance with these findings are the findings of a comparative study in imaging infection using ^{99m}Tc-labeled C5a and C5a des Arg^{74} (C5adR) (*22*). The complement anaphylatoxin C5a (74 amino acids) differs from its natural metabolite C5adR in just one additional C-terminal amino acid residue for C5a. Both act on a common receptor on different cell types, including neutrophils and monocytes. The receptor binding affinity of C5a exceeds that of C5adR by 1-2 orders of magnitude. For infection imaging ^{99m}Tc-labeled C5a showed much better characteristics than C5adR: uptake in the abscess was five-fold higher for C5a than for C5adR (*22*).

The importance of the C-terminal domain in the function of CXC-chemokines was illustrated in the present study by radiolabeled NAP-2 and three C-terminally truncated isoforms. Differences in biologic (and scintigraphic) behavior are attributed to the physicochemical properties of the deleted residues (*14*). Full size NAP-2 bears three acidic amino acids in the C-terminal ending: D_{66}, E_{67} and D_{70}. The loss of particularly the acidic residues D_{70} and E_{67} caused subsequent increases in biologic activity and binding to neutrophils, and the loss of a third acidic residue in NAP-2 resulted in NAP-2(1-63), the most active NAP-2 isoform. Further deletion of the C-terminal L_{63} was associated with a threefold reduction of the capacity of NAP-2(1-63) to bind to and activate neutrophils (*14*). Apparently, L_{63} is a functionally important residue within the structure of NAP-2. The present study showed a discrepancy with these reported findings: here, the most suitable NAP-2 derivative for infection imaging was radiolabeled NAP-2(1-66) and not NAP-2(1-63). This difference might be ascribed to the diverse effects of chemical modification on receptor binding. The chemokines were labeled with ^{99m}Tc using a succinimidyl-hydrazinonicotinamide (S-HYNIC) derivative as bifunctional agent. S-HYNIC is reacted with primary aminogroups, i.e., the α-aminogroup of the N-terminal amino acid residue or the ε-aminogroup of lysine residues within the protein. The conjugation of S-HYNIC might interfere with receptor binding. It is tempting to speculate that the fraying C-terminal end of NAP-2(1-66) might prevent effective reaction of S-HYNIC with the lysines at critical positions 61 and 62 near to L_{63}. This might explain the preferential qualities for infection imaging of ^{99m}Tc-labeled NAP-2(1-66) as compared to NAP-2(1-63).

The importance of the N-terminal domain in the function of the CXC-chemokines is exemplified in the pair of closely related proteins CTAP-III and NAP-2 in our study, and also in a comparison between two naturally existent isoforms of IL-8 (*2*). The most abundant form of naturally occurring IL-8 is 72 amino acids long. This form has three residues in front of the ELR-sequence. A 77 amino acid variant of IL-8 is produced by endothelial cells and is extended at the N-terminus by five amino acids. The longer protein is some ten-fold less potent than the shorter protein in attracting and activating neutrophils. The differences might, again, be attributed to the negative interference of the longer fraying N-terminal end of IL-8(77) in the binding of the protein to CXC-receptors. IL-8(72) has a high affinity for both the CXCR1 and CXCR2 receptor and its potency as a neutrophil chemoattractant has been estimated to be threefold higher than that of NAP-2 (*23*). The potential of radiolabeled IL-8(72) for imaging infection has been extensively explored by us (*16-18*) and is, not surprisingly, superior to that of other CXC-chemokines, including the NAP-2 analogues.

It must be emphasized here that neutrophil receptor affinity is not the only factor determining the uptake of a radiolabeled chemokine in the abscess. In general, localization of radiolabeled proteins in the focus of infection is a result of both specific and non-specific mechanisms. For non receptor binding proteins it was shown in a rat model of *S.aureus* infection that abscess accumulation is mainly driven by sustained blood levels (*24*). Blood residence time appeared to be the principal factor that determines localization of a nonspecific tracer protein in infectious foci. In the rabbit models of intramuscular *E.coli* infection, blood levels for ^{99m}Tc-labeled IL-8 were twice as high as for the ^{99m}Tc-labeled NAP-2 analogues at six hours post injection and these sustained higher blood levels will contribute to the uptake in the abscess in addition to the specific receptor interactions of the protein. However, in case of ^{99m}Tc-IL-8 it was estimated that non-specific uptake accounts for less than 10% of the total uptake in the abscess. Accumulation of ^{99m}Tc-IL-8 in the abscess is a predominantly neutrophil-driven (i.e., receptor interaction driven) process as was shown in a comparison between abscess uptake in neutropenic rabbits and that in immunocompetent rabbits in which the immunocompetent rabbits showed a ten-fold higher abscess uptake than the neutropenic animals (*25*).

In conclusion, this study showed a clear relationship between affinity to receptors on neutrophils and suitability for infection imaging. Of the NAP-2 variants, NAP-2(1-66) combined highest affinity to CXCR2 with best characteristics for imaging. IL-8, having a clearly higher affinity for the CXCR1 and CXCR2 receptor than NAP-2(1-66), showed a superior imaging quality. The other CXC-chemokines tested showed to be less suitable for infection imaging.

REFERENCES

1. Rennen HJ, Boerman OC, Oyen WJ, Corstens FH. Imaging infection/inflammation in the new millennium. *Eur J Nucl Med.* 2001;28:241-252.
2. Rollins BJ. Chemokines. *Blood.* 1997;90:909-928.
3. Abrams MJ, Juweid M, tenKate CI, Schwartz DA, Hauser MM, Gaul FE, Fuccello AJ, Rubin RH, Strauss HW, Fischman AJ. Technetium-99m-human polyclonal IgG radiolabeled via the hydrazino nicotinamide derivative for imaging focal sites of infection in rats. *J Nucl Med.* 1990;31:2022-2028.
4. Zlotnik A, Yoshie O. Chemokines: a new classification system and their role in immunity. *Immunity.* 2000;12:121-127.
5. Lee J, Horuk R, Rice GC, Bennett GL, Camerato T, Wood WI. Characterization of two high affinity human interleukin-8 receptors. *J Biol Chem.* 1992;267:16283-16287.
6. Ahuja SK, Murphy PM. The CXC chemokines growth-regulated oncogene (GRO) alpha, GRObeta, GROgamma, neutrophil-activating peptide-2, and epithelial cell-derived neutrophil-activating peptide-78 are potent agonists for the type B, but not the type A, human interleukin-8 receptor. *J Biol Chem.* 1996;271:20545-20550.
7. Wuyts A, Proost P, Lenaerts JP, Ben Baruch A, Van Damme J, Wang JM. Differential usage of the CXC chemokine receptors 1 and 2 by interleukin-8, granulocyte chemotactic protein-2 and epithelial-cell- derived neutrophil attractant-78. *Eur J Biochem.* 1998;255:67-73.
8. Clark-Lewis I, Dewald B, Geiser T, Moser B, Baggiolini M. Platelet factor 4 binds to interleukin 8 receptors and activates neutrophils when its N terminus is modified with Glu-Leu-Arg. *Proc Natl Acad Sci U S A.* 1993;90:3574-3577.
9. Dewald B, Moser B, Barella L, Schumacher C, Baggiolini M, Clark-Lewis I. IP-10, a gamma-interferon-inducible protein related to interleukin-8, lacks neutrophil activating properties. *Immunol Lett.* 1992;32:81-84.
10. Brandt E, Petersen F, Ludwig A, Ehlert JE, Bock L, Flad HD. The beta-thromboglobulins and platelet factor 4: blood platelet-derived CXC chemokines with divergent roles in early neutrophil regulation. *J Leukoc Biol.* 2000;67:471-478.
11. Walz A, Baggiolini M. Generation of the neutrophil-activating peptide NAP-2 from platelet basic protein or connective tissue-activating peptide III through monocyte proteases. *J Exp Med.* 1990;171:449-454.
12. Brandt E, Van Damme J, Flad HD. Neutrophils can generate their activator neutrophil-activating peptide 2 by proteolytic cleavage of platelet-derived connective tissue- activating peptide III. *Cytokine.* 1991;3:311-321.
13. Ehlert JE, Petersen F, Kubbutat MH, Gerdes J, Flad HD, Brandt E. Limited and defined truncation at the C terminus enhances receptor binding and degranulation activity of the neutrophil-activating peptide 2 (NAP-2). Comparison of native and recombinant NAP-2 variants. *J Biol Chem.* 1995;270:6338-6344.
14. Ehlert JE, Gerdes J, Flad HD, Brandt E. Novel C-terminally truncated isoforms of the CXC chemokine beta-thromboglobulin and their impact on neutrophil functions. *J Immunol.* 1998;161:4975-4982.
15. Krijgsveld J, Zaat SA, Meeldijk J, van Veelen PA, Fang G, Poolman B, Brandt E, Ehlert JE, Kuijpers AJ, Engbers GH, Feijen J, Dankert J. Thrombocidins, microbicidal proteins from human blood platelets, are C-terminal deletion products of CXC chemokines. *J Biol Chem.* 2000;275:20374-20381.
16. Rennen HJ, Boerman OC, Oyen WJ, van der Meer JW, Corstens FH. Specific and rapid scintigraphic detection of infection with 99mTc- labeled interleukin-8. *J Nucl Med.* 2001;42:117-123.
17. Rennen HJ, van Eerd JE, Oyen WJ, Corstens FH, Edwards DS, Boerman OC. Effects of coligand variation on the in vivo characteristics of ^{99m}Tclabeled interleukin-8 in detection of infection. *Bioconjug Chem.* 2002;13:370-377.
18. Gratz S, Rennen HJ, Boerman OC, Oyen WJ, Corstens FH. Rapid imaging of experimental colitis with (99m)Tc-interleukin-8 in rabbits. *J Nucl Med.* 2001;42:917-923.
19. Schwartz DA, Abrams MJ, Giadomenico CM, Zubieta JA. Certain pyridyl hydrazines and hydrazides useful for protein labeling. US patent nr. 5,206,370. 27-4-1993.
20. Loetscher P, Seitz M, Clark-Lewis I, Baggiolini M, Moser B. Both interleukin-8 receptors independently mediate chemotaxis. Jurkat cells transfected with IL-8R1 or IL-8R2 migrate in response to IL-8, GRO alpha and NAP-2. *FEBS Lett.* 1994;341:187-192.
21. Malkowski MG, Lazar JB, Johnson PH, Edwards BF. The amino-terminal residues in the crystal structure of connective tissue activating peptide-III(des10) block the ELR chemotactic sequence. *J Mol Biol.*1997;266:367-80
22. Rennen HJ, Oyen WJ, Cain SA, Monk PN, Corstens FH, Boerman OC. Tc-99m-labeled C5a and C5a des Arg(74) for infection imaging. *Nucl Med Biol.* 2003;30:267-272.
23. Leonard EJ, Yoshimura T, Rot A, Noer K, Walz A, Baggiolini M, Walz DA, Goetzl EJ, Castor CW. Chemotactic activity and receptor binding of neutrophil attractant/activation protein-1 (NAP-1) and structurally related host defense cytokines: interaction of NAP-2 with the NAP-1 receptor. *J Leukoc Biol.* 1991;49:258-265.
24. Rennen HJ, Makarewicz J, Oyen WJ, Laverman P, Corstens FH, Boerman OC. The effect of molecular weight on nonspecific accumulation of (99m)T- labeled proteins in inflammatory foci. *Nucl Med Biol.* 2001;28:401-408.
25. Rennen HJ, Boerman OC, Oyen WJ, Corstens FH. Kinetics of 99mTc-labeled interleukin-8 in experimental inflammation and infection. *J Nucl Med.* 2003;44:1502-1509.

Chapter 11

Conclusions and future prospects

Imaging of infection and inflammation by targeting receptors on leukocytes
Scintigraphic imaging of microbial and nonmicrobial foci of inflammation is a powerful diagnostic tool in the management of patients with inflammatory disorders. Rapid and accurate diagnosis of an inflammatory process allows early and adequate treatment and may prevent the onset of complications. Most inflammatory foci can be visualized accurately with ex vivo radiolabeled autologous leukocytes. The use of ex vivo labeled white blood cells is the standard nuclear medicine technique for imaging of inflammatory foci. However, this technique has several disadvantages: a.o., laborious preparation; requirement of specialized equipment and skills; handling of potentially contaminated blood. Therefore there is a continued search for an alternative agent with similar diagnostic power. After the relatively poor results obtained with large size monoclonal antibodies directed against surface antigens of leukocytes, radiolabeled small molecules that specifically bind to receptors on circulating leukocytes appeared to have more promise.

As the leukocyte subpopulation of neutrophils play a prominent role in inflammatory disorders, especially in their acute phases, targeting receptors on neutrophils is of particular importance and involves several interesting features and choices for selection and optimization.

The choice of the receptor(s).
In this thesis three different neutrophil receptors for high-affinity binding were tested as target for imaging of inflammatory foci with radiolabeled receptor binding peptides and proteins: C5a and C5adR target the C5a-receptor (Chapter 9); the chemokines IL-8, NAP-2 and others target the chemokine receptor CXCR2 (Chapters 4-8, 10); IL-8 targets the chemokine receptor CXCR1 as well. The CXC-receptors, expressed in high numbers on neutrophils, appeared to be suitable targets for infection imaging with radiolabeled chemokines, especially with IL-8. IL-8 binds with high affinity to both CXCR1 and CXCR2 (Chapters 4-5). Alternative receptors for radiolabeled compounds, not investigated in this thesis, include the N-formyl-peptide receptors (FPR), which are high affinity binding receptors for chemotactic peptides such as Formyl-Met-Leu-Phe (fMLF) and its derivatives, and the Leukotriene B-4 (LTB-4) receptor BLT1, to which LTB-4 analogues bind with high affinity. These targets on the neutrophil proved to be suitable targets for radiolabeled compounds such as fMLFK and the LTB-4 receptor antagonists RP517 and DPC11870.

High and exclusive expression of receptors on neutrophils is a prerequisite for specific targeting of neutrophils in vivo. The choice of the proper ligand for such a receptor opens a myriad of possibilities. This choice may be guided principally by two main characteristics of a candidate compound: affinity for the receptor and induction

of biologic effects ("side-effects") following i.v. administration. In addition, finetuning of radiolabeling conditions may be applied in order to improve receptor binding and to improve the clearance (rate and route) of the radiolabeled compound from the blood and from non-target tissues.

High affinity receptor binding

High affinity for the receptor of choice should be in the nanomolar range and is definitely a requirement for effective imaging of inflammation as described in Chapters 9 and 10. A clear relationship between affinity for the receptor on neutrophils and suitability for infection imaging was found in an experimental study in which the targeting characteristics of radiolabeled NAP-2 and NAP-2 derivatives were compared (Chapter 10). The NAP-2 variant NAP-2(1-66) combined highest affinity to CXCR2 with best characteristics for imaging. IL-8 binds to both CXCR1 and CXCR2 with high affinity and showed a superior imaging quality. The receptor binding affinity of C5a is in the nanomolar range and exceeds that of C5adR by 1-2 orders of magnitude. For infection imaging ^{99m}Tc-labeled C5a showed considerable uptake in the focus but C5adR showed suboptimal imaging characteristics (Chapter 9). From the point of view of high (nanomolar) affinity for the receptor, IL-8, fMLF analogues, LTB-4 antagonists and, to some lesser degree, NAP-2(1-66) and C5a are interesting candidates for imaging of infection.

Induction of side-effects

The choice of the most suitable ligand is further also determined by the concern that most of the neutrophil receptor binding compounds elicit a biologic response after binding to the receptor. Side-effects such as leukopenia, leukocytosis, fever, hypotension, etc, are undesirable for a diagnostic utility in routine clinical practice. The biologic activities of high-affinity binding compounds as C5a and also the fMLF analogues prevent the clinical use of these agents as infection imaging agents. The induction of side-effects can be addressed in several ways. First, a receptor antagonist can be applied as replacement for the agonist. However, in most cases receptor affinity and agonistic activity are closely related, resulting in lower affinity with less biological activation. Apparantly, the LTB-4 receptor antagonists RP517 and DPC11870 are an exception to this rule. These agents appear not to trigger signal transduction following binding to the receptor. In most cases, however, high affinity binding receptor antagonists are not available and radiochemistry has to overcome potential side-effects. The biologic effect of the agent can be reduced by substantially increasing the specific activity of the radiolabeled agent. Successful efforts were made using state-of-the-art radiochemical approaches to increase the specific activity of ^{99m}Tc-labeled IL-8, thereby reducing the biologic effect of a diagnostic dose of

[99mTc]-IL-8 (Chapter 5). Using the bifunctional coupling agent S-HYNIC and a selected set of coligands, the protein administration dose was lowered a factor 350 compared to the iodinated IL-8 preparation used previously (Van der Laken et al., J Nucl Med 2000;41:463-9). Based on pharmacokinetic data, at the low protein doses of [99mTc]-labeled IL-8, side-effects are not expected in humans.

[99mTc]-HYNIC-IL-8 for imaging of infection and inflammation

[99mTc]-HYNIC-IL-8 has excellent characteristics as an infection and inflammation imaging agent. As demonstrated in the animal experiments presented in this thesis, it surpasses the current standard, labeled white blood cells, in ease and safety of preparation, preparation time and quality of imaging (Target-to-Background ratios). Patient studies with [99mTc]-HYNIC-IL-8 will have to demonstrate its safety (side-effects) and its value as a diagnostic tool in various clinical settings. None of the other chemotactic proteins for infection imaging described in this thesis could match the characteristics of IL-8 as infection imaging agent.

Competitive new agents are positron emission tomography (PET) using [18F]-fluorodeoxyglucose (FDG) and the recently described LTB-4 receptor antagonist, DPC11870 (Van Eerd et al., J Nucl Med 2003;44:1087-91). In various clinical studies in patients with inflammatory disorders FDG-PET has already proved to be useful. The mechanism of accumulation is based on the fact that granulocytes and macrophages at the site of infection have an enhanced glucose metabolism. However, FDG-PET does not allow the discrimination between tumor lesions and inflammatory lesions. Moreover, FDG-PET is a rather expensive imaging modality and is not yet widely available.

The [111In]-labeled LTB-4 receptor antagonist, DPC11870, also has great potential as a new infection imaging agent. DPC11870, a small (3 kDa) nonpeptide compound, clearly delineated infectious foci in various rabbit models of infection and inflammation. It was reported to induce no biologic effects after intravenous administration. A disadavantage here is the choice of [111In] as radiometal. [99mTc] has much more favorable physical characteristics. In future studies the [111In] chelating DTPA moiety of DPC11870 will be replaced by a [99mTc] chelating HYNIC moiety.

Alternative labeling strategies for IL-8

The IL-8 molecule is an ideal playground for the radiochemist. It offers opportunities for alternative labeling strategies with [99mTc] and [18F]. It offers opportunities for more selective, site-directed labeling strategies which do not impede binding of labeled IL-8 to the receptors on neutrophils. A further development, not limited to IL-8 for its application, is the modification of the bifunctional coupling agent S-HYNIC, which might facilitate clearance of the radiolabel from the body and the kidneys.

IL-8 is a 72 amino acid protein and contains 9 lysine residues. The 9 primary ε-amino groups of the lysine residues and the N-terminal α-amino group of serine are potential sites for reaction with activated esters as the succinimidyl moiety in succinimidyl-hydrazinonicotinamide (S-HYNIC), the bifunctional coupling agent most extensively applied in this thesis. A careful selection of conditions for the conjugation reaction of S-HYNIC with IL-8 resulted in a HYNIC-IL-8 conjugate that could be labeled with ^{99m}Tc with high specific activity in combination with preservation of the neutrophil binding capacity (Chapters 4 and 5).

The tricarbonyl approach: labeling IL-8 with $[^{99m}Tc(CO)_3(H_2O)_3]^+$

The two histidine residues of IL-8 might be used in an alternative method to label IL-8 with ^{99m}Tc: labeling with ^{99m}Tc using the tricarbonyl method. In this method an organometallic aquaion $[^{99m}Tc(CO)_3(H_2O)_3]^+$ is formed as a precursor. This precursor complex can be used to label IL-8 with ^{99m}Tc presumably via the histidine residues of IL-8. Preliminary experiments, not reported in this thesis, indicated that ^{99m}Tc-IL-8 preparations prepared according to the tricarbonyl method showed distinctive differences in biodistribution in rabbits with infection as compared to ^{99m}Tc-IL-8 using S-HYNIC as bifunctional coupling agent. Relatively modest specific activities were obtained with the ^{99m}Tc-tricarbonyl method and future experiments will focus on the modification of IL-8 with an N_α-histidinyl acetate group to facilitate complexation with the ^{99m}Tc-aquaion complex and in order to produce a radiochemically better defined product. However, in comparison to the labeling of proteins with ^{99m}Tc via HYNIC, the ^{99m}Tc-tricarbonyl approach in its current phase is more laborious and more time consuming. The ^{99m}Tc-tricarbonyl approach takes two reaction steps involving radioactive ^{99m}Tc instead of one step in case of direct labeling of HYNIC-conjugated proteins with ^{99m}Tc.

Site-specific conjugation of HYNIC to IL-8

As mentioned above, the 10 primary amino groups of IL-8 can potentially react with S-HYNIC. The HYNIC-moieties are more or less randomly linked to these primary amino groups and could potentially interfere with receptor binding. Introduction of a HYNIC-group into IL-8 in a chemically well-defined manner, at a region of the molecule not involved in receptor binding, could potentially improve the characteristics of ^{99m}Tc-labeled IL-8 for imaging of infection. IL-8 has a serine residue at the N-terminus of the protein, a distinctive and rather unique feature. The N-terminal serine residue can be selectively oxidized under mild conditions to give a reactive glyoxyl function. Peptides with an N-terminal cysteine residue can react with the glyoxyl function forming a thiazolidine-ring which is highly stable over a broad range of pH and temperature conditions. For site-specific conjugation of HYNIC to IL-8, small peptides containing an

N-terminal cysteine residue and a HYNIC-moiety as attached to an adjacent amino acid residue, were synthesized by solid-phase synthesis. The in vivo characteristics of site-specifically HYNIC-conjugated IL-8 are currently under investigation in experimental models of infection.

Cleavable linkers for faster clearance and excretion

As indicated in Chapters 4 and 5, ^{99m}Tc-HYNIC-IL-8 is cleared mainly via the kidneys, but is only partially excreted to the urine. It has been shown for bifunctional chelating agents linked to antibodies that the biodistribution of the radiolabeled antibody is strongly dependent on the nature of the linker. Antibody-conjugates containing cleavable linkers exhibit faster whole-body clearance and excretion from the body as compared to antibody-conjugates containing noncleavable linkers. Future efforts will be directed towards synthesis of an S-HYNIC derivative including additional ester groups between the hydrazinonicotinic (HYNIC) moiety and the succinimidyl (S) moiety for faster clearance and excretion. Such a derivative could find a broad range of applications, not restricted to conjugation to IL-8.

Positron emission tomography (PET) using ^{18}F-IL-8

The 10 amino groups in IL-8 can potentially be used to label IL-8 with ^{18}F for positron emission tomography (PET). For instance, N-succinimidyl 4-[^{18}F]fluorobenzoate (SFB) contains a succinimidyl-group and can be coupled to IL-8 in a similar way as used for coupling of S-HYNIC to IL-8. PET using ^{18}F-IL-8 is feasible because of rapid and high accumulation of radiolabeled IL-8 in foci of infection. PET-imaging is of particular interest for its high spatial resolution. High spatial resolution is of particular importance, e.g., when it is crucial to discriminate soft tissue infection from bone infection in cases of osteomyelitis.

Limitations

The utility of neutrophil binding compounds is limited, once a discrimination between infection and sterile inflammation is required such as in, e.g., the evaluation of infection of orthopaedic prostheses. For application in those cases, radiolabeled agents that specifically bind to micro-organisms have been proposed (Infecton, ^{99m}Tc-labeled antimicrobial peptides). Though an attractive concept, directly targeting micro-organisms is still in a premature state, and most radiopharmaceuticals currently under investigation show a lack of targeting and/or specificity. The utility of neutrophil binding compounds is also limited in diagnosing infection and inflammation in deeply neutropenic patients. In those cases, agents not relying on neutrophil receptor binding such as, e.g., radiolabeled polyclonal IgG, could be applied.

Summary

Patients with inflammatory disorders may pose a diagnostic problem to their physicians. Rapid and accurate detection of inflammatory foci is a challenging problem in clinical practice, because it may have important implications for the treatment of patients with presumed or established inflammatory disorders. Over the last 30 years various approaches to visualize inflammatory foci scintigraphically have been developed. **Chapter 1** presents a survey of the different approaches currently in use or under investigation. In response to inflammation, white blood cells move massively to inflammatory foci and localize there in great numbers. The use of ex vivo labeled white blood cells is currently the gold standard nuclear medicine technique for imaging of inflammatory foci. The limitations of this approach have encouraged the continued search for an alternative agent with at least a similar diagnostic power.

The aim of the studies described in this thesis is to investigate the potential of ^{99m}Tc-labeled interleukin-8 (IL-8) for imaging infection and inflammation. IL-8 is a small protein that binds with high affinity to receptors on white blood cells in general and especially to receptors on the white blood cell subpopulation of neutrophils. IL-8 was labeled with the radionuclide ^{99m}Tc using a derivative of hydrazinonicotinamide (HYNIC) as bifunctional coupling agent. The HYNIC-derivative is first coupled to IL-8 and is used subsequently to bind ^{99m}Tc.

In two fundamental studies the chemistry of labeling proteins with ^{99m}Tc via HYNIC is investigated. The effects of conjugation ratio, reaction temperature, pH and protein concentration on HYNIC-substitution ratio, labeling efficiency and biologic activity were studied in a series of proteins (molecular weight between 6.5 and 17 kDa) (**Chapter 2**). It was found that HYNIC-conjugation was most efficient at 0 ^{0}C (as compared to 20 and 40 ^{0}C), at pH 8.2 (as compared to 6.0, 7.2 and 9.5) and at protein concentrations $\geq$ 2.5 mg/ml. Labeling efficiency improved with increasing molar conjugation ratio HYNIC/protein. For receptor binding proteins, biologic activity was best preserved under relatively mild conjugation conditions.

In **Chapter 3**, the effect of molecular weight on non-specific accumulation of ^{99m}Tc labeled proteins in inflammatory foci is studied in a rat model. Eleven proteins in a broad molecular weight range from 2.5 kDa up to 800 kDa were labeled with ^{99m}Tc via HYNIC. Rats with an intramuscular *S. aureus* infection were injected intravenously with the ^{99m}Tc-labeled proteins and scintigraphic images were acquired. Proteins of intermediate size (66 kDa – 206 kDa) showed moderate hepatic and moderate renal clearance with sustained high blood levels and showed highest localization in inflammatory foci. This study showed that the circulatory half-life is the main characteristic of a non-specific tracer protein that determines its suitability for infection imaging. From the proteins tested here, IgG and serum albumin showed the best characteristics.

In **Chapter 4** the first in vivo characterization of ^{99m}Tc-HYNIC-IL-8 in rabbits with an intramuscular infection is described. It was shown that the white blood cell receptor binding capacity was preserved after labeling. Gamma camera imaging rapidly visualized the abscess from 1 hour after injection onwards, with abscess/background ratios improving with time up to 22 at 8 hour after injection versus 2.7 for a ^{99m}Tc-labeled control protein lysozyme. The only mild transient drop of white blood cell counts shortly after injection suggested that ^{99m}Tc-HYNIC-IL-8 may be suitable as an imaging agent with only mild and transient side-effects.

In **Chapter 5** a further optimization of the labeling of IL-8 with ^{99m}Tc is described. The propylaldehyde hydrazone formulation of HYNIC was introduced to enhance the shelf-life of HYNIC-IL-8. ^{99m}Tc-HYNIC-IL-8 was prepared using 5 different coligands. The effects of these coligands on the *in vitro* characteristics and *in vivo* behavior of ^{99m}Tc-HYNIC-IL-8 in rabbits with *E.coli* induced intramuscular infection were investigated. The most optimal infection imaging characteristics were obtained when nicotinic acid/tricine was used as coligand system. This preparation combined a high specific activity (up to 80 MBq/µg) with a high *in vitro* stability and high abscess/background ratios (>20) at 6 hour after injection. As a result of the high specific activity, protein doses to be administered were as low as 70 ng/kg bodyweight. At these low protein doses side effects are not to be expected in the human system.

The importance of the careful choice of the radiolabeling conditions for the imaging characteristics was stressed once more in the **Addendum to Chapter 5**.

In addition to its suitability to delineate infectious and inflammatory foci in rabbits with intramuscular infection, ^{99m}Tc-HYNIC-IL-8 demonstrated its utility as an imaging agent in rabbit models of colitis and pulmonary infection.

In rabbits with chemically-induced acute colitis, inflammatory lesions were visualized scintigraphically after injection of ^{99m}Tc-HYNIC-IL-8 (**Chapter 6**). Within 4 hour after injection, ^{99m}Tc-labeled IL-8 allowed a meticulous evaluation of the severity of inflammatory bowel disease.

^{99m}Tc-labeled IL-8 was tested for imaging of pulmonary infection in three experimental rabbit models: aspergillosis in immunocompromised rabbits, pneumococcal (gram-positive) pneumonia and *E.coli*-induced (gram-negative) pneumonia in immunocompetent rabbits (**Chapter 7**). ^{99m}Tc-HYNIC-IL-8 enabled early (within 2 hour after injection) and excellent visualization of localization and extent of pulmonary infection in each of the three models of pulmonary infection. ^{99m}Tc-labeled IL-8 offers many advantages over the conventionally used radiopharmaceuticals to image pulmonary infection, ^{67}Ga-citrate and radiolabeled white blood cells, i.e., rapid and easy preparation, short time span between injection

and imaging, low radiation burden and, most importantly, a clear delineation of the infectious foci.

The pharmacokinetics of ^{99m}Tc-HYNIC-IL-8 are studied in detail in **Chapter 8**. To address specificity of uptake of ^{99m}Tc-labeled IL-8 in the abscess, uptake in turpentine-induced abscesses in neutropenic rabbits was compared to uptake in turpentine-induced abscesses in normal rabbits. Abscess uptake in immunocompetent rabbits was ten times higher than that in neutropenic rabbits, demonstrating specificity of the target uptake of ^{99m}Tc-IL-8. Substantial support is provided for the hypothesis that ^{99m}Tc-labeled IL-8 localizes in the abscess mainly by binding to peripheral neutrophils. As assessed by *in vivo* and *ex vivo* analysis, the total fraction that accumulates in the inflamed tissue was extremely high (more than 15% of the injected dose).

In **Chapters 9** and **10** other leukocyte receptor binding ligands were investigated.
The complement factor C5a and its natural metabolite C5a des Arg^{74} (C5adR) both act on a common receptor expressed on neutrophils. The receptor binding affinity of C5a is in the nanomolar range and exceeds that of C5adR ten to hundred fold. ^{99m}Tc-labeled C5a and C5adR were tested for imaging of infection in a rabbit model of intramuscular infection (**Chapter 9**). For infection imaging ^{99m}Tc-labeled C5a showed excellent in vivo characteristics. However, C5a is an extremely bioactive protein, impeding its clinical use as an infection imaging agent. C5adR is biologically less active but showed suboptimal imaging characteristics. This study suggested that for adequate localization of a receptor binding ligand affinities for the receptor in the nanomolar range are required.

The CXC-chemokines are a family of closely related chemotactic cytokines, which bind to, attract and activate neutrophils. In **Chapter 10** the relationship between neutrophil binding affinity and suitability for infection imaging was investigated in a selected group of CXC-chemokines, including NAP-2, three NAP-2 variants, IL-8, CTAP-III, GCP-2, ENA-78, PF-4 and IP-10. The ^{99m}Tc-labeled CXC-chemokines were tested for imaging of infection in rabbits with intramuscular *E.coli* infections. This study showed a clear relationship between neutrophil receptor affinity and suitability for infection imaging. Of the NAP-2 variants, NAP-2(1-66) combined highest affinity to CXCR2 with best characteristics for imaging.

Conclusion
^{99m}Tc-HYNIC-IL-8 has almost ideal characteristics as an infection imaging agent. As demonstrated in the animal experiments presented in this thesis, it surpasses the current standard, labeled white blood cells, in ease and safety of preparation, preparation time and quality of imaging. Patient studies with ^{99m}Tc-HYNIC-IL-8 will have to demonstrate its safety and its value as a new diagnostic tool in various clinical settings.

Samenvatting

De diagnose van ontstekingen bij patiënten is vaak moeilijk. Snel en adequaat detecteren van ontstekingshaarden is een ware uitdaging in de klinische praktijk, met belangrijke gevolgen voor de behandeling van patiënten met een mogelijke dan wel reeds vastgestelde ontsteking. De afgelopen 30 jaar zijn er diverse methodes ontwikkeld om ontstekingshaarden zichtbaar te maken met gebruik van radioactieve stoffen en detectie met behulp van gammacamera's. In **Hoofdstuk 1** wordt een overzicht gegeven van de diverse technieken die momenteel in de kliniek worden toegepast en van technieken die in ontwikkeling zijn. In reactie op de ontsteking bewegen witte bloedcellen zich massaal naar de ontstekingshaard en verblijven daar in groten getale. Het gebruik van radioactief gelabelde witte bloedcellen vormt nog altijd de gouden standaard binnen het vakgebied van de nucleaire geneeskunde voor het scintigrafisch zichtbaar maken van ontstekingshaarden. Deze techniek kent zijn beperkingen en er wordt dan ook naarstig gezocht naar een alternatief middel met een op zijn minst gelijkwaardige diagnostische kwaliteit.

Het doel van de studies zoals beschreven in dit proefschrift is om Technetium-99m (^{99m}Tc) gelabeld interleukine-8 (IL-8) te onderzoeken op zijn kwaliteiten om ontstekingen zichtbaar te maken. IL-8 is een klein eiwit dat met hoge affiniteit bindt aan receptoren op witte bloedcellen in het algemeen en aan receptoren op een subpopulatie van witte bloedcellen, de neutrofielen, in het bijzonder. Om IL-8 te labelen met het radionuclide ^{99m}Tc werd gebruik gemaakt van een hydrazinonicotinamide (HYNIC) derivaat als bifunctioneel koppelingsreagens. Het HYNIC derivaat wordt eerst aan IL-8 gekoppeld en wordt vervolgens benut om ^{99m}Tc te binden.

In twee fundamentele studies wordt de chemie van het labelen van eiwitten met ^{99m}Tc via HYNIC nader bekeken. De effecten van de conjugatieratio, de reactietemperatuur, pH en eiwitconcentratie op de HYNIC-substitutie ratio, de labelingsefficiëntie en de biologische activiteit werden onderzocht in een reeks eiwitten met een molecuulgewicht tussen de 6.5 en 17 kDa (**Hoofdstuk 2**). De conjugatie bleek het meest efficiënt te verlopen bij 0 ^{0}C (in vergelijking met 20 en 40 ^{0}C), bij pH 8.2 (in vergelijking met pH 6.0, 7.2 en 9.5) en bij eiwitconcentraties boven 2.5 mg/ml. De labelingsefficiëntie nam toe bij een toenemende molaire conjugatie ratio HYNIC/eiwit. In geval van receptor bindende eiwitten bleek de biologische activiteit het beste behouden te blijven onder relatief milde conjugatie condities.

Hoofdstuk 3 beschrijft het effect van het molecuulgewicht van het eiwit op de niet-specifieke opname van ^{99m}Tc-gelabelde eiwitten in ontstekingshaarden in ratten. Elf

eiwitten variërend in molecuul gewicht tussen de 2.5 en 800 kDa werden gelabeld met ^{99m}Tc via HYNIC. Ratten met een door *S.aureus* bacteriën geïnduceerde infectie in de dijbeenspier werden intraveneus geïnjecteerd met de radioactief gelabelde eiwitten. Vervolgens werden op verschillende tijdstippen opnames van de ratten gemaakt met een gamma-camera. Eiwitten van gemiddelde grootte (66 kDa – 206 kDa) vertoonden een bescheiden mate van klaring door de lever en de nieren, een aanhoudend hoge bloedspiegel en de hoogste opname in de ontstekingshaarden. Deze studie toonde aan dat de circulatietijd voor niet-specifieke tracer eiwitten de belangrijkste factor is ter bepaling van de geschiktheid voor scintigrafische detectie van ontstekingen. Van de geteste eiwitten bleken polyclonaal immunoglobuline G en serum albumine het meest geschikt.

In **Hoofdstuk 4** wordt de eerste in vivo karakterisering van ^{99m}Tc-HYNIC-IL-8 in konijnen met een spierontsteking beschreven. Uit deze studies bleek dat dit preparaat ook na labeling nog in staat was om te binden aan receptoren op witte bloedcellen. Reeds vanaf 1 uur na de injectie konden de ontstekingen met een gamma-camera zichtbaar gemaakt worden. De verhouding tussen de opname in de ontsteking en de achtergrond (abces/achtergrond ratio) nam geleidelijk aan toe tot een waarde van 22, 8 uur na toediening van het preparaat. Ter vergelijking, de abces/achtergrond ratio van een controle eiwit, ^{99m}Tc-gelabeld lysozyme, bedroeg 2,7. Als gevolg van de injectie met ^{99m}Tc-HYNIC-IL-8 werd een slechts geringe en tijdelijke daling van het aantal witte bloedcellen gezien, hetgeen aangeeft dat de bijwerkingen van toediening van ^{99m}Tc-HYNIC-IL-8 mild en tijdelijk zijn.

In **Hoofdstuk 5** wordt een verdere optimalisatie van de labeling van IL-8 met ^{99m}Tc beschreven. Om de houdbaarheid van HYNIC-IL-8 te vergroten werd de propylaldehyde hydrazon formulering van HYNIC geïntroduceerd. Vervolgens werden ^{99m}Tc-HYNIC-IL-8 preparaten met behulp van vijf verschillende coliganden gelabeld. Het effect van deze coliganden op de in vitro karakteristieken en het in vivo gedrag van ^{99m}Tc-HYNIC-IL-8 werd bestudeerd in konijnen met ontstekingen in de dijbeenspier geïnduceerd door *E.coli* bacteriën. Het gebruik van nicotinezuur/tricine als coliganden gaf de meest optimale eigenschappen om ontstekingen te visualiseren. Dit preparaat combineerde een hoge specifieke activiteit (tot 80 MBq/μg) met een goede in vitro stabiliteit en hoge abces/achtergrond ratio's (>20), 6 uur na toediening. Als gevolg van de hoge specifieke activiteit komt de toegediende hoeveelheid eiwit in mensen niet boven de 70 ng/kg lichaamsgewicht uit. Bij deze lage eiwitdoses worden geen bijwerkingen verwacht.

Het belang van een zorgvuldige keuze van de radiolabeling condities voor de kwaliteit van de scintigrafische detectie wordt nogmaals benadrukt in het **Addendum bij Hoofdstuk 5**.

^{99m}Tc-HYNIC-IL-8 is niet alleen bruikbaar om ontstekingen in spieren in konijnen te visualiseren, maar bleek ook geschikt als diagnosticum in experimentele modellen van colitis en longontsteking in konijnen.

In konijnen met chemisch geïnduceerde acute colitis werden de ontstekingshaarden scintigrafisch zichtbaar gemaakt met behulp van ^{99m}Tc-HYNIC-IL-8 (**Hoofdstuk 6**). Binnen 4 uur na injectie van ^{99m}Tc-HYNIC-IL-8 is een nauwgezette beoordeling van de ernst van de ontsteking in de darm mogelijk.

^{99m}Tc-HYNIC-IL-8 werd getest als diagnosticum voor longontstekingen in drie experimentele modellen in konijnen: aspergillosis in konijnen met een verzwakt afweersysteem, pneumococcen (gram-positieve) pneumonie en *E.coli* geïnduceerde (gram-negatieve) pneumonie in konijnen met een normaal afweersysteem (**Hoofdstuk 7**). Met behulp van ^{99m}Tc-HYNIC-IL-8 kon binnen twee uur na toediening de plaats en ernst van de ontsteking uitstekend bepaald worden in elk van de drie modellen. ^{99m}Tc-HYNIC-IL-8 biedt diverse voordelen boven de conventionele radiofarmaca voor de detectie van longontsteking, namelijk ^{67}Ga-citraat en radioactief gelabelde witte bloedcellen. Deze voordelen zijn een snelle en eenvoudige bereiding, een korte tijdsspanne tussen het injecteren en het maken van de opnames, een lage stralingsbelasting en, niet onbelangrijk, een scherpere aftekening van de ontstekingshaarden op de opnames.

De farmacokinetiek van ^{99m}Tc-HYNIC-IL-8 wordt in detail bestudeerd in **Hoofdstuk 8**. Om te onderzoeken in welke mate de aanwezigheid van neutrofielen een rol speelt bij de opname van ^{99m}Tc-gelabeld IL-8 in een ontsteking, werd de opname van ^{99m}Tc-HYNIC-IL-8 in steriele ontstekingen in konijnen met zeer weinig neutrofielen (neutropene konijnen) vergeleken met de opname in steriele ontstekingen in konijnen met normale aantallen neutrofielen (normale konijnen). De opname van ^{99m}Tc-HYNIC-IL-8 in ontstekingen in normale konijnen was tien keer hoger dan de opname in ontstekingen in neutropene konijnen, een goede demonstratie van de (neutrofiel afhankelijke) specificiteit van opname van ^{99m}Tc-IL-8 in ontstekingen. Verder wordt aannemelijk gemaakt dat ^{99m}Tc-gelabeld IL-8 in de ontstekingshaard terechtkomt hoofdzakelijk middels binding aan neutrofielen in de bloedbaan. Uit zowel in vivo als ex vivo analyses bleek de totale fractie van het geïnjecteerde preparaat dat uiteindelijk in het ontstoken weefsel terecht komt extreem hoog (meer dan 15%) te zijn.

In de **Hoofdstukken 9 en 10** worden andere eiwitten die binden aan receptoren op witte bloedcellen onderzocht.

C5a, een eiwit dat deel uit maakt van het complementsysteem, en zijn natuurlijke metaboliet C5a des Arg[74] (C5adR) binden beide de zelfde receptor op witte bloedcellen. De bindingsaffiniteit van C5a is in de orde van grootte van 10^{-9} M, een factor 10-100 hoger dan in geval van C5adR. ^{99m}Tc-gelabeld C5a en C5adR werden getest op hun vermogen om ontstekingen zichtbaar te maken in konijnen met spierontstekingen (**Hoofdstuk 9**). ^{99m}Tc-gelabeld C5a vertoonde uitstekende eigenschappen om ontstekingen te visualiseren. C5a is echter biologisch zeer actief, hetgeen een gebruik in de kliniek als beeldvormend middel voor ontstekingen belemmert. C5adR is een biologisch minder actief eiwit maar is als diagnosticum suboptimaal. Deze studie gaf aan dat voor een adequate lokalisatie van een receptor bindend eiwit bindingsaffiniteiten in de orde van grootte van 10^{-9} M vereist zijn.

De CXC-chemokines zijn een familie van nauw verwante chemotactische cytokinen, die binden aan neutrofielen, deze aantrekken en activeren. In **Hoofdstuk 10** wordt de relatie tussen bindingsaffiniteit voor neutrofielen en mate van geschiktheid voor het zichtbaar maken van ontstekingen onderzocht in een selectie van CXC-chemokines, waaronder NAP-2, drie NAP-2 varianten, IL-8, CTAP-III, GCP-2, ENA-78, PF-4 en IP-10. De ^{99m}Tc-gelabelde CXC-chemokines werden getest op hun vermogen om ontstekingen zichtbaar te maken in konijnen met spierontstekingen geïnduceerd door *E.coli*. Deze studie toonde een duidelijk verband aan tussen receptoraffiniteit voor neutrofielen en de mate van geschiktheid voor het zichtbaar maken van ontstekingen. Van de NAP-2-varianten combineerde NAP-2(1-66) een hoogste affiniteit voor de CXCR2 receptor met de beste eigenschappen voor beeldvorming.

Conclusie

De dierexperimentele studies zoals beschreven in dit proefschrift laten zien dat ^{99m}Tc-HYNIC-IL-8 beter is dan de huidige standaard, gelabelde witte bloedcellen, voor het scintigrafisch zichtbaar maken van ontstekingen. De bereiding is sneller en eenvoudiger en er bestaat geen kans op besmetting door bloedproducten. Tevens is de kwaliteit van de scintigrafische opnames veel beter dan die van gelabelde witte bloedcellen. De veiligheid van ^{99m}Tc-HYNIC-IL-8 voor de patiënt en de klinische toepasbaarheid dienen nog nader onderzocht te worden.

List of publications

1. Rennen HJJM, Boerman OC, Koenders EB, Oyen WJG, Corstens FHM. Labeling proteins with [99mTc] via hydrazinonicotinamide (HYNIC): optimization of the conjugation reaction. *Nucl Med Biol.* 2000;27:599-604.

2. Rennen HJJM, Boerman OC, Oyen WJG, van der Meer JWM, Corstens FHM. Specific and rapid scintigraphic detection of infection with [99mTc]-labeled interleukin-8. *J Nucl Med.* 2001;42:117-123.

3. Rennen HJJM, Boerman OC, Oyen WJG, Corstens FHM. Imaging infection/inflammation in the new millennium. *Eur J Nucl Med.* 2001;28:241-252.

4. Rennen HJJM, Makarewicz J, Oyen WJG, Laverman P, Corstens FHM, Boerman OC. The effect of molecular weight on nonspecific accumulation of [99mTc]-labeled proteins in inflammatory foci. *Nucl Med Biol.* 2001;28:401-408.

5. Gratz S, Rennen HJJM, Boerman OC, Oyen WJG, Corstens FHM. Rapid imaging of experimental colitis with [99mTc]-interleukin-8 in rabbits. *J Nucl Med.* 2001;42:917-923.

6. Rennen HJJM, Corstens FHM, Oyen WJG, Boerman OC. New concepts in infection / inflammation imaging. *Q J Nucl Med.* 2001;45:167-173.

7. Gratz S, Rennen HJJM, Boerman OC, Oyen WJG, Burma P, Corstens FHM. [99mTc]-interleukin-8 for imaging acute osteomyelitis. *J Nucl Med.* 2001;42:1257-1264.

8. Boerman OC, Rennen HJJM, Oyen WJG, Corstens FHM. Radiopharmaceuticals to image infection and inflammation. *Semin Nucl Med.* 2001;31:286-295.

9. Rennen HJJM, van Eerd JE, Oyen WJG, Corstens FHM, Edwards DS, Boerman OC. Effects of coligand variation on the in vivo characteristics of [99mTc]-labeled interleukin-8 in detection of infection. *Bioconjug Chem.* 2002;13:370-377.

10. Rennen HJJM, Boerman OC, Oyen WJG, Corstens FHM. Scintigraphic imaging of inflammatory processes. *Curr Med Chem.- Anti-Inflammatory & Anti-Allergy Agents.* 2002;1:63-75.

11. Gratz S, Rennen HJJM, Boerman OC, Oyen WJG, Mast P, Behr TM, Corstens FHM. [99mTc]-HMPAO-labeled autologous versus heterologous leukocytes for imaging infection. *J Nucl Med.* 2002;43:918-924.

12. Rennen HJJM, Boerman OC, Oyen WJG, Corstens FHM. Labeling method largely affects the imaging potential of interleukin-8. *J Nucl Med.* 2002;43:1128.

13. Rennen HJJM, Oyen WJG, Cain SA, Monk PN, Corstens FHM, Boerman OC. [99mTc]-labeled C5a and C5a des Arg(74) for infection imaging. *Nucl Med Biol.* 2003;30:267-272.

14. Rennen HJJM, Boerman OC, Oyen WJG, Corstens FHM. Molecular imaging of infection and inflammation. *In:* Feinendegen LE, Shreeve WW, Eckelman WC, Bahk YW, Wagner HN, *ed*: Molecular Nuclear Medicine. The challenge of genomics and proteomics to clinical practice. 1st ed. Berlin, Springer-Verlag; 2003:233-252.

15. Van Eerd JE, Oyen WJG, Harris TD, Rennen HJJM, Edwards DS, Liu S, Ellars CE, Corstens FHM, Boerman OC. A bivalent leukotriene B(4) antagonist for scintigraphic imaging of infectious foci. *J Nucl Med.* 2003;44:1087-1091.

16. Rennen HJJM, Boerman OC, Oyen WJG, Corstens FHM. Kinetics of Tc-99m-labeled Interleukin-8 in experimental inflammation and infection. *J Nucl Med.* 2003;44:1502-1509.

17. Rennen HJJM, Boerman OC, Oyen WJG, Corstens FHM. Scintigraphic imaging of inflammatory processes. *Med Chem Rev Online.* 2004;1 (in press).

18. Rennen HJJM, Bleeker-Rovers CP, van Eerd JE, Frielink C, Oyen WJG, Corstens FHM, Boerman OC. [99mTc]-labeled Interleukin-8 for scintigraphic detection of pulmonary infection. *Submitted.*

19. Rennen HJJM, Frielink C, Brandt E, Zaat SAJ, Boerman OC, Oyen WJG, Corstens FHM. Relationship between neutrophil binding affinity and suitability for infection imaging: Comparison of [99mTc]-NAP-2 and three C-terminally truncated isoforms. *Submitted.*

20. Van Eerd JE, Rennen HJJM, Oyen WJG, Harris TD, Edwards DS, Corstens FHM, Boerman OC. Scintigraphic detection of pulmonary aspergillosis in rabbits with a radiolabeled Leukotriene B4 antagonist. *Submitted.*

Dankwoord

Mijn dank gaat uit naar de velen die aan de totstandkoming van dit proefschrift hebben bijgedragen:

Mijn promotores, Prof. Dr. F.H.M. Corstens en Prof. Dr. W.J.G. Oyen, en co-promoter, Dr. O.C. Boerman, voor hun onverzettelijk geloof in mij, wat ze reeds tijdens mijn vorige promotie van facilitair medewerker tot junior onderzoeker tentoonspreidden. Otto, vooral jij zag potentie in je studiegenoot die voor jaren slechts vertrouwd was met de toegepaste chemie van detergentia, een schone zaak!

Annemieke Soede, Cathelijne Frielink en Julliëtte van Eerd hebben mij met ware offerbereidheid in de experimenten terzijde gestaan. En niet te vergeten Emile Koenders voor zijn handige tips en ondersteuning bij de uitvoering van menige kritische reactie.

Alle "Aquarium"-genoten, zij die het Aquarium aspireerden en zij die voortijdig ruimer sop gekozen hebben, in het bijzonder Peter Laverman, Frank van Schaijk en Lioe-Fee de Geus-Oei voor hun warme collegialiteit. In Chantal Bleeker-Rovers heb ik het volste vertrouwen dat de IL-8 patiëntenstudie het "most promising" stadium zal passeren.

Daarnaast dank aan alle overige collega's van de afdeling Nucleaire Geneeskunde, voor de gezellige werksfeer die ze bieden, en de collega's annex disgenoten van het Urologisch Research Lab.

De medewerkers van het Centraal Dierenlaboratorium, Gerrie Grutters en Hennie Eijkholt, wil ik gaarne bedanken voor hun humane behandeling van de dieren die hun leven voor de wetenschap gegeven hebben.

En niet op de laatste plaats dank aan Prof. Dr. R.M.J. Liskamp, John Kruijtzer en Matthias Broekema van de Universiteit Utrecht, afdeling Medicinal Chemistry, voor de genoten gastvrijheid op hun afdeling en vakkundige ondersteuning in het synthesewerk.

Curriculum vitae

De schrijver van dit proefschrift werd geboren op 24 januari 1959 te Woensdrecht. In 1977 behaalde hij het VWO gymnasium β diploma aan het Moller Lyceum te Bergen op Zoom. Vervolgens studeerde hij scheikunde en filosofie aan de Katholieke Universiteit te Nijmegen. Het doctoraalexamen scheikunde omvatte het hoofdvak biochemie (onderzoek aan ooglenseiwitten), als bijvakken biofysische chemie en filosofie, en werd behaald in 1985. Daarna volgde een periode van afwisselende werkzaamheden (o.a. programmeur/systeemanalist bij Philips Nijmegen en facilitair medewerker in het St. Radboud ziekenhuis te Nijmegen) en uitgebreide omzwervingen in Azië (met name de Himalaya's). In november 1998 trad hij in dienst als junior onderzoeker op de afdeling Nucleaire Geneeskunde van het Universitair Medisch Centrum St. Radboud te Nijmegen (hoofd: Prof. Dr. F.H.M. Corstens). Mede dankzij subsidie van de Technologiestichting STW kon het promotieonderzoek verricht worden dat resulteerde in dit proefschrift.